Remote Sensing the Radionuclide Contaminated Belarusian Landscape: Predicting ^{137}Cs Content in *Pinus sylvestris*

Paul Christian Goldsmith

This Thesis is being Submitted in Partial Fulfilment of the Requirements for the Degree of Doctor of Philosophy

Submitted September 2007

School of Earth Sciences and Geography
Kingston University

Abstract

The 1986 Chernobyl accident resulted in distribution of Radiocaesium (^{137}Cs) throughout much of the northern hemisphere. ^{137}Cs still persists in the environment, particularly in Belarus where up to 80% of the radioactive fallout occurred. Monitoring ^{137}Cs across space and through time is essential to remediate contamination and remote sensing, particularly imaging spectrometry has potential to provide information at appropriate spatial and temporal scales. This thesis explores that potential by assessing whether imaging spectrometry can be used to monitor ^{137}Cs content of vegetation.

The research has three main components; field radiometry, laboratory experimentation and spaceborne hyperspectral imagery (EO-1 Hyperion). Field radiometry collected spectral and biochemical data from *Pinus sylvestris* growing on the Belarusian landscape contaminated with varying levels of ^{137}Cs, and investigated the links between foliar biochemistry, ^{137}Cs specific activity and spectral reflectance. Significant differences exist between spectra of *Pinus sylvestris* contaminated with different levels of ^{137}Cs as well as key foliar biochemicals of chlorophyll, nitrogen, cellulose, lignin and water. Partial correlation identified which parts of the electromagnetic spectrum ^{137}Cs contamination had impacts upon in relation to particular biochemicals. Prediction of leaf/needle biochemicals from spectra was possible using regression techniques, but predicting ^{137}Cs specific activity from biochemicals was not possible at a statistically significant level.

Laboratory experimentation results supported fieldwork findings and exhibited significant differences in spectral response between contaminated and non-contaminated trees, also highlighting non-linearity in uptake and response of *Pinus sylvestris* to ^{137}Cs (with subsequent remote sensing implications). Spectra extracted from hyperspectral imagery also show significant difference in their spectra despite assumptions and constraints in interpretation of this imagery. The thesis concludes by suggesting that presently, the use of imaging spectrometry to monitor ^{137}Cs specific activity of vegetation (0.07 - 39.9 Bq/g) is not feasible; mainly due to immature understanding of ^{137}Cs impacts on plant biochemicals and the links between foliar biochemistry and ^{137}Cs content. Research limitations present opportunities for further research which may allow future monitoring of ^{137}Cs levels using imaging spectrometry.

Acknowledgements

There are a number of people who I must not simply acknowledge, but thank, for their considerable input in helping me bring this research to fruition. Firstly, I would like to thank Kingston University for providing me with a PhD studentship, without which, none of this work would have happened. Central to the process of research have been my supervisors, each of whom has supported me in different ways and at different times throughout; all have been excellent. Long evenings spent with Alan Flowers in his office were wonderful for musing and discussing the latest Belarusian politics. Speaking of politics, the expulsion from Belarus (and interruption to fieldwork) due to Alan's supposed 'secret' scientific work along with the subsequent media coverage and addition to the KGB's forbidden persons list was an interesting aside from studying. Jane Entwistle was an asset in the field and was most helpful in setting up a two-week research visit to Northumbria University. Her attention to detail and patience have been vital in completing parts of this work. Mike Smith has been a solid port of call for support with various aspects of my work and teaching. I enjoyed testing Mike's kites as potential platforms for aerial imagery, but didn't enjoy the bites from chiggers we received whilst on the Dunstable Downs! I couldn't ask for more from Doreen Boyd who has been supportive and always available from start to finish, despite her numerous moves over the course of the PhD. Doreen has been understanding and inspirational throughout and I sincerely thank her for all her help. My family have been a motivational force and have assisted monetarily and practically. I'd like to thank my dad for his continued interest in the progress of the PhD and my mum, who gave up a great deal of time to help with laborious weighing and potting procedures. Special thanks also to my Nan, Clare, who has always been interested in my work. Cheryl and Janice have been a source of motivation, mainly via the telephone. My deepest thanks also go to the Hawker family (Malcolm, Jo, Josh, Jen and Harrison) who have all been incredibly helpful during the final write up. Long wordy acknowledgments are not my preferred style, so before I bring these to a close I would like to add thanks to Claire Ivison at Kingston, who assisted with diagrams, maps and printing. At the University of Southampton, I appreciate Ted Milton's provision of the computer running ENVI. Thanks also to the NERC FSF for loans of the ASD FieldSpec and the SAS Institute who were generous in providing a free student copy of the SAS JMP software. Finally, I would like to thank the Belarusian people for their hospitality and fieldwork assistance, particularly Dr Alexander Dvornik and all those at the Svetolovichi Sanatorium.

Contents

	Page
Abstract	i
Acknowledgements	ii
Contents	iii
List of Figures	viii
List of Tables	xiii
List of Acronyms	xvii
Chapter 1	
Introduction	1
1.1 Contamination of Land by Radionuclides	1
1.2 Remote Sensing Radionuclide Contamination	3
1.3 Belarus as a Natural Environmental Laboratory	5
1.3.1 The Chernobyl Accident	5
1.3.2 Contamination of Land by Radiocaesium (^{137}Cs)	7
1.4 Research Objectives	7
1.5 Thesis Structure	8
Chapter 2	
Remote Sensing Vegetation Status and Contamination	11
2.1 Introduction	11
2.2 Remote Sensing	11
2.3 Remote Sensing Contamination	12
2.3.1 Contamination causing Visible or Thermal Impacts	12
2.3.2 Contamination Detectable in Spectral Changes	14
2.4 The Importance of Remote Sensing Vegetation	16
2.5 Vegetation as a Prisoner of Its Environment	16
2.6 Spectral Response and Remote Sensing of Vegetation	18
2.7 Imaging Spectrometry	23
2.8 Remote Sensing of Vegetation Stress	26

2.8.1 Laboratory Experimentation to Understand Vegetation Responses to Stress 26
2.8.2 Crop Responses to Environmental Stress 27
2.8.3 Remote Sensing Forest Scale Response to Environmental Stress 28
2.9 Radioecological Effects of ^{137}Cs 29
2.10 Summary 31

Chapter 3
Study Site, Data and Instrumentation 33

3.1 Introduction 33
3.2 Study Site and Environment 34
3.2.1 Belarus as a Natural Environmental Laboratory 34
3.2.2 The Artificial Laboratory Environment 35
3.2.3 Imaging Spectrometry 35
3.3 Data Collection Strategies 35
3.3.1 Spectral Measurement 36
3.3.2 Spectral Processing 39
3.3.3 First Derivative Spectra 39
3.3.4 Continuum Removal 40
3.3.5 Biochemical Assay 43
3.3.6 Chlorophyll Concentration 44
3.3.7 Lignin Cellulose and AD Fibre 46
3.3.8 Water 47
3.3.9 Nitrogen 48
3.3.10 Gamma Spectrometry 49
3.4 Summary 51

Chapter 4
Feasibility of Imaging Spectrometry for Remote Sensing 52
^{137}Cs Contamination: A Pilot Study

4.1 Introduction 52
4.2 Background to Data Collection Strategies 52
4.3 Study Sites and Data Collection 52

4.4 Analysis of Spectral Reflectance 56
4.5 Discussion 61
4.6 Summary and Suggested Modifications to Future Fieldwork 63

Chapter 5
Predicting ^{137}Cs levels from Spectra 64

5.1 Introduction 64
5.2 Data Collection Strategy and Biochemical Variability 66
5.3 Assessing Whether Significant Differences 71
Exist Between Spectra Contaminated with High and Low Levels of ^{137}Cs
5.4 Assessing Differences Between Key Foliar Biochemicals 75
5.5 Partial Correlations to Determine ^{137}Cs Effects on Foliar Biochemicals 77
5.6 Prediction of Foliar Biochemicals From Spectra 88
5.6.1 Stepwise Multiple Linear Regression 88
5.6.1.1 Water 92
5.6.1.2 AD Fibre 93
5.6.1.3 Cellulose 94
5.6.1.4 Lignin 95
5.6.1.5 Total Chlorophyll 96
5.6.1.6 Chlorophyll *a* 97
5.6.1.7 Chlorophyll *b* 98
5.6.1.8 Elemental Nitrogen 99
5.6.1.9 ^{15}N 99
5.6.1.10 ^{137}Cs 100
5.6.2 Testing Validity of Stepwise Regression Using Randomised Data 101
5.6.3 Determining Causality with Forced Entry Stepwise Regression 103
5.6.4 Testing Validity of Forced Entry Stepwise Regression 104
5.6.5 Partial Leased Squares to Predict Foliar Biochemical Content 105
5.7 Predicting ^{137}Cs from Foliar Biochemicals 108
5.7.1 Multiple Regression 108
5.7.2 Artificial Neural Networks 111
5.8 Summary 114

Chapter 6

Detecting ^{137}Cs Levels in *Pinus sylvestris* Grown in Artificial Laboratory Environment 117

6.1 Introduction 117

6.2 Trees and Growing Conditions 117

6.2.1 Dosing the Trees with ^{137}Cs 119

6.2.2 Measuring Reflectance Spectra 120

6.2.3 Measuring Specific ^{137}Cs Activity 121

6.2.4 Measuring Plant Health Using Chlorophyll Fluorescence 121

6.3 Analysis and Discussion 123

6.3.1 Specific ^{137}Cs Activity and Plant Health 123

6.3.2 Spectral Analysis 126

6.4 Summary 133

Chapter 7

Detecting ^{137}Cs from a Spaceborne Platform: Hyperion Imagery 136

7.1 Introduction 136

7.2 The Hyperion Hyperspectral Instrument 137

7.3 Data Acquisition over the Belarus Landscape 138

7.4 Prepossessing of Imagery 142

7.4.1 Atmospheric Correction Using FLAASH 142

7.4.2 Geometric Correction 143

7.5 Extraction of Spectra from Pixels 143

7.6 Analysis of Image Spectral Information 144

7.7 Summary 150

Chapter 8

Discussion and Conclusion 152

8.1 Introduction 152

8.2 Are Changes in Spectral Response Caused by Differing ^{137}Cs Levels? 152

8.3 Does ^{137}Cs Contamination Have Any Effect on Key 154

Foliar Biochemicals and At What Regions of the
Optical Range of the Electromagnetic Spectrum Are These Detectable?
8.4 Can Key Foliar Biochemicals be Predicted from Spectral Response and in turn used to Infer Levels of ^{137}Cs Contamination? 157
8.5 Can Any ^{137}Cs Impacts on Spectral Response and Foliar Biochemicals be Monitored from Space Using Imaging Spectrometry? 159
8.6 Research Limitations 160
8.7 Further Research Opportunities 161
8.8 Conclusion 162

References 164
Appendices 187

List of Figures

Figure 1.1	Photo showing road markings at the entrance to a restricted area where the forests are contaminated with radionuclides.	6
Figure 1.2	Photo of evacuated and derelict farmland after the Chernobyl nuclear accident.	6
Figure 2.1	Typical spectral reflectance of healthy green vegetation.	18
Figure 3.1	Map of Belarus, it regions and bordering countries.	34
Figure 3.2	Map of Gomel region of Belarus and general contamination levels where the data collection took place.	36
Figure 3.3	Photo showing rope and wire saw method for collecting branches.	37
Figure 3.4	Conceptual diagram of continuum removal.	41
Figure 3.5	Six absorption features selected for continuum removal.	42
Figure 3.6	Photo showing foil weigh boats and portable balance in Belarus laboratory.	48
Figure 4.1	Location of the four study site chosen for investigation.	56

Figure 4.2	Mean spectral response for the *Pinus sylvestris* needles sampled at each site.	57
Figure 5.1	Conceptional diagram of the top down approach taken in the chapter.	65
Figure 5.2	Location of the three study site chosen for investigation.	67
Figure 5.3	Student's t-test for high versus low spectra using the domestic fuel wood limit as a cut off point.	72
Figure 5.4	Student's t-test for high versus low spectra using the lumber limit as a cut off point.	74
Figure 5.5	Partial correlation – an illustration of the concept.	78
Figure 5.6	Difference between first order partial and zero order correlation for water	80
Figure 5.7	Difference between first order partial and zero order correlation for AD fibre.	81
Figure 5.8	Difference between first order partial and zero order correlation for cellulose.	82
Figure 5.9	Difference between first order partial and zero order correlation for lignin.	83
Figure 5.10	Difference between first order partial and zero order correlation for total chlorophyll.	84
Figure 5.11	Difference between first order partial and zero order correlation for chlorophyll *a*.	84

Figure 5.12	Difference between first order partial and zero order correlation for chlorophyll *b*.	85
Figure 5.13	Difference between first order partial and zero order correlation for elemental nitrogen.	86
Figure 5.14	Difference between first order partial and zero order correlation for ^{15}N.	87
Figure 5.15	Multiple linear regression to predict ^{137}Cs using all nine foliar biochemicals as inputs.	109
Figure 5.16	Multiple linear regression to predict regression from the conditionally independent biochemicals.	110
Figure 5.17	Multiple linear regression to predict regression from the conditionally dependent biochemicals.	111
Figure 5.18	Artificial neural network conceptual diagram showing nine biochemical inputs.	112
Figure 5.19	Artificial neural network conceptional diagram showing four conditionally independent biochemical inputs.	113
Figure 5.20	Artificial neural network conceptional diagram showing four conditionally dependent biochemical inputs.	114
Figure 6.1	An annotated photo summarising the laboratory conditions and set-up during the experiment.	119

Figure 6.2	Conceptual illustration of the process of chlorophyll fluorescence and parameters measured.	122
Figure 6.3	Mean specific ^{137}Cs activity for each group of trees.	125
Figure 6.4	Average Fv/Fm values as measured by chlorophyll florescence.	126
Figure 6.5	Mean spectral reflectance of each group of trees.	127
Figure 6.6	Coefficient of determination between raw spectra and specific ^{137}Cs.	128
Figure 6.7	Coefficient of determination between raw spectra and Fv/Fm.	129
Figure 6.8	Mean first derivative spectra for each group of trees.	129
Figure 6.9	Coefficient of determination between FDS and specific ^{137}Cs.	130
Figure 6.10	Coefficient of determination between FDS and Fv/Fm.	131
Figure 6.11	Coefficient of determination between BDNA and specific ^{137}Cs activity.	132
Figure 6.12	Coefficient of determination between BDNA and Fv/Fm values.	133
Figure 7.1	Approximate true colour display of Hyperion imagery collected from the high site.	140

Figure 7.2 Approximate true colour display of Hyperion imagery collected from the medium site. 141

Figure 7.3 Student's t-test for high versus low FDS extracted from Hyperion pixels. 143

Figure 7.4 Student's t-test for high versus medium FDS extracted from Hyperion pixels. 145

Figure 7.5 Student's t-test for medium versus low FDS extracted from Hyperion pixels. 146

Figure 7.6 Comparison of statistically significant t-values for spectra taken from Hyperion pixels and spectra collected with the ASD field spectrometer in Belarus (0.74 Bq/g). 148

Figure 7.7 Comparison of statistically significant t-values for spectra taken from Hyperion pixels and spectra collected with the ASD field spectrometer in Belarus (1.85 Bq/g). 149

Figure 7.8 Comparison of statistically significant t-values for spectra taken from Hyperion pixels and field spectra. 150

List of Tables

Table 2.1	List of forty-two absorption features in the visible and near infrared portion of the electromagnetic spectrum that have been related to certain foliar biochemicals.	20
Table 2.2	Example of selected airborne and spaceborne spectrometers along with abridged technical details.	24
Table 3.1	Selected technical characteristics of the ASD FieldSpec Pro.	38
Table 4.1	Site designation, location and mean dose rate at 1m above ground and mean needles specific activity.	55
Table 4.2	Wavelength for which significantly different BDNA spectra were found between needles with low and high ^{137}Cs contamination levels.	59
Table 5.1	Site designation, location and mean dose rate at 1m above ground and mean needle specific ^{137}Cs.	68
Table 5.2	Descriptive statistics of biochemical data.	70
Table 5.3	Intercorrelation between foliar biochemicals.	71
Table 5.4	Student's t-test between biochemicals which have been split up according to domestic fuel wood limit.	75

Table 5.5	Student's t-test between biochemicals which have been split up according to the lumber wood limit.	76
Table 5.6	Results from unconstrained regressions on four transformations of the spectra.	91
Table 5.7	BNC wavelengths selected by the stepwise procedure for use in the water regression model.	93
Table 5.8	BDNA wavelengths selected by the stepwise procedure for use in the AD fibre regression model.	94
Table 5.9	FDS wavelengths selected by the stepwise procedure for use in the cellulose regression model.	95
Table 5.10	BDNA wavelengths selected by the stepwise procedure for use in the lignin regression model.	96
Table 5.11	BNC wavelengths selected by the stepwise procedure for use in the total chlorophyll regression model.	96
Table 5.12	BNC wavelengths selected by the stepwise procedure for use in the chlorophyll *a* regression model.	97
Table 5.13	BNC wavelengths selected by the stepwise procedure for use in the chlorophyll *b* regression model.	98

Table 5.14	FDS wavelengths selected by the stepwise procedure for use in the elemental nitrogen regression model.	99
Table 5.15	Absolute reflectance wavelengths selected by the stepwise procedure for use in the ^{15}N regression model.	100
Table 5.16	FDS wavelengths selected by the stepwise procedure for use in the ^{137}Cs regression model.	101
Table 5.17	Results from unconstrained regressions using randomised datasets from four transformations of the spectra.	102
Table 5.18	Results from constrained regression on four transformations of the spectra.	103
Table 5.19	Results form constrained regressions using randomised datasets from four transformations of the spectra.	104
Table 5.20	Results from partial least squares modelling using two transformations of the spectra.	106
Table 5.21	Results from PLS modelling using two further transformations of the spectra.	106
Table 5.22	Results of a comparison between the power of predictive biochemistry models derived from stepwise and PLS techniques.	107
Table 5.23	SAS suggested settings for generating a neural network.	113

Table 6.1 Approximate ^{137}Cs added to the different groups of *Pinus sylvestris.* 120

Table 6.2 Specific ^{137}Cs activities for each tree as measured by gamma spectrometry. 124

Table 7.1 Summary of Hyperion technical specifications. 138

List of Acronyms

ACORN	Atmospheric Correction Now
AD Fibre	Acid Digestible Fibre
ASD	Analytical Spectral Devices
ATREM	Atmospheric Removal Program
BDNA	Band Depth Normalised to Area
BNC	Band Depth Normalised to Centre
CF	Chlorophyll Fluorescence
CNPP	Chernobyl Nuclear Power Plant
CTAB	Cetyltrimethylammonium Bromide
DAR	Data Acquisition Request
DN	Digital Number
EA-IRMS	Elemental Analyser Isotope Ratio Mass Spectrometry
ENVI	The Environment for Visualising Images
EO-1	Earth Observing 1
ERICA	Environmental Risk from Ionising Contaminants: Assessment and Management
ETR	Electron Transport Rate
EU	European Union
FASSET	Framework for Assessment of Environmental Impact
FDR	First Derivative Reflectance
FLAASH	Fast Line-of-Sight Atmospheric Analysis of Spectral Hypercubes
FSF	Field Spectroscopy Facility
Fv/Fm	Ratio of Variable to Maximum Fluorescence
GCP	Ground Control Point
GPS	Global Positioning System
HATCH	High Accuracy Atmospheric Correction for Hyperspectral Data
HDF	Hierarchical Data Format
HPGe	High Purity Germanium
IAEA	International Atomic Energy Agency
IFOV	Instantaneous Field of View
LAI	Leaf Area Index
Landsat ETM+	Landsat Enhanced Thematic Mapper Plus

Landsat TM	Landsat Thematic Mapper
LIBERTY	Leaf Incorporating Biochemistry Exhibiting Reflectance and Transmittance Yield
MODIS	Moderate Resolution Imaging Spectrometer
MODTRAN	Moderate Resolution Atmospheric Transmission
NASA	National Aeronautical and Space Administration
NDVI	Normalised Difference Vegetation Index
NERC	Natural Environment Research Council
NPL	National Physical Laboratory
PAM	Pulse Amplitude Modulation
PLS	Partial Least Squares
qN	Non Photochemical Quenching
qP	Photochemical Quenching
REP	Red Edge Position
RMS	Root Mean Square
RMSE	Root Mean Square Error
RSI	Research Systems Inc.
SNR	Signal to Noise Ratio
SPOT	Satellite Pour l'Observation de la Terre
SWIR	Short Wavelength Infrared
SWMLR	Stepwise Multiple Linear Regression
UN	United Nations
USGS	United States Geological Survey
USSR	Union of Soviet Socialist Republics
VNIR	Visible and Near Infrared

Chapter 1

Introduction

1.1 Contamination of Land by Radionuclides

Humans have affected Earth's biosphere, atmosphere and lithosphere with the term 'Anthropocene' being coined by some (e.g. Crutzen and Stoermer 2000) to illustrate the extent of human impact on the natural environment. In order to understand these anthropogenic effects there is a need to monitor the impacts across space and through time. This is especially so of contaminated land (Plant *et al.* 2001). Despite large amounts of research into the global environment, most pertains to climate change; there has been relatively little research into the quality of Earth's land surface and life support systems other than studies commissioned on an *ad hoc* basis in response to specific problems. One exception to this has been the EU funded ERICA project which has provided necessary methods to allow societal and scientific issues regarding environmental exposure to radiation to be dealt with in a robust and comprehensive way (Brown *et al.* 2008). The importance of developing national and international frameworks for dealing with the effects of ionising radiation on biota is corroborated by Copplestone *et al.* (2004). This illustrates the importance of understanding and monitoring contamination of the environment by radionuclides. Environmental contamination may be described as the impact of chemical compounds, technologies and other human manifestations on the environment (Cajaraville 2000); though it is important to note that contamination is not always anthropogenic in its origins (e.g. Farias *et al.* 2003). Spatial and temporal information is critical for global and regional change studies including contamination (Senay and Elliott 2000). This is especially so with contamination of land by radionuclides due to their spatial and temporal dynamics. Radionuclides can be described as any unstable nuclide which undergoes natural radioactive decay (Walker 1999). Spatially there is constant cycling and transfer of radioactive material through environmental systems and secondary events such as biomass burning, which can carry radionuclides into other

territories (Abduragimov and Odnolko 1993). Temporally there are constantly changing contamination levels based on half-lives of different radioactive isotopes. Natural radionuclides are argued on average to account for 79% of radiation to which humans are exposed, whilst 19% is from medical exposure and only 2% from fallout via nuclear weapons testing and the nuclear power industry (Zhu and Shaw 2000). Despite the relatively small exposure to artificial radioactivity, Salbu (2001) indicates that artificial radionuclides from nuclear fuel cycling, nuclear weapons activity and accidents represent a significant problem. Major deposition of manmade radionuclides has occurred in large-scale weapons testing during the late 1950s and early 1960s and in the 1986 Chernobyl accident (Gaso *et al.* 1998). Future potential threats from radionuclide contamination include nuclear waste and accidents (Baklanov *et al.* 2002) and terrorism (Oumeish 2002). The need to understand spatial and temporal dynamics of contamination, combined with significant problems caused by current radionuclide contamination and potential of future radionuclide threats mean suitable monitoring techniques are required. Currently, a variety of methods exist to measure and map environmental radioactivity. Broadly speaking the monitoring technique used, depends on the particular radionuclide being measured. Radionuclides emitting exclusively α or β radiation (e.g. ^{90}Sr) require chemical separation and non-destructive techniques cannot be used (Michel 2001). For radionuclides emitting γ radiation, the non-destructive method of gamma spectrometry can be utilised. Both laboratory and *in situ* field adaptations have been made to these techniques in order to characterise environmental radioactivity. Indeed, according to Debauche (2004) the gap between laboratory and field measurements of radioactivity has closed. To gather environmental radioactivity data at appropriate spatial scales and in a time efficient way, airborne gamma spectrometry has been the method of choice since the early 1980s but is not always precise for low levels of radiation (Guillot 2001). The techniques mentioned so far are concerned with the direct measurement of radionuclides however, using these techniques, the impacts of radioactivity on biota can only be inferred based on levels of particular radionuclides or by performing additional fieldwork to assess impacts. Remote sensing, specifically imaging spectrometry, may hold unique potential in monitoring radionuclide contamination by providing a measure of impact on biota. This is discussed further in section 1.2.

1.2 Remote Sensing Radionuclide Contamination

It is important at this stage to clarify the remit of the term 'remote sensing' as used in this thesis. As mentioned above, methods exist to monitor radionuclides using airborne gamma spectrometry (e.g. Cresswell *et al.* 2006) and could be broadly classified as remote sensing techniques. The term 'remote sensing' in this thesis means the use of instruments sampling in the optical range of the electromagnetic spectrum and more specifically, imaging spectrometry (described in chapter two). Formally, remote sensing can be described as the sensing of electromagnetic energy to record images of the environment which can then be interpreted to yield useful information about that environment (Curran 1985).

Remote sensing techniques have been demonstrated as key in understanding issues of global change such as biogeochemical cycles (e.g. Schimel 1995) deforestation patterns (e.g. Boyd *et al.* 2002) urban change (e.g. Chen *et al.* 2006) and other patterns of land use change. Indeed, Rees (1990) suggests that due to sheer number it would be impossible to note all the applications of remote sensing. In addition, remote sensing is often the only method available at appropriate spatial and temporal resolutions for a variety of studies (Alves and Skole 1996). A wide body of literature exists utilising remote sensing as a tool to aid the mapping of contamination (e.g. Webster *et al.* 1999, Zellmer and Eastman 1997). Curran (1994) suggests the advent of imaging spectrometry, which samples the electromagnetic spectrum in many narrow wavebands, gives the ability to estimate subtle changes in physical and chemical variables of the environment (such as vegetation).

This in turn has enabled remote sensing to be used in monitoring health of vegetation (e.g. Belluco *et al.* 2006). Some studies have already investigated the potential of imaging spectrometry as applied to environmental contamination. Jago *et al.* (1999) for example, investigate the effect that soil contamination and nitrogen application have upon spectral response in the form of the red edge. More recently, Kooistra *et al.* (2004) investigated the relationship between vegetation reflectance and the elevated concentrations of heavy metals in river floodplain soils. Likewise, Koponen *et al.* (2001) attempt to use imaging spectrometry (amongst other remote sensing techniques) to monitor chlorophyll *a* concentrations within a Finnish lake to derive the lake's water quality through the characterisation of algal blooms. Potential has been shown by Davids and Tyler (2003) for

inferring levels of radionuclide contamination via remote sensing techniques, but the study does not comprehensively investigate the possibilities of using remote sensing to monitor such contamination. If remote sensing could be used to monitor radionuclide contamination it would offer several benefits, namely:

- Measuring contamination indirectly by using vegetation as a bioindicator of radionuclide contamination would allow an assessment of the ecological impact of radiation
- Repeat coverage of contaminated areas would facilitate the monitoring of ecological recovery
- Measuring the impact on vegetation would allow the commercial potential of forest wood to be exploited
- Spatial variability of radionuclide contamination within forest ecosystems could be measured
- Opportune spatial and temporal coverage of contaminated areas could be utilised
- Cost effective spatial coverage could be offered (especially if existing operational spaceborne sensors could be used)

Of these benefits, perhaps the most important and unique, is the potential of remote sensing to provide an assessment of the ecological impact of radionuclide contamination and in turn, through continued temporal coverage, provide a means for measuring ecological recovery. This thesis aims to assess whether remote sensing techniques can be used to monitor vegetation contaminated by radionuclides. In order to achieve this research aim, an area of land contaminated by radionuclides was required. Belarus contains large continuous areas of vegetation contaminated with radionuclides from the largest nuclear accident at the Chernobyl Nuclear Power Plant (CNPP), Ukraine (formerly part of the USSR along with Belarus).

1.3 Belarus as a Natural Environmental Laboratory

1.3.1 The Chernobyl Accident

The Chernobyl accident occurred on April 26th, 1986 at the CNPP, Ukraine, releasing approximately 12 x 10^{18} Bq of radioactivity into the environment and was the result of flawed Soviet reactor design, lack of adequate training and an ethos which did not have proper regard for safety (World Nuclear Association 2001). The Chernobyl accident released 85PBq of Radiocaesium (^{137}Cs) into the environment with the majority of fall out occurring in Russia, Ukraine and Belarus (Gaso *et al.* 1998). The effects of the Chernobyl accident are wide ranging in terms of both spatial extent and diversity of effects upon people and the environment. Although Ukraine, Russia and Belarus were the three countries closest to the Chernobyl nuclear power plant and received the majority of contaminants, Rahu (2003) states that lower concentrations affected much of the northern hemisphere. Rahu (2003) goes on to describe the Chernobyl accident not simply as an event, but an ongoing process, which is still affecting people and the environment. This is especially true in Belarus, which was exposed to around 70% of the Chernobyl fallout (Soukhova *et al.* 2003). Almost immediately after the accident, a 30km exclusion zone was set up around the power plant, and in the months and years following, areas of Belarus were evacuated and restrictions placed on land use. Figures 1.1 and 1.2 show some of these restricted areas.

Figure 1.1: Photo showing road markings at the entrance to a restricted area where the forests are contaminated with Chernobyl-derived radionuclides.

Figure 1.2: Photo of evacuated and derelict farmland after the Chernobyl nuclear accident.

1.3.2 Contamination of Land by Radiocaesium (^{137}Cs)

Approximately 23% of the Belarusian landscape is contaminated with radionuclides (Vargo 2000). Immediately after the accident ^{131}I was the radionuclide causing most radiological concern, however over longer timescales and in the foreseeable future ^{137}Cs is the radionuclide of most interest due to its relatively long half-life and mobility in ecosystems (IAEA 2006). ^{90}Sr is also of interest, but is less volatile than ^{137}Cs and far less (c. 10PBq) was released into the environment than ^{137}Cs (IAEA 2006). The contamination has meant formerly productive forest resources and agricultural fields have been restricted in their use, which has in turn strained the political, economic and social infrastructure of Belarus (IAEA 1996). Amiro and Ipatyev (1999) suggest that many of the most contaminated areas have the best potential for harvesting lumber, thus aggravating economic impacts. The UN (2003) alarmingly argues that in the 21 years since the Chernobyl accident the problems have not gone away whilst international interest and assistance has diminished. Unsurprisingly, Chernobyl is listed as one of the top ten most polluted places on Earth (Blacksmith Institute 2007). Central to the UN's CORE programme (Co-operation for rehabilitation of living conditions in Chernobyl affected areas of Belarus) is the need to accurately and regularly monitor the radiological quality of the Belarusian landscape. In this research Belarus was used as a natural environmental laboratory, having large continuous areas of radionuclide contaminated land. *Pinus sylvestris* (Scots pine) was dominant on the contaminated areas of the Belarusian landscape and was focused on in order to minimise confounding variables during the study. The research also focused on the radionuclide causing most current and future interest, ^{137}Cs (IAEA 2006). ^{137}Cs is a radioactive pollutant causing much concern due to its relatively long half life (30.2 years), high bioavailability and behaviour in ecosystems in a way similar to potassium (causing high levels of uptake) (Gommers *et al.* 2005).

1.4 Research Objectives

The principal research question answered by this thesis is, 'can ^{137}Cs contamination be detected using imaging spectrometry techniques?'

From this central question come a set of research objectives:

- Assess if there are changes in spectral reflectance caused by differing ^{137}Cs levels (addressed in chapters four, five, six and seven)
- Characterise whether ^{137}Cs contamination has any effects on key foliar biochemicals (chlorophylls, cellulose, lignin, nitrogen and water) and at what regions of the optical range of the electromagnetic spectrum these are detectable (addressed in chapters four and five)
- Determine if key foliar biochemicals can be predicted from spectral response and in turn if these biochemicals can be used to infer levels of ^{137}Cs contamination (addressed in chapter five)
- Ascertain whether any ^{137}Cs impacts on spectral response and foliar biochemicals can be monitored from space using imaging spectrometry (addressed in chapter seven)

These research objectives are met in the thesis chapters, as described below in section 1.5.

1.5 Thesis Structure

The thesis consists of eight chapters, the contents of which are described below.

Chapter 2, Remote Sensing Vegetation Status/Contamination:
This chapter reviews literature concerning the use of remote sensing, particularly imaging spectrometry, to monitor the status of vegetation including foliar biochemical concentrations, biophysical properties and applications pertaining to monitoring status, stress and contamination. Literature concerning ^{137}Cs and radionuclide contamination in general is mentioned, where appropriate, in specific chapters. This chapter concludes by drawing out gaps in the literature and highlighting the opportunity for research focussed on in this thesis.

Chapter 3, Laboratories and Instrumentation:
To meet the objectives three main components of study were undertaken; fieldwork, laboratory experimentation and hyperspectral imaging. This chapter outlines the rationale behind these components starting with the two laboratories used in the research. Belarus (introduced in section 1.3) was used as natural environmental laboratory to undertake

fieldwork and is described. In addition to the natural environmental laboratory, an artificial laboratory was created to isolate the effects of ^{137}Cs from other environmental variables. This was in the form of an experiment in Kingston University's radiochemistry laboratory. The rationale behind the experiment is also described in this chapter. The third component of this research involved collecting hyperspectral imagery from study sites in Belarus. The reasoning behind choosing the Hyperion sensor is discussed. The chapter also summarises the necessary instrumentation and techniques used to collect data required for the research.

Chapter 4, Feasibility of Imaging Spectrometry for Remote Sensing ^{137}Cs Contamination: A Pilot Study:

This chapter describes pilot research undertaken on data collected from Belarus in order to assess feasibility and potential of remote sensing to monitor radionuclide contamination and as a method to inform and refine further study in the natural environmental laboratory. This chapter is based on the paper by Boyd *et al.* (2006) published in the *International Journal of Remote Sensing.*

Chapter 5, Predicting ^{137}Cs from Spectra:

This chapter contains the results form the extended fieldwork campaign in Belarus. It includes analyses of spectra using the statistical techniques of Student's t-tests, correlation analysis and predictions using stepwise multiple regression and partial least squares. Using these techniques, the links between spectra, foliar biochemicals and ^{137}Cs content are assessed.

Chapter 6, Artificial Laboratory Study:

This chapter describes results from research carried out in the artificial laboratory experiment to isolate ^{137}Cs effects and corroborate the results from fieldwork. It looks at the effects of ^{137}Cs dose on spectral response and ^{137}Cs uptake as well as the content of ^{137}Cs in relation to the health and spectral response of *Pinus sylvestris.*

Chapter 7, Detecting ^{137}Cs from a Spaceborne Platform: Hyperion Imagery:

This chapter looks at imagery collected from the fieldwork study sites in Belarus to determine if spectra collected from space concur with results from spectra collected in the field and in the artificial laboratory setting.

Chapter 8, Summary/Conclusion:

In this chapter a summary of results and a discussion are provided. Implications for remote sensing ^{137}Cs contamination are determined as well as research limitations and possibilities for further study.

Chapter 2

Remote Sensing Vegetation Status and Contamination

2.1 Introduction

This chapter outlines the context for the research presented in this thesis. It discusses and analyses key research relevant to the overall research aim and objectives marked in chapter one. It also presents central theoretical concepts and their relevance to existing research as well as this thesis. Finally, it draws out gaps in current knowledge and identifies opportunities for research which are exploited in this thesis.

2.2 Remote Sensing

To begin, it is necessary to identify the scope and meaning of remote sensing before moving onto some of its uses, in particular its application to remote sensing of contamination and specifically, contamination of vegetation. Remote sensing uses the interaction of electromagnetic waves with materials on the Earth's surface to derive useful information about the composition of those materials (Vincent 1997). Further, the composition of material on Earth's surface can be used to infer properties of such material and in turn processes which have acted upon these (Campbell 1996). Kerr and Ostrovsky (2003) suggest that environmental applications require data at a variety of spatial and temporal scales, which are often unavailable using traditional field-based methods. Clearly, this indicates the theoretical promise which remote sensing shows in monitoring the Earth's environment and processes. Scale is one of the most fundamental aspects of any research (Quattrochi and Goodchild 1997) and this is reflected in the number of studies utilising the spatial and temporal scale remote sensing techniques provide in order to monitor contamination.

2.3 Remote Sensing Contamination

Remote sensing of contamination can broadly be split into two main categories. Firstly, studies which use the visible impact of contamination in remotely sensed imagery (including thermal effects) and secondly, those which analyse changes in spectral response of the Earth's surface in response to contaminants. This is in parallel with the development of remote sensing techniques which have developed from mainly visual (e.g. panchromatic aerial images) to multispectral and more recently hyperspectral data (Rajitha *et al.* 2007). This section uses these two main categories to steer through literature relating to remote sensing of contamination.

2.3.1 Contamination Causing Visible or Thermal Impacts

A wide body of literature exists using remote sensing as a tool to aid the mapping of contamination. The majority of studies however rely on the contaminants having a visible effect on the landscape. Webster *et al.* (1999) for example use aerial photography in order to map and provide an inventory for polychlorinated biphenyl contamination in the Donna Reservoir, southern Texas. Similarly, Zellmer and Eastman (1997) use historic aerial photographs to conduct an environmental site assessment. In addition, Brown *et al.* (1996) use the synoptic view and rapidity of data collection offered by remote sensing to enhance the response in cleaning up oil spillage in the St Lawrence River. Again though, this study uses remote sensing to map visible changes, as opposed to collect useful data about the nature of contamination (e.g. effects on biota, levels of contamination).

Remote sensing has often been used to detect visible changes over time and in doing so has monitored land which has become more or less contaminated. Vagen (2006) for example assess changes in landscape and identify contamination in Madagascar, specifically contamination from the effects of fire on the landscape. Detecting contamination from fire is a key area of remote sensing research and is exemplified by Dwyer *et al.* (2000) who attempt to derive spatial and temporal distribution of vegetation fire and subsequent contamination of the environment from satellite observations. Whilst their work provides data on a scale that may not have been possible without remote sensing, fires are

ephemeral events and as such the temporal resolution of the sensor used meant an underestimation of fire numbers.

Yamano and Tamara (2004) discuss the suitability of using remote sensing to monitor contamination of coral reefs, specifically through coral bleaching. Although there is potential in using remote sensing to monitor the visual changes in coral after bleaching, the majority of operational satellites are stated by Yamano and Tamara (2004) to be too coarse in their spatial resolution to detect subtle changes in an otherwise spatially heterogeneous area of coral. As spatial resolutions of operational remote sensing systems become finer, this barrier to use may be removed.

Whilst several studies seem to use remote sensing to detect the visual impact of contamination, a number of studies use Landsat thermal data in an analytical way in order to assess variables such as salinization in coastal waters (e.g. Bayari and Kurttas, 2002). More recently, uh din *et al.* (2008) have used the thermal band from Landsat TM in combination with a custom algorithm to map hydrocarbon pollution across contaminated sites. This follows research such as that by Kwarteng (1998) which uses multi-temporal imagery to monitor oil pollution from the 1991 gulf war.

It is not just contamination of natural systems which are monitored via remote sensing techniques. City areas are studied by Chen *et al.* (2006) who compare urban heat intensity from historical Landsat TM data to more recent heat intensity data from Landsat ETM+. This is also compared to land use and land change patterns to assess effects of contamination of land on urban heat intensity in China.

So far, remote sensing of contamination has been discussed in terms of examples which rely on a visible (affecting the visible part of the electromagnetic spectrum) or thermal effect of contamination to be detected. As remote sensing has progressed from aerial photos and panchromatic images to multispectral and more recently hyperspectral data, research has attempted to characterise contamination through effects detectable in spectral changes on the Earth's surface.

2.3.2 Contamination Detectable in Spectral Changes

Whilst examples mentioned in section 2.3.1 above have utilised the synoptic coverage offered by spaceborne and airborne sensors, remote sensing contamination via spectral information has often utilised *in situ* spectral data as well as data gathered from airborne or spaceborne platforms. Oron and Gitelson (1996) for example are able to monitor the real time quality of wastewaters through spectral information provided by a portable spectroradiometer. Other research aims to use both *in situ* spectral data as well as data from airborne or spaceborne platforms. *In situ* field radiometry is usually to corroborate airborne or spaceborne data and Rajitha *et al.* (2007) illustrate this in research into water pollution caused by chemicals associated with shrimp culture in India. Further to this, Giardino *et al.* (2007) compare hyperspectral data collected from space to *in situ* spectral data and get comparable results when monitoring contamination of Lake Garda.

Both traditional broadband sensors and newer hyperspectral instruments (section 2.6) have been used to monitor changes in spectral response due to contamination. Often, remotely sensed data is used in combination with ancillary data in order to aid in the understanding or monitoring of contamination. For example, Du *et al.* (2008) assess the environmental impact of chemicals on tree health by using a combination of multispectral and environmental impact data.

Research into remote sensing of contamination falls into one of three land cover categories namely, the contamination of water (e.g. Vignolo *et al.* 2006, Hellweger *et al.* 2004), contamination of urban areas (e.g. Chen *et al.* 2006, Miller and Small 2003) or contamination of vegetation (e.g. Li *et al.* 2005, Jago *et al.* 1999).

In terms of vegetation, spectral data has been used in an attempt to detect contamination via its effects on biochemical properties of vegetation. For example Jago *et al.* (1999) used shifts in the red edge inflection point to determine contamination of sites by oil. Li *et al.* (2005) used a comparable technique to detect oil induced vegetation stress in New Mexico using imagery collected before and after an oil spill event. Similarly, Kooistra *et al.* (2003) attempted to link spectral response to contamination of vegetation on Dutch floodplains by heavy metals, though they tried to infer a direct link without measurement of foliar

biochemicals and did not demonstrate accuracy levels suitable for operational use. Davids and Tyler (2003) present results from a reconnaissance study aimed at assessing whether contamination of land by radionuclides can be detected via remote sensing techniques. This is an apt use of remote sensing given the spatial and temporal dynamics of contamination from radionuclides which have a spatial element in terms of movement and cycling of radionuclides through the environment and a temporal element in terms of constantly changing radioactivity levels based on the half-lives of different radioactive isotopes. These spatial and temporal dynamics match the potential abilities of imaging spectrometry. Remote sensing radionuclide contamination has not been fully investigated and due to current and potential impacts of radioactive contamination (Baklanov *et al.* 2002, Oumeish 2002) would be a useful application of imaging spectrometry. This thesis aims to exploit the lack of research into remote sensing radionuclide contamination and does so via its effects on vegetation. To investigate this, there is a need for an area of contiguous radionuclide contamination, which is present in the Republic of Belarus (chapter one and three), a country contaminated by fallout from the Chernobyl nuclear accident which has left a legacy of ^{137}Cs on the landscape, particularly affecting large forest stands composed of *Pinus sylvestris*. Smith *et al.* (2000) suggest ^{137}Cs will persist in the rooting zone and as such, the vegetated landscape itself for many years. In this thesis, Belarus (chapters one and three) was therefore used as natural environmental laboratory to exploit the potential of imaging spectrometry and whether it can be used to monitor ^{137}Cs impacts on *Pinus sylvestris*.

Imaging spectrometry has never been used operationally to monitor radionuclide contamination. Aerial gamma-ray surveys have been utilised to monitor nuclear contamination (e.g. Sanderson *et al.* 2004) but do not give an indication of impacts on biota. As stated in chapter one, remote sensing has some unique benefits if it could be utilised in monitoring radionuclide contamination.

Before considering this research opportunity further, it is first necessary to understand the importance and theoretical concepts behind remote sensing of vegetation, before investigating current research relating to remote sensing of vegetation stress and contamination.

2.4 The Importance of Remote Sensing Vegetation

Vegetation is a key component of the Earth's surface and monitoring vegetative land cover is often cited as a fundamentally important application of remote sensing due to the role vegetation plays in maintaining life on Earth (e.g. Roberts *et al.* 2003). Vegetation has links to various terrestrial physical and social processes. These include biogeochemical cycles (e.g. Sato *et al.* 2007), whereby the spatial variation of vegetation regulates energy, water and carbon fluxes within the climate (Kuchment *et al.* 2006). Economic systems are also affected, with vegetation often providing a valuable economic resource. The tropical rainforests for example, have been deforested primarily for economic reasons (e.g. Heal and Conrad 2006). Changes in terrestrial vegetation patterns have ramifications for climate change with remote sensing techniques being signalled as a method to provide necessary data for understanding and monitoring these changes. For example, Rosenqvist *et al.* (2000) respond to Kyoto protocol information requirements by discussing the contribution that can be made from remote sensing of vegetation. Pollution of the biosphere and atmosphere via biomass burning is a further application of remote sensing of vegetation and commands a large body of research (e.g. Liu *et al.* 2005, Smith *et al.* 2005, Wittenberg *et al.* 2007, Clemente *et al.* 2006). The importance of monitoring vegetation changes and the use of remote sensing has been introduced in this section. Detailed applications of remote sensing of vegetation stress are revisited later after some of the reasons as to why vegetation acts as a useful discriminator of environmental conditions are considered.

2.5 Vegetation as a Prisoner of its Environment

Since vegetation cannot move it is a prisoner of its environment and must, where necessary, adapt to that environment in order to survive (Grime 2001). This allows vegetation to be used indirectly as a discriminator of the quality or state of the Earth's surface. This has been utilised in a large proportion of remote sensing studies which aim to collect information about the environment through monitoring vegetation. Perhaps one of the most well known uses of remote sensing in vegetation has been the development of the normalised difference vegetation index (NDVI) (Jiang *et al.* 2006) and other associated indices. Funk and Brown (2006) for example use NDVI for assessing drought condition

and rainfall patterns in Africa. Lunetta *et al.* (2004) provide estimates of land cover change via analysis of imagery derived NDVI.

Whilst NDVI has been used to infer biomass and sometimes quality of the environment it has generally been used to gain only basic information about vegetation albeit at useful and synoptic spatial scales. Millington *et al.* (2003) perceptively capture the idea of a discontinuity between the theory of what remote sensing techniques can provide and the practical constraints in their operational use. Shaw *et al.* (1998) suggest that the development of remote sensing to monitor vegetation has been slow to develop and is partly due to different habitat and vegetation types exhibiting similar spectral properties. This has often meant *in situ* fieldwork is necessary to unravel the relationship between spectral response and vegetative properties. Blackburn (2002) demonstrates the need to use *in situ* data and collection methods in order to fully understand the relationship between spectral response and vegetation properties at the leaf and canopy level. Jayaraman and Srivastava (2002) go further and suggest that such fieldwork is also necessary to correspond the spectral response of vegetation in the field to the spectral response exhibited in remotely sensed imagery. This presents a small quandary, especially for imaging spectrometry; whilst remote sensing is commonly perceived as quick and easy to obtain as well as providing a synoptic coverage and fine temporal scale, high spectral resolution spectrometry, although offering greater power of analysis, initially requires time, effort and expense in establishing the relationship between spectral response and absorption/scattering properties. This has meant that whilst imaging spectrometry has been seized as an extremely useful tool, it has required a significant scientific issue or commercial incentive to be fully exploited. Many may argue that this is the case for all data collection techniques, however it may help to explain why Shaw *et al.* (1998) describe the development of the technique as slow. As stated above, a particular problem in monitoring vegetation with remote sensing is the similarity of spectral reflectance of various species and types of vegetation. Whilst vegetation itself has a distinctive spectral response (section 2.5) the subtle changes in spectral response from species to species or from differing environmental conditions cannot always be detected using traditional broadband sensors such as Landsat TM or ETM+. Some studies however show how subtle variations can be detected by decorrelation techniques such as Principle Components Analysis (PCA) (e.g. Tyler *et al.* 2006). The advent of hyperspectral remote sensing and imaging spectrometry has enabled some of the mismatches between theory and practice to

be eliminated and allows subtle changes in spectral response, which were previously undetectable, to be resolved (Liang and Fang 2004). The spectral signature of vegetation is crucial to the utilisation of imaging spectrometry and therefore before considering imaging spectrometry and vegetation stress research it is necessary to outline the spectral response (or signature) of vegetation itself.

2.6 Spectral Response and Remote Sensing of Vegetation

The typical spectral reflectance of a healthy green leaf, along with the main absorption points and the associated controlling biochemicals is shown in figure 2.1.

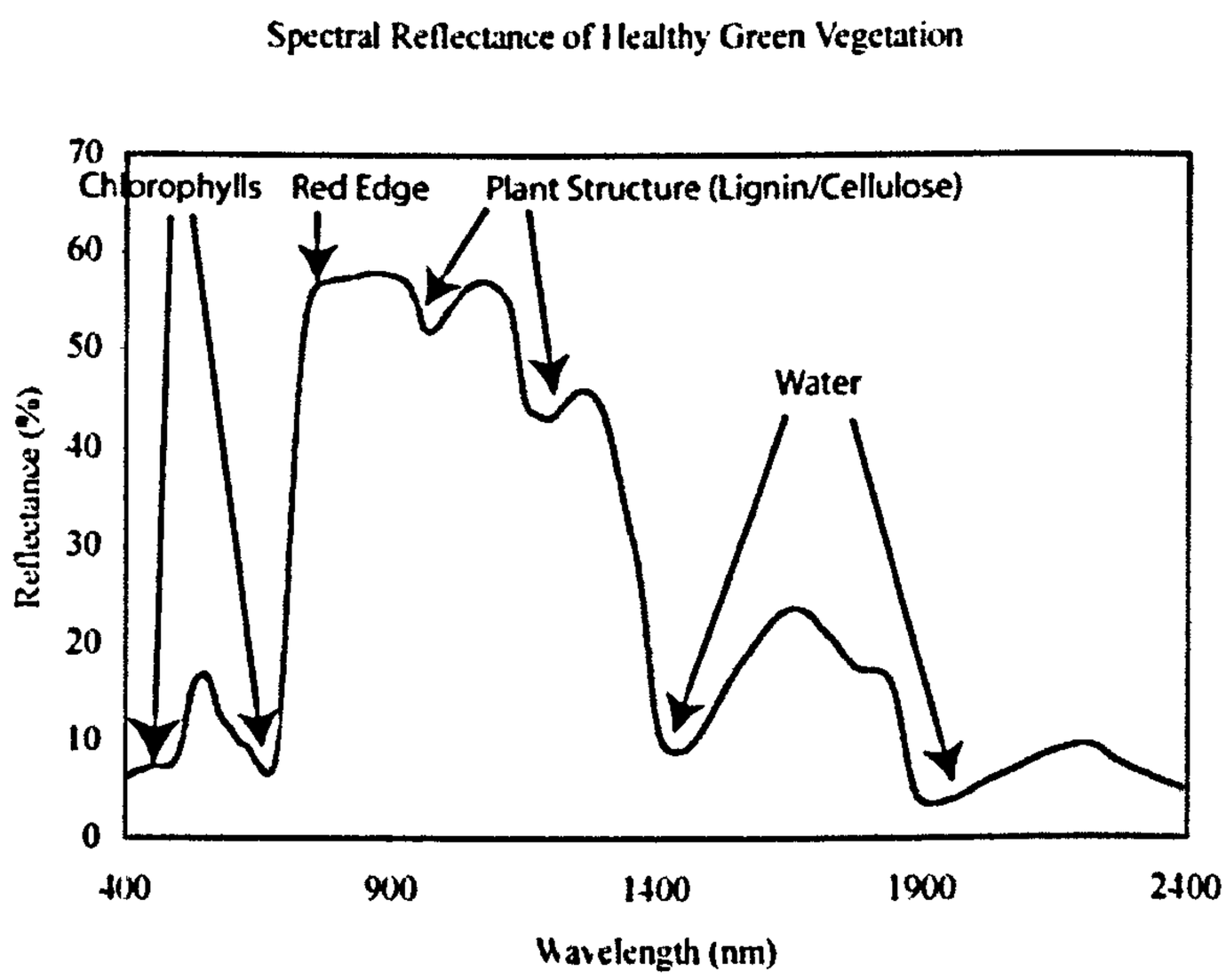

Figure 2.1: Typical spectral reflectance of healthy green vegetation along with the key absorption points and the biochemicals responsible for this absorption.

At the leaf (or needle) scale, spectral reflectance is controlled mainly by biochemical content and changes in reflectance over the 400-2400nm range have been shown to change in response to stress agents (Carter 1993). Chlorophyll for example reflects electromagnetic energy strongly in the near infrared portion of the electromagnetic spectrum and absorbs electromagnetic energy in the red (Lillesand *et al.* 2004). Figure 2.1 shows the main absorption features and the key biochemicals (chlorophyll, water, lignin, cellulose) known to be responsible for such absorption. Table 2.1 shows forty-two absorption features, as well as the associated biochemical, responsible for absorption at that wavelength. Figure 2.1 is a visual representation of the biochemicals responsible for

controlling absorption of electromagnetic energy, whilst table 2.1 is in essence a text version of figure 2.1 with each absorption feature listed, along with the biochemical known to be responsible for that absorption.

Wavelength	Electron Transition or Bond Vibration	Biochemical
430	Electron transition	**Chlorophyll *a***
460	Electron transition	**Chlorophyll *b***
640	Electron transition	**Chlorophyll *b***
660	Electron transition	**Chlorophyll *a***
910	C-H stretch, 3rd overtone	Protein
930	C-H stretch, 3rd overtone	Oil
970	O-H bend, 1st overtone	**Water,** Starch
990	O-H stretch, 2nd overtone	Starch
1020	N-H stretch	Protein
1040	C-H stretch, C-H deformation	Oil
1120	C-H stretch, 2nd overtone	Lignin
1200	O-H bend, 1st overtone	**Water,** cellulose, starch, lignin
1400	O-H bend, 1st overtone	Water
1420	C-H stretch, C-H deformation	Lignin
1450	O-H stretch, 1st overtone, C-H stretch, C-H deformation	Starch, sugar, lignin, water
1490	O-H stretch, 1st overtone	Cellulose, sugar
1510	N-H stretch, 1st overtone	**Protein, nitrogen**
1530	O-H stretch, 1st overtone	Starch
1540	O-H stretch, 1st overtone	Starch, cellulose
1580	O-H stretch, 1st overtone	Starch, sugar
1690	C-H stretch, 1st overtone	**Lignin,** starch, protein, nitrogen
1780	C-H stretch, 1st overtone / O-H stretch / H-O-H deformation	**Cellulose, sugar,** starch
1820	O-H stretch / C-O stretch, 2nd overtone	Cellulose
1900	O-H stretch, C-O stretch	Starch
1940	O-H stretch, O-H deformation	**Water,** lignin, protein, nitrogen, starch, cellulose
1960	O-H stretch / O-H bend	Sugar, starch
1980	N-H asymmetry	Protein
2000	O-H deformation, C-O deformation	Starch
2060	N=H bend, 2nd overtone / N=H bend / N-H stretch	Protein, nitrogen
2080	O-H stretch / O-H deformation	Sugar, starch
2100	O=H bend / C-O stretch / C=O stretch / C-N stretch	**Starch,** cellulose
2130	N-H stretch	Protein
2180	N-H bend, 2nd overtone / C-H stretch / C-O stretch / C=O stretch / C-N stretch	**Protein, nitrogen**
2240	C-H stretch	Protein
2250	O-H stretch, O-H deformation	Starch
2270	C-H stretch / O-H stretch CH_2 bend /CH_2 stretch	Cellulose, sugar, starch
2280	C-H stretch / CH_2 deformation	Starch, cellulose
2300	N-H stretch, C=O stretch, C-H bend, 2nd overtone	Protein, nitrogen
2310	C-H bend, 2nd overtone	Oil
2320	C-H stretch / CH_2 deformation	Starch
2340	C-H stretch / O-H deformation / C-H deformation / O-H stretch	Cellulose
2350	CH_2 bend, 2nd overtone, C-H deformation, 2nd overtone	Cellulose, protein, nitrogen

Table 2.1: Forty-two absorption features in the visible and near infrared portion of the electromagnetic spectrum that have been related to certain foliar biochemicals. Adapted from Curran (1989).

Despite the theoretical promise of remote sensing in monitoring vegetation, practically speaking, there are a variety of issues which act as a constraint on its use and these are shown in various studies. One such constraint is the difficulty of understanding the relationship between spectral reflectance in the leaf and spectral reflectance at the canopy. When scaling to the canopy as opposed to leaf level, biophysical properties also affect spectral reflectance and understanding how these biophysical properties affect spectral reflectance and subsequently the remotely sensed image has been, and remains a key tenet of research. Asner (1998) points out that vegetation reflectance is a function of leaf tissue properties and biophysical properties going on to state that biophysical issues have not been adequately addressed. Serrano *et al.* (2002) for example highlight the need to separate structural from biochemical signals when interpreting remotely sensed data. At the leaf scale and in continuous green canopies several studies have successfully estimated concentrations of foliar biochemicals such as nitrogen and lignin (e.g. Martin and Aber 1997, Hlavka *et al.* 1997, Curran *et al.* 1997). However, in order to separate biochemical from structural signals, canopy biophysical properties themselves need to be identified. Schlerf *et al.* (2005) discover that forest biophysical variables such as leaf area index (LAI) are estimated at a greater accuracy using hyperspectral versus multispectral data, which holds potential for future applications of the estimation of foliar biochemistry, and go on to state this is feasible at a high accuracy with hyperspectral and not multispectral data. Lee *et al.* (2004) and Thenkabail *et al.* (2004[b]) corroborate the findings of Schlerf *et al.* (2005) by again indicating the increased ability of hyperspectral remote sensing to monitor canopy biophysical properties. Coniferous forests exhibit the greatest challenges in terms of their biophysical properties due to their dense small scale clumping (Smolander and Stenberg 2003) inherent understory and complex structure causing multiple scattering of electromagnetic energy (Rautiainen 2005). Having illustrated challenges, Zarco-Tejada *et al.* (2004) highlight the use of radiative transfer models to show the possibilities of linking leaf and canopy concentrations of chlorophyll.

Modelling spectral reflectance has often been implemented to understand the effects biochemical constituents of vegetation have on spectral reflectance, for example Dawson *et al.* (1998) developed the Leaf Incorporating Biochemistry Exhibiting Reflectance and Transmittance Yield model (LIBERTY) to simulate the optical properties of coniferous needles when various biochemical parameters are changed.

When remote sensing vegetation, there are a variety of factors influencing the image such as atmospheric effects, geometric distortions and the resolution of the sensors (both spatial and spectral). Research has attempted to overcome atmospheric impact through correcting the image via empirical or modelling techniques (e.g. Adler-Golden *et al.* 1999, Felde *et al.* 2003). Removing or improving geometric distortions have also been strong research foci, though Chavez (1989) suggests that geometric correction has moved at a rate faster than the research and improvements into atmospheric correction. In essence, the gap between remote sensing theory and what can be achieved in practice is being reduced through research.

Sensor resolution is sometimes, though not always considered a constraint when monitoring vegetation. The coarse spectral resolution of traditional broadband sensors (e.g. Landsat TM, SPOT) has meant the reflectance spectra of vegetation has not always been fully understood from a spaceborne platform. The advent of hyperspectral remote sensing in the mid-1980s (Goetz *et al.* 1985) has enabled detailed spectra to be collected from airborne and spaceborne platforms and resulted in research which is able to apply the fine spectral resolution of imaging spectrometers to gather information on biochemical and biophysical properties of Earth surface features in a way which is analogous to laboratory spectra (Ben dor *et al.* 2004).

Influences of the atmosphere, sensor geometry and biophysical factors all reduce the ability of remote sensing to monitor vegetation. Spatial and spectral resolution are also sometimes limiting factors, dependent on the application. For example, in monitoring global vegetation, moderate spatial resolutions are preferred (Morisette *et al.* 2006). Broadband sensors do not sample the electromagnetic spectrum at a fine enough resolution to fully understand the complex spectral reflectance of vegetation shown in Figure 2.1.

The mismatch between theory and practice mentioned so far means that some changes in spectral response due to environmental processes remain undetected. Hyperspectral remote sensing is a relatively new technique which samples in many rather than few wavebands. Imaging spectrometry utilises high spectral resolution sensors on board airborne or spaceborne platforms to build a datacube for each pixel with finely detailed spectral information.

2.7 Imaging Spectrometry

Recent advances in remote sensing mean researchers can understand physical and chemical changes in the environment rather than just map them. Curran (1994) describes the process of remote sensing in the following terms:

$$R = f(x, t, \lambda, \theta).$$

Where, R is the remotely sensed radiation, which is a function (f) of location (x), time (t), wavelength (λ) and viewing geometry (θ). Remote sensing can provide information when a change in x, t, λ or θ gives a detectable change in R. Curran (1994) goes on to argue that traditional remote sensing systems sample the spectrum in wavebands which are too broad to detect changes and suggests imaging spectrometry has the potential to sample the spectrum in many narrow bands, in turn giving an ability to estimate physical and chemical variables of the environment. It is the measurement of such physical and chemical variables that provides the potential to monitor environmental contamination.

Spectroscopy is arguably one of the most important methods for analytical chemists (Gunzler and Gremlich 2002) and the use of laboratory spectrometers to illuminate and subsequently measure the radiation spectrum of a substance is common. Milton (2003) argues that spectrometry differs from traditional remote sensing in its focus on absorption spectra as opposed to the energy reflected and emitted from an object, plotted against its wavelength. Before continuing, it is necessary to eliminate the confusion often caused between the interchangeable nature of the terms spectroscopy, and spectrometry. The word spectroscopy, like the technique, is well known in analytical chemistry, however, the word spectrometry is preferred in remote sensing as the aim is to measure the absorption spectrum, not simply observe it (Milton 2003). As such, for the remainder of this thesis, the word spectrometry will be used when referring to remotely sensed hyperspectral images. When referring to the technique of gamma ray spectrometry to determine ^{137}Cs specific activities, the term gamma spectrometry will be used.

The theoretical potential in narrow band, high spectral resolution spectrometry has resulted in a variety of different spectrometers. These spectrometers range in their platforms from

portable field spectrometers, to airborne and, more recently spaceborne sensors. Table 2.2 describes the main properties of a selection of common spectrometers currently in use.

Name	Full Name	Number of Bands	Spatial Resolution (in m)	Spectral Range (in nm)	Airborne or spaceborne platform?
AHS	Airborne Hyperspectral Scanner	64	Dependent on flying height	433 - 12700	Airborne
AVIRIS	Airborne Visible/Infrared Imaging Spectrometer	224	Dependent on flying height	400 - 2500	Airborne
CASI	Compact Airborne Spectrographic Imager	288	Dependent on flying height	400 - 1050	Airborne
CHRIS	Compact High Resolution Imaging Spectrometer	19 (programmable)	20m	415 - 1050	Spaceborne
HYPERION	HYPERION	220	30m	400-2400	Spaceborne
MERIS	Medium Resolution Imaging Spectrometer	15 (programmable)	300m	390 - 1040	Spaceborne
MODIS	Moderate Resolution Imaging Spectrometer	36	250m (bands 1-2) 500m (bands 3-7) 1000m (bands 8-36)	400 - 1440	Spaceborne

Table 2.2: Examples of selected airborne and spaceborne spectrometers along with abridged technical details.

It logically follows from Curran's (1994) description of remote sensing that in order to monitor environmental changes, the changes need to have a measurable effect upon the biochemical or biophysical characteristics of the vegetation growing in that environment. To monitor biochemical properties of vegetation, imaging spectrometry operates in the optical range of the electromagnetic spectrum and attempts to measure changes in these key foliar biochemicals through associated changes in spectral wavebands. Many studies utilise the selective depletion of foliar biochemicals to monitor vegetative quality and status of the environment (e.g. Mutanga *et al.* 2004).

Imaging spectrometry requires an ability to use spectral wavebands to predict biochemicals which is commonly performed using a variety of statistical methods. The advent of these methods traditionally lie in analytical laboratory spectrometry (Barton 2002). Investigation of leaf biochemistry using statistics has frequently used the technique of stepwise multiple regression to select wavebands with the greatest ability to predict biochemical content (e.g. Jacquemoud *et al.* 1995). Despite the disapproval of the technique by much statistical literature (e.g. Foster and Stine 2006) several studies have shown successful use of the technique (and various modifications) in selecting wavebands most suited to predicting biochemicals (Dawson *et al.* 1995, LaCapra *et al.* 1996). Many of these studies fail to accurately apply their regression models to testing data sets and this has been discussed by Grossman *et al.* (1996). Recently, partial least squares (PLS) has been suggested as a possibility for greater accuracy in predicting biochemicals (Ourcival *et al.* 1999).

Hyperspectral remote sensing has allowed for applications of remote sensing which were not possible with broadband remote sensing. Schmidt and Skidmore (2003) discriminate between 27 vegetation types in a challenging wetland environment showing that hyperspectral data is key to that discrimination. Further studies utilising fine spectral resolution to distinguish similar species are evident (e.g. Galvao *et al.* 2004). Early focus of hyperspectral research was on prediction of foliar biochemistry from spectra (e.g. Yoder and Pettigrew-Crosby 1995). Current research continues to try to improve accuracy of biochemistry prediction, for example by separating plant water content from atmospheric water (Schaepman 2007) or by applying novel statistical techniques to improve accuracy (e.g. Kokaly and Clark 1999, Curran *et al.* 2001). More recent research has focused on the potential applications of this predicted biochemical data. Mutanga *et al.* (2005) use hyperspectral data in conjunction with statistical techniques to predict pasture quality indirectly through the foliar biochemistry of grass. The status of vegetation *per se* is sometimes investigated (e.g. Dobrowski *et al.* 2005, Zarco-Tejada *et al.* 2003) but more often than not, remote sensing of foliar biochemistry is used as an indirect method to monitor status of the terrestrial environment. Rosso *et al.* (2005) investigate the links between heavy metal and petroleum contamination of the spectral reflectance properties of *Salicornica virginica* and suggest that there were sufficient changes in spectral response caused by changes in foliar biochemistry which were utilised in order to detect this contamination remotely (using imaging spectrometry). Smith *et al.* (2005) assessed

abilities of remote sensing in detecting between plant stress caused by gas leakage and other forms of stress and attempted to use differences in chlorophyll concentrations as an indicator of stress. What these examples show is that there are a wide variety of studies investigating the remote sensing of vegetation stress. This is investigated further in section 2.8.

2.8 Remote Sensing of Vegetation Stress

So far, this chapter has explored literature pertaining to remote sensing *per se*, the remote sensing of contamination and remote sensing techniques to monitor vegetation. This section brings these themes together by exploring remote sensing to monitor vegetation stress caused by natural and anthropogenic influences. It is split into three subsections which are representative of themes in the literature and are, (i) laboratory investigations into how vegetation responds to plant stress (in a remote sensing context), (ii) agronomical and agricultural research into how remote sensing may be used for the monitoring of stress in crops and (iii), how remote sensing may be utilised to monitor environmental stress within coniferous and deciduous forests.

2.8.1 Laboratory Experimentation to Understand Vegetation Responses to Stress

To understand vegetation's response to stress and resulting signature in remotely sensed imagery, there is a need to understand processes at the leaf or needle scale (Disney *et al.* 2006). This has resulted in a number of studies which utilise laboratory experimentation to assess the effects stressors may have on vegetation at the leaf or needle scale and the resulting changes in spectral signature which may be detected using airborne or spaceborne remote sensing platforms.

Two recent studies investigated heavy metal impacts on vegetation and resulting spectral changes. Firstly, Dungan *et al.* (2007) grew mustard spinach plants under controlled laboratory conditions to assess if any detectable changes in spectra were present between mercury contaminated plants and control plants finding that red edge position changes relative to the control plants. Sridhar *et al.* (2007) assessed the impact of Arsenic and

Chromium on Chinese brake fern to assess feasibility of using spectral reflectance for monitoring Arsenic and Chromium accumulation. This was again under controlled laboratory conditions and results showed the possibility of using a unique ratio index to monitor changes in plants due to Chromium with the results inferring possibilities of using the infrared reflectance of plant canopies to be used to monitor plants grown in heavy metals. Interestingly, in a further study, Su *et al.* (2007) also investigate the effect the natural isotopes of Caesium and Strontium have on Indian mustard. The study suggests Caesium has an effect on pigment concentrations and internal structure of the plants and resulting spectral changes. This signifies potential in using spectral reflectance to monitor ^{137}Cs in vegetation.

Whilst laboratory experimentation to understand spectral reflectance in response to contaminants has been evident in recent literature, a wide body of research investigates crop responses to environmental stress. This is mainly due to industrial and economic needs to understand plant physiological status in order to grow crops in the most efficient way possible (Dorigo *et al.* 2007).

2.8.2 Crop Responses to Environmental Stress

Due to the need for continually efficient and improved methods of growing crops, remote sensing techniques, with a broad spatial and fine temporal resolution have been welcomed by the agricultural industry to monitor health and status of crops (Dorigo *et al.* 2007). Much research has sought to understand the effects certain chemical additives (such as fertilisers) have on crop quality. For example, Zhao *et al.* (2005) attempt to maximise the output of wheat crops by identifying crops which require nitrogen application. This is performed through an analysis of crops using Landsat TM data. Similar research has also been concerned with the quality of crops and how to assess best practice in managing and harvesting crops. Du *et al.* (2008) monitor citrus tree health in the Rio Grande valley in an attempt to enhance productivity of citrus crops through precision farming. There are also attempts to monitor changes of crop health throughout time and this is exemplified by Tottrup and Rasmussen (2004) who monitor crop productivity changes in Senegal and whether these changes are due to differences in rainfall patterns or anthropogenic impacts.

In terms of practical issues, remote sensing of crops is arguably easier than remote sensing of forest ecosystems. This is due to the spatial and spectral heterogeneity present in most crop types (Dorigo *et al.* 2007). Despite this, the importance of forest ecosystems has meant remote sensing research into monitoring forest physiological status has been wide ranging (Penuelas and Filella 1998).

2.8.3 Remote Sensing Forest Scale Response to Environmental Stress

Literature associated with remotely sensing forest responses to stress can broadly be classified into one of two types. This is dependent on whether the research is concerned with understanding vegetation response to stress at a needle/leaf scale or at the canopy scale. The canopy scale often brings associated problems such as the effects of biophysical properties and technical issues such as geometric and atmospheric correction (Treitz and Rogan 2004).

The presence or susceptibility of a species to pathogens is often a domain of remote sensing forest stress. Coops *et al.* (2006) for example use Landsat TM data to assess stands which have been attacked by mountain pine beetle and those stands which are at greater risk of attack. Other studies use the synoptic coverage provided by remote sensing to detect changes in forest land cover caused by contamination or stress. This is shown in a study by Latifovic *et al.* (2005) who use Landsat TM scenes to monitor vegetation loss after contamination following mining development in Canada.

Soil water deficit and its resulting impacts on ecosystem productivity and forest physiological status is a key area of research (e.g. Grant *et al.* 2006). *In situ* field studies (e.g. Eitel *et al.* 2006) attempt to characterise the effects of water stress in a species specific environment and then apply it to imagery like that collected by Asner *et al.* (2005). Asner *et al.* (2005) use hyperspectral Hyperion data to explore the development and functioning of rainforests in Hawaii by determining tree age and rainfall status from imagery.

Lu *et al.* (2007) looks at stress in vegetation after the exploitation of coal and subsequent effects in terms of reducing nutrients available for vegetative growth. Utilising Landsat

TM images in the red and infrared regions of the electromagnetic spectrum, synoptic coverage is provided and found to be compatible with observations on the ground. The advent of hyperspectral imagery (section 2.6) has resulted in detection of biochemical properties of forests to detect stress. For example, salinity stress is often monitored using spectral changes (Penuelas and Filella 1998) and this exemplified in research by Metternicht and Zinck (2003) who use hyperspectral imagery to infer soil salinity through spectral information collected about vegetation growing on that soil. le Maire *et al.* (2004) monitor forest chlorophyll status as a surrogate for natural or anthropogenic stressors. This is taken further by studies such as that by O'Neill *et al.* (2002) who examine spatial variability of biochemicals in a spruce canopy. Added challenges arise according to whether the forest is composed of coniferous, deciduous or a mixture of tree types. Coniferous trees bring added challenges in that they are often more complex in terms of structure, clumping and have multiple canopy layers.

So far this chapter has considered the remit of the term remote sensing, has gone on to investigate remote sensing of contamination and then identified an opportunity to monitor radionuclide contamination with remote sensing. The chapter has then focussed on the importance of remotely sensing vegetation, the methods and concepts used to remotely sense vegetation and lastly, has looked specifically at examples of remote sensing vegetation stress. As already stated in section 2.3.2 remote sensing of radionuclide contamination, specifically ^{137}Cs contamination of *Pinus sylvestris* represents a research opportunity. Before considering this opportunity in more detail, the radiological effects of ^{137}Cs on vegetation are considered.

2.9 Radioecological Effects of ^{137}Cs

Grime (2001) suggests functional differences in plants lead to differences in their uptake and cycling of ^{137}Cs, in turn showing factors such as growth rate and life span of the plant to be significant in ^{137}Cs uptake rates. This suggests any research investigating the potential of imaging spectrometry to monitor ^{137}Cs should minimise confounding variables by focusing initially on one species. Current research is still attempting to fully understand all the radionuclide pathways and this is reflected by Thiry *et al.* (2002) who investigate the distribution of ^{137}Cs in *Pinus sylvestris*. They discover that in both young (17 years)

and old (58 years) trees, the largest concentration of ^{137}Cs is within the inner bark, the lowest within stemwood and medium levels in the outer bark. Though this study provides useful and relevant data about the stores of radionuclides in relation to tree age, recently Soukhova *et al.* (2003) have sought to infer more about the transfer processes within tree rings in contaminated Russian territory. The study not only investigates *Pinus sylvestris*, but also silver birch (*Betula pendula*) and does so at four forest sites across a variety of age ranges. There is an increased interest in effects of ionising radiation on biota and this is illustrated by initiatives such as the Framework for Assessment of Environmental Impact (FASSET) and the Environmental Risk from Ionising Contaminants: Assessment and Management (ERICA) (Copplestone *et al.* 2004, Ciffroy *et al.* 2007). Soukhova *et al.* (2003) state the economic impact of contamination on forest ecosystems as the motivation for their study. Such a motivation is reflected by Sandalls *et al.* (1993) who state that the current behaviour and ultimate fate of radionuclides in the environment is a major issue of concern for those countries affected. As a potential solution, Vandenhove *et al.* (2002) suggest that changing land use based on radiologically acceptable risks can assure an economic return and a feasible remediation option. However, in order to decide which land poses a significant risk, and which does not, a regular, accurate and efficient method of monitoring is necessary.

Despite other research seeking to assess ^{137}Cs uptake factors (e.g. Zhu and Smolders 2000) there is very little research into the effects of ^{137}Cs on key foliar biochemistry or spectral reflectance. Davids and Tyler (2003) show that plant pigments are likely to be affected by ^{137}Cs through vegetation indices, although they did not collect any biochemical data. Willey and Tang (2006) indicate that nitrogen is affected by and alters ^{137}Cs within plants. Additionally, work by Mykhaylo *et al.* (2005) shows ^{137}Cs to bind to lignin and cellulose, suggesting these biochemicals may exhibit changes in response to varying ^{137}Cs levels. Whilst the effects of ^{137}Cs on plant foliar biochemicals are not fully established, the literature discussed suggests ^{137}Cs may have an effect on each one of the principal foliar chemicals of a leaf and as such may be detectable in the spectral response of vegetation. Having said this, research into ^{137}Cs in the environment pertains mostly to storage, transport and uptake (e.g. Poiarkov *et al.* 1995). There is substantial interest in understanding plant mechanisms of ^{137}Cs uptake (White and Broadley 2000) with the view to genetically altering gene expression of plants to either increase ^{137}Cs uptake rates (for remediation) or reduce them (to prevent dangerous levels in food crops) (Payne *et al.*

2004). The lack of research into ^{137}Cs effects on biochemistry and ultimately spectra presents a research opportunity and is necessary to fully assess whether imaging spectrometry can be used to monitor ^{137}Cs.

2.10 Summary

The following has emerged from this review of the literature:

- Remote sensing of vegetation is an important application of the technique. A mismatch between theoretical promise and practical application has meant research has often been able to partly characterise contamination and not fully characterise the spectral response of vegetation.

- Imaging spectrometry presents a new opportunity in terms of its spectral resolution and has the ability to acquire detailed spectra which in some cases can be used in a way analogous to laboratory spectroscopy and thus has potential to monitor subtle changes of vegetation and the environment.

- There are some successful studies of imaging spectrometry at monitoring contamination, and potential shown in monitoring radionuclide contamination (albeit in an area of little economic use). The spatial and temporal dynamics of radionuclide contamination fit well with the spatial and temporal abilities of imaging spectrometry and so might be well suited to monitor radionuclide contamination indirectly through the selective depletion of key foliar biochemicals.

- Belarus has been identified as a natural environmental laboratory having large contiguous areas of *Pinus sylvestris* forest which were contaminated by the fallout (mainly ^{137}Cs) from the Chernobyl nuclear accident (probably through artificially induced rain).

- Radioecological literature provides insight into the behaviour of radionuclides in the environment, the mechanisms of uptake by plants and ways to alter gene expression in order to manipulate that uptake. Some promise has been shown that

foliar biochemicals are selectively depleted or altered as a result of ^{137}Cs (e.g. Davids and Tyler 2003, Willey and Tang 2006) but more understanding is needed to ascertain how ^{137}Cs affects foliar biochemistry and ultimately spectral response.

The research undertaken in this thesis therefore attempts to understand the effects of ^{137}Cs on foliar biochemicals and ultimately spectral response in order to address gaps in both radioecological and imaging spectrometry research and does so through the objectives and overall aim set out in chapter one. From this chapter has come a research opportunity which is exploited in the remainder of the research. This opportunity comes from the gaps identified in the literature which are, (i) that remote sensing has not been utilised to monitor radionuclide contamination, (ii) the effects of ^{137}Cs on the spectral reflectance of vegetation have not been fully considered by the research and may have detectable impacts on plant biochemicals and (iv) there is a need to regularly and accurately monitor radionuclide contamination in Belarus following ^{137}Cs deposition from the 1986 Chernobyl accident. These gaps form the basis of the research opportunity investigated by this thesis; namely, can imaging spectrometry be used to monitor ^{137}Cs contamination of *Pinus sylvestris* through an indirect effect on plant biochemical content?

Chapter 3

Study Site, Data and Instrumentation

3.1 Introduction

To remotely sense radionuclide contaminated vegetation requires a causal relationship to exist between spectral response of vegetation and levels of radionuclide contamination. Fundamentally, if there is no link between spectral response and contamination then the use of remote sensing techniques are prohibited. The starting point of the research is therefore to determine if such a relationship does exist. For the research objectives to be met, a number of processes and links need to be investigated and understood. This chapter describes the data, and instrumentation used to investigate these processes and links. It begins by outlining aspects of the natural environmental laboratory, artificial laboratory and hyperspectral imagery collected over the study site (Belarus). It then moves into methods of data collection, data needed to drive the research and the subsequent instrumentation used to collect such data. It is important to note that whilst conducting fieldwork in Belarus, the trip was curtailed due to political intervention (appendix A3). Whilst all samples had been collected and measured for spectral response and chlorophyll concentration, water content could not be measured for all samples whilst in Belarus (as originally planned) and approximately half of the samples had to be frozen and returned to the UK for water analysis. Plans for other analyses such as gamma spectrometry had always been to return samples to the UK to be measured and so were not affected by the curtailment.

3.2 Study Site and Environment

3.2.1 Belarus as a Natural Environmental Laboratory

Belarus is a landlocked republic located in eastern Europe and is bordered by Ukraine in the south, Poland, Lithuania and Latvia in the west and north-west and Russia in the north and east (Figure 3.1). Formerly a republic of the Soviet Union, Belarus declared independence in 1991 becoming the Republic of Belarus when the Soviet Union was dissolved. Administratively, Belarus is split into six regions with the capital city being Minsk. Population is approximately 10 million people and Belarus covers approximately 207 sq km with 36% being covered by forest, 45% farmland, 2% water and 18% classified as other land cover. In April 1986, Belarus was contaminated by radionuclides as a result of and accident at the Chernobyl nuclear power plant (CNPP).

Figure 3.1: Map of Belarus, its regions and bordering countries.

As mentioned in chapter one, Belarus was used as a natural environmental laboratory as it has large areas of its landscape contaminated with ^{137}Cs. Two field campaigns took place in Belarus, the results of which are described in chapters four and five. Before considering these results it is necessary to underline the methods and strategies used to collect data in the natural environmental laboratory.

3.2.2 The Artificial Laboratory Environment

As well as fieldwork in the natural environmental laboratory, an experiment took place in Kingston University's radiochemistry laboratory. Specific details regarding the laboratory set up and strategies are discussed in chapter six, but the methods used to collect spectral data are the same as those for the natural environmental laboratory.

3.2.3 Imaging Spectrometry

Hyperspectral imagery was a further component of this research. Hyperspectral imagery with the appropriate spectral and spatial resolution to provide spectra compatible with field and laboratory data was required. This was collected from the Hyperion hyperspectral instrument onboard NASA's EO-1 platform. The methods used to collect and analyse this hyperspectral imagery are specific to the particular research undertaken in chapter seven, and as such are discussed in that chapter.

3.3 Data Collection Strategies

The direct measurement of radionuclides is limited largely to laboratory equipment. This means, in the natural environment an indirect discriminator of contamination levels is needed. The intimacy of plants with their environment, especially their inability to move means they are highly sensitive and responsive to changes in that environment (Herbert 2002). Similarly, remote sensing is established in vegetation studies and is therefore well suited to monitoring the state of vegetation (chapter two). Data collection focused on collecting spectral measurements of *Pinus sylvestris* along with key foliar biochemical measurements and, central to this research, ^{137}Cs levels. These key pieces of data allowed the links and processes between ^{137}Cs contamination, foliar biochemicals and spectral response to be investigated through statistical analysis.

To assess the potential of remote sensing ^{137}Cs contamination, a comparison of contaminated and non-contaminated vegetation was necessary. Ambient background radiation levels, combined with radiological maps were used to pick sites in Belarus with differing contamination levels. Ambient dose rates were measured using a portable

radioactivity meter, measuring background radioactivity in μSv/h. Levels of background radiation at fieldsites ranged from 0.05 to 2.91 μSv/h. Two sets of fieldwork were carried out and the strategies used to pick the sites are described in each of the relevant chapters (chapters four and five) and their location shown in Figure 3.2. After harvesting branches (section 3.3.1) needles were removed and retained in a dark coolbox in preparation for biochemical, gamma spectrometry and spectral analysis. These analyses methods are described in the subsequent sections of this chapter.

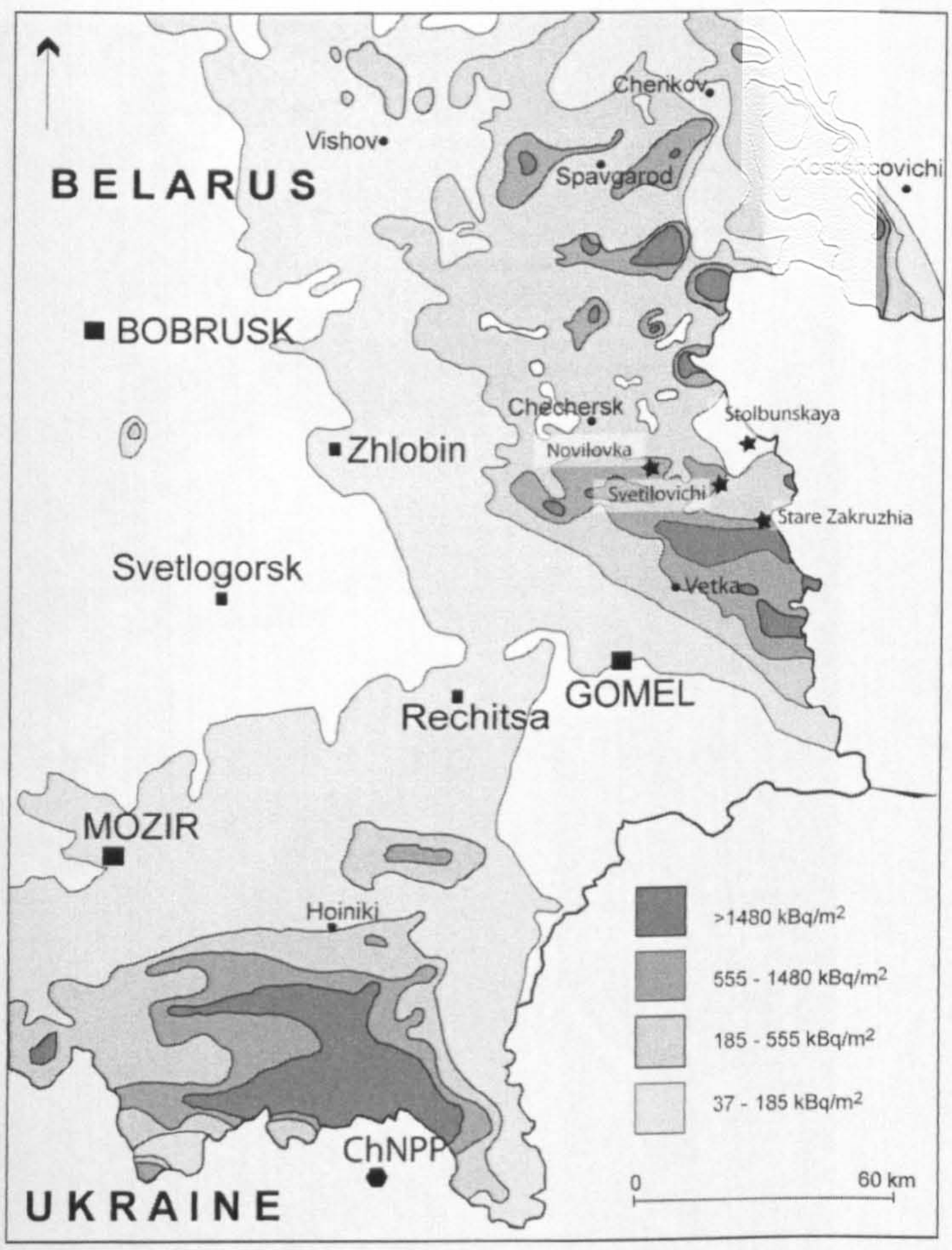

Figure 3.2: Map of the Gomel region of Belarus and general contamination levels where the data collection took place. The fieldsites from the two sets of fieldwork are marked with a star. The fieldwork base and laboratory was at the Svetilovichi Sanatorium during both sets of fieldwork.

3.3.1 Spectral Measurement

At each field site, *Pinus sylvestris* trees were chosen to represent the site and what might be seen in a remotely sensed pixel (30m x 30m). Branches were selected from the edge of forests to account for edge effects as well as across the rest of each site. In addition

branches were selected from different positions on the trees so that needles were representative of the ^{137}Cs contaminated forests. Branches were collected from the tree using a variety of different methods. As many of the branches were beyond unaided human reach, a method was devised which used wire saws attached to rope. The rope could then be thrown over a branch and with two operators a sawing movement was created which cut the branch from the tree. This rope and wire saw method is shown in figure 3.3. Other branches were cut using telescopic secateurs (if within reach) or by using a ladder in combination with the secateurs or sawing method.

Figure 3.3: The rope and wire saw method used to collect branches from tree samples. Rope was thrown over and the saw pulled into place and with two operators a sawing action was created to cut the branch from the tree.

After representative branches were removed from selected trees, the new growth needles were picked from the branches and preserved for spectral measurement. Preservation included wrapping the base of the needles in black insulation tape in order to prevent structural degradation of the needles. The needles were then bagged, labelled and placed in a dark coolbox to minimise chlorophyll degradation. For every sample, enough needle

KINGSTON UNIVERSITY LIBRARY

material was collected and preserved to allow for spectral, biochemical and gamma spectrometry measurements. This was approximately 250g of needles for each sampled tree.

To accurately and efficiently measure the spectral response of vegetation collected in Belarus, a portable spectroradiometer was used. This was in the form of an Analytical Spectral Devices (ASD) Fieldspec Pro spectrometer, loaned from the Natural Environment Research Council (NERC) Field Spectroscopy Facility (FSF) (Formerly Equipment Pool for Field Spectroscopy). This is ASD's flagship model (ASD 2004) and has a spectral range of 350-2500nm. Table 3.1 concisely conveys the technical attributes of the ASD field spectroradiometer.

ASD FieldSpec Pro System	
Spectral Range:	350 – 2500nm
Spectral Bandwidth:	1.4nm at 350-1050nm
	2nm at 1000-2500nm
	10nm at 1400 and 2100nm
	3nm at 700nm
Sampling Time:	100 milliseconds

Table 3.1: Selected technical characteristics of the ASD FieldSpec Pro (ASD 2004).

Harvested needles were measured on the day they were collected at a temporary laboratory created at the Svetolovichi Sanatorium, Belarus (Figure 3.2). In the laboratory experiment described in chapter six, needles were measured for spectral reflectance at Kingston University. Needles measured for spectral reflectance in Belarus and Kingston University were subject to the same methodology. Approximately 5g of needle material was placed into a custom made black container to maintain a constant geometry and illumination when measuring spectral reflectance. For each sample, four spectral measurements were taken, with the pot being turned 90° between each measurement. The four measurements were then averaged to give a single spectral reflectance measurement for each sample. The pot was always filled to the same level (top of pot) in order to standardise the procedure and amount of needle material in the pots. The needles were measured using the contact reflectance probe, which provides an artificial light source in the form of a 100w halogen reflectorised lamp (NERC FSF 2004). Use of an artificial light source minimised error associated with changing irradiance conditions, and provided flexibility in measuring the

needles. The contact probe was placed directly over the custom black pots and created a seal between needles and light source. The use of airborne or spaceborne remote sensing would inevitably be affected by atmospheric effects, but the use of the contact probe during field spectrometry minimised factors to take into consideration and helped focus primarily on whether a relationship exists between radionuclide levels, foliar biochemical concentrations and ultimately, spectral response. Raw ASD spectra were processed to absolute reflectance using a white spectralon calibration tile and bespoke ASD calibration software, resulting in spectra showing absolute reflectance from 400-2400nm at 1nm intervals. After collecting spectral measurements, various pre-processing transformations of the spectra were performed prior to any analysis. These are described below in section 3.3.2.

3.3.2 Spectral Processing

Absolute reflectance spectra were part of the analysis routine, but spectra were also processed into various other manifestations (first derivative spectra, continuum removed spectra) in order to compensate for noise in the spectra and to attempt to draw out subtle changes and differences between spectra. These processing routines and manifestations are described in this section.

3.3.3 First Derivative Spectra

Derivative spectroscopy has been used for a number of years in analytical chemistry and is powerful in enhancing small fluctuations in the reflectance spectrum as well as aiding in the separation of closely related absorption features and minimising noise or background effects (Louchard *et al.* 2002). First derivative spectra were calculated according to equation 3.0.

$$FDR_{\lambda(i)} = (R_{\lambda(j+1)} - R_{\lambda(j)})/\Delta_{\lambda} \qquad \text{[equation 3.0]}$$

Where FDR is the first derivative reflectance, i is the midpoint between spectral wavebands j and j+1. $R_{\lambda(j)}$ is reflectance at waveband j, $R_{\lambda\,(j+1)}$ is reflectance at waveband j+1, and Δ_{λ} is the difference in wavebands between j and j+1 (Dawson *et al.* 1998,

Mutanga *et al.* 2004). In addition to derivative spectroscopy, absolute reflectance spectra were also manipulated through the technique of continuum removal.

3.3.4 Continuum Removal

Continuum removal isolates absorption features and standardises reflectance across them (Underwood *et al.* 2006). Continuum removal is in essence a feature selection technique (Kokaly and Clark 1999, Curran *et al.* 2001, Mutanga *et al.* 2004) which isolates absorption features from the rest of the spectrum using a continuum line. Once absorption features have been isolated using this continuum line then the continuum-removed reflectance is normalised using a variety of methods in order to ease intercomparison of reflectance and provide different manifestations of the spectra. Kokaly and Clark (1999) and Curran *et al.* (2001) have shown continuum removed spectra to provide higher r^2 values when using regression models to predict foliar biochemicals and given the need to accurately assess key foliar biochemicals in this research, continuum removal was employed on the spectra. Figure 3.4 shows a conceptual diagram of continuum removal.

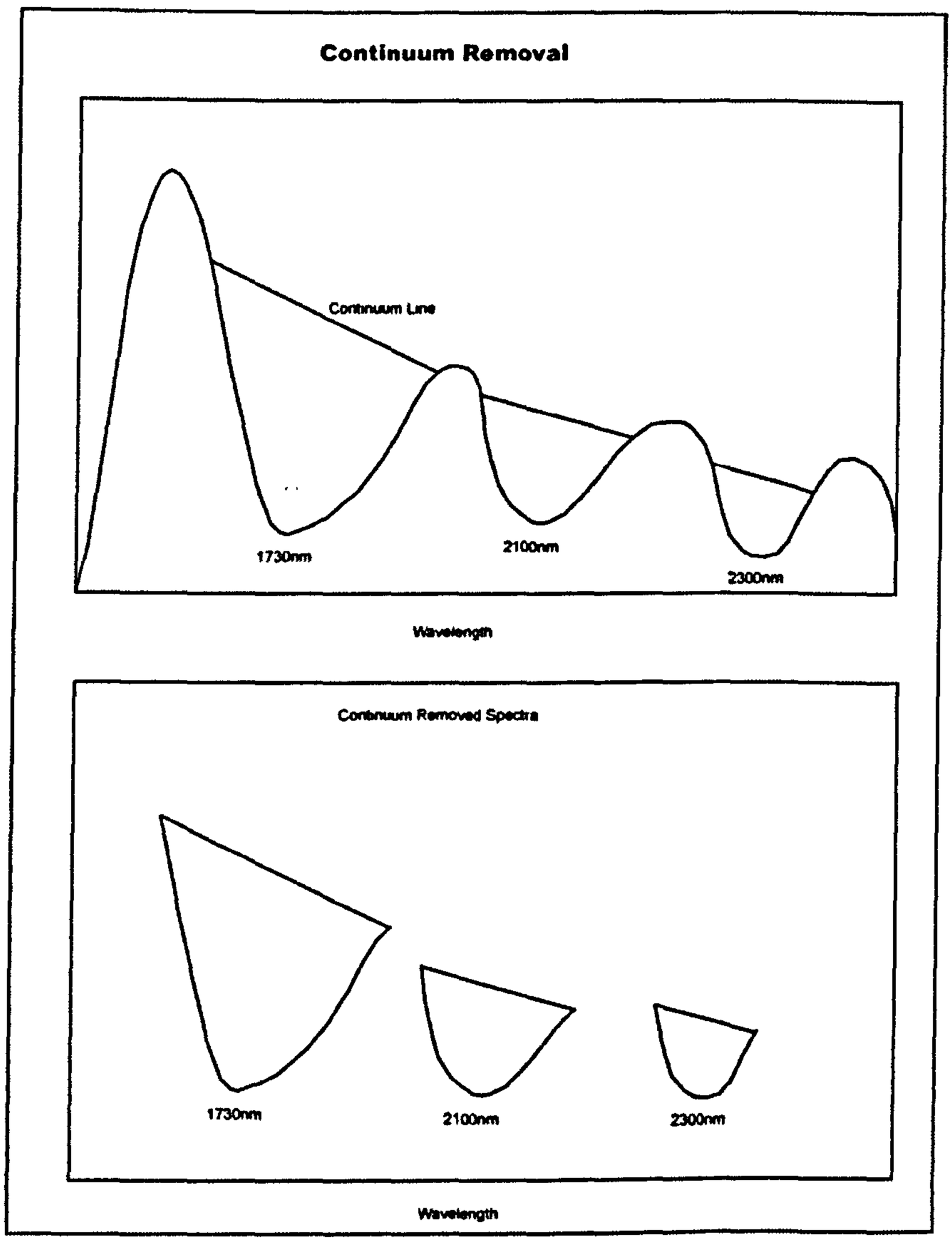

Figure 3.4: Conceptual diagram of continuum removal. Each absorption feature is isolated from the rest of the spectra using a continuum line. The reflectance is then standardised using a variety of methods for intercomparison.

Six absorption features were selected for continuum removal based on the spectra collected and literature pertaining to biochemical absorption (e.g. Curran 1989). These are shown, together with the continuum line, in figure 3.5. Figure 3.5 shows why six absorption features were chosen; these six features adequately represent the absorption features evident in the spectral response of *Pinus sylvestris*.

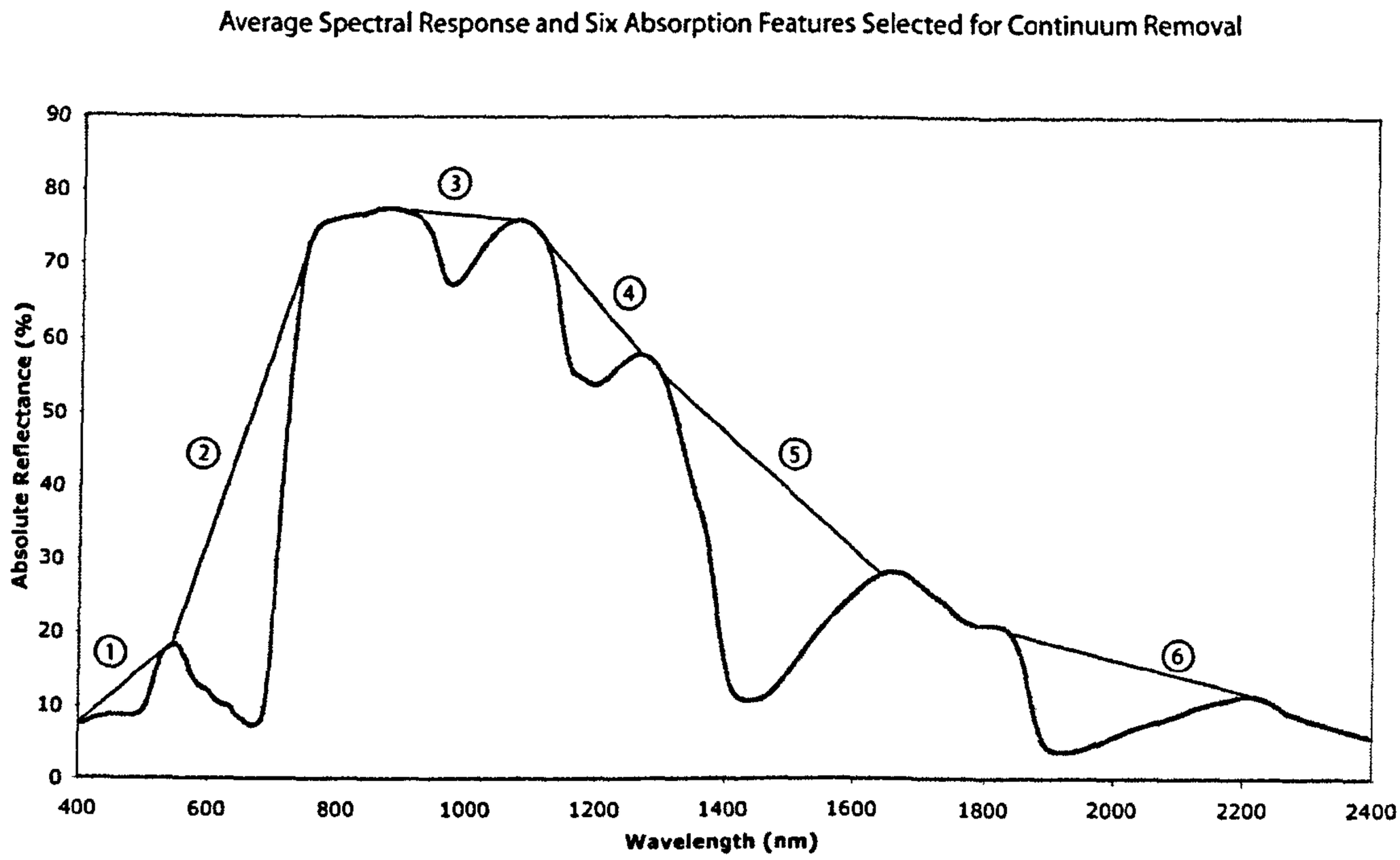

Figure 3.5: Six absorption features selected for continuum removal. The average spectral response is shown together with the continuum line and the six absorption features which are labelled from one to six.

The continuum line was derived using maxima and minima of a particular absorption feature and linear interpolation in between. The continuum at a particular wavelength can be described in equation 3.1 below.

$$C_{(\lambda i)} = (\lambda_i - \lambda_1) * (\tfrac{R_2 - R_1}{\lambda_2 - \lambda_1}) + R_1 \qquad \text{[equation 3.1]}$$

Equation 3.1 defines the continuum line (basically linear interpolation); R_1 and R_2 are the minima and maxima reflectance endpoints, λ_1 and λ_2 are the wavelengths at those endpoints, C is the continuum and λ_i is the wavelength where the continuum is to be determined. Continuum removed reflectance is then calculated from equation 3.2, where R' is continuum removed reflectance and C is the continuum reflectance at a particular wavelength (which is derived from equation 3.1).

$$R' = R / C \qquad \text{[equation 3.2]}$$

The continuum-removed reflectance is then normalised in two different ways to create two transformations of the spectra for analysis. Initially, the band depth was calculated as in equation 3.3.

$$BD = 1 - R' \qquad \text{[equation 3.3]}$$

The band depth was then normalised to either the area (BDNA) or centre (BDNC) of the continuum removed absorption feature. Calculation of BDNA involved dividing the band depth at a particular wavelength by the sum of all band depths inside the absorption feature. Calculation of BDNC involved dividing band depth at a particular wavelength by the centre of the absorption feature (wavelength of maximum depth). BDNA and BDNC calculations are shown below in equations 3.4 and 3.5.

$$BDNA = BD/(\Sigma BD) \qquad \text{[equation 3.4]}$$

$$BDNC = BD/MAXBD \qquad \text{[equation 3.5]}$$

Where MAXBD is the band depth wavelength with maximum depth inside the absorption feature.

These various transformations of the spectra allowed the links between spectral response, ^{137}Cs contamination and key foliar biochemicals to be fully investigated.

3.3.5 Biochemical Assay

In order to ascertain whether a link exists between spectral response of vegetation and levels of radionuclide contamination, key foliar biochemical contents were obtained. Foliar biochemical contents measured were, chlorophylls *a* and *b*, total chlorophyll, acid digestible fibre (AD fibre), lignin, cellulose, water, elemental nitrogen and nitrogen 15 (^{15}N). These six biochemicals have been shown to be the principal biochemicals within a leaf and are often selectively depleted due to plant stress (Carter 1993). The measurement of these foliar biochemicals also allowed isolation of any other environmental factors, which might be causing any vegetative stress. Measuring water content for example, might indicate water deficiency as a cause of changes to spectral response, rather than contamination. Conversely, it may suggest that water deficiency is not causing the plant stress and reveal that changes to the spectra are due to radionuclide contamination. In the sections below, the techniques for biochemical assay are described.

3.3.6 Chlorophyll Concentration

Chlorophyll is an important photosynthetic light-harvesting pigment. Vegetative content of chlorophylls *a* and *b* has been shown as an important indicator of plant stressors (le Maire *et al.* 2004). In addition, chlorophyll volume has been statistically linked to vegetation reflectance (Zarco-Tejada *et al.* 2004) and this correlation has allowed the use of remote sensing to monitor the state of such vegetation. Chlorophyll varies across species and with different stressors and therefore the relationship between chlorophyll and plant stress is not a simple one. Rather it is one which often requires *in situ* data to derive the link between chlorophyll, plant stress and reflectance.

To determine foliar levels of chlorophyll demanded the use of wet chemistry techniques. These were carried out on the same day as the needles were harvested and at same time as spectral measurements were collected. In Belarus, the temporary laboratory at the Svetolovichi Sanatorium was used to undertake chlorophyll analysis on the evening of the day the needles were collected. It was important to carry out chlorophyll analysis as quickly as possible after harvesting the needles in order to prevent chlorophyll degeneration. For each sample, a selection of needles was randomly sub-sampled for chlorophyll analysis. The needles were cut into smaller pieces before chlorophyll was extracted in a pestle and mortar. Care was taken to ensure each part of the needle was included in the analysis for chlorophyll as opposed to just the needle tip or base. The most frequently used assay for chlorophyll content in higher plants and green algae is the method introduced by Arnon (1949). This method was chosen due to its commonality, simplicity and the confidence in results as corroborated by the frequency of its use in the literature. It was performed in a darkened room to prevent any chlorophyll degradation during measurement. The method involves chlorophyll extraction (using a pestle and mortar) in a buffered 90% aqueous acetone solution (10% water), then a determination of the extinction point of chlorophyll *a* (664nm) and *b* (647nm). This extinction was measured using a Hach DRC2010 portable spectrophotometer and the results from the extinction points were then placed into a set of simultaneous equations in order to determine chlorophyll concentration. Finally, the chlorophyll is related to the volume of aqueous acetone as well as the sample weight to give chlorophyll concentration in mg g^{-1}. To maintain confidence in results, for every fifth sample, chlorophyll measurement was

replicated. A handheld portable chlorophyll meter was taken to Belarus in an attempt to derive duplicate measurements and add confidence to results. The Minolta SPAD-502 measures relative chlorophyll content in SPAD units. SPAD units are defined by Minolta's Soil Plant Analysis Division (SPAD) and range from 0 (lowest) to 100 (highest). The Minolta SPAD-502 has been designed primarily for agricultural and crop science applications, with an emphasis on measuring crop health and inferring Nitrogen levels. In terms of practicality the SPAD-502 is very quick at taking readings and simply clamps on the leaf. However, when applying the device to pine needles in the field a set of challenges arose. The long and thin biophysical properties of needles meant the SPAD-502 could not simply clamp over the needle. Results from the SPAD-502 were too variable, with inconsistencies caused by lack of compatibility of needles with the SPAD-502 device and therefore could not be used in the research.

Porra (2002) suggests that the specific extinction coefficients used by Arnon (1949) may be erroneous by up to 19% when determining chlorophyll *a* and 14% when measuring chlorophyll *b* concentration. As a result, the more accurate simultaneous equations developed by Lichtenthaler (1987), and Porra (2002) were used when determining chlorophyll. These newer specific extinction coefficients were determined by Mg-atomic absorption spectrometry. The equations used are below.

$$Chla(mg/ml) = 12.25E^{664} - 2.55E^{647} \qquad \text{[equation 3.6]}$$

$$Chlb(mg/ml) = 20.31E^{647} - 4.91E^{664} \qquad \text{[equation 3.7]}$$

$$TotalChl(mg/ml) = 20.31E^{647} - 4.91E^{664} \qquad \text{[equation 3.8]}$$

Where E^{664}, and E^{647} are absorptions at 664nm and 647nm respectively. To relate the chlorophyll amount to the volume of aqueous acetone and original sample weight the chlorophyll amount was then multiplied by the volume of solution, and divided by the sample weight in mg. This resulted in chlorophyll concentration in mg/g. Equation 3.9 shows the calculation. Chlorophyll was accurately reported to a precision of two decimal places.

$$ChlConcentration(mg/g) = chlorophyll(mg/ml) * volume(ml) / sampleweight(mg)$$

[equation 3.9]

3.3.7 Lignin, Cellulose and AD Fibre

Lignin and cellulose are the structural components of vegetation, and are biochemically and physiologically inactive (Jacquemoud *et al.* 1995). Kokaly and Clark (1999) highlight the links between ecosystem function, lignin and cellulose content, and spectral reflectance at the leaf and canopy levels. More specifically, Curran (1989) has identified specific absorption features in generic spectra of vegetation, which can be related to lignin and cellulose. Thus, spectral response may vary in these wavelengths as a function of radionuclide contamination and therefore it was important to derive lignin and cellulose contents from the vegetation samples. Rowland and Roberts (1994) review and compare a number of acid-detergent fibre methods in order to determine content of lignin and cellulose in a variety of vegetation types, and find that they produce accurate results. The H_2SO_4 variant was used in this study, as it was found by Rowland and Roberts (1994) to be easy to implement, reliable, precise and, unlike the alternative permanganate variant, was suitable for application to a wide variety of vegetative materials.

Unlike chlorophylls, lignin and cellulose are resistant to decomposition and therefore the pine needles could be powdered, and brought back to the UK for analysis. The method began by weighing out 1g of randomly sub-sampled air dried powdered needle material for each sample and went through a series of acid digestion stages after which the sample was re-weighed. These weights were placed into simple formulas to derive quantity of acid digestible fibre (AD Fibre), cellulose and, after an ignition at 550°C, lignin. The method first involved digestion of the 1g powdered sample in a CTAB solution (0.5m sulphuric acid and cetylrimethyl bromide) with slight heating. After filtering the sample through a sintered glass crucible (porosity 1μm) the material was dried at 105°C and weighed. The sample was then digested in 72% H_2SO_4 for three hours, filtered, dried at 105°C then re-weighed. Finally, the sample was ignited at 550°C for 2-3 hours until only lignin remained. The sample was then weighed and the following calculations used to determine acid digestible fibre, lignin and cellulose.

$$\%ADFibre = (W3 - W2) * 100 / W1 \quad \text{[equation 3.10]}$$

$$\%Cellulose = (W3 - W4) * 100 / W1 \quad \text{[equation 3.11]}$$

$$\%Lignin = (W4 - W5) * 100 / W1 \quad \text{[equation 3.12]}$$

Where W1 is the weight of the original powdered sample, W2 is the starting weight of the sintered crucible, W3 is the weight after the CTAB digestion and drying, W4 is the weight after the H_2SO_4 digestion and drying, and W5 is the weight after ignition at 550°C. All weights are to three decimal places to gain an accurate determination when working with small numbers.

Throughout the procedure, levels of laboratory equipment meant samples were assayed for AD fibre, lignin and cellulose in batches of 15. In order to maintain consistency and check standards between batches, every fifth sample was repeated but in a different batch to minimise error and isolate real variation in lignin and cellulose quantities from experimental error or inconsistencies.

3.3.8 Water

Water content was measured via a simple loss on ignition method. Approximately 1g of each needle sample (selected randomly) was weighed when fresh, dried overnight (24 hours) in a 70°C oven and was reweighed after drying and cooling. A simple equation then allowed percentage water content to be derived.

$$\%Water = (W1 - W2) / W1 * 100 \quad \text{[equation 3.13]}$$

Where W1 and W2 are weights before and after drying.

In Belarus, some of the samples were measured for moisture using ovens in the Svetolovichi Sanatorium and a portable balance with foil weigh boats. Figure 3.6 illustrates the portable balance and weigh boats. Some samples were kept frozen (using

freezers in Belarus and a coolbox during transit) and transported to the UK for moisture analysis due to political reasons forcing a premature exit from Belarus (section 3.1, appendix A3). The procedures in the UK and Belarus for water analysis were identical and once again, every fifth measurement was replicated to monitor standards and ensure data quality.

Figure 3.6: Foil weigh boats and portable balance used to measure water content of needles in Belarus.

3.3.9 Nitrogen

Nitrogen is used in varying forms by plants and there is often variation in nitrogen uptake and assimilation, dependent on sources of nitrogen, other nutrients and the growth environment (Liu *et al.* 2006). In addition, nitrogen content is often used to predict plant growth, efficiency and function (Broadley *et al.* 2000). As a result, nitrogen was considered to be an important foliar biochemical in this study and was measured in two forms, ^{15}N and elemental nitrogen (^{14}N).

Nitrogen analysis was the only biochemical in this research which was measured externally and was carried out by Iso-Analytical, Sandbach, UK. Powdered needle material was sent for each sample and was then sub-sampled at random by Iso-Analytical for nitrogen analysis. The laboratory report is included in appendix A1. The technique used for analysis was EA-IRMS (elemental analyser isotope ratio mass spectrometry).

Elemental nitrogen was measured as a percentage content of the sample. ^{15}N was measured in per mil notation versus the international reference standard of air. To minimise error and add confidence to results, an international reference standard was used in addition to every fifth sample being duplicated.

Due to budgetary constraints in this research, half of the samples were measured for nitrogen. Half of the high, medium and low ^{137}Cs concentration groups were randomly selected and sent to Iso-Analytical.

3.3.10 Gamma Spectrometry

Accurate measurement of radionuclide levels inside the physiologically active part of the trees (i.e. the needles) was pivotal in linking spectral response to radionuclide contamination levels. Section 3.3 described the selection of sites using a portable dosimeter, which gave ambient dose rates in the growing environment and not specific activity inside the needles. Needle specific activity was measured in samples of dried needles at Kingston University using gamma spectrometry. The needles for each sample were dried for a period of at least 12 hours in a 70°C oven before being packed into containers ready for gamma spectrometry.

Approximately 20g of dried needles per sample were placed in plastic beakers. These were placed inside the lead shielding of a high-purity germanium detector (HPGe) where gamma rays were counted over a period of 25000 seconds. With each sample, care was taken to ensure geometry of counting remained constant. This was secured by maintaining full pots of needles and ensuring the needle density inside the pots remained constant for each sample. To determine density, the pots were weighed before and after filling with needles in order to accurately determine needle mass inside the pots. The aim was to keep this as close as possible to 20g whilst continually checking fill levels and spacing of needles in the pots. Care was also taken in the placement of the pot inside the gamma spectrometer counting chamber and each sample was placed on a marker to ensure there was no deviation from the HPGe crystal between each sample. The ^{137}Cs peak in the resulting gamma spectra was analysed using Canberra Genie 2000 spectroscopic software to give net area (representing total counts) at the ^{137}Cs energy channel (662KeV).

The count rate was calculated by dividing the area of the ^{137}Cs energy channel by the count time. A decay time correction factor was calculated by determining the number of days between the gamma spectrometer measurement date and the reference date when samples were collected (15th July 2003 for pilot study fieldwork, 15th July, 2004 for the second field campaign and 4th August 2005 for the laboratory data). This then enabled decay corrected count rates to be calculated. HPGe detector efficiency was calculated using a National Physical Laboratory (NPL) standard solution (appendix A2) added to a volume and mass of pine needles equivalent to the standard sample mass (equation 3.14 below).

$$Efficiency = \frac{NetArea}{(LiveTime)(Activity)(Yield)} \qquad \text{[equation 3.14]}$$

Where the activity (in Bq) is for a pine needle standard, yield is the radionuclide branching ratio for the measured gamma ray and live time is the counting time of the NPL standard.

The HPGe efficiency and ^{137}Cs branching ratio were then used along with the decay corrected count rate in equation 3.15 in order to compute needle specific activity.

$$A(inBq) = DC/(\varepsilon * BR) \qquad \text{[equation 3.15]}$$

Where A is the activity in Bq. DC is the decay corrected count rate, ε is the efficiency of the detector and BR is the branching ratio of 662KeV measured gamma ray.

Finally, the specific activity (Bq/g) was calculated using the weight of the sample.

$$SA(Bq/g) = A/W \qquad \text{[equation 3.16]}$$

Where SA(Bq/g) is the needle specific activity, A is the activity in Bq calculated in equation 3.15 and W is the sample weight of needles.

These specific activity levels could then be compared to the foliar biochemicals and reflectance spectra of the needles in order to investigate links between ^{137}Cs contamination, foliar biochemicals and reflectance spectra.

3.4 Summary

This chapter has described methods used to collect and analyse data as well as the instrumentation used along with techniques used to ensure consistency and validity of data. These methods and associated instrumentation are crucial to the research and underpin the research and analyses in subsequent chapters.

Chapter 4

Feasibility of Imaging Spectrometry for Remote Sensing ^{137}Cs Contamination: A Pilot Study

4.1 Introduction

This chapter reports results from pilot field radiometry work undertaken in Belarus. It begins by outlining the background to the contaminated *Pinus sylvestris* in Belarus and then describes strategies of data collection. It goes on to illustrate analyses performed and results achieved. Research outlined in this chapter forms the basis for field radiometry work in chapter five and with regards to the objectives set out in chapter one, considers the following:

- To assess whether there are changes in spectral reflectance caused by differing ^{137}Cs levels

- To characterise whether ^{137}Cs has any effects on key foliar biochemicals and at what regions of the optical range of the electromagnetic spectrum these are detectable.

4.2 Background to Data Collection Strategies

The contamination of forest ecosystems by ^{137}Cs has been the focus of much field-based and modelling research aimed at determining the transport process of ^{137}Cs (e.g. Ipatyev *et al.* 1999, Malek *et al.* 2002). Such research has shown forests to be efficient sinks for ^{137}Cs, with a number of implications for humans who may use the forest (Gaso *et al.* 1998). Currently, many Belarusian forests pose a major radiological hazard to the local

population (Amiro and Ipatyev 1999). There is a need to regularly review the potential to regain the economic function of the forests and identify those areas that can provide clean timber (< 0.74Bq/g) and other resources. Frequently updated information on radionuclide concentration over large areas is important for determining forestry practices and land-use planning. Imaging spectrometry techniques (as described in chapter two) may enable large areas of the Belarusian landscape to be monitored simultaneously. The resulting spectra collected from imaging spectrometers can conceivably be used to estimate quantities and spatial distributions of canopy biochemicals which could then in turn be used as a discriminator of ^{137}Cs contamination (chapter two). Davids and Tyler (2003) highlighted imaging spectrometry as having potential in monitoring two forest species (*Pinus sylvestris* and *Betula pendula*) though their study focused on the Chernobyl exclusion zone where high levels of contamination effectively preclude economic use of the forest for many decades to come. In contrast, much of Belarus was exposed to lower contamination levels, mainly by fission products with approximately 30-year half-lives (chapters one and three). In Belarus, the authorities stipulate specific radioactivity levels at which timber may be utilised; 1.85Bq/g for lumber wood and 0.74Bq/g for domestic fuel wood (Goor and Thiry 2004). The pilot study research focuses on locations with known radioactive fission product contamination (^{137}Cs) that has been taken out of economic use, but may have potential to be returned to economic use in the next few decades. This chapter presents field radiometry research which is an initial step towards meeting the overall aim of the thesis which is to assess whether ^{137}Cs can be monitored using imaging spectrometry techniques. Two main assumptions were made whilst conducting the fieldwork. Firstly it was assumed that the specific activity of ^{137}Cs in the needles was representative of the soil contamination. This assumption has limitations in terms of different transfer factors and other variables which may affect the transfer of ^{137}Cs from soil to needle, meaning the needle concentration of ^{137}Cs may not be representative of the contamination in the soil. As this research was focussing on the relationship between ^{137}Cs needle concentration and spectral reflectance, this assumption was not considered as having serious impacts on results, but is important to be aware of when considering the work in context, particularly when thinking about spatial resolution of ^{137}Cs. Chapter six illustrates this assumption in terms of transfer factors between the growing material and needle not always being linear. The second assumption made was that the dose rates measured in the field were representative of the ^{137}Cs contamination in the soil and needles. This was not the case, as illustrated by discrepancies between dose rate and contamination measured within the

needles. This assumption had to be made as ambient dose rate with a portable dosimeter was the only quick method available in the field which could provide an indication of ^{137}Cs contamination at a particular site or sample.

4.3 Study Sites and Data Collection

Forest sites located within the Belarus part of the Bryansk-Belarus radioactive fallout spot (centred 200km north-northeast of the Chernobyl reactor) were the focus of the pilot study (table 4.1). This contaminated region was formed on 28-29th April 1986, probably as a result of fallout which was artificially induced by the USSR via cloud seeding. Ground deposition of ^{137}Cs exceeded 1.5MBq/m^2 and reached, in some parts, 5MBq/m^2. Within the Bryansk-Belarus spot is the Vetka region, which comprises a number of contiguous forest plantations, the predominant species of which is *Pinus sylvestris*. These forests were the focus of study and were sampled according to two factors; radiation dose and tree age. Tree age was considered important since transport and storage of radionuclides within trees depends partly on age (Ipatyev *et al.* 1999, Thiry *et al.* 2002).

Four sites were chosen in July 2003 based on the ambient radiation dose rate levels measured using a portable dose rate meter at one metre above ground level (table 4.1). Two ranges of dose rates were identified, and described as either 'high' (1.50μSv/h to 2.90μSv/h) or 'low' (0.05μSv/h to 0.08μSv/h). One old (c. 35 years) forest and one young (c. 15 years) forest were sampled for each dose rate range. The sites are designated in table 4.1 as High Old, High Young, Low Old and Low Young and their location mapped on figure 4.1. At each of the four sites between 2 and 13 trees were sampled (table 4.1). Whilst more samples would have been preferred the number of samples represents the pilot nature of the research in this chapter and constraints on time in the field meant at some sites, a representative number of samples were not collected. This was a key aim of research in chapter five; to expand and gather a representative sample from each selected site.

Branches facing north, south, east and west were taken to avoid introducing bias from different growing conditions. In terms of stand position, trees from the forest edge as well as in the middle of the stand were collected in order to fully represent the trees growing on

each site. Mean height for old trees was 18m, whilst the mean girth (at chest height) was 80cm. For the young trees the mean height was 3m and mean girth was 20cm. Needles (<1 year old) were removed from the branches and subsampled for spectral measurements and ^{137}Cs specific activity according to the spectral and gamma spectrometry methods described in chapter three (sections 3.3.1 and 3.3.10). For each tree, four spectral measurements were taken and averaged (according to methods described in chapter 3, section 3.3.1), giving one spectral measurement per sampled tree. Mean ^{137}Cs specific activity for *Pinus sylvestris* needles sampled from each of the four sites is reported in table 4.1.

Site Designation (Nearest Village)	Site Location (Latitude and Longitude)	Mean Dose Rate (µSv/ h)	Mean Needles ^{137}Cs Specific Activity (Bq/g)
Old High (OH) (Staraja Zakruzza)	52 39.269'N 031 29.456'E	2.33 +/- 0.32 (n=22)	13.37 +/- 9.52 (n=13)
Old Low (OL) (Stolbunskaya)	52 50.110'N 031 27.767'E	0.15 +/- 0.03 (n=12)	0.38 +/- 0.19 (n=9)
Young High (YH) (Bartolomeevka)	52 39.809'N 031 22.785'E	1.59 +/- 0.36 (n=14)	5.27 +/- 3.68 (n=11)
Young Low (YL) (Romanovichi)	52 26.882'N 031 06.187'E	0.06+/- 0.01 (n=22)	0.46 +/- 0.19 (n=2)

n = number of trees.

Table 4.1: site designation, location and mean dose rate at 1m above ground (+/- 1SD) and mean needle specific activity (+/- 1SD).

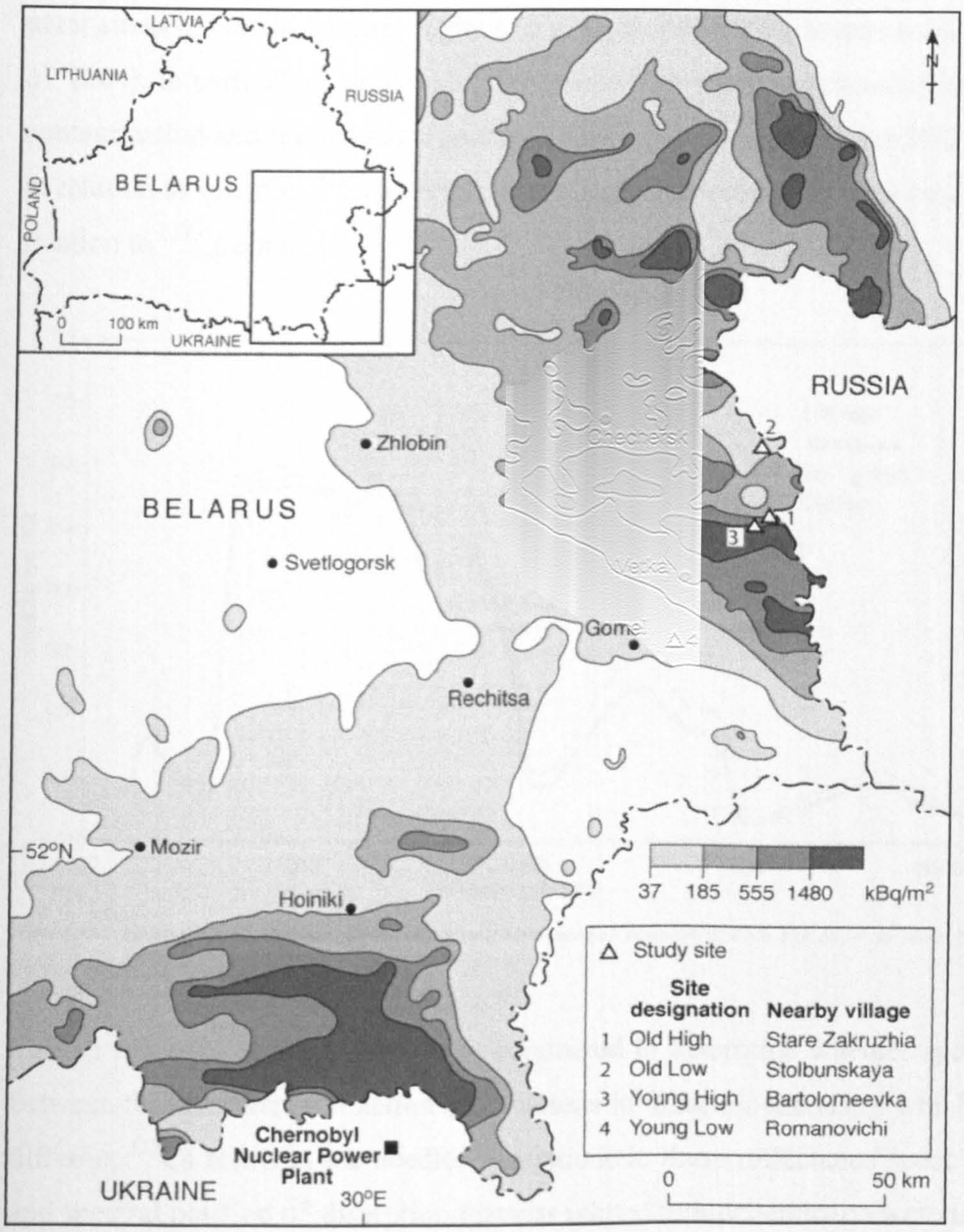

Figure 4.1: Location of the four study sites chosen for investigation. Note that the site designation information matches the detail in table 4.1.

4.4 Analysis of Spectral Reflectance

Mean reflectance spectra (%) of the four sites were different across the spectral range studied (figure 4.2). The largest spectral reflectances were for old growth forest whose needles also exhibited the highest mean levels of ^{137}Cs specific activity (mean 13.7 Bq/g) for the four sites studied. The coincidence of high pine needle specific ^{137}Cs activity with high spectral reflectances, particularly in the visible and near infrared regions, suggests plant stress. Other authors have noted the association between high spectral reflectance and

plant stress in certain spectral regions (e.g. Jago *et al.* 1999, Moran *et al.* 2000, Kooistra *et al.* 2004). In particular, Jago *et al.* (1999) showed a strong relationship between vegetation contamination and the red edge position (REP). In this research, the REP was investigated in relation to specific ^{137}Cs activity, but no significant changes were evident in the REP in relation to ^{137}Cs content.

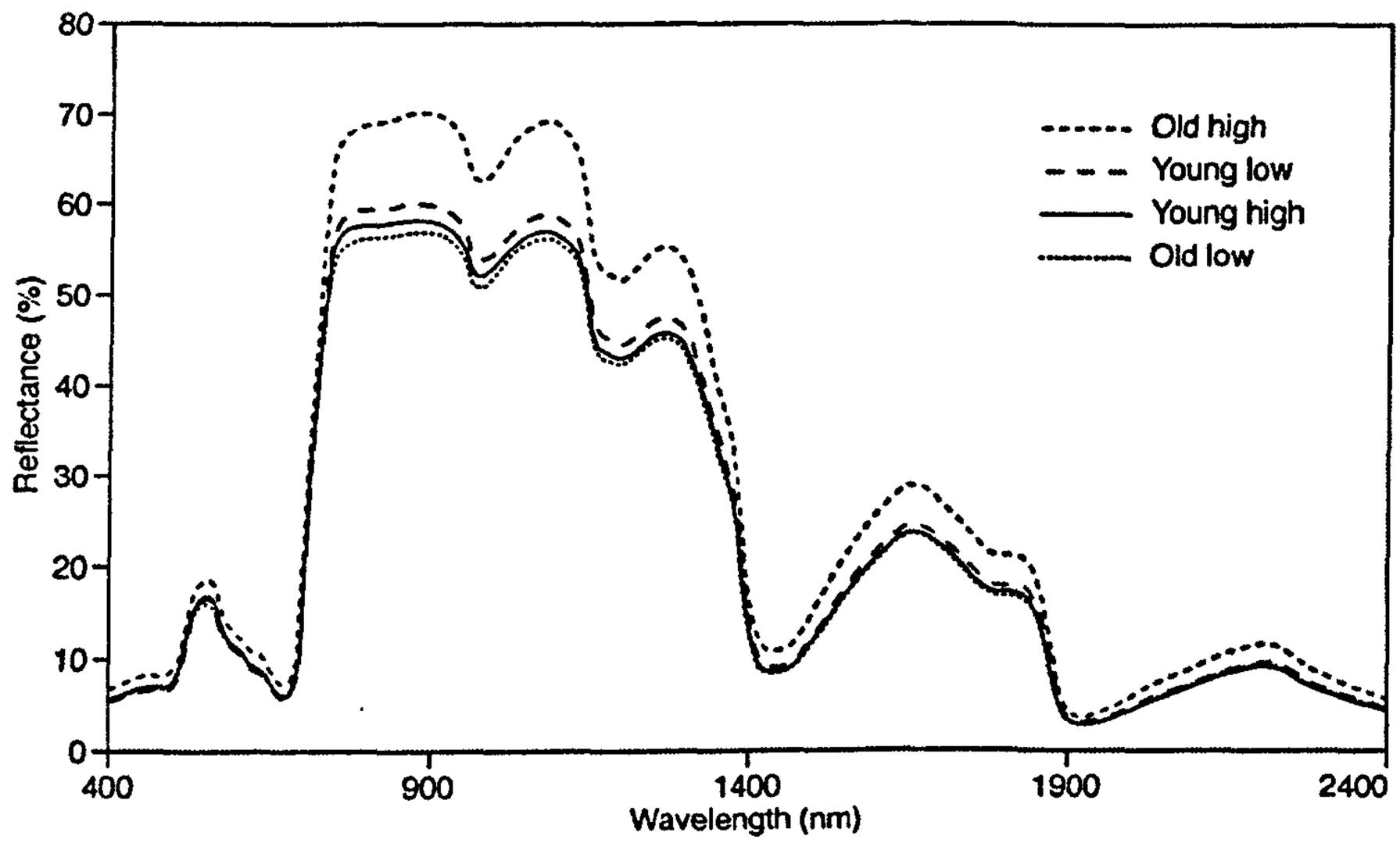

Figure 4.2: Mean spectral response for the Pinus sylvestris needles sampled at each site (refer to table 4.1 for further details on abbreviations and ^{137}Cs contamination levels).

Further analyses of the spectra were conducted to determine whether spectral differences between the sites were a function of variations in foliar biochemistry which may arise from different ^{137}Cs levels in the needles. Variations in these reflectance spectra (such as depth and spectral position of absorption features related to biochemicals) were isolated using the feature selection technique of continuum removal (Kokaly and Clark 1999, Curran *et al.* 2001, Mutanga *et al.* 2004) (described in chapter three). Feature selection involves the search for a subset of the original data which will aid in the decision making process regarding the number, location and width of spectral bands which are significant (Warner and Shank 1997). Six continuum-removed absorption features were identified using both visual analyses of the spectra and by considering specific absorption features noted in the literature (e.g. Curran 1989). These features had their centre located around 470nm, 670nm, 920nm, 1200nm, 1360nm and 1840nm (chapter three, section 3.3.4).

A statistical comparison between the BDNA spectral value for each wavelength at each of the six absorption features between high and low contaminated sites for the young and old

forests was undertaken. This comparison was to ascertain whether there was a statistically significant difference between the spectra based on differing ^{137}Cs levels and to ascertain at which wavelengths this difference was detectable. In turn, wavelengths identified could then possibly be associated with foliar biochemical absorption points to determine if a link exists between spectral reflectance, foliar biochemicals and ^{137}Cs specific activity. The Runs test was employed, being a non-parametric test able to accommodate the small sample sizes. The test was used to establish wavelengths displaying statistically significant differences (at 0.05 significance level) between sites of high and low contamination levels. None of the wavelengths in any of the six absorption features were significantly different between the high and low contaminated needles sampled from the young forest sites. This was not the case however, for the new growth needles measured from the old forest site where a large number of wavelengths in each of the six absorption features were found to be statistically different (at 0.05 significance level) between the needles with low and high ^{137}Cs contamination levels (table 4.2).

Significant Wavelengths (nm)	Association with Biochemical
Absorption feature of 470nm	
478	Chlorophyll (460nm)
522-526	Unattributable
Absorption feature of 670nm	
596-600	Unattributable
637-641	Chlorophyll (640nm)
647-653	Chlorophyll (660nm)
693	Unattributable
736	Chlorophyll (724nm)
742-749	Unattributable
Absorption feature of 920nm	
921	Nitrogen (910nm)
926	Nitrogen (910nm)
947	Unattributable
954-960	Unattributable
966	Water (970nm)
973-974	Water (970nm)
976	Water (970nm)
978-989	Cellulose (978nm)
995	Cellulose (978nm)
Absorption feature of 1200nm	
1145-1146	Unattributable
1155-1180	Lignin (1174nm)
1186	Lignin (1174nm)
1197-1199	Water (1200nm); Cellulose (1194nm); Cellulose (1200nm)
1217	Cellulose (1216nm)
1241	Unattributable
1245	Unattributable
1264	Cellulose (1275nm)
1266-1277	Cellulose (1275nm)
1280	Cellulose (1275nm)
1283	Cellulose (1275nm)
Absorption feature of 1360nm	
1361-1408	Water (1400nm); Cellulose (1368nm)
1422-1341	Nitrogen (1426nm); Lignin (1420nm)
1432-1499	Nitrogen (1446nm); Nitrogen (1456nm); Nitrogen (1462nm); Lignin (1442); Lignin (1450nm); Cellulose (1484nm); Cellulose (1490nm)
Absorption feature of 1840nm	
1841 -1842	Unattributable
1843 – 1888	Unattributable
1926-1975	Water (1940nm); Nitrogen (1974nm); Lignin (1940nm); Cellulose (1924nm); Cellulose (1940nm)

Table 4.2: Wavelengths for which significantly different BDNA spectra (at 0.05 significance level) were found between spectra of new growth needles with low and high ^{137}Cs contamination levels. (Note all spectra were from the old forest sites.) Many of these wavelengths are located within ±20nm of one of the five principal biochemicals within a leaf; chlorophyll, nitrogen, lignin, cellulose and water.

Table 4.2 also indicates which of the wavelengths are located within ± 20nm of one of the five principal biochemicals within a leaf; chlorophyll, nitrogen/protein, lignin, cellulose and water (Curran 1989, Curran *et al.* 2001). Examination of the first absorption feature in the visible region (centred at 470nm) revealed that the wavelength at 478nm can be attributable to the electron transition of chlorophyll 436nm. For the absorption feature of 670nm, it was the wavelengths at 637-641nm attributable to the electronic transmission of chlorophyll at 640nm; at 647-653nm attributable to the electronic transmission of chlorophyll at 660nm; and the wavelengths at 736nm and 742-744nm attributable to the electronic transmission of chlorophyll at 724nm that exhibited significant differences in the BDNA spectral response between the high and low contaminated sites. Theory has related absorption features in the visible portion of the electromagnetic spectrum to chlorophyll content and at the far edge of the feature is the aforementioned red edge position, a phenomenon well-documented and used to monitor changes in chlorophyll content and vegetation stress (Jago *et al.* 1999). Specifically the REP has been associated with the chlorophyll content of vegetation (e.g. Pinar and Curran 1996) as well as energy scattering related to nitrogen levels (Mutanga *et al.* 2004), The position of the red edge and in turn chlorophyll content and scattering properties are often useful indicators of photosynthetic processes and the health of vegetation but in the investigations of the REP in this pilot research and in the field radiometry described in chapter five, the REP did not vary significantly and therefore the REP is not a useful discriminator of ^{137}Cs contamination, possibly due to the non-linear response of *Pinus sylvestris* to ^{137}Cs contamination, as discussed in chapters five, six and eight.

Within the near infrared part of the spectrum two absorption features were examined. For the absorption feature of 920nm, significant differences were seen at a large number of wavelengths, many of which can be attributable to the biochemicals of nitrogen (C-H stretch at 910nm); water (O-H bend at 970nm) and cellulose (O-H stretch at 978nm). The absorption feature of 1200nm had significantly different wavelengths attributable to the biochemicals of lignin (C-H stretch at 1174nm); cellulose (C-H stretch at 1194nm; O-H bend at 1200nm; C-H stretch at 1216nm and C-H stretch at 1275nm) and water (O-H bend at 1200nm). Two further absorption features were examined, both in the shortwave infrared portion of the spectrum, both of which had a very large number of wavelengths with statistically significant differences in BDNA values (at 0.05 level of significance). Specifically, the 1360nm absorption feature had wavelengths attributable to the

biochemicals of cellulose (C-H stretch and C-H deformation at 1368nm; O-H stretch at 1484nm and O-H stretch at 1490nm); water (O-H bend at 1400nm); lignin (C-H stretch and C-H deformation at 1420nm; O-H stretch and C-H stretch and C-H deformation at 1442nm and O-H stretch and C-H stretch and C-H deformation at 1450nm) and nitrogen (N-H symmetrical stretch at 1426nm; N-H stretch at 1446nm; N-H stretch at 1456nm; N-H stretch at 1462nm). The absorption feature of 1840nm had wavelengths attributable to the biochemicals of water (O-H stretch and O-H deformation at 1940nm); nitrogen (N-H asymmetrical stretch at 1974nm); lignin (O-H stretch and O-H deformation at 1940nm) and cellulose (O-H 1924nm and O-H stretch and O-H deformation at 1940nm). These results indicate that there may be selective depletion of these biochemicals, which indicates significant structural differences between the needles from the high contaminated site and the low contaminated sites. Similar findings have been associated with other contaminants (Jago *et al.* 1999, Kooistra *et al.* 2003).

4.5 Discussion

The analysis of these absorption features using a continuum-removed transformation of the spectral reflectance demonstrates that there are statistically significant differences in processed spectra between *Pinus sylvestris* needles exhibiting ^{137}Cs contamination levels partitioned according to radiological risk. Of particular note is that this was only the case for the older trees (c. >20 years). This may be due to the higher levels of radionuclides within the old trees (see chapter six), or that the trees have been exposed to contamination for longer periods. In further research, analyses are required to link the spectral response of *Pinus sylvestris* needles to their foliar biochemicals and to ^{137}Cs specific activity. The possibility that by measuring the biochemical concentrations of vegetation compartments, estimates of the level of radionuclide contamination can be derived also warrants further investigation. This pilot study has indicated that tree age is an important consideration and old trees (c. >20 years) have most potential in using their spectral response to monitor ^{137}Cs. Not only do old trees show significant differences between spectral transformations based on ^{137}Cs, but they also harbour most economic potential. The World Bank (2006) emphasise the increased production of wood as a key opportunity in developing Belarus' energy supply in the future. This is dependent on the availability of wood which does not pose a radiological hazard (<0.74Bq/g) and again highlights the need for regular and

accurate monitoring of ^{137}Cs contaminated areas so that as forest ecosystems recover, those forests which no longer pose a radiological risk can be put back into economic function.

Results from this chapter have shown that ^{137}Cs contamination may affect the spectral reflectance properties of *Pinus sylvestris* needles, particularly the new growth needles of older forests (c. >20 years). A number of wavelengths within six continuum-removed absorption features exhibited significantly different BDNA values (at 0.05 significance level) between new growth pine needles of old forests with high and low specific ^{137}Cs activities. Several of these significant wavebands were near to known absorption features that are causally related to the five principal foliar biochemicals of chlorophyll, lignin, cellulose, nitrogen and water.

This pilot research has shown potential in using spectral reflectance and foliar biochemistry to monitor ^{137}Cs specific activity. Differences in spectral reflectance at wavelengths associated with principal foliar biochemicals have highlighted the possibility of using partial correlation and predictive regression routines to link spectral reflectance, foliar biochemistry and ^{137}Cs levels. This is undertaken in chapter five which makes use of a greatly extended dataset which was collected in Belarus on a field campaign after the analysis of the pilot study data. The pilot research has shown potential in using imaging spectrometry and also helped to inform future data collection and analyses. Limitations in this pilot chapter such as a lack of data, assumptions about transfer between soil and needle as well as ambient dose rate not being representative of ^{137}Cs concentration in needles have been considered in terms of the overall aims of the research and are acted upon in chapters five and six, as well as being considered in the discussion and conclusion in chapter eight. Modifications to fieldwork and analyses based on this chapter are described below in section 4.6.

4.6 Summary and Suggested Modifications to Future Fieldwork

Suggested modifications to future fieldwork based on the pilot research presented in this chapter are:

- The potential shown in this chapter has been based on relatively small samples sizes and as such a recommendation for future fieldwork and analysis is to increase sample size. This would allow greater confidence in results and a wider variety of statistical analyses methods to be performed. This is acted upon in an extended field campaign and is presented in chapter five.

- A focus on old trees is recommended as these show statistically significant differences between ^{137}Cs specific activity and spectral reflectance as well as holding greatest economic potential. Fieldwork in chapter five thus focuses on old trees, as does the imagery collected and described in chapter seven.

- Pilot research has used *Pinus sylvestris* containing (relatively) very low ^{137}Cs specific activities and contrasted this with relatively high levels of ^{137}Cs. Future research should consider a greater range of ^{137}Cs levels to better represent the range in the Belarusian landscape and ascertain at what levels an effect becomes detectable in spectra. This is represented in the data collection strategy of data presented in chapter five and in the dosing of *Pinus sylvestris* grown in the laboratory and is presented in chapter six.

These recommendations are acted upon in subsequent chapters to meet the overall thesis aim of investigating whether imaging spectrometry can be used to monitor ^{137}Cs contamination.

Chapter 5

Predicting ^{137}Cs Levels from Spectra

5.1 Introduction

This chapter describes the results from the main field study in Belarus. It encompasses results from two tailed Student's t-tests, regression analyses to predict biochemicals from spectra and finally attempts to predict ^{137}Cs levels from this biochemical data. The chapter is organised in a top-down scientific approach according to the diagram in figure 5.1 which shows conceptually how ^{137}Cs might be monitored using remote sensing techniques. The chapter begins outlining the protocol of fieldwork and data collection used in this part of the thesis. It then describes results of testing the spectra to see if any differences exist between high and low contamination levels. This is followed by testing whether any differences exist between key foliar biochemical contents at high and low contamination levels. In turn, partial correlation is used to assess whether ^{137}Cs is having an effect on any of these biochemicals and at which parts of the electromagnetic spectrum. The chapter then describes statistical procedures (including stepwise regression and partial least squares) to predict foliar biochemicals from the spectra and finally assesses whether ^{137}Cs content can be predicted from these key foliar biochemicals by utilising multiple regression and artificial neural networks. This chapter addresses three of the four research objectives, as set out in chapter one:

- To assess if there are changes in spectral reflectance caused by differing ^{137}Cs levels.

- To characterise whether ^{137}Cs contamination has any effects on key foliar biochemicals and at what regions of the optical range of the electromagnetic spectrum these are detectable.

- To determine if key foliar biochemicals can be predicted from spectral response and in turn if these biochemicals can be used to infer levels of ^{137}Cs contamination.

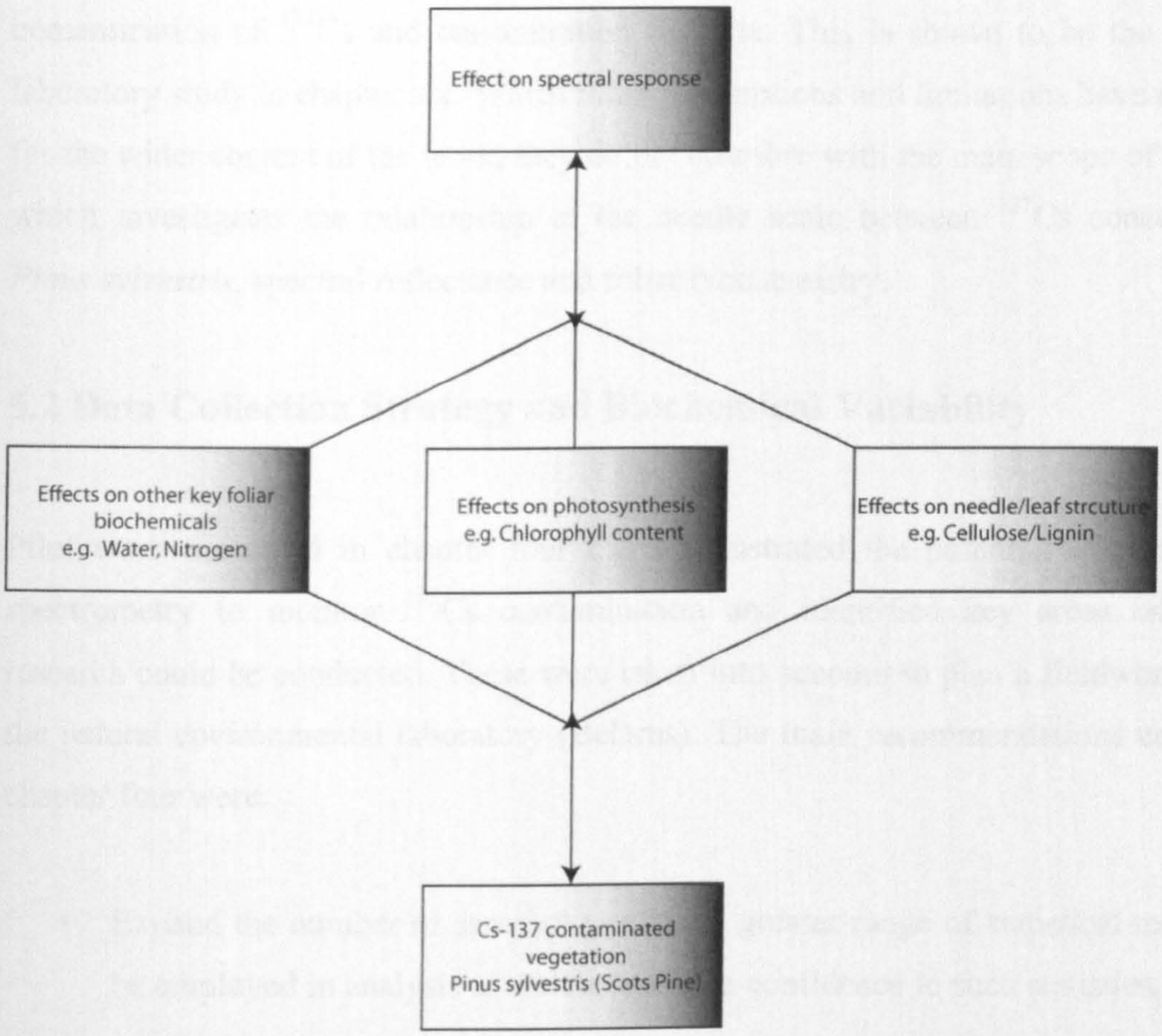

Figure 5.1: Conceptual diagram of the top-down approach taken in this chapter.

There are some key assumptions and limitations which are inherent in the research in this chapter and should be noted before proceeding. Firstly, the approach focuses on the relationship between foliar biochemicals, ^{137}Cs and spectral reflectance of *Pinus sylvestris* at the expense of exploring biophysical data and its effect on this relationship. This is for two reasons. Primarily this is due to pilot research in chapter four showing statistically significant differences in spectra between relatively high and low ^{137}Cs contaminated spectra and at regions known to be causally related to certain foliar biochemicals (e.g. chlorophyll, lignin). Secondly, political reasons prevented a further field trip to Belarus in order to investigate biophysical properties in relation to ^{137}Cs concentration. As in chapter four, other assumptions and limitations are that the ambient dose rate was assumed to be a good indicator for ^{137}Cs contamination of a forest when in reality, ambient dose rate and ^{137}Cs specific activity of needles do not always correspond. It was also assumed that ^{137}Cs concentration in *Pinus sylvestris* needles was representative of contamination in the soil. Again, in reality there is not always a linear relationship between growing medium

contamination of ^{137}Cs and concentration in biota. This is shown to be the case in the laboratory study in chapter six. Whilst these assumptions and limitations have implications for the wider context of the work, they do not interfere with the main scope of this chapter which investigates the relationship at the needle scale between ^{137}Cs concentration of *Pinus sylvestris*, spectral reflectance and foliar biochemistry.

5.2 Data Collection Strategy and Biochemical Variability

Pilot work discussed in chapter four has demonstrated the potential of using imaging spectrometry to monitor ^{137}Cs contamination and identified key areas where future research could be conducted. These were taken into account to plan a fieldwork season in the natural environmental laboratory (Belarus). The main recommendations coming from chapter four were:

- Expand the number of samples to allow a greater range of statistical techniques to be employed in analysis as well as enhance confidence in such statistics.

- Focus on old trees (c. >20 years) since they show most promise in using imaging spectrometry and have economic potential (see chapter four).

- Look at a greater range of contamination levels in order to better represent those present in Belarus and to ascertain which levels might have a detectable effect on spectral reflectance of *Pinus sylvestris*.

To act upon these recommendations data collection took place in Belarus during July and August 2004. Field sites were in the Bryansk-Belarus fallout spot described in chapter four (section 4.3) and are shown in figure 5.2.

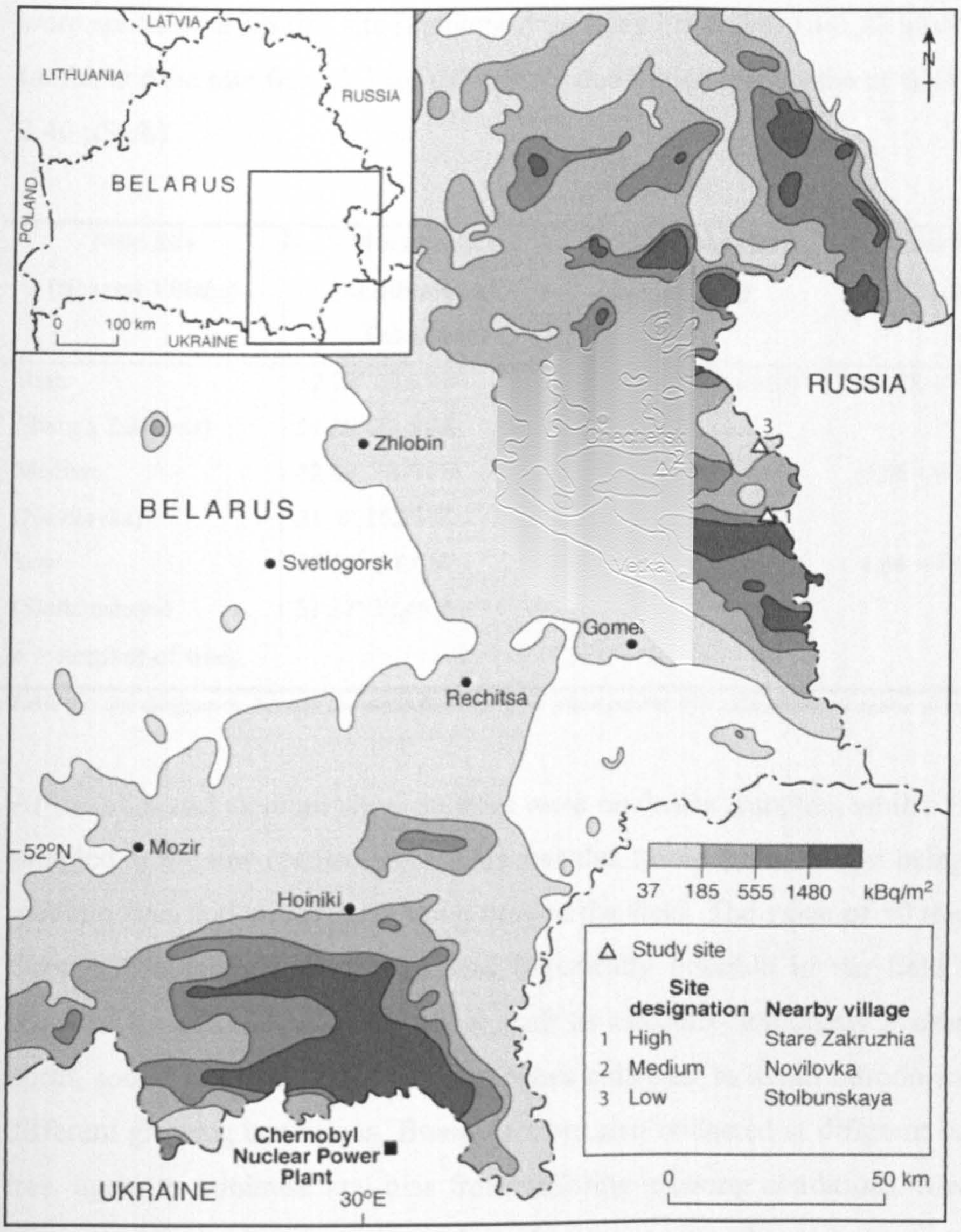

Figure 5.2: Location of the three study sites chosen for investigation during July/August 2004. Note that the site designation information matches the detail in table 5.1.

In the field, sites were categorised according to their ambient radioactive dose rate. Ambient dose rate provided a quick indication of contamination levels although specific ^{137}Cs soil characterisation would have been preferred. Since there was no access to a laboratory or any *in situ* devices capable of measuring specific ^{137}Cs activity of soil, ambient dose rate was the chosen method of site characterisation. As the focus was on old trees (c. >20 years) sites were made up only of mature *Pinus sylvestris*. A portable dosimeter was used to measure ambient dose rate in the field. The location and mean dose rates for each site are shown in table 5.1. Levels of background radiation ranged from 0.05 to 2.91 μSv/h. Three sites were chosen based on dose rates 1m above ground level and

were split into a control site (ambient dose rates from 0.07 to 0.22 μSv/h), a medium site (ambient dose rate from 0.3 to 0.97 μSv/h) and a high site (ambient dose rate from 0.91 to 2.46 μSv/h).

Field Site (Nearest Village)	Site Location (Latitude and Longitude)	Mean Dose Rate (μSv/h)	Mean Needles ^{137}Cs Specific Activity (Bq/g)
High (Staraja Zakruzza)	52 39' 20.67'N 31 29' 52.54'E	2.03 +/- 0.32 (n=50)	11.78 +/- 10.33 (n=50)
Medium (Novilovka)	52 49' 18.04'N 31 6' 16.27'E	1.07 +/- 0.36 (n=50)	4.56 +/- 4.21 (n=50)
Low (Stolbunskaya)	52 50' 2.77'N 31 27' 32.46'E	0.14 +/- 0.03 (n=15)	1.68 +/- 1.60 (n=15)

n = number of trees.

Table 5.1: Site designation, location and mean dose rate at 1m above ground (+/- 1SD) and mean needle specific activity (+/- 1SD).

At the high and medium sites, 50 trees were randomly sampled, whilst 15 were randomly sampled at the low (control) site. This was due to the main interest being in the high and medium sites and a restriction upon time in the field. The value of 50 trees was settled on through a combination of what was logistically possible in the field and the number required for confidence in statistical analysis methods. Randomly chosen trees each had north, south, east and west facing branches collected to avoid introducing any bias from different growing conditions. Branches were also collected at different heights from each tree, again to minimise any bias from differing growing conditions. Mean height of the trees was 19m whilst the mean girth at chest height was 89cm. In terms of stand position, trees from the edge of the forest as well as within were sampled to maintain a representative set of data. At this point, since the work was investigating effects of ^{137}Cs at the leaf scale, regard for spatial resolution of imaging spectrometers was not taken into consideration. Rather, a variety of trees from across the site were collected. In terms of imaging spectrometry new growth needles (since this is predominantly what the sensor would monitor) were collected. Whilst old growth needles may be important at certain times of year (seasonality) the pilot study and imagery were all collected during the new growth summer period hence the focus was upon new growth needles. After harvesting branches, needles were removed and retained in a dark coolbox in preparation for

biochemical, gamma spectrometry and spectral analysis which was performed using the instrumentation and methodologies described in chapter three.

Before moving into the main sections of the chapter, it is necessary to note basic variation in foliar biochemistry and ^{137}Cs data illustrated through basic statistical summaries. This achieved three simple objectives:

- To establish if variability between foliar biochemicals exists, as without these variations, changes in spectral reflectance may not be detectable.

- To examine variability of ^{137}Cs, as without this, there will be no changes in ^{137}Cs levels to detect using imaging spectrometry.

- To determine if any interrelationships exist between the foliar biochemicals.

Biochemical and ^{137}Cs statistical summaries are shown in table 5.2, with intercorrelations of biochemicals shown in table 5.3. It is pertinent to note that the number of nitrogen samples assayed was reduced in relation to other foliar biochemicals. This was due to lack of suitable pre-processed needle material after an interruption in post-fieldwork processing in Belarus because of political reasons (appendix A3).

	Water Concentration (%)	AD Fibre Concentration (%)	Lignin Concentration (%)	Cellulose Concentration (%)	^{15}N Concentration (%)
Mean	64.14	41.60	17.78	24.18	-3.94
StDev	4.62	6.11	7.52	3.26	1.91
Coefficient of Variance (%)	7.21	14.69	42.29	13.47	-48.48
Number of Samples	112	112	112	112	59
Min	37.27	33.57	10.17	13.89	-7.20
Median	64.34	39.83	14.35	24.58	-4.33
Max	85.99	58.67	38.02	30.14	1.41
	Chl *a* (mg/g)	**Chl *b* (mg/g)**	**Total Chl (mg/g)**	**Elemental N Concentration (%)**	**^{137}Cs Specific Needle Activity (Bq/g)**
Mean	0.73	0.29	1.02	1.44	6.94
StDev	0.12	0.06	0.18	0.11	7.77
Coefficient of Variance (%)	15.88	21.45	17.30	7.67	111.86
Number of Samples	116	116	116	59	114
Min	0.44	0.16	0.61	1.18	0.07
Median	0.73	0.29	1.02	1.45	3.86
Max	1.14	0.54	1.69	1.69	39.89

Table 5.2: Descriptive statistics of biochemical data. Note the high coefficient of variance for ^{137}Cs specific needle activity. This is due to the high variability of ^{137}Cs both across each site and between each site.

Maximum and minimum values as well as the coefficient of variance indicate that there is variance in each biochemical, which is key for detecting changes in spectral response. As expected, the greatest variance is in ^{137}Cs and this indicates that imaging spectrometry might be used to monitor variation in foliar biochemicals to ultimately ascertain ^{137}Cs contamination. Aside from ^{137}Cs variance, the greatest relative variance is ^{15}N concentration. This is followed in order by lignin, chlorophyll *b*, total chlorophyll, chlorophyll *a*, AD fibre, cellulose, elemental nitrogen and water.

	A:	*B:*	*C:*	*D:*	*E:*
A: Water	**1.00**	**0.26**	**0.26**	0.16	-0.03
B: AD Fibre	**0.26**	**1.00**	**0.79**	**0.84**	0.13
C: Lignin	**0.26**	**0.79**	**1.00**	**0.36**	0.04
D: Cellulose	0.16	**0.84**	**0.36**	**1.00**	0.19
E: Chl *a*	-0.03	0.13	0.04	0.19	**1.00**
F: Chl *b*	-0.19	0.04	-0.04	0.12	**0.94**
G: Total Chl	-0.09	0.10	0.01	0.17	**0.99**
H: Elemental N	-0.06	**-0.33**	-0.13	**-0.36**	0.18
I: ^{15}N	**-0.40**	**-0.46**	**-0.45**	**-0.34**	**-0.27**
J: ^{137}Cs	0.05	0.19	0.08	**0.22**	-0.11

	F:	**G:**	**H:**	**I:**	**J:**
A: Water	-0.19	-0.09	-0.06	**-0.40**	0.05
B: AD Fibre	0.04	0.10	**-0.33**	**-0.46**	0.19
C: Lignin	-0.04	0.01	-0.13	**-0.45**	0.08
D: Cellulose	0.12	0.17	**-0.36**	**-0.34**	**0.22**
E: Chl *a*	**0.94**	**0.99**	0.18	**-0.27**	-0.11
F: Chl *b*	**1.00**	**0.97**	0.22	-0.15	-0.10
G: Total Chl	**0.97**	**1.00**	0.20	-0.23	-0.11
H: Elemental N	0.22	0.20	**1.00**	0.05	-0.15
I: ^{15}N	-0.15	**-0.23**	0.05	**1.00**	**-0.39**
J: ^{137}Cs	-0.10	-0.11	-0.15	**-0.39**	**1.00**

Table 5.3: Intercorrelation between foliar biochemicals and ^{137}Cs. Data are normally distributed. Bold denotes statistically significant correlation at the 95% confidence interval.

Table 5.3 shows that strong correlations exist between similar biochemical data (e.g. the three forms of chlorophyll). This is to be expected given the methods used to assay these biochemicals (chapter three). Greatest correlation with ^{137}Cs is between ^{15}N. This is followed in order by cellulose, AD fibre, elemental nitrogen, chlorophyll *a*, total chlorophyll, chlorophyll *b*, lignin and finally water. This interrelationship between foliar biochemicals and ^{137}Cs is promising in using spectra to monitor changes in ^{137}Cs via variability in key foliar biochemicals. The chapter now continues to assess these relationships in greater detail in order to achieve the objectives set out in chapter one and reiterated at the beginning of this chapter.

5.3 Assessing Whether Significant Differences Exist Between Spectra Contaminated with High and Low Levels of ^{137}Cs

Spectra were collected using the ASD FiedSpec Pro radiometer and statistically transformed using first derivative and continuum-removal techniques according to the methods described in chapter three. The spectra were split up into one of two groups

according to their ^{137}Cs content. Two activity groupings were chosen, the first using the domestic fuel wood limit (0.74Bq/g) as a cut off between high and low contamination levels and the second group utilising the lumber fuel wood limit (1.85Bq/g) imposed by the Belarusian authorities on use of lumber wood.

The first logical step in the research was to see if any differences existed between spectra grouped according to contamination levels. Differences were expected, since pilot work in chapter four suggested variance existed between spectra partitioned according to ^{137}Cs specific needle activity. In the first instance a two-tailed Student's t-test was performed on first derivative spectra to see whether any statistically significant differences existed between those spectra grouped into high and low ^{137}Cs contamination according to the levels described above as well as ascertaining where in the spectrum any such differences existed. The two-tailed Student's t-test was performed on normally distributed first derivative spectra as this contained all spectral information. Feature selection using continuum removal is useful for analysing absorption features with regards to prediction of biochemicals (section 5.6) but before data reduction, the whole spectral reflectance was assessed for significant differences. Figures 5.3 and 5.4 show the results of a Student's t-test using the domestic fuel wood (0.74Bq/g) and lumber wood limit (1.85Bq/g) to split the spectra into high and low groups. Only significant t-values (at the 95% confidence level) are shown.

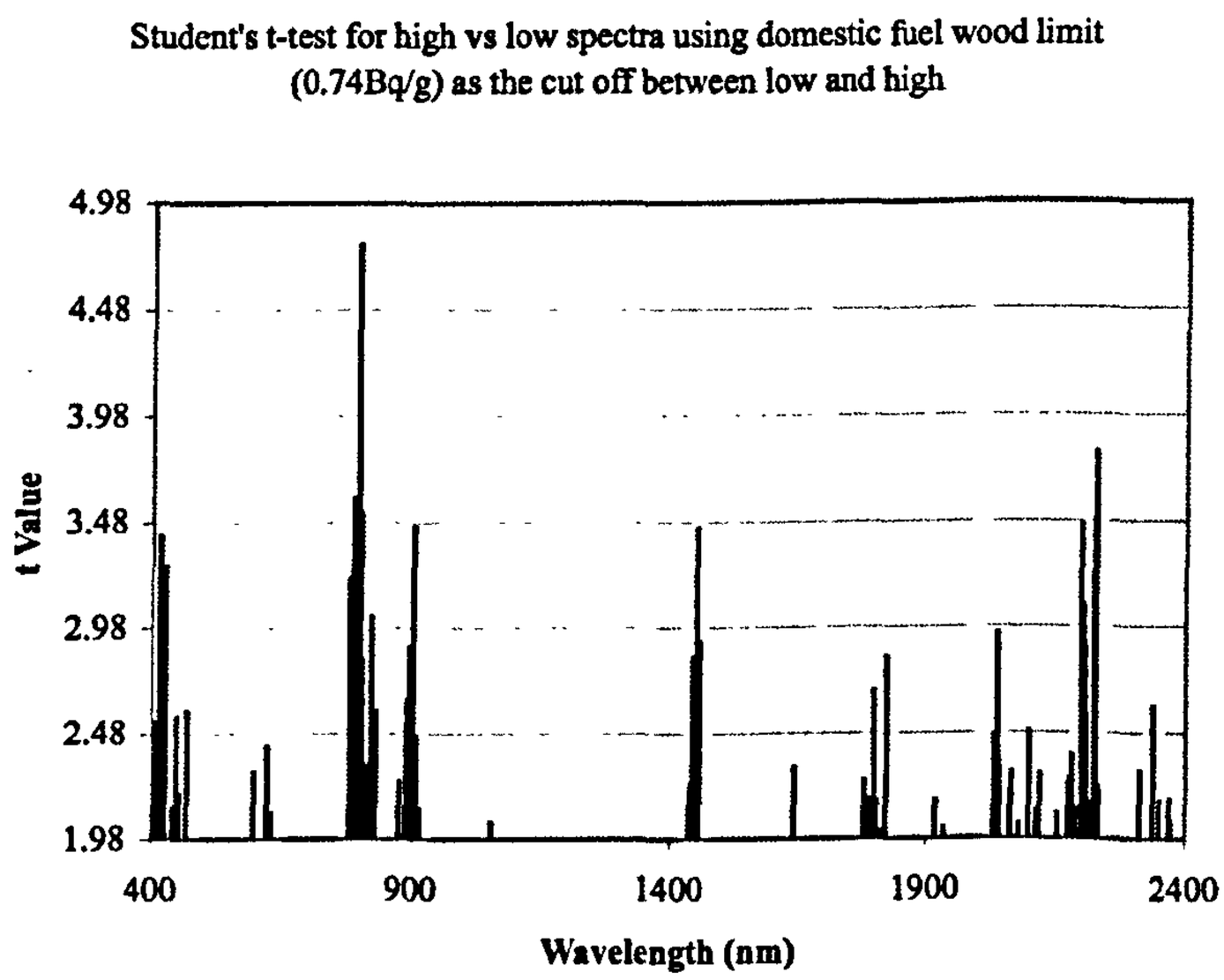

Figure 5.3: Student's t-test for high versus low spectra using the domestic fuel wood limit as a cut off point between low and high ^{137}Cs levels. Data are normally distributed.

Using the domestic fuel wood limit as a cut off point, there are statistically significant differences across the 400-2400nm range of the electromagnetic spectrum. This corroborates pilot work outlined in chapter three which signified that differences existed between spectra partitioned by ^{137}Cs content. This is a promising and fundamental result in the research, as without these differences between spectra, the use of remote sensing techniques to monitor ^{137}Cs is precluded.

The highest t-value is at 795nm and associated with the far shoulder of the red edge portion of the electromagnetic spectrum. This is followed by 2227nm, associated in the literature with cellulose and other sugars and starches (Curran, 1989) then by 902nm which is associated with plant proteins, then by 1451nm which is controlled by starches, sugars and lignin. At this stage it is fruitless to mention all wavelengths highlighted by the t-test as the main purpose is to check the spectra for differences. As stated above, the key aspect of this result is that it shows there is a statistically significant difference between spectra containing different levels of ^{137}Cs. It shows some of the wavelengths exhibiting difference are in regions of the spectrum known to be associated with certain foliar biochemicals (chapter two, table 2.1) however, before causality between foliar biochemicals and spectra can be investigated it is necessary to see if there is also a statistically significant difference between foliar biochemicals. This is to assess whether differences in spectra between varying levels of ^{137}Cs correspond to differences in foliar biochemicals and are not due to other factors affecting spectral response. Prior to looking at differences between foliar biochemicals the t-test results from spectra grouped according to the lumber fuel wood limit are discussed.

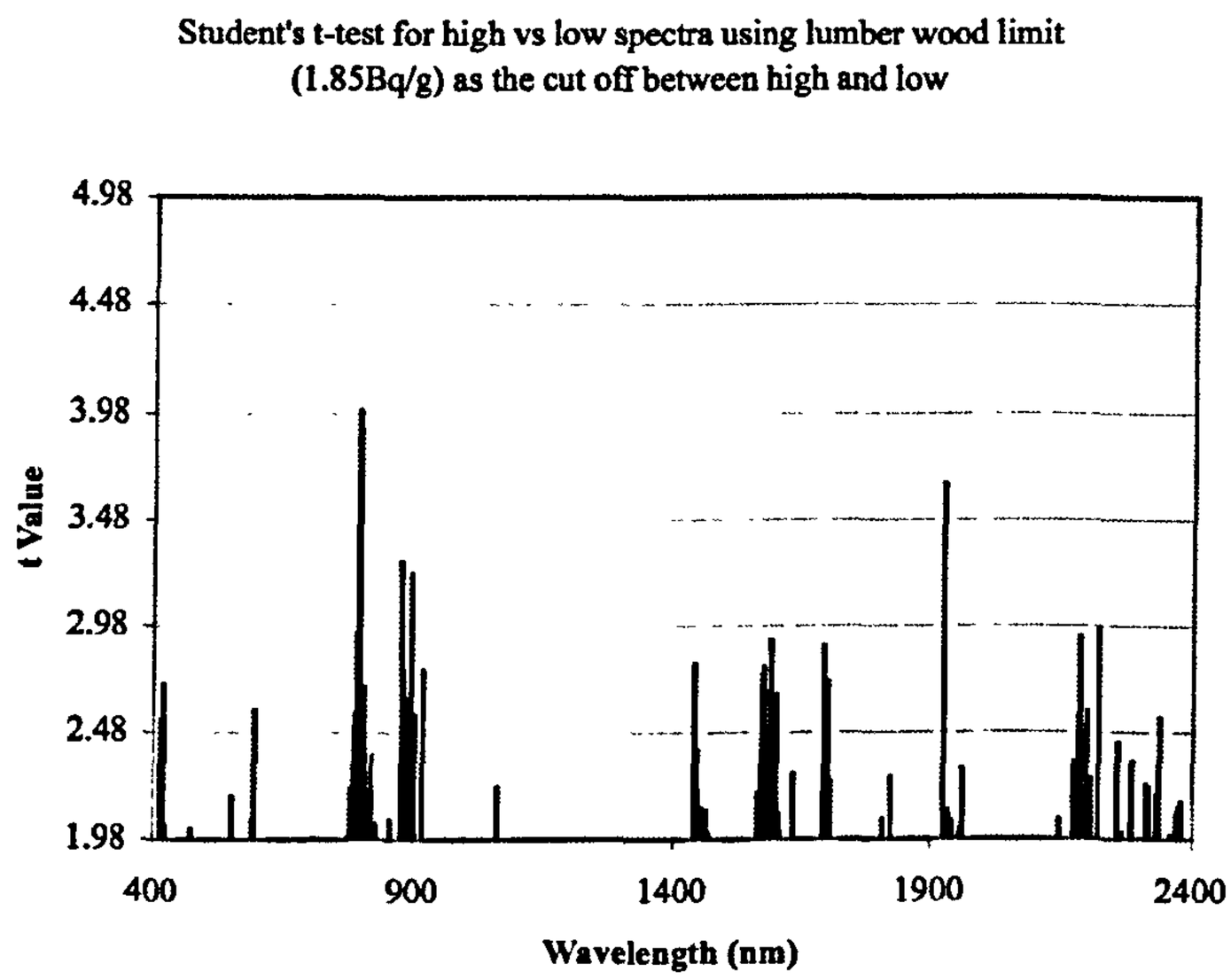

Figure 5.4: Student's t-test for high versus low spectra using the lumber limit as a cut off point between low and high ^{137}Cs levels.

In the lumber wood grouping there are also statistically significant differences across the spectrum, again showing promise in the utilisation of imaging spectrometry as a ^{137}Cs monitoring technique. The peak t-value is 794nm, again at the far end of the red edge shoulder. It is followed by 1926nm , an area of the spectrum controlled by oil according to the literature (Curran, 1989). In both the t-test using domestic fuel wood limits and the t-test using lumber wood limits, a similar pattern of statistically significant differences exist. From these t-tests the key result conveyed is that there are statistically significant differences between spectra from varying ^{137}Cs levels which is crucial for remote sensing since no difference between spectra would render imaging spectrometry incompatible with monitoring ^{137}Cs through the spectral response of vegetation.

Differences across the spectrum are in regions controlled by pigmentation/photosynthesis, structure (lignin/cellulose), nitrogen and water. It appears that ^{137}Cs may be having an effect on these key foliar biochemicals and in turn an effect across the spectrum. Before turning to correlation analysis, there is now a need to determine whether there are also statistically significant differences between key foliar biochemicals.

5.4 Assessing Differences between Key Foliar Biochemicals

Central to this research was the accurate determination of key foliar biochemicals and whether such biochemicals were affected by ^{137}Cs. Having seen in section 5.3 that there are statistically significant differences between spectra from *Pinus sylvestris* contaminated with relatively high and low levels of ^{137}Cs, the next step is to see if statistically significant differences also exist between key foliar biochemicals. Since spectral response is partly a manifestation of foliar biochemical content and the spectral response has shown significant differences (chapter four, chapter 5, section 5.3) it follows that statistically significant differences between foliar biochemicals would be observed. It was important to check that differences did exist (partly as a method to check reliability of instrumentation) and to ascertain which biochemicals ^{137}Cs may be impacting upon, and which parts of the spectrum this effect might be seen. Tables 5.4 and 5.5 show the results of two Student's t-tests between key foliar biochemicals. The Student's t-tests are for each grouping of contamination (domestic fuel wood and lumber limits).

Biochemical	*T-Value*
Water (n=21)	-0.52
AD Fibre (n=21)	1.00
Lignin (n=21)	**2.11[a]**
Cellulose (n=21)	**-3.12[b]**
Chlorophyll *a* (n=21)	-0.35
Chlorophyll *b* (n=21)	-0.74
Total Chlorophyll (n=21)	-0.49
Elemental N (n=10)	**2.11[a]**
^{15}N (n=10)	1.80
^{137}Cs (n=21)	**-6.52[b]**

Table 5.4: T-test between biochemicals which have been split up according to the domestic fuel wood limit (0.74Bq/g). Bold denotes t-value is indicative of a statistically significant difference. Superscript a or b indicate 95% and 99% confidence limits respectively.

The domestic fuel wood limit grouping shows lignin, cellulose, elemental nitrogen and ^{137}Cs to have a statistically significant difference between high and low groups. At the 99% confidence interval cellulose and ^{137}Cs exhibit statistically significant differences. It would be expected that ^{137}Cs shows statistically significant differences as the groups have been organised by the level of ^{137}Cs and if performed correctly, the Student's t-test should show this difference. In essence the ^{137}Cs t-value provides a form of benchmark to add

confidence to the results obtained for other biochemicals. Despite the spectra showing statistically significant differences in regions shown to be associated with chlorophyll content (section 5.3, figures 5.3 and 5.4) the t-test on the biochemicals has not shown a significant difference between any of the chlorophylls, thus suggesting ^{137}Cs may not be having a detectable effect on measured chlorophyll content, or is somehow indirectly affecting the red edge portion of the spectrum, but this does not manifest itself in measured differences in chlorophyll content. Red edge position was calculated for each sample using linear interpolation but there was no statistically significant difference between red edge positions. This may be through the causal relationship that exists between the foliar biochemicals, as described in the literature (e.g. Mutanga and Skidmore 2004) and shown through the inter-correlation of biochemistry in the descriptive statistics (section 5.2).

Biochemical	*T-Value*
Water (n=41)	-0.04
AD Fibre (n=41)	**2.63** [b]
Lignin (n=41)	**3.04** [b]
Cellulose (n=41)	**-2.17** [a]
Chlorophyll *a* (n=41)	0.08
Chlorophyll *b* (n=41)	-0.39
Total Chlorophyll (n=41)	-0.09
Elemental N (n=19)	**2.01** [a]
^{15}N (n=19)	**3.99** [b]
^{137}Cs (n=41)	**-7.72** [b]

Table 5.5: T-test between biochemicals which have been split up according to the lumber wood limit (1.85Bq/g). Bold denotes t-value is indicative of a statistically significant difference. Superscript a or b indicate 95% and 99% confidence limits respectively.

In the t-test performed using the lumber wood limit as the cut off point, structural components (AD fibre, lignin and cellulose) as well as the two types of nitrogen (^{15}N and elemental nitrogen) are highlighted as having statistically significant differences between the two groups. Once more ^{137}Cs is shown as having statistically significant differences at the 99% confidence interval which again, would be expected given the way the biochemicals have been grouped according to ^{137}Cs level. With this grouping having a higher level of ^{137}Cs content as the cut off between high and low, there are additional biochemicals which show as being significantly different. In addition, some of the confidence levels for the biochemicals change. ^{15}N and AD fibre have been highlighted as showing significant differences. ^{15}N is significant at the 99% confidence interval, whilst cellulose and lignin have reversed their confidence intervals in this grouping with lignin

having a 99% confidence interval and cellulose lowering to a 95% interval. Elemental nitrogen has reduced to a 95% confidence interval whilst AD fibre is significant at the 99% confidence interval. This finding is reinforced by literature suggesting nitrogen and lignin are affected by ^{137}Cs (e.g. Willey and Tang 2006, Mykhaylo *et al.* 2005).

Whilst the Student's t-test has exposed biochemicals that are significantly different between high and low contamination groupings, it has not identified whether the difference is due to ^{137}Cs or at which parts of the spectrum ^{137}Cs is having an impact on such biochemicals. To determine ^{137}Cs impact on biochemicals and to ascertain which parts of the spectrum may be affected, the technique of partial correlation was employed.

5.5 Partial Correlations to Determine ^{137}Cs effects on Foliar Biochemicals

As with the Student's t-test, partial correlation made use of first derivative spectra. This was again to make full use of the spectral data and not reduce spectral information though feature selection, which may lead to effects of ^{137}Cs on foliar biochemistry and spectra being undiscovered. Partial correlation is a type of correlation analysis which measures the correlation coefficient between two variables, whilst holding the effects of a third variable constant (Nelson 1998). In essence, a third variable or effect is partialled out to ascertain what the correlation coefficient would be without the interference of the third variable. Figure 5.5 shows the conceptual basis for partial correlation and illustrates that three variables, x, y, and z may each be correlated with one another, but that there is an area where the relationship between each individual variable and another may be affected by the third variable. This area is coloured red in figure 5.5 and is the portion of the relationship which partial correlation attempts to isolate in order to see the relationship between two variables without the influence of the third. Raw, or standard Pearson correlation is known as zero order correlation while the correlation coefficient between two variables whilst holding the effects of a third constant is known as first order partial correlation. It is also possible to calculate second, third and higher orders of partial correlation whereby a number of effects are partialled out from the correlation coefficient. In this research, first order partial correlation was used to isolate the effect of ^{137}Cs on each key foliar biochemical. The correlation analysis was between each of the key foliar biochemicals at every wavelength whilst holding the effect of ^{137}Cs constant (see figure 5.5 caption). All samples were included in the partial correlation as the aim was to see if ^{137}Cs

level had an effect on biochemicals and at what wavelength. Equation 5.1 shows how the partial correlation coefficient was calculated for each biochemical.

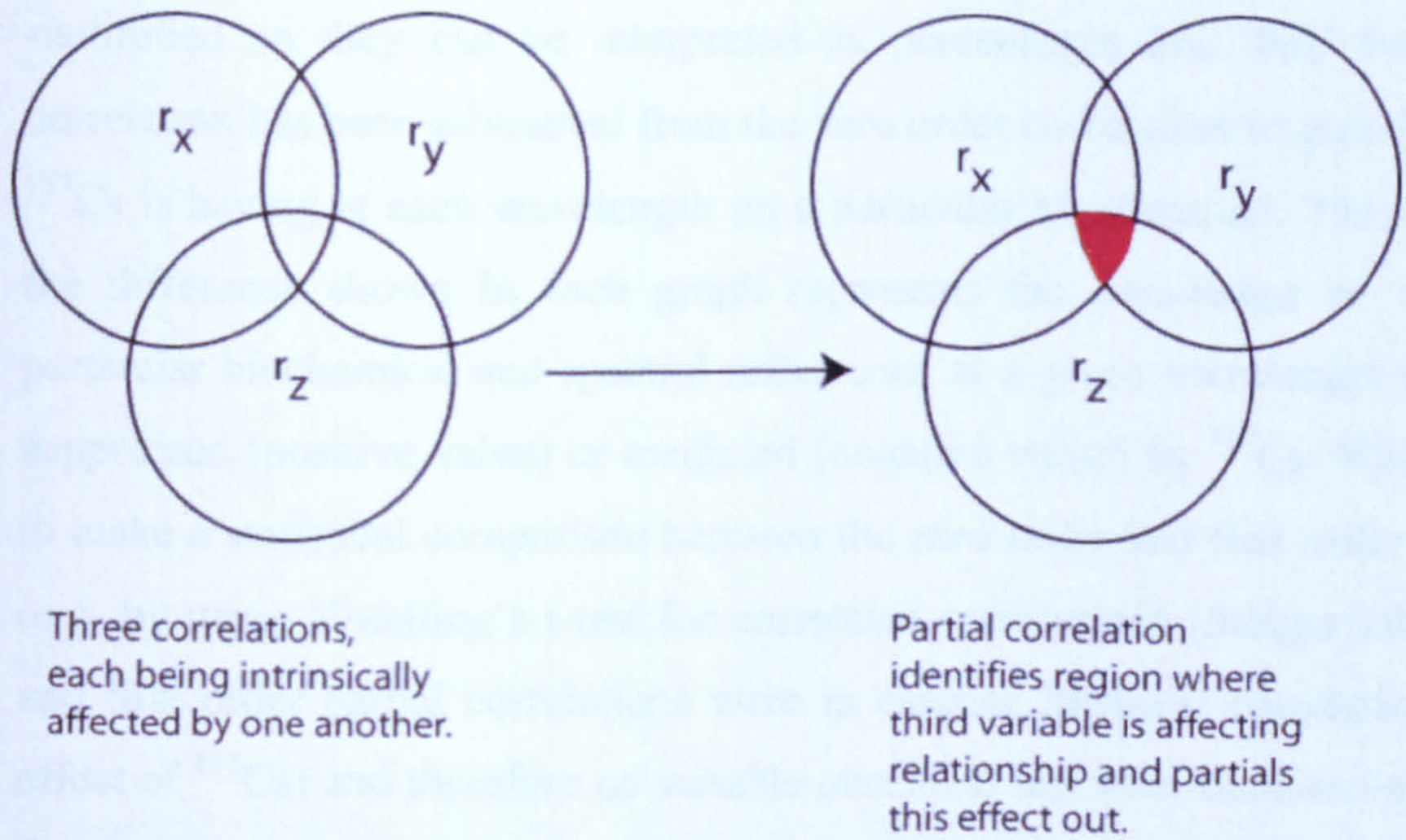

Figure 5.5: Partial correlation partials out the effect of a third variable (shaded red) on the correlation coefficient (relationship) between two variables. At each wavelength, the three partial correlation variables are, 1. correlation between spectral reflectance and foliar biochemistry 2. correlation between spectral reflectance and ^{137}Cs 3. correlation between ^{137}Cs and foliar biochemistry.

Interpretation of partial correlation results hinges on how different the partial correlation coefficient is from the original zero order correlation. Essentially, the partial correlation can be one of three things when compared to the original zero order correlation:

- Identical (i.e. no change in correlation coefficient)
- The correlation coefficient increases
- The correlation coefficient decreases

If the correlation is identical, it can be assumed that the variable partialled out is having no effect on the relationship (correlation) between the other two variables. If it increases it can be assumed that the partialled variable is suppressing the relationship and if it decreases it can be assumed the partialled variable is mediating the relationship. Partial correlation therefore statistically uncovers whether the partialled variable is:

- having no effect on the relationship (variables are conditionally independent)
- is mediating the relationship (variables are conditionally dependent)
- is suppressing the relationship (variables are conditionally dependent)

The results of partial correlation analysis are presented here as the difference between zero and first order partial correlation where ^{137}Cs is the variable which has been partialled out. The correlation coefficients have been squared (coefficient of determination) and multiplied so they can be interpreted as percentages and then the first order partial correlation has been subtracted from the zero order correlation to give the percentage effect ^{137}Cs is having at each wavelength on a particular biochemical. The interpretation is that the difference shown in each graph represents the percentage of variance between a particular biochemical and spectral reflectance at a given wavelength that has been either suppressed (positive value) or mediated (negative value) by ^{137}Cs. Whilst it was desirable to make a statistical comparison between the zero order and first order partial correlations (e.g. by using Hotelling's t-test for correlated correlations (Steiger 1980)) the zero order and first order partial correlations were in essence identical correlations (aside from the effect of ^{137}Cs) and therefore no suitable statistical test was found to have existed. Making links to known absorption points by particular foliar biochemicals is undertaken, making use of table 2.1 (shown in chapter two).

$$r_{xyz} = \frac{(r_{xy})-(r_{xz})-(r_{yz})}{\sqrt{(1-r^2_{xz})}*\sqrt{(1-r^2_{yz})}} \qquad \text{[equation 5.1]}$$

Equation 5.1: Calculating first order partial correlations to account for the effect of ^{137}Cs on the relationship between spectral response and a particular foliar biochemical.

Figure 5.6 shows that there is very little (if any) difference between zero order and partial correlation for water. This adds validity to other results such as the t-tests for foliar biochemicals since they point to no difference between high and low contamination levels, thus also suggesting water and ^{137}Cs are not linked. This is a useful finding since it rules out stress from water and a link to ^{137}Cs. It also supports findings from the student's t-test on foliar biochemicals where it showed there was no statistically significant difference between water from relatively high and low contaminated *Pinus sylvestris* (section 5.4).

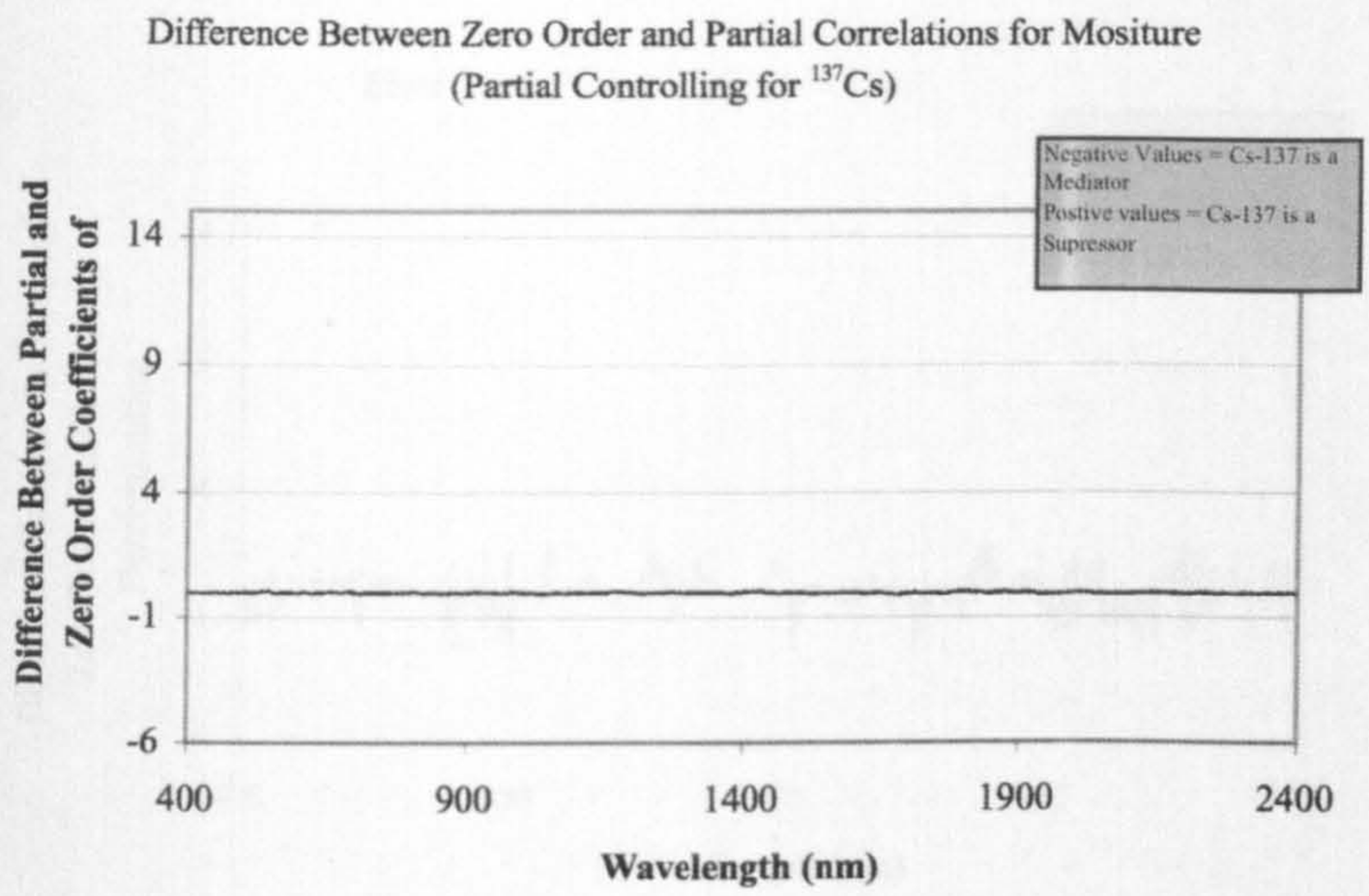

Figure 5.6: Difference between first order partial and zero order correlation at each wavelength with the effect of ^{137}Cs being partialled out of the relationship between spectral response and water.

Compared to water, there are some identifiable differences between zero and first order partial correlations for AD fibre (figure 5.7). At shorter wavelengths the difference is smallest and any differences seem to be negative, indicating ^{137}Cs is mediating the relationship at these wavelengths. The spectral bands where differences exist do seem to be related to absorption by structural components of vegetation, hence the pattern is as might be expected for AD fibre, which is a measure of the structural components of the *Pinus sylvestris* needles. It also exhibits a very similar pattern to the partial correlation results for lignin and cellulose which might be expected given that AD fibre, lignin and cellulose are all inherently linked through the methodology used to measure them (chapter three, section 3.3.7). This links to the foliar biochemical t-test result for the domestic fuel wood limit (section 5.4) which showed statistically significant differences between AD fibre split up according to ^{137}Cs contamination levels.

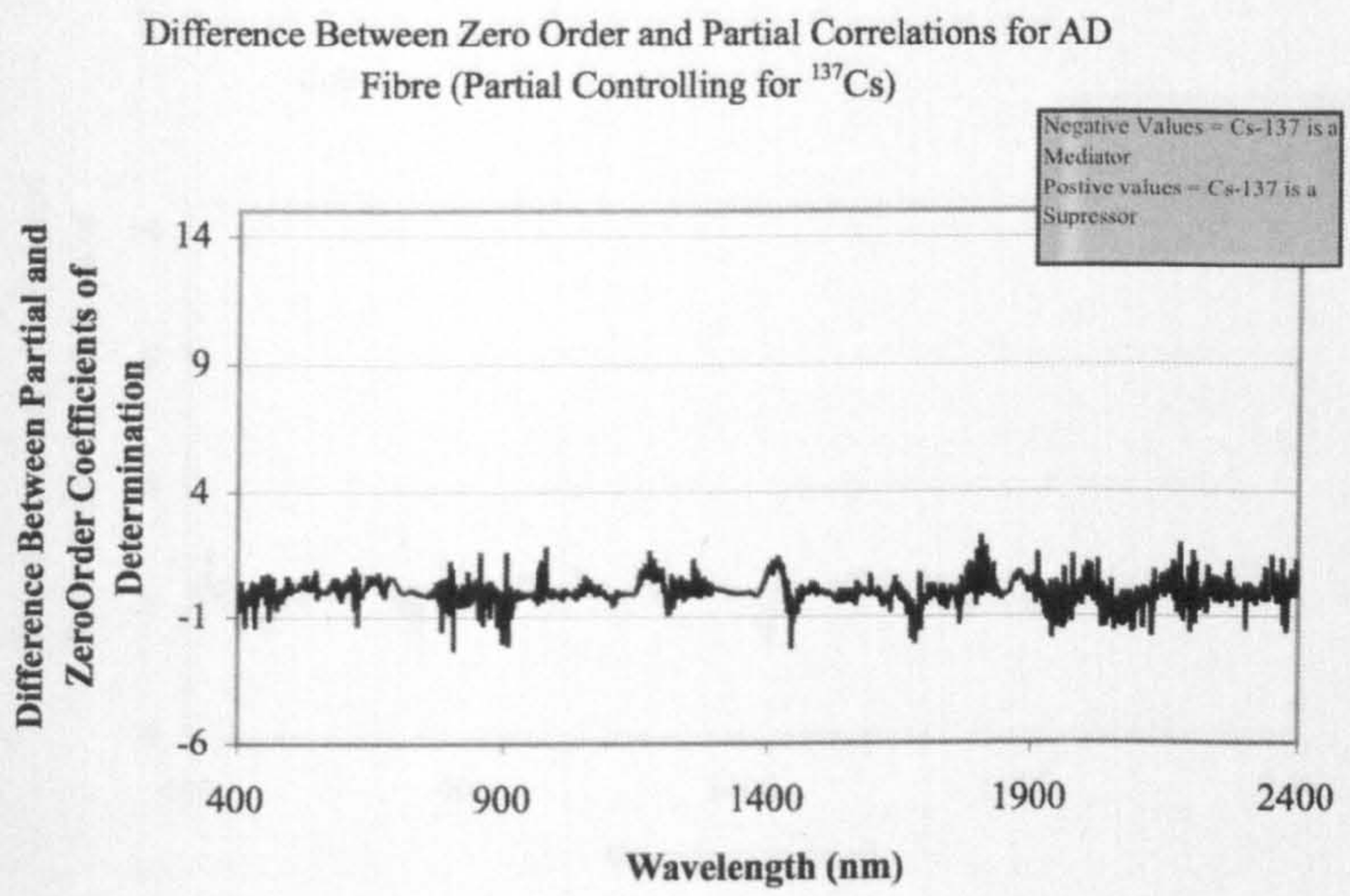

Figure 5.7: Difference between first order partial and zero order correlation at each wavelength with the effect of ^{137}Cs being partialled out of the relationship between spectral response and AD Fibre.

For cellulose (figure 5.8) differences are greater than for the chlorophylls (figures 5.10, 5.11 and 5.12), but not as large as the nitrogen differences (figures 5.13 and 5.14). The largest positive differences (suggesting ^{137}Cs is acting to suppress the relationship between cellulose and spectral reflectance) are at 439nm (associated with chlorophyll *a*), 1259nm (associated with water, cellulose, starch and lignin) and 2308nm (associated with oil). The largest negative differences, which suggest ^{137}Cs is mediating the correlation are at 540nm (associated with the accessory pigment phycoerythrobilin), 820nm, 1442nm (associated with starch, sugar, lignin and water) and 1816nm (associated with cellulose). Like the AD fibre result, the cellulose result is corroborated by the foliar biochemical t-test results which showed a statistically significant difference in both the lumber and domestic fuel wood groupings for cellulose.

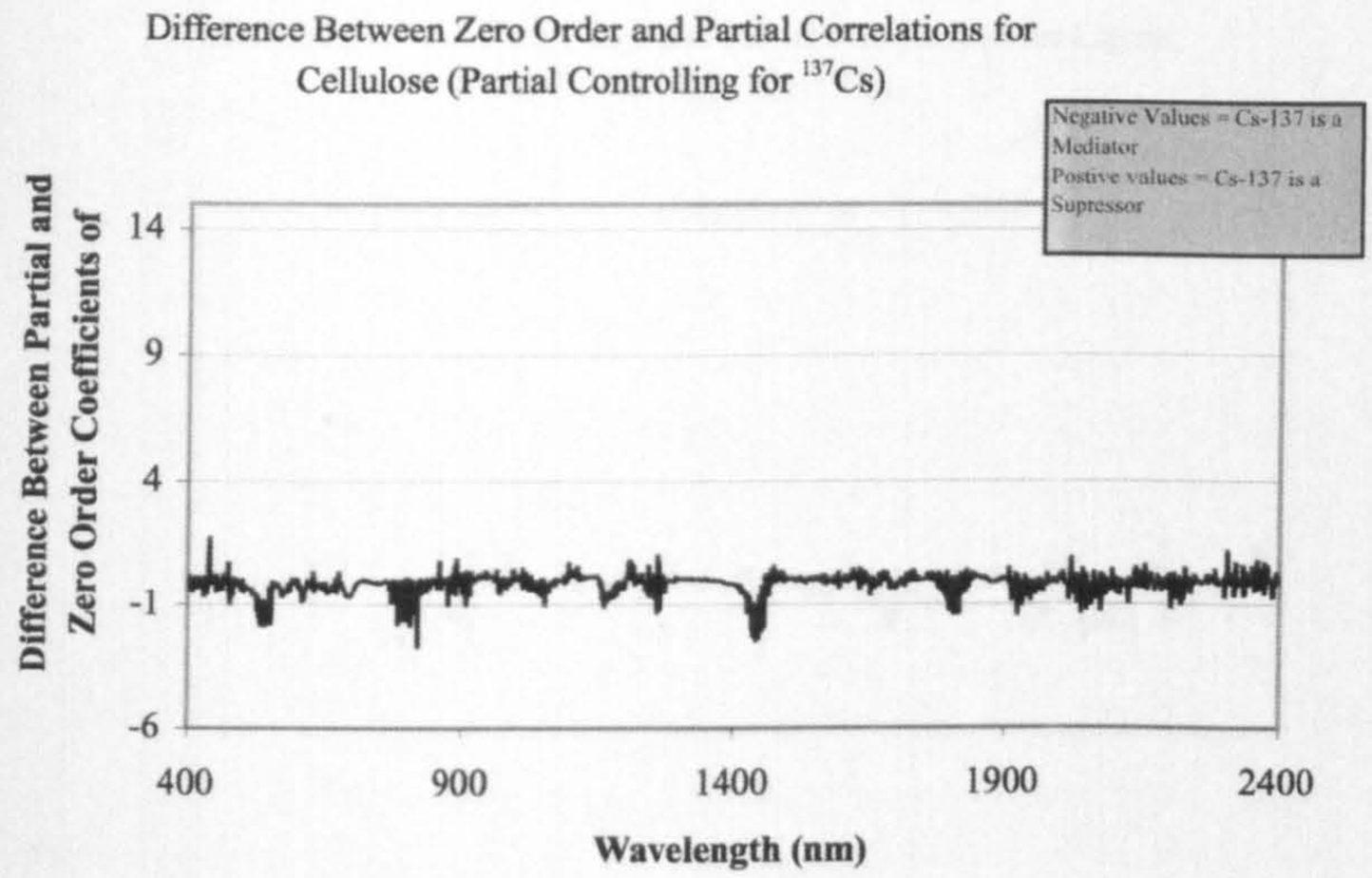

Figure 5.8: Difference between first order partial and zero order correlation at each wavelength with the effect of ^{137}Cs being partialled out of the relationship between spectral response and Cellulose.

Partial correlation results for lignin are shown in figure 5.9 and exhibit a similar pattern to cellulose, but with slightly greater differences, and some shifts in which wavelengths display a difference. The greatest positive differences occur at 439nm and 621nm (associated with chlorophyll), 857nm (associated with lignin), 906nm (associated with protein), 981nm (associated with starch), 1260nm and 2181nm (associated with protein and nitrogen). The largest negative values are at 807nm and 909nm (both associated with protein), 1445nm (associated with starch, sugar, lignin and water), 1682nm and 1942nm (associated with lignin), 2129nm and 2303nm (associated with protein). Many of these wavelengths highlighted by the partial correlation as having the relationship between spectral reflectance and lignin affected by ^{137}Cs are in areas of the spectrum associated with structural components of vegetation. So far, the results from the partial correlation have demonstrated that ^{137}Cs has very little (if any) effect on the relationship between water and spectral reflectance. The structural components (i.e. AD fibre, cellulose and lignin) do seem to have their relationships mediated or suppressed by ^{137}Cs at certain wavelengths which are associated with structural areas of the electromagnetic spectrum. These results also fit with the results of the foliar biochemical t-tests which demonstrate that there is no statistically significant difference between water based on groups of *Pinus sylvestris* spectra split up according to ^{137}Cs contamination level but that there are significant differences between the structural components.

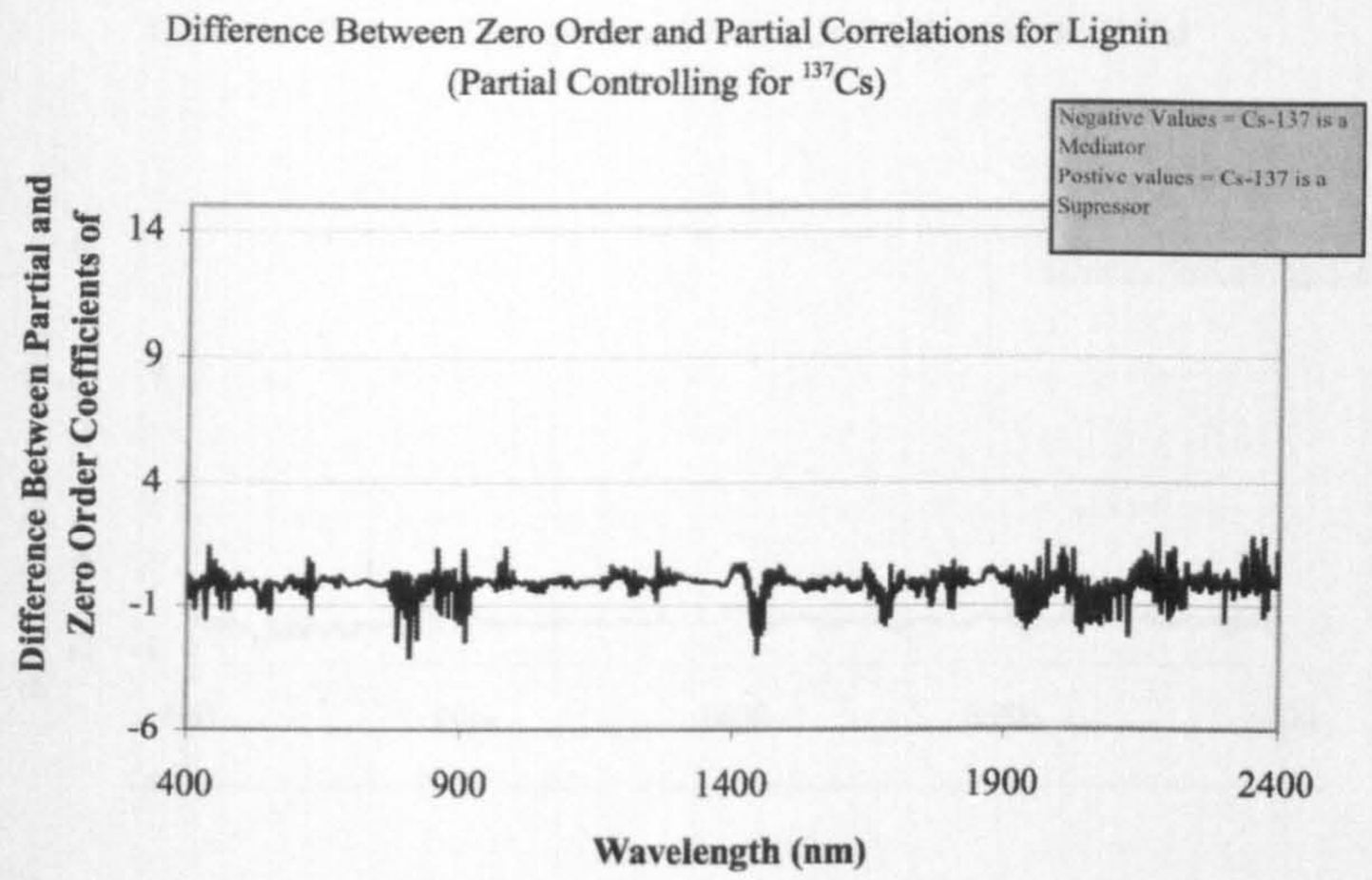

Figure 5.9: Difference between first order partial and zero order correlation at each wavelength with the effect of ^{137}Cs being partialled out of the relationship between spectral response and Lignin.

For total chlorophyll (figure 5.10) difference between zero order and partial correlation are very small and smaller than the differences shown by the structural biochemicals. The largest difference is negative at 540nm which is associated with the region of the spectrum controlled by pigmentation and suggests ^{137}Cs is slightly mediating correlation at this wavelength. The largest positive difference is at 849nm. Whilst the differences shown are small, the nosiest part of figure 5.10 is in the chlorophyll region which would be expected given that the partial correlation is attempting to isolate the effect ^{137}Cs is having on spectral reflectance and total chlorophyll concentration. Once again, the results from the partial correlation echo the biochemical t-test results which show that total chlorophyll is not significantly different between ^{137}Cs contamination levels.

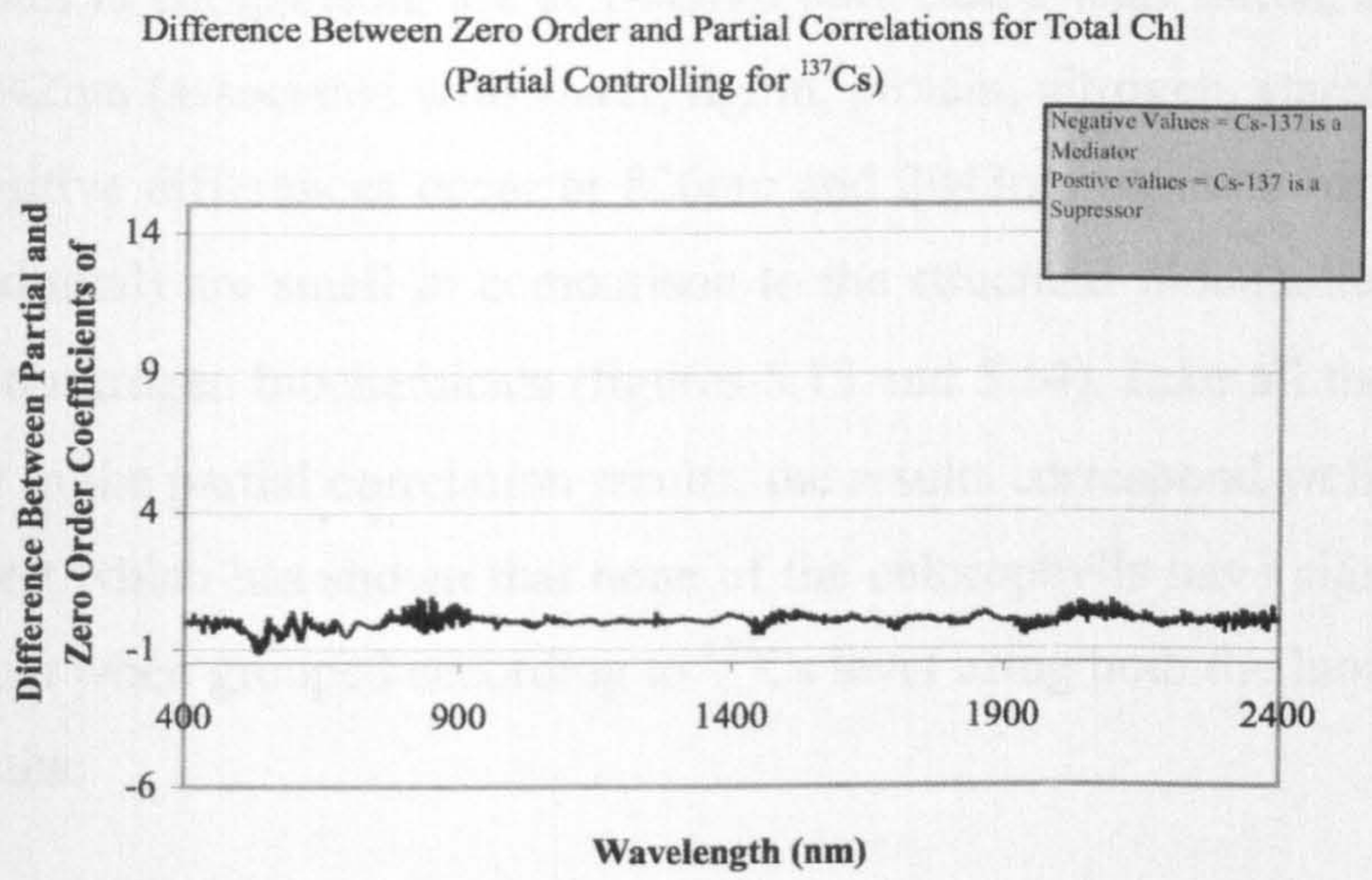

Figure 5.10: Difference between first order partial and zero order correlation at each wavelength with the effect of ^{137}Cs being partialled out of the relationship between spectral response and total Chlorophyll.

Results for chlorophyll *a* mirror the patterns in the results from total chlorophyll and chlorophyll *b* (figures 5.10 and 5.12). Differences between partial and zero order correlation are on the whole, slightly lower than for chlorophyll *b*. The greatest negative difference is identical to total chlorophyll and chlorophyll *b* and lies at 540nm whilst the greatest positive differences are at slightly longer wavelengths than chlorophyll *b* and are at 849nm and 2100nm (associated with starch and cellulose).

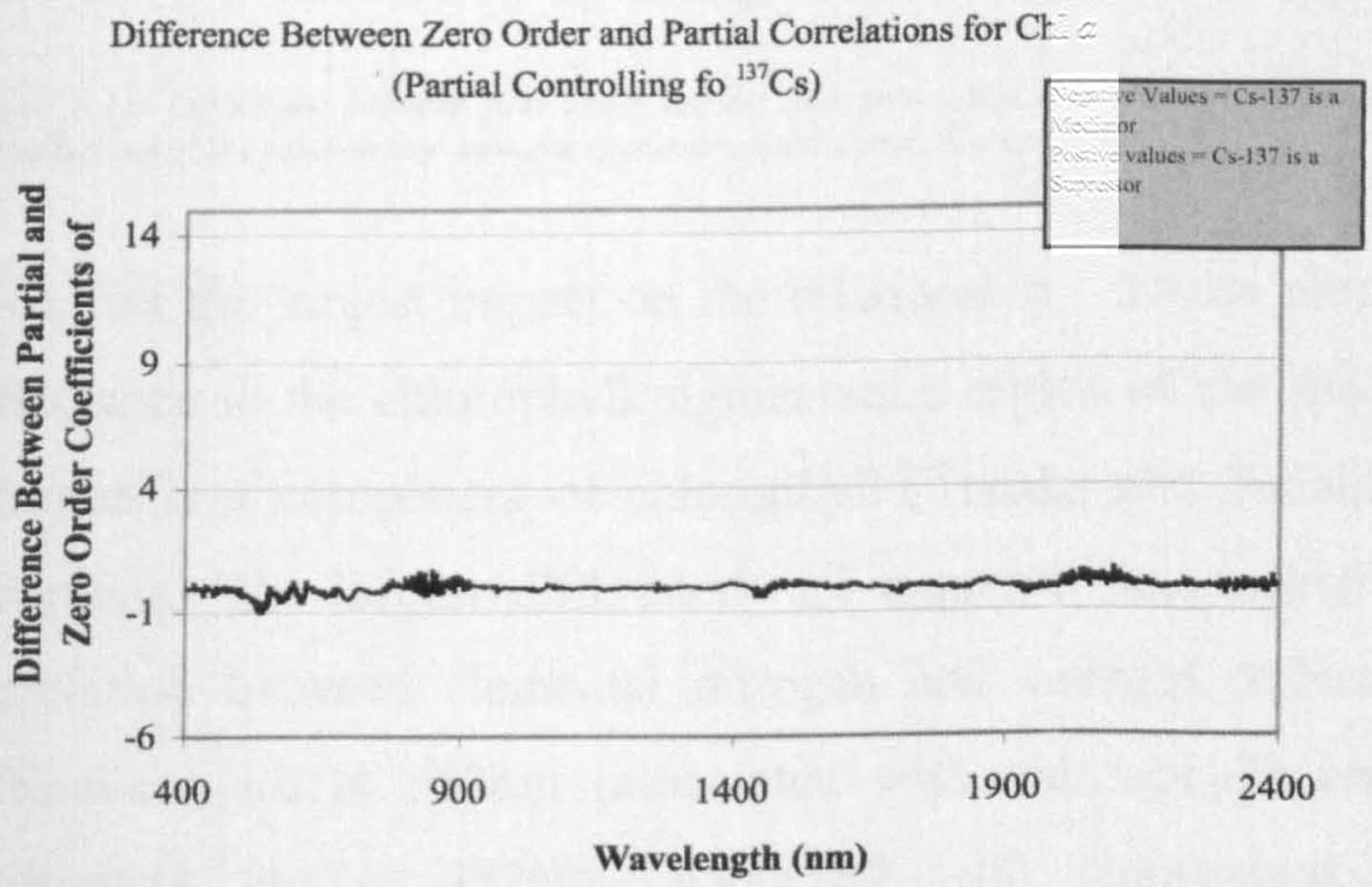

Figure 5.11: Difference between first order partial and zero order correlation at each wavelength with the effect of ^{137}Cs being partialled out of the relationship between spectral response and Chlorophyll a.

The largest difference for chlorophyll *b* is at 540nm and is associated with the accessory pigment phycoerythrobilin. This difference is still relatively small in comparison to the structural biochemicals and the two nitrogen isotopes. Other negative differences, again

small in comparison, are at 1445nm (associated with starch, sugar, lignin and water) and 1942nm (associated with water, lignin, protein, nitrogen, starch and cellulose). The largest positive differences occur at 826nm and 2043nm. Results for all three chlorophylls (*a*, *b* and total) are small in comparison to the structural biochemicals and the results from the two nitrogen biochemicals (figures 5.13 and 5.14). Like all the biochemicals discussed so far in the partial correlation results, the results correspond well with the foliar biochemical t-test which has shown that none of the chlorophylls have significant differences between them when grouped according to ^{137}Cs level using both the lumber and domestic fuel wood limits.

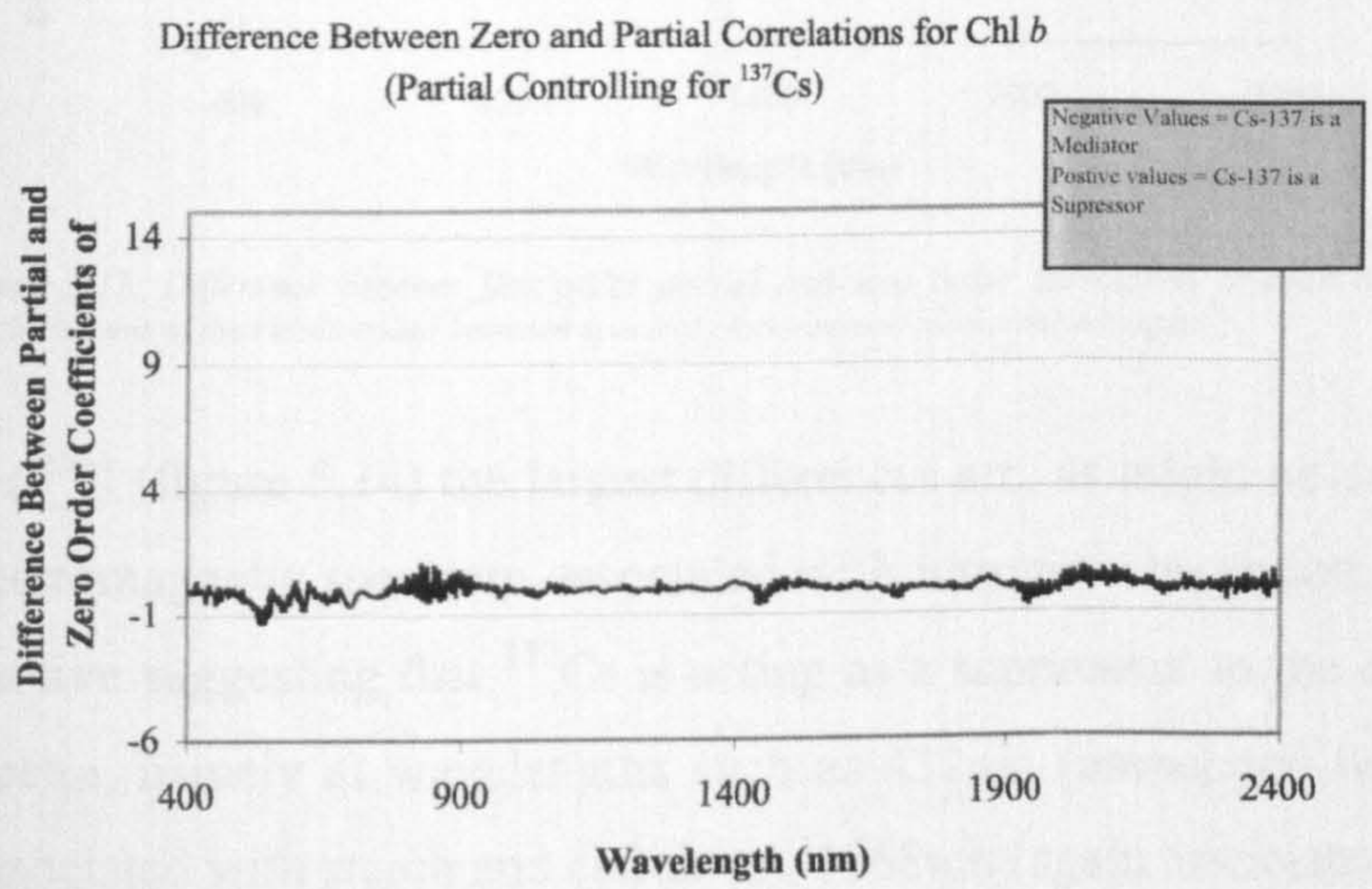

Figure 5.12: Difference between first order partial and zero order correlation at each wavelength with the effect of ^{137}Cs being partialled out of the relationship between spectral response and chlorophyll b.

^{137}Cs has the largest impact on the relationship between elemental nitrogen and spectral reflectance in the chlorophyll/pigmentation region of the spectrum. Given that elemental nitrogen is a component of chlorophyll (Tanaka and Tanaka 2006) this is perhaps not surprising. The largest differences are negative, suggesting ^{137}Cs is a mediator of the correlation between elemental nitrogen and spectral reflectance. The largest negative differences are at 552nm (associated with chlorophyll) and 794nm. Largest positive differences are at 437nm (associated with chlorophyll), 577nm (associated with chlorophyll), 1677nm (associated with protein, lignin, starch and nitrogen) and 2209nm (associated with protein). The differences are relatively larger than for water or the chlorophylls suggesting ^{137}Cs might be having an impact upon nitrogen and manifesting itself in spectral reflectance (discussed further in chapter eight, section 8.3). The foliar biochemical t-tests shown in section 5.4 indicate that there is a significant difference

between elemental nitrogen in both the lumber and domestic fuel wood ^{137}Cs groupings which seems to be reproduced in these partial correlation results.

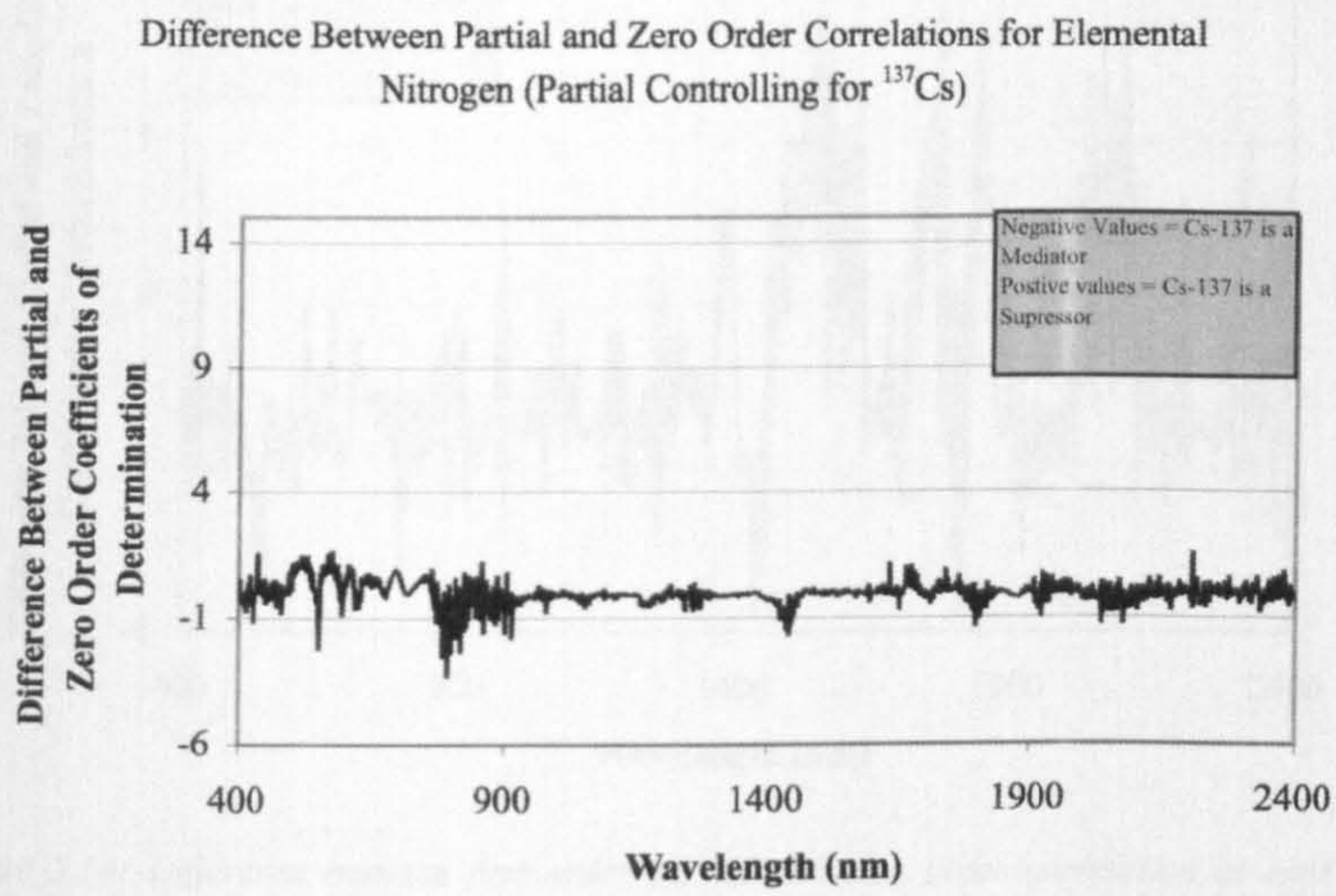

Figure 5.13: Difference between first order partial and zero order correlation at each wavelength with the effect of ^{137}Cs being partialled out of the relationship between spectral response and elemental nitrogen.

For ^{15}N (figure 5.14) the largest differences are, as might be expected, in the region of the electromagnetic spectrum associated with nitrogen absorption. The largest differences are positive suggesting that ^{137}Cs is acting as a suppressor to the correlation between ^{15}N and spectra, namely at wavelengths such as 432nm (associated with chlorophyll *a*), 1545nm (associated with starch and cellulose), 1768nm (again associated with cellulose and starch), 1846nm (associated with cellulose and starch), 2062nm (associated with nitrogen) and 2322nm (associated with starch). Negative differences suggest ^{137}Cs is mediating the correlations at 1436nm (associated with lignin and starch) and 1809nm (associated with cellulose). In comparison with all the other foliar biochemicals ^{15}N has a much greater difference between its zero order and partial correlations. In the foliar t-test domestic fuel wood grouping ^{15}N is not shown to have statistically significant differences yet in the lumber wood group is statistically significant at the 99% confidence interval. This suggests there may be a cut off point or certain level of ^{137}Cs required to have an effect on ^{15}N. The relatively large impact which ^{137}Cs appears to have upon the relationship between spectral reflectance and ^{15}N is interesting as there is evidence that ^{137}Cs uptake and nitrogen are linked (Willey and Tang, 2006).

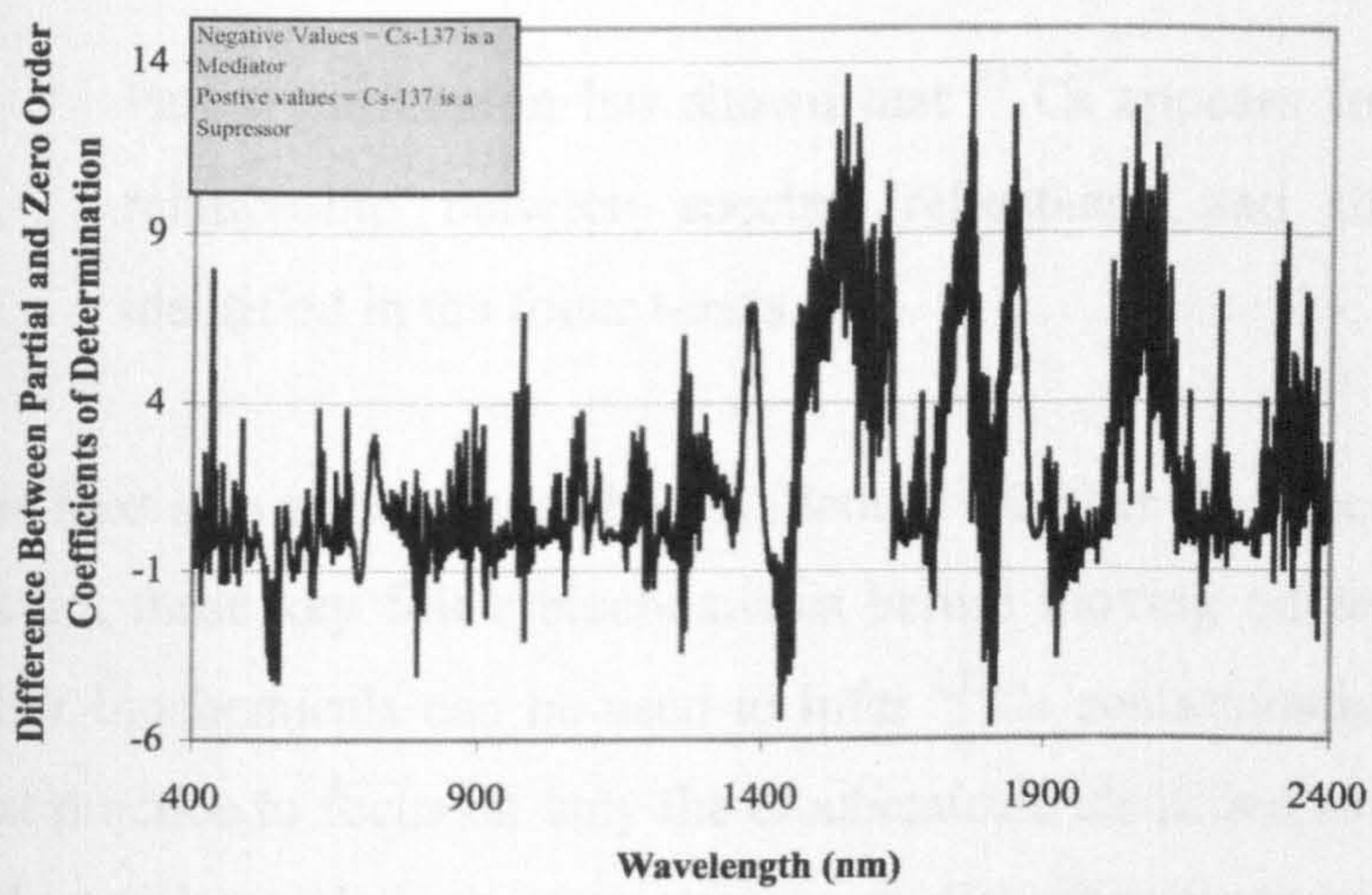

Figure 5.14: Difference between first order partial and zero order correlation at each wavelength with the effect of ^{137}Cs being partialled out of the relationship between spectral response and ^{15}N.

Partial correlation results have shown ^{137}Cs has very little impact on the correlation between water and the three chlorophylls. Water appears to be conditionally independent from ^{137}Cs. The structural biochemicals (AD fibre, cellulose, lignin) and two nitrogen isotopes have the largest differences between zero order and partial correlation with ^{15}N showing the largest differences of all biochemicals. The wavelengths where ^{137}Cs has any impact appear to be as expected in terms of where in the electromagnetic spectrum they lie in relation to the particular biochemical. The results also concur with the foliar t-test performed in section 5.4 where the biochemicals with a statistically significant difference were also the structural biochemicals and two nitrogen isotopes. Whilst correlation does not measure causation it remains a very good indicator of interactions between variables (Raghuraj-Rao and Lakshminarayanan 2007) hence the correlation combined with the Student's t-tests seem to so far indicate that:

- There are statistically significant differences between spectra from different contamination levels.

- There are statistically significant differences between some key foliar biochemicals, namely the structural biochemicals (AD fibre, lignin, cellulose) and

the two nitrogen isotopes (^{15}N, elemental nitrogen) which have been split up according to ^{137}Cs contamination levels.

- Partial correlation has shown that ^{137}Cs appears to be having an impact on the relationship between spectral reflectance and the same foliar biochemicals identified in the foliar t-tests.

The next step in the research is to identify whether the spectral reflectance can be used to predict these key foliar biochemicals before moving on to finally consider whether the foliar biochemicals can be used to infer ^{137}Cs contamination levels. Whilst it may seem best practice to focus on only the biochemicals identified as being significant in the t-tests and partial correlations, attempting to predict other biochemicals acts as a benchmark and helps to ascertain whether foliar biochemicals that are not conditionally independent from ^{137}Cs are harder to predict than those which are affected by ^{137}Cs.

5.6 Prediction of Foliar Biochemicals from Spectra

5.6.1 Stepwise Multiple Linear Regression

In the literature (chapter two) foliar biochemical absorption has been related to specific areas of the electromagnetic spectrum (e.g. Curran 1989) however absorption from different plant materials is similar and overlapping, meaning a single absorption band cannot always be isolated and directly related to a particular biochemical content (Kokaly and Clark 1999). This has resulted in the use of statistics in attempt to select spectral wavebands, which are causally and strongly related to biochemical content and which can in turn be used to predict foliar biochemical content (e.g. Jacquemoud *et al.* 1995, Kokaly and Clark 1999). This in turn would allow the possibility of predicting foliar biochemistry from imaging spectrometry and depending on the relationship between ^{137}Cs and foliar biochemicals may allow ^{137}Cs content to be determined from an image.

One such statistical technique which has been commonly used in the literature (e.g. Mutanga *et al.* 2005, Kokaly and Clark 1999, Jacquemoud *et al.* 1995, Curran *et al.* 2001) is stepwise multiple linear regression (SWMLR). SWMLR has its roots in laboratory based

near infrared spectroscopy (Barton 2002) and is often used by many laboratories in place of analytical chemical techniques when determining composition of dried ground vegetative samples (Williams and Norris 1987). The technique works by fitting an observed dependant variable (e.g. concentration of a particular foliar biochemical) using a linear set of independent variables (e.g. FDR at a number of discrete wavelengths) (Kokaly and Clark 1999). The process moves in a stepped fashion (hence its title) either entering or removing variables into the regression equation based on user-defined significance probabilities. Wavelengths most highly correlated with the dependent variable are added to a regression equation, the second wavelength is then added based on partial correlations with all other wavelengths and the wavelength with the highest partial correlation is added to the equation (Ourcival *et al.* 1999). The process continues until no further improvement in the R^2 value is made. Following the addition of each wavelength, every regressor is reassessed and may be added or removed depending on its contribution to the regression equation. The direction of the stepwise process can be forwards (where the regressors most improving the model's fit are brought in), backwards (where regressors which affect the regression fit the least are removed) and finally, mixed, which is a combination of forward and backward processes iterated until no more regressors can be entered or removed from the regression equation, again based upon the significance levels set by the user.

Stepwise regression is not without problems and one of its worst attributes is that it is known to overfit data, especially when the number of predictors is greater than the number of observations (Foster and Stine 2006). This is particularly so with applications of stepwise regression to spectroscopy since it is common for there to be many more predictors (i.e. wavelengths) than observations. Harrell (2006) goes on to describe several additional problems associated with the use of stepwise regression procedures, some of which are:

- It yields R^2 values which are biased towards being too high.
- It has problems in the presence of colinearity.
- It allows the analyst not to think about the problem.
- Models identified by stepwise procedures have a high likelihood of capitalising on chance features and often fail when applied to new datasets and are rarely tested this way.

Despite this, the technique is commonly used and several papers in the remote sensing domain demonstrate successful use of SWMLR in predicting foliar biochemicals (e.g. Jacquemoud *et al.* 1994, Curran 2001, Mutanga *et al.* 2004). Attempts were made to minimise these problems and were considered when analysing results.

In this research SWMLR was used to attempt prediction of each key foliar biochemical. ^{137}Cs was included as a biochemical in this analysis to see whether ^{137}Cs could be predicted directly from spectral reflectance. The procedure was undertaken using JMP 6 statistical software from SAS institute. Mixed stepwise regression was performed (a combination of forward and backward modes) and the entry and exit probabilities (f-values) for each variable were set at 0.15 according to levels recommended by Grossman *et al.* (1996). To check the predictive power of wavebands chosen by the procedure, a third of the data was held back from the regression procedure (according to Grossman *et al.* 1996) and used to test accuracy (see table 5.2 for number of samples). To verify that predictions were not spurious a randomised set of data was created from the original data by randomising the association between foliar biochemical and spectral response. Randomisation was conducted using a similar procedure to that described in Grossman *et al.* (1996) whereby a random set of numbers were generated and used as a sort key to randomise the order of the biochemicals. The randomised biochemicals were then assigned to the spectral data to create an artificial dataset which contained no real relationships between biochemical and spectral response. Stepwise regression was then performed on this randomised dataset to see how well it performed in comparison to the real dataset. This randomisation helped to avoid the pitfall identified by Harrell (2006) where stepwise regression capitalises on chance features in the data. The use of a training and testing dataset as well as the randomised dataset was undertaken in order to try to minimise some of the key problems associated with stepwise regression.

Table 5.6 shows the results from the stepwise regressions. All wavelengths have been used (i.e. stepwise regression was unconstrained) and the stepwise procedure has selected the most suitable wavelengths for the regression model. In each case the quantity of wavebands was not allowed to surpass one-fifth the number of observations to prevent overfitting (Thenkabail *et al.* 2004[a]). The stepwise procedure was performed on four transformations of the spectra (each described in chapter three); absolute reflectance, first derivative spectra (FDS) and the two continuum removed transformations, band depth

normalised-to-area (BDNA), and band depth normalised-to-centre (BNC). This was undertaken since Kokaly and Clark (1999) and Curran *et al.* (2001) show that continuum-removed reflectance is often able to predict certain biochemicals with a higher accuracy than absolute reflectance or first derivative spectra.

	Absolute Reflectance		**FDS**		**BDNA**		**BNC**	
Biochemical	Regression R^2	Validation R	Regression R^2	Validation R	Regression R^2	Validation R	Regression R^2	Validation R
Water	0.70[b]	0.60[b]	0.96[b]	0.58[b]	0.90[b]	0.52[b]	0.65[b]	**0.65[b]**
AD Fibre	0.77[b]	0.25	0.89[b]	0.04	0.49[b]	**0.39[a]**	0.29	0.21
Lignin	ns	ns	0.90[b]	0.21	0.45[b]	**0.52[b]**	0.66[b]	0.34[a]
Cellulose	ns	ns	0.91[b]	-0.06	0.67[b]	0.19	0.54[b]	**0.28**
Chl *a*	0.70[b]	0.51[b]	0.93[b]	0.49[b]	0.85[b]	0.38[a]	0.73[b]	**0.69[b]**
Chl *b*	0.84[b]	0.44[b]	0.95[b]	0.53[b]	0.92[b]	0.53[b]	0.79[b]	**0.68[b]**
Total Chl	0.79[b]	0.53[b]	0.94[b]	0.54[b]	0.93[b]	0.44[b]	0.68[b]	**0.70[b]**
Elemental N	0.34	0.13	0.86[b]	-0.12	0.61[b]	**0.30**	0.32	0.16
^{15}N	0.63[b]	**0.70[b]**	0.88[b]	0.42	0.71[b]	0.48[a]	0.62[b]	0.33
^{137}Cs	0.30	-0.11	0.91[b]	0.08	0.62[b]	**0.14**	0.58[b]	0.09

ns = no significant R^2 or R [a] = significant at 95% confidence [b] = significant at 99% confidence

Table 5.6: Results from unconstrained regressions on four transformations of the spectra. Bold type denotes the highest predictive power amongst the different spectral transformations.

The results shown in table 5.6 are organised according to the transformation of the spectra. Each transformation contains two columns. The first column shows the regression R^2 and illustrates the goodness of fit between the data and the regression model for the particular biochemical. The second column pertains to the validation of the regressions using the testing data set. The validation was performed on data excluded from the model creation and is the correlation coefficient between the actual excluded data and the values predicted for those excluded data by the regression model.

In terms of the regression R^2 value, stepwise regression performs well in most transformations of the spectra. FDS and BDNA have R^2 values statistically significant at the 99% confidence interval for every biochemical. This is followed by BNC which fails to model AD fibre or elemental nitrogen at statistically significant levels. Absolute reflectance is worst and fails to predict lignin, cellulose or elemental nitrogen. The biochemicals which are unable to be significantly predicted by BNC or absolute

reflectance are those that are shown to be conditionally dependent (i.e. affected by ^{137}Cs) in the partial correlations from section 5.4. This perhaps suggests that the effect of ^{137}Cs on some of the biochemicals makes their prediction more difficult. Interestingly FDS, BDNA and BNC are able to model ^{137}Cs content at a statistically significant level. At ^{137}Cs prediction, FDS performs best with an R^2 of 0.91 followed by BDNA and BNC. Looking solely at the ability of the stepwise procedure to model the data is however, flawed in two ways. These are both akin to problems suggested with the stepwise method described above. These two problems are:

- The model rarely fits other data (i.e. the model has power of description but not prediction).
- The analyst does not think about the problem.

To overcome these issues, the validation of the model using the testing data set was performed. This allowed the overall research problem to be thought about (i.e. that simply describing the data but not having predictive power was not enough for this study) and therefore the validation of the testing data allowed the true predictive power of the regression model to be realised. As a further failsafe, the randomised dataset results were compared to the real results.

Results for predictive power of the regression models are discussed for each biochemical as well as the presentation of the wavebands selected by the stepwise procedure for each regression model.

5.6.1.1 Water

For water, predictive power is relatively high in each transformation of the spectra. BNC performs best with an R value (correlation between predicted and actual value) of 0.65 whilst BDNA performs least well. Predictions from each transformation of the spectra are statistically significant at the 99% confidence interval. This is in contrast to results from the t-tests and partial correlations where water was not statistically significant and not identified as being impacted upon by ^{137}Cs. It implies that ^{137}Cs is not having an effect on water and in turn is not affecting the ability to predict it from spectral reflectance. Table

5.7 shows the wavelengths identified by SWMLR for the water model. Only wavelengths from the spectral transformation with the highest predictive power are shown, however full tables of selected wavelengths are available in the appendices.

Waveband Selected (nm)	Biochemical Association	R^2 (Descriptive Power)
1301	Unattributable	0.38
1427	Lignin	0.49
969	Water, starch	0.55
1426	Lignin	0.60
1470	Nitrogen/protein	0.61
1268	Cellulose	0.62
1270	Cellulose	0.63
1471	Nitrogen/protein	0.65

Table 5.7: BNC wavelengths selected by the stepwise procedure for use in the water regression model. Incremental changes in R^2 are shown based on the addition of each waveband.

The majority of wavelengths selected cannot be causally linked to water content. One band selected is within 1nm of the 970nm water absorption waveband. The majority of the other bands selected are associated with structural components of the plant. There are no wavebands selected at short wavelengths. This is unsurprising as the longer wavelengths are associated with water content. In short, whilst wavebands selected give a reasonable prediction accuracy of the testing data set, there is a lack of causality associated with the wavebands selected by the stepwise process.

5.6.1.2 AD Fibre

AD fibre has greatest predictive ability using BDNA with an R value of 0.39 (table 5.6). Whilst this is a lower accuracy than water it is significant at the 95% confidence interval. The two continuum-removed reflectances provide best predictive ability but only BDNA is able to predict in a statistically significant way. FDS has a high R^2 value indicating the model can describe existing data but fails when applied to new information. From a remote sensing perspective, predictive power is key to enable vegetation status (^{137}Cs) to be inferred.

Waveband Selected (nm)	Biochemical Association	R^2 (Descriptive Power)
2020	unattributable	0.18
904	protein	0.27
910	protein	0.36
960	Starch	0.44
964	Water, starch	0.47
956	Unattributable	0.49

Table 5.8: BDNA wavelengths selected by the stepwise procedure for use in the AD fibre regression model. Incremental changes in R^2 are shown based on the addition of each waveband.

Aside from one long wavelength at 2020nm, the majority of wavelengths selected are around 900nm and associated with protein and starch. These are wavelengths which might be expected for AD fibre. The first waveband (2020nm) which adds the greatest weight to the regression model is unattributable, again highlighting the inability to infer causality from model results. Unlike water, AD Fibre is shown in the partial correlations (section 5.5) to be conditionally dependent on ^{137}Cs and this may explain why predictive power for AD fibre is relatively low and is only statistically significant in one transformation of the spectra.

5.6.1.3 Cellulose

Cellulose is harder to predict than AD fibre with none of the spectral transformations giving statistically significant predictive power (table 5.6). Absolute reflectance fails to provide any significant model at all, whilst FDS, BDNA and BNC provide a decreasing descriptive ability respectively.

Waveband Selected (nm)	Biochemical Association	R^2 (Descriptive Power)
1440	Starch, sugar, lignin, water	0.24
1206	Water, cellulose, starch, lignin	0.38
2057	Protein, nitrogen	0.47
799	unattributable	0.54
2356	Cellulose, protein, nitrogen	0.60
2210	unattributable	0.65
1773	Cellulose, sugar, starch	0.69
2099	Starch, cellulose	0.72
2079	Sugar, starch	0.77
1789	Cellulose, sugar, starch	0.80
1765	lignin	0.83
2024	unattributable	0.86
1937	Water, lignin, protein, nitrogen, starch	0.88
434	Chlorophyll *a*	0.90
2342	cellulose	0.91

Table 5.9: FDS wavelengths selected by the stepwise procedure for use in the cellulose regression model. Incremental changes in R^2 are shown based on the addition of each waveband. Whilst the model has high descriptive ability in the form of an R^2 of 0.91, it cannot predict significantly when applied to the testing data.

The wavebands chosen for cellulose appear to be generally related to cellulose and its constituents (e.g. lignin, starch). Some of the wavebands are unattributable, again hampering inference of causality. In the foliar biochemical t-test (section 5.4) aside from ^{137}Cs, cellulose had the greatest t-value and was the only biochemical in the domestic fuel wood grouping to be significantly different at the 99% confidence interval. It is pertinent that this biochemical has not been able to be successfully predicted yet is statistically different based on ^{137}Cs contamination levels.

5.6.1.4 Lignin

Like cellulose, absolute reflectance is unable to provide any significant model when utilising absolute reflectance. FDS provides greatest descriptive power (table 5.6) with an R^2 of 0.90 but fails to predict when applied to testing datasets. The continuum-removed reflectances both provide statistically significant predictive ability, though BDNA is greatest with an R of 0.52. Whilst this is higher than AD fibre and better than cellulose (for

which there was no significant predictive ability) it is not as high as water, which has been shown to be conditionally independent of ^{137}Cs content.

Waveband Selected (nm)	Biochemical Association	R^2 (Descriptive Power)
2020	Unattributable	0.18
530	Chlorophyll	0.28
904	Protein	0.34
910	Protein	0.38
915	Protein	0.42
1466	Starch, sugar, lignin, water	0.45

Table 5.10: BDNA wavelengths selected by the stepwise procedure for use in the lignin regression model. Incremental changes in R^2 are shown based on the addition of each waveband.

5.6.1.5 Total Chlorophyll

Total chlorophyll was described and could predict at the 99% confidence interval for every transformation of the spectra. FDS had the highest descriptive ability but BNC had the greatest predictive ability when applied to the testing dataset, with an R value of 0.70 (table 5.6), the highest prediction R value of the biochemicals discussed so far.

Waveband Selected (nm)	Biochemical Association	R^2 (Descriptive Power)
1341	Unattributable	0.22
552	Chlorophyll	0.42
910	Protein	0.50
905	protein	0.56
2051	Protein, nitrogen	0.59
1052	Oil	0.62
531	Chlorophyll	0.65
909	Protein	0.67
901	Protein	0.68

Table 5.11: BNC wavelengths selected by the stepwise procedure for use in the total chlorophyll regression model. Incremental changes in R^2 are shown based on the addition of each waveband.

Wavebands chosen by the stepwise procedure include some wavebands directly attributable to chlorophyll, with the majority at regions associated with protein at around

900nm. This again highlights the limitations to causality associated with unconstrained stepwise regression.

5.6.1.6 Chlorophyll *a*

Chlorophyll *a* follows a similar pattern to total chlorophyll in terms of prediction and description. FDS again gives the highest model R^2 of 0.93 and BNC gives the highest predictive power with an R value of 0.69, which is statistically significant at the 99% confidence interval. BDNA performs least well in predictive ability. The use of different transformations of the spectra with each one providing differences in their power to model biochemicals is corroborated by Kokaly and Clark (1999) and Curran *et al.* (2001).

Waveband Selected (nm)	Biochemical Association	R^2 (Descriptive Power)
552	Chlorophyll	0.44
916	Protein	0.51
531	Chlorophyll	0.55
1899	Starch	0.59
913	Protein	0.63
1302	Unattributable	0.66
1305	Unattributable	0.67
1304	Unattributable	0.69
1309	Unattributable	0.70
905	Protein	0.72
910	Protein	0.73

Table 5.12: BNC wavelengths selected by the stepwise procedure for use in the chlorophyll a regression model. Incremental changes in R^2 are shown based on the addition of each waveband.

Two of the top three wavebands chosen by the stepwise procedure can be directly attributed to chlorophyll (531nm and 552nm), which when combined with the relatively high predictive ability adds confidence to the technique and the ability of using spectral reflectance to predict chlorophyll *a*. The majority of other wavebands chosen are associated with protein or are unattributable.

5.6.1.7 Chlorophyll *b*

Like the other two chlorophylls discussed so far, chlorophyll *b* has statistically significant models and predictions for all transformations of the spectra. Once again, FDS has the highest model R^2 and BNC has the greatest predictive R value of 0.68 (lowest of the three chlorophylls). The similarity in modelling and prediction of the three chlorophylls is to be expected since they are intrinsically linked by the methodology used for their assay (chapter three, section 3.3.6).

Waveband Selected (nm)	Biochemical Association	R^2 (Descriptive Power)
1336	Unattributable	0.22
645	Chlorophyll *b*	0.37
1974	Starch	0.43
695	Chlorophyll, red edge	0.47
723	Red edge region	0.59
905	Protein	0.62
1443	Starch, sugar, lignin, water	0.65
1302	Unattributable	0.69
1901	Starch	0.71
1306	Unattributable	0.73
1064	Nitrogen/protein	0.74
912	Protein	0.76
924	Oil	0.77
926	Oil	0.78
923	Oil	0.80

Table 5.13: BNC wavelengths selected by the stepwise procedure for use in the chlorophyll b regression model. Incremental changes in R^2 are shown based on the addition of each waveband.

Some of the wavelengths selected are directly attributable to chlorophyll *b* or the chlorophyll region of the spectrum. Many are unattributable or linked to other biochemicals which again starts to prevent causation and may be why there is a divergence between the power of the regression models and their ability to predict. So far, the chlorophyll models have had the highest predictive ability of the biochemicals. Water and the chlorophylls have both had similar levels of predictability and are all biochemicals which are shown in the foliar t-tests (section 5.4) not to be significantly different between

groupings based on ^{137}Cs contamination levels. This suggests that ^{137}Cs may be inhibiting the ability to predict biochemicals affected by it.

5.6.1.8 Elemental Nitrogen

Elemental nitrogen has statistically significant models only for FDS and BDNA spectra. It has no statistically significant predictive abilities for any of the spectral transformations. When linking this to the foliar t-test and partial correlations it is a biochemical with significant differences between groupings of high and low ^{137}Cs content in both the domestic fuel and lumber wood groupings (section 5.4) and is shown by partial correlation to be conditionally dependent on ^{137}Cs (section 5.5). Like the structural biochemicals (AD fibre, cellulose, lignin) elemental nitrogen is a biochemical which appears to be affected by ^{137}Cs and in turn cannot be predicted from the spectra.

Waveband Selected (nm)	Biochemical Association	R^2 (Descriptive Power)
785	unattributable	0.32
674	Chlorophyll *a*	0.48
1233	unattributable	0.59
1928	Water, lignin, protein, nitrogen, starch, cellulose	0.70
1223	cellulose	0.78
1457	Starch, sugar, lignin, water	0.82
1814	cellulose	0.86

Table 5.14: FDS wavelengths selected by the stepwise procedure for use in the elemental nitrogen regression model. Incremental changes in R^2 are shown based on the addition of each waveband.

None of the wavelengths selected by SWMLR (table 5.14) are directly attributable solely to nitrogen and most are not attributable to nitrogen at all. This may explain why the model has relatively good descriptive power (R^2) in comparison to predictive power when applied to the testing data set.

5.6.1.9 ^{15}N

Unlike elemental nitrogen, ^{15}N has some statistically significant predictive models. These are derived from absolute reflectance and BDNA spectra. Absolute reflectance has the highest predictive power with an R of 0.70. Description of ^{15}N by the regression models is

significant for all transformations of the spectra. This is surprising given the pattern so far in terms of ^{137}Cs impacts, which seem to impede predictive ability in some biochemicals. Partial correlations (section 5.5) showed that the relationship between spectral reflectance and ^{15}N was the one most affected by ^{137}Cs. This is promising as if ^{15}N can be successfully predicted from spectra and crucially has a relationship with ^{137}Cs level it may allow the use of the spectra to predict ^{137}Cs.

Waveband Selected (nm)	Biochemical Association	R^2 (Descriptive Power)
1694	Lignin, starch, protein, nitrogen	0.16
1412	water	0.54
1695	Lignin, starch, protein, nitrogen	0.59
1331	unattributable	0.63

Table 5.15: Absolute Reflectance wavelengths selected by the stepwise procedure for use in the ^{15}N regression model. Incremental changes in R^2 are shown based on the addition of each waveband.

Only four wavebands were chosen for this model, two of which can be attributed to nitrogen. Of the other two, one is unattributable and the other attributable to water.

5.6.1.10 ^{137}Cs

Table 5.6 shows that FDS and BNC spectra produce statistically significant models for ^{137}Cs, but fall down completely when applied in a predictive fashion to the testing data set. As expected, this result precludes using unconstrained stepwise regression to predict ^{137}Cs directly from spectral reflectance and therefore prediction hinges on whether ^{137}Cs can be predicted indirectly from the foliar biochemicals. Before testing this, other statistical prediction methods are trialled to see if prediction accuracy can be enhanced, however prior to these additional methods, SWMLR results using the randomised data set are presented to assess the validity of the stepwise results so far.

Waveband Selected (nm)	Biochemical Association	R^2 (Descriptive Power)
1928	cellulose	0.16
1947	Water, lignin, protein, nitrogen, starch, cellulose	0.24
2188	Protein, nitrogen	0.45
417	Chlorophyll *a*	0.51
1432	lignin	0.60
2369	unattributable	0.65
435	Chlorophyll *a*	0.69
2195	Protein, nitrogen	0.74
2234	cellulose	0.77
2121	protein	0.80
2148	unattributable	0.83
2061	Protein, nitrogen	0.85
1454	Starch, sugar, lignin, water	0.86
982	starch	0.89
2225	cellulose	0.91

Table 5.16: FDS wavelengths selected by the stepwise procedure for use in the ^{137}Cs regression model. Incremental changes in R^2 are shown based on the addition of each waveband.

Wavebands chosen by SWMLR for the ^{137}Cs regression model (table 5.16) are on the whole associated with cellulose and nitrogen. This links to other results so far (foliar biochemical t-tests, partial correlations) which suggest ^{137}Cs is affecting ability to predict these biochemicals.

5.6.2 Testing Validity of Stepwise Regression using Randomised Data

Table 5.17 shows the results for unconstrained stepwise regressions performed on the randomised data for each biochemical. The stepwise procedure was identical to that described in section 5.6.1 other than using the randomised relationship between biochemical data and spectral response.

	Absolute Reflectance		FDS		BDNA		BNC	
Biochemical	Regression R^2	Validation R	Regression R^2	Validation R	Regression R^2	Validation R	Regression R^2	Validation R
Water	0.39	0.03	0.92	-0.17	0.10	0.08	0.42	0.00
AD Fibre	ns	ns	0.88	-0.25	0.40	-0.22	0.31	0.10
Lignin	ns	ns	0.83	0.26	0.44	-0.31	0.38	0.28
Cellulose	ns	ns	0.79	-0.03	0.66	-0.04	0.45	-0.02
Chl A	0.08	0.20	0.86	0.10	0.68	-0.05	0.49	-0.23
Chl B	0.06	0.18	0.81	-0.03	0.68	-0.03	0.25	0.01
Total Chl	0.07	0.19	0.89	0.10	0.64	0.00	0.45	0.02
Elemental N	ns	ns	0.91	-0.00	0.37	0.40	0.30	0.22
^{15}N	0.08	0.07	0.88	-0.09	0.26	0.20	0.11	-0.10
Cs-137	0.30	0.05	0.88	-0.14	0.52	0.50	0.46	0.02
ns = no significant R^2 or R								

Table 5.17: Results from unconstrained regressions using randomised datasets from four transformations of the spectra.

Descriptive and predictive power of the models is on the whole orders of magnitude lower than when using the real data set. This adds confidence that the stepwise procedure is identifying real relationships in the data and selecting appropriate wavebands to model those relationships. Worryingly, FDS have relatively high R^2 values but these fall down when applied to the testing data set. This highlights the need for a testing data set and supports Harrell's (2002) view that SWMLR can often capitalise on chance features of the data.

Overall, unconstrained stepwise regression on the real data has chosen wavebands which are able to predict foliar biochemical contents with comparable accuracies to other studies (e.g. Mutanga *et al.* 2003, Curran *et al.* 2001). Although some bands selected by the regression are close to known absorption points for the particular foliar biochemical, the bands are, on the whole, unique to the current dataset meaning there is a lack of causality and repeatability in the technique. Causality and repeatability are important when attempting to use spectra collected from remote sensing platforms to try to predict biochemicals and ultimately ^{137}Cs. Dawson *et al.* (1995) have demonstrated that the use of forced entry stepwise regression with bands known to be associated with particular foliar biochemicals can bypass the hindrance to causality associated with unconstrained stepwise regression.

5.6.3 Determining Causality with Forced Entry Stepwise Regression

Problems with unconstrained regression often centre on the lack of causality between the biochemicals and chosen wavelengths for the regression model. In constrained (or forced entry) regression, wavelengths known to be associated with particular biochemical absorption points were entered into regression equations along with wavelengths identified in the partial correlations (section 5.5). These wavelengths were entered simultaneously to force a regression and taken out sequentially based on changes in the f-values. In table 5.18 below, four transformations of the spectra are used (described in chapter three, section 3.3.2) and again are validated using a testing data set which was excluded from the creation of the regression models. Since the literature does not provide absorption bands for AD fibre of ^{137}Cs, these biochemicals were not used in the constrained regressions.

	Absolute Reflectance		FDS		BDNA		BNC	
Biochemical	Regression R^2	Validation R	Regression R^2	Validation R	Regression R^2	Validation R	Regression R^2	Validation R
Water	0.55	0.64[b]	0.51	0.68[b]	0.65	0.52[b]	0.49	**0.77[b]**
Lignin	0.80	0.29	0.79	0.36[a]	0.37	0.27	0.43	**0.43[b]**
Cellulose	0.67	0.43[b]	0.74	0.22	0.50	0.53[b]	0.49	**0.55[b]**
Chl *a*	0.63	0.61[b]	0.63	0.56[b]	0.66	0.38[a]	0.49	**0.68[b]**
Chl *b*	0.68	0.57[b]	0.63	0.53[b]	0.62	0.45[b]	0.46	**0.66[b]**
Total Chl	0.65	0.58[b]	0.66	0.63[b]	0.60	0.29	0.48	**0.68[b]**
Elemental N	0.76	**-0.67[b]**	0.94	-0.12	0.74	0.36	0.48	-0.16
^{15}N	0.97	0.23	0.96	**0.53[a]**	0.75	0.33	0.73	0.34

ns = no significant R^2 or R [a] = significant at 95% confidence [b] = significant at 99% confidence

Table 5.18: Results from constrained regressions on four transformations of the spectra.

BNC spectra appears to have the highest predictive ability for most of the biochemicals. Unlike unconstrained regression, all biochemicals have models with statistically significant predictive power. Lowest predictive power is for lignin with an R value of 0.43 whilst the highest is 0.77 for water. On the whole, the pattern remains the same as in unconstrained regression in that water and chlorophylls have models with highest predictive power with the structural components and ^{15}N having lower predictive power. Having said this, elemental nitrogen which could not be predicted significantly at all in unconstrained regression has an R value of -0.67 (statistically significant at 99% confidence interval) using absolute reflectance.

5.6.4 Testing Validity of Forced Entry Stepwise Regression Using Randomised Data

Table 5.19 shows the results of constrained regression using the randomised data set. There is one model in this table which significantly predicts lignin, but at a lower level than the real dataset. The rest of the table shows that none of the models can significantly predict any of the other biochemicals. This result is similar to the randomised data in the unconstrained stepwise regression and again adds confidence to the models generated from the constrained regression.

	Absolute Reflectance		FDS		BDNA		BNC	
Biochemical	Regression R^2	Validation R	Regression R^2	Validation R	Regression R^2	Validation R	Regression R^2	Validation R
Water	ns	ns	0.22	-0.04	0.04	-0.05	0.08	0.06
Lignin	0.60	0.05	0.70	-0.12	0.49	-0.17	0.26	0.41[a]
Cellulose	0.66	0.24	0.22	-0.07	0.26	-0.20	0.32	0.15
Chl *a*	0.13	0.06	0.06	-0.15	0.14	0.04	0.14	-0.14
Chl *b*	0.12	0.00	0.05	-0.15	0.14	0.06	0.16	-0.04
Total Chl	0.13	0.04	0.06	-0.15	0.14	0.05	0.13	-0.17
Elemental N	0.93	-0.06	ns	ns	0.70	0.15	0.45	0.37
^{15}N	ns	ns	ns	ns	0.73	0.07	0.61	0.10

ns = no significant R^2 or R [a] = significant at 95% confidence

Table 5.19: Results from constrained regressions using randomised datasets from four transformations of the spectra.

By using wavebands known to be associated with each particular biochemical a causal link between wavebands and foliar biochemicals can be made leading to greater confidence in the technique and is shown in table 5.18 by some higher R values and statistically significant predictive models for all biochemicals entered into the stepwise procedure. The wavebands used in the regressions along with their biochemical association are listed in appendix A4. If ^{137}Cs is to be inferred from foliar biochemical content, then the successful prediction of each biochemical is central to the research. Whilst stepwise procedures have exhibited predictive power, recently, in laboratory-based near infrared spectroscopy the statistical technique of partial least squares (PLS, also known as projection to latent structures) has surpassed stepwise regression in its ability to predict content of samples (Barton 2002). PLS was applied to this research to see if predictions of foliar biochemicals can be any more accurate than using stepwise regression procedures.

5.6.5 Partial Least Squares to Predict Foliar Biochemical Content

Partial least squares (PLS) attempts to overcome the difficulty of overfitting often associated with regression techniques (Davies 2001). PLS was developed in the 1960s by Herman Wold and is often used in spectroscopic techniques to try to identify the few underlying factors which account for most of the variation in the response (Tobias 1997). Recent remote sensing literature has suggested that the use of PLS to predict foliar biochemicals might be a more accurate technique than SWMLR (e.g. Huanga *et al.* 2004, Ourcival *et al.* 1999). Since accurate prediction of key foliar biochemicals is central in this research in order to infer ^{137}Cs contamination levels, PLS was applied to the spectra and biochemicals to see if an improvement over stepwise techniques could be made.

Table 5.20 shows PLS results for absolute reflectance and FDS whilst table 5.21 shows PLS results for the continuum-removed spectra. The overall pattern of predictive power remains the same as the stepwise procedures. The biochemicals exhibiting models with the greatest predictive power are those for water and chlorophyll and are the biochemicals shown not to be statistically different in ^{137}Cs contamination groupings and are also shown to be conditionally independent of ^{137}Cs by partial correlation. ^{15}N was again an outlier in the argument since it is shown in the partial correlation (section 5.5) to be most conditionally dependent on ^{137}Cs yet it is significantly predicted by models from three transformations of the spectra in the PLS method.

	Absolute Reflectance				FDS			
Biochemical	Percent Variance Accounted For	Optimum Number of latent vectors	RMSE	Validation R	Percent Variance Accounted For	Optimum Number of latent vectors	RMSE	Validation R
Water	97.146	5	0.764	0.74[b]	16.27	1	0.768	0.76[b]
AD Fibre	27.16	2	1.021	-0.09	62.327	6	0.928	**0.36[a]**
Lignin	94.943	4	1.021	-0.09	19.622	2	0.901	0.36[a]
Cellulose	55.52	1	1.042	-0.20	39.526	3	0.942	**0.26**
Chl *a*	82.929	3	0.761	0.49[b]	56.921	5	0.62	0.53[b]
Chl *b*	97.892	5	0.751	0.35[a]	56.848	5	0.582	0.50[b]
Total Chl	99.116	6	0.751	0.46[b]	56.899	5	0.596	0.52[b]
Elemental N	76.33	2	1.024	**0.25**	21.23	2	0.983	0.17
^{15}N	81.384	3	0.804	0.63[a]	39.42	2	0.839	**0.77[b]**
Cs-137	59.77	1	1.018	-0.10	22.14	1	1.045	-0.01

Table 5.20: Results from partial least squares modelling using two transformations of the spectra. [a] = significant at 95% confidence [b] = significant at 99% confidence Bold denotes highest validation figure out of four spectra transformations.

	BDNA				BNC			
Biochemical	Percent Variance Accounted For	Optimum Number of latent vectors	RMSE	Validation R	Percent Variance Accounted For	Optimum Number of latent vectors	RMSE	Validation R
Water	49.33	2	0.677	0.61[b]	38.67	2	0.803	**0.81[b]**
AD Fibre	28.27	1	0.997	0.18	19.88	1	1.002	0.02
Lignin	36.35	2	0.985	**0.39[a]**	16.11	1	1.02	-0.04
Cellulose	31.63	1	0.994	0.17	23.91	1	1.019	0.21
Chl *a*	84.903	7	0.653	0.56[b]	48.11	3	0.817	**0.73[b]**
Chl *b*	84.173	7	0.701	0.62[b]	39.78	2	0.842	**0.64[b]**
Total Chl	84.855	7	0.66	0.59[b]	38.66	2	0.821	**0.68[b]**
Elemental N	35.21	2	1.017	0.16	10.96	1	0.996	0.01
^{15}N	34.33	1	0.819	0.73[b]	48.19	2	0.695	0.43
Cs-137	16.76	1	1.046	**0.32**	16.8	1	1.039	-0.06

Table 5.21: Results from partial least squares modelling using two further transformations of the spectra. [a] = significant at 95% confidence [b] = significant at 99% confidence Bold denotes highest validation figure out of four spectra transformations.

Whether PLS can produce models with greater predictive power than stepwise techniques is the main question of interest for this research. To simplify this comparison, the R values taken from the best predictive model for each approach are displayed in table 5.22, along with the spectral transformation used and whether the PLS method has higher or lower predictive power in comparison to the stepwise methods.

Biochemical	Highest PLS R value	Spectral Transformation		Highest Stepwise R value	Spectral Transformation and type of regression	PLS higher or lower accuracy than stepwise?
Water	0.81	BNC	*VS.*	0.77	BNC Constrained	**Higher**
AD fibre	0.36	FDS	*VS.*	0.39	BDNA Unconstrained	**Lower**
Cellulose	0.26	FDS	*VS.*	0.55	BNC Constrained	**Lower**
Lignin	0.39	BDNA	*VS.*	0.52	BDNA Unconstrained	**Lower**
Total Chl.	0.68	BNC	*VS.*	0.70	BNC Unconstrained	**Lower**
Chl. *a*	0.73	BNC	*VS.*	0.69	BNC Unconstrained	**Higher**
Chl. *b*	0.64	BNC	*VS.*	0.68	BNC Unconstrained	**Lower**
Elemental nitrogen	0.25	Abs. Ref.	*VS.*	-0.67	Abs. Ref. Constrained	**Lower**
^{15}N	0.77	FDS	*VS.*	0.70	Abs. Ref. Unconstrained	**Higher**

Table 5.22: Results of a comparison between the power of predictive biochemistry models derived from stepwise and PLS techniques.

Table 5.22 illustrates that PLS is able to predict only three out of nine biochemicals with a greater accuracy than stepwise methods. These are ^{15}N and chlorophyll *a*. Stepwise performs better on the other seven biochemicals. On biochemicals shown to be unaffected by ^{137}Cs (water, chlorophylls) the two methods provide very similar results in terms of R value and spectral transformation used. Since the PLS method is to some degree a function of all the inputs, individual wavebands cannot be singled out and this is a hindrance in two ways:

1. It hides causality which might be gained from knowing wavebands.
2. Input data used to derive the prediction equation may not match spectral resolution of future input data, thus rendering the prediction equation unusable.

These two issues coupled with the generally lower predictive power of PLS mean in this research, stepwise procedures are favoured.

So far, this chapter has shown that spectra split into high and low contamination levels according to ^{137}Cs content exhibit statistically significant differences. It has gone on to illustrate foliar biochemistry also shows significant differences when split up according to ^{137}Cs level. Partial correlation was used to demonstrate which biochemicals had their relationship with spectral reflectance affected by ^{137}Cs. In section 5.6 the chapter has

focused on techniques to predict foliar biochemistry from spectral response and shown stepwise techniques to be desirable over PLS methods. The final key in terms of using spectra to infer ^{137}Cs levels is whether the biochemistry can be used to derive ^{137}Cs content. If this is case then it signals the opportunity of using spectral reflectance to predict biochemistry and in turn ascertain levels of ^{137}Cs. The final section of this chapter looks at the link between leaf biochemistry and ^{137}Cs content.

5.7 Predicting ^{137}Cs from Foliar Biochemicals

5.7.1 Multiple Regression

Initially, a simple multiple linear regression was performed to attempt prediction of ^{137}Cs using foliar biochemistry. The foliar biochemicals were used as the independent variables and ^{137}Cs was set as the dependent variable. The first model is shown in figure 5.15 and uses all nine foliar biochemicals as inputs.

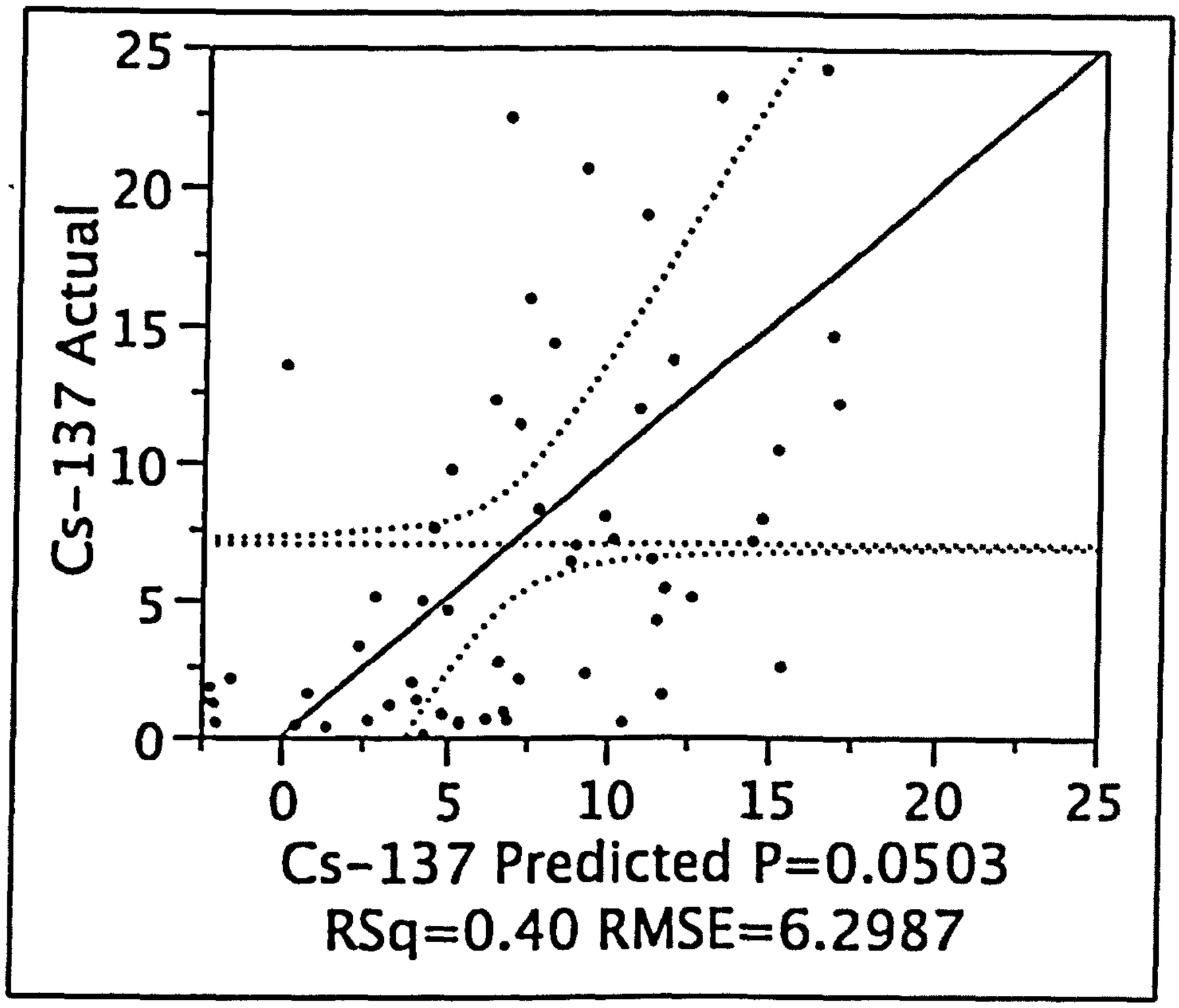

Figure 5.15: Multiple linear regression model to predict ^{137}Cs specific activity using all nine foliar biochemicals as inputs

The model R^2 of 0.40 is not statistically significant and means it cannot be used with regards to the ability of using foliar biochemistry to predict ^{137}Cs specific activity. Since previous techniques of analysis have shown a difference in the effects of ^{137}Cs on certain biochemicals, the biochemicals were split into two groups and then input separately into two further regression models. The two biochemical groups were based on whether the particular biochemical had been identified as significant in the foliar t-test (section 5.4) and if it was conditionally dependent or independent as signified by the partial correlations (section 5.5). Conditionally dependent biochemicals were identified as elemental nitrogen, ^{15}N, lignin, cellulose and AD fibre. Conditionally independent biochemicals were identified as water, and the three variants of chlorophyll (*a*, *b* and total). The two multiple regression models using these separate biochemical groups are shown in figures 5.16 and 5.17.

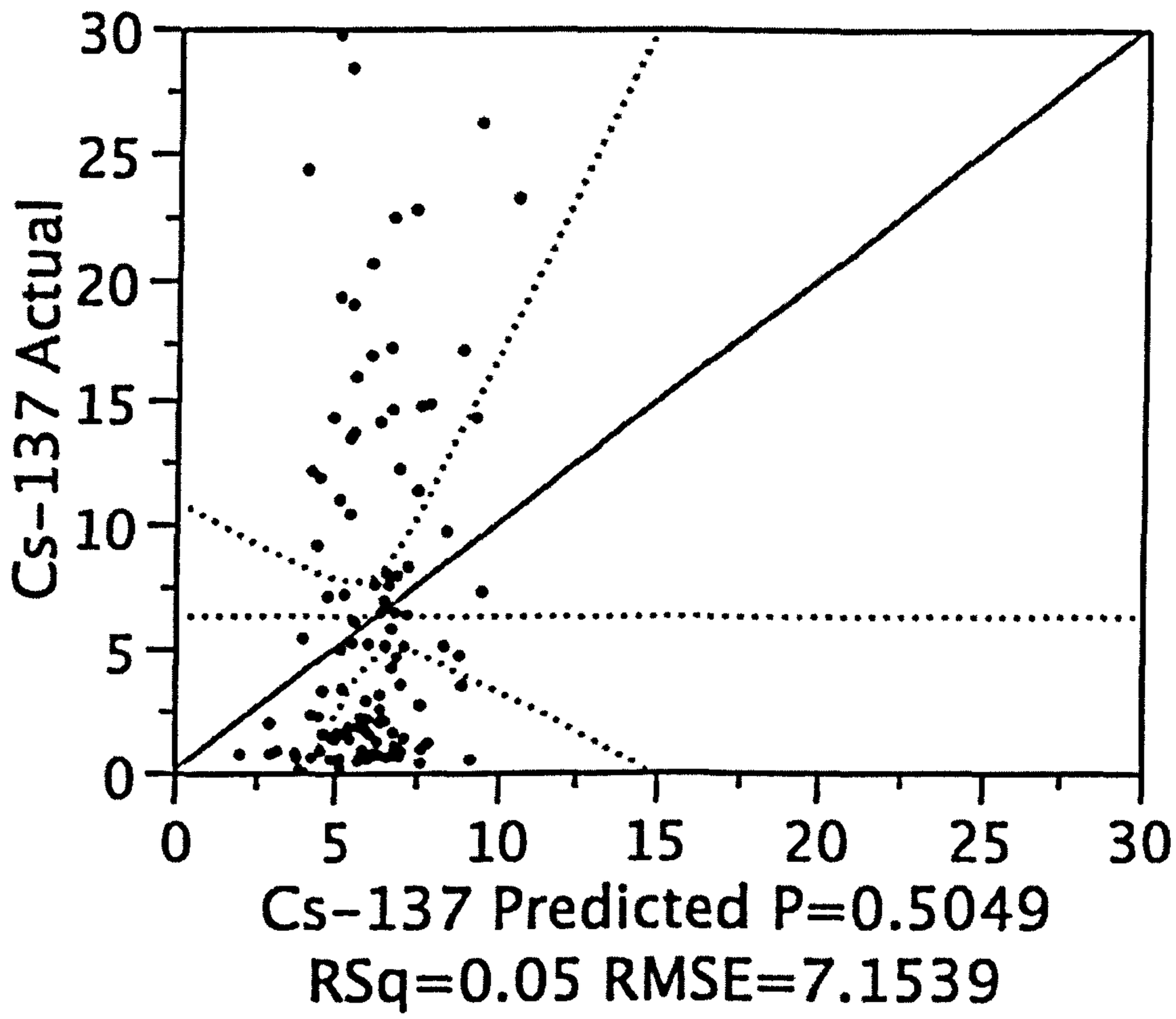

Figure 5.16: Multiple linear regression model to predict ^{137}Cs specific activity from the conditionally independent biochemicals (water and three variants of chlorophyll).

The conditionally independent biochemicals produced an R^2 of 0.05, corroborating that they are unaffected by ^{137}Cs and showing that they do not have any power in predicting ^{137}Cs specific activity on their own. This represents a research paradox since the biochemicals which can be predicted with highest accuracies in the stepwise procedures are those which have been shown not to be affected by ^{137}Cs. In contrast, the biochemicals identified in stepwise models as having lower prediction accuracies seem to have the best potential for inferring ^{137}Cs levels.

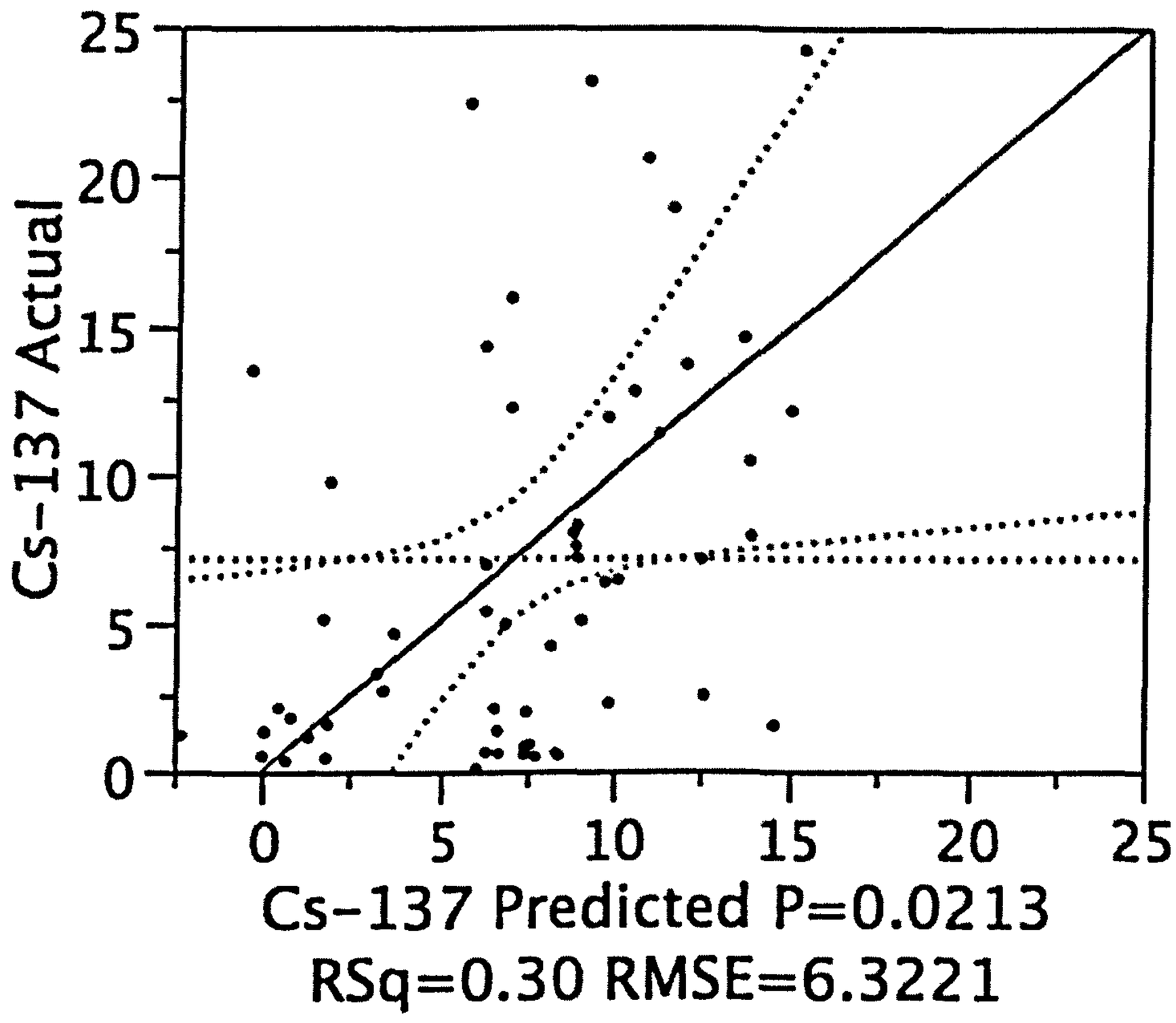

Figure 5.17: Multiple linear regression model to predict ^{137}Cs specific activity from the conditionally dependent biochemicals (three structural biochemicals and two isotopes of nitrogen).

Using biochemicals shown to be conditionally dependent of ^{137}Cs the R^2 is 0.30 which although not statistically significant is a far higher level than the conditionally independent biochemicals can provide.

The final link between foliar biochemistry seems to be missing or is not being uncovered by the multiple regression models. Literature suggests this link might be non-linear (e.g. Calabrese and Baldwin 2000). As such, neural networks, with their strengths in modelling non-linear relationships, may prove a better predictive tool than multiple regression.

5.7.2 Artificial Neural Networks

Artificial neural networks are a form of machine vision (Carpenter *et al.* 1999) and have been utilised in aspects of research, particularly when linear models do not suit the data. Simple neural networks were investigated using SAS institute's JMP statistical exploration

software to ascertain whether they might have potential for modelling the relationship between ^{137}Cs and spectra. Figure 5.18 shows a conceptual diagram of an artificial neural network using all foliar biochemicals.

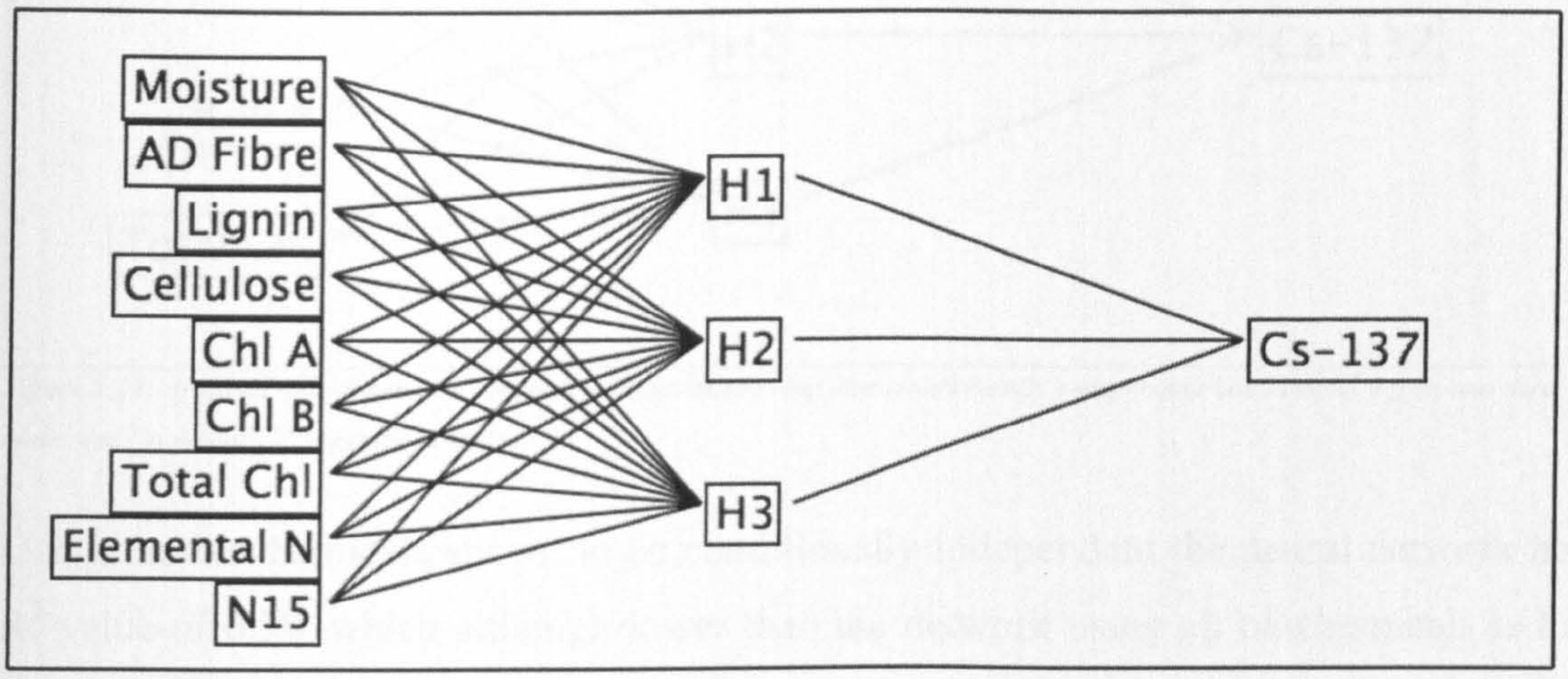

Figure 5.18: Artificial neural network conceptual diagram showing nine biochemical inputs and three hidden nodes used to model ^{137}Cs specific activity.

The neural network using all nine biochemicals as inputs produces a high R^2 value of 0.98 which is far higher than the multiple regression model. When this was applied to a test dataset however, the predictive ability was not statistically significant with an R value of 0.30. This illustrates how neural networks have good ability in modelling given data, but perform poorly when applied to new data sets. Before continuing, the neural network method followed the same approach used in the multiple regression section and tested models using biochemicals which were split into two groups. These groupings are the same as described in section 5.7.1.

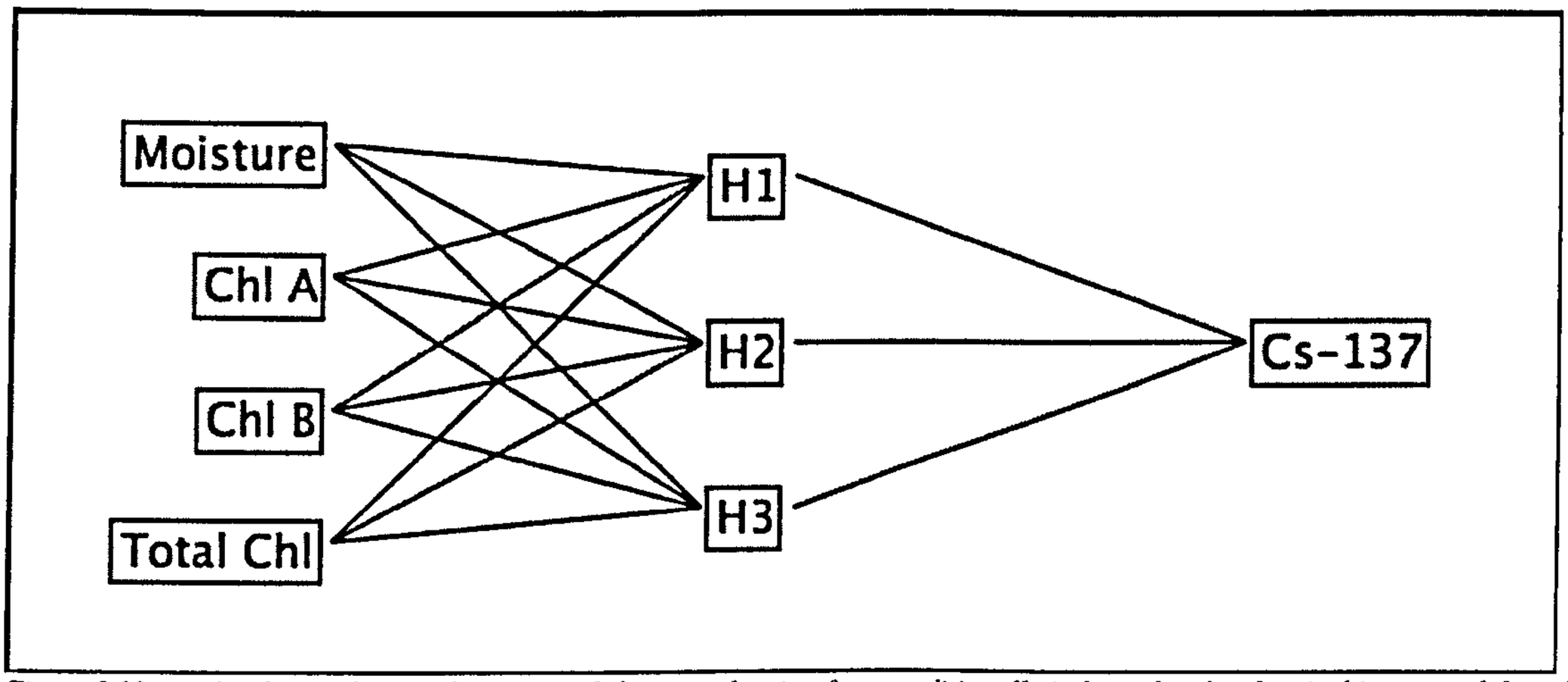

Figure 5.19: Artificial neural network conceptual diagram showing four conditionally independent biochemical inputs and three hidden nodes used to model ^{137}Cs specific activity.

Using the biochemicals shown to be conditionally independent the neural network had an R^2 value of 0.39, which although lower than the network using all biochemicals is higher than the multiple regression model using the same biochemicals as inputs. When applied to the testing dataset, the neural network predicted versus actual values had a correlation coefficient of 0.13 which is not statistically significant and is much lower than when using all the biochemicals as inputs to the network. Figure 5.20 shows the conceptual diagram for the neural network using the conditionally dependent biochemicals as inputs. As an exploration of neural networks to assess if improvements over linear regression could be made, SAS suggested settings (SAS 2005) were used in the generation of the networks. These are shown in table 5.23.

Neural Network Settings	
Hidden nodes	3
Overfit penalty	0.001
Number of tours	20
Maximum iterations	50
Convergence criterion	0.00001

Table 5.23: SAS suggested settings for generating a neural network as used in this research.

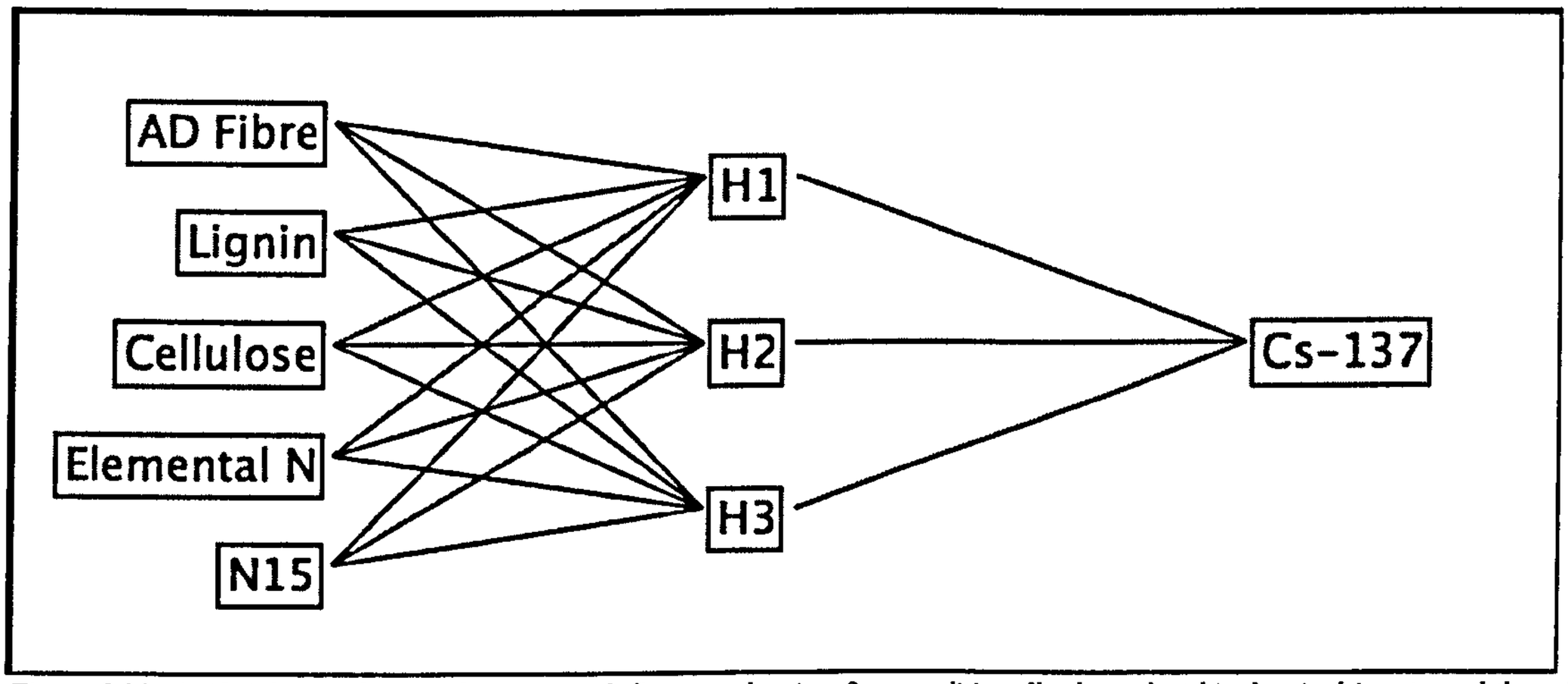

Figure 5.20: Artificial neural network conceptual diagram showing five conditionally dependent biochemical inputs and three hidden nodes used to model ^{137}Cs specific activity.

Using the conditionally dependent biochemicals only, the R^2 value is 0.83 and although slightly lower than when using all nine biochemicals in the model is much larger than the model which used only the conditionally dependent biochemicals. A third of the data was held back randomly to use as a testing data set (training n= 75, testing n=37). For prediction using the test data, the model had a correlation coefficient between actual and predicted of 0.24 which is not statistically significant. The value is similar to that when using the entirety of biochemicals in the model.

So far, multiple regression and artificial neural networks have failed to predict ^{137}Cs from foliar biochemistry with statistically significant levels. This signals that either the link between measured foliar biochemicals and ^{137}Cs does not exist or that it is not being uncovered by these modelling techniques. The multiple regression and artificial neural networks have corroborated other results which show that ^{137}Cs has an impact on structural components and nitrogen, but little or no impact on water or chlorophylls.

5.8 Summary

This chapter has so far shown the following:

- *Pinus sylvestris* spectra grouped based on their specific ^{137}Cs activity differ at a statistically significant level across various wavelengths.

- Foliar biochemistry from *Pinus sylvestris* grouped based on their specific ^{137}Cs activity also differ at a statistically significant level for AD fibre, cellulose, lignin,

elemental nitrogen and ^{15}N. Total chlorophyll along with chlorophylls *a b* and water do not differ at statistically significant levels.

- Partial correlation has corroborated the foliar t-tests and shown ^{137}Cs affects the relationship between spectral reflectance and elemental nitrogen, ^{15}N, AD fibre, lignin and cellulose but not water or the three variants of chlorophyll. The foliar biochemical t-test and partial correlations have led to the designation of biochemicals into one of two groups, either conditionally dependent of ^{137}Cs or conditionally independent of ^{137}Cs.

- Prediction of foliar biochemicals from spectra can be performed at statistically significant levels for all nine foliar biochemicals using one of four transformations of the spectra. Stepwise regression both unconstrained and constrained was tested along with PLS, but stepwise regression was shown to be more suitable for this research. The predictive ability of the models highlighted a research paradox; that the biochemicals conditionally independent of ^{137}Cs could be predicted with greater accuracy than those conditionally dependent on ^{137}Cs.

- Ultimately the chapter investigated the final link in attempting to use spectra to infer ^{137}Cs specific activity but showed that predicting ^{137}Cs specific activity from foliar biochemistry does not seem possible at statistically significant levels using multiple regression or artificial neural networks. This may be due to a missing relationship or the lack of ability in terms of the statistical techniques used to model ^{137}Cs from biochemistry.

To sum up, ^{137}Cs is impacting on some biochemicals and affecting spectra, but there is a missing link between ^{137}Cs and biochemistry. This may be due to the immaturity of biological understanding concerning ^{137}Cs impacts upon plant biochemistry. Also, whilst this chapter has shown spectra differ between ^{137}Cs activity levels, the spectra might be affected by intrinsic environmental variables and natural processes which are hiding the link between ^{137}Cs and spectral response. The limitations described in section 5.1 provide opportunities for further research in order to understand more fully the results from this chapter. In particular, if returning to the field, the measurement of biometric properties such as leaf area index (LAI) of needles and canopy structural properties would be a key

area to develop and research further and may help to understand the relationship between ^{137}Cs contamination and spectral reflectance. This is especially so in terms of providing understanding to results from hyperspectral images (chapter seven) where the canopy and biophysical properties are inherent in the data (image). The next chapter uses an artificial environmental laboratory in order to filter out external environmental variables and assess the impacts of ^{137}Cs on *Pinus sylvestris* when no other confounding variables are present.

Chapter 6

Detecting ^{137}Cs Levels in *Pinus sylvestris* Grown in an Artificial Laboratory Environment

6.1 Introduction

Field radiometry results from chapters four and five have shown significant differences in spectra from samples with differing levels of ^{137}Cs, but a major research obstacle is the inability to conclusively and causally relate changes in spectra to ^{137}Cs. This is due to the number of biochemical and biophysical variables in the natural environment, which could also be responsible for changes in spectral response. Research described in this chapter illustrates results from a laboratory-based experiment designed to isolate the effects of ^{137}Cs on spectral response of *Pinus sylvestris*. By performing the experiment in a controlled laboratory setting, all variables could be held constant other than ^{137}Cs levels. This chapter begins by outlining the concept, methodology and set up of the experiment. It then describes uptake of ^{137}Cs by the trees before analysing the health of the trees, as assessed by the technique of chlorophyll fluorescence (CF). This chapter finally looks at the spectral reflectance of the trees in relation to ^{137}Cs and plant health.

6.2 Trees and Growing Conditions

Trees were grown hydroponically in Kingston University's radiochemistry laboratory. The experiment utilised young *Pinus sylvestris* trees of approximately three years old. In total, 20 trees were used, and these were split into four groups, each containing five trees. Ideally, more trees would have been grown, but logistical and regulatory constraints in Kingston University's radiochemistry laboratory meant a maximum of 20 trees could be

grown. The tree groupings corresponded to the levels of radioactivity added to the growing conditions (dose) and are detailed in table 6.1, but can be broadly described as relatively high, medium and low levels of ^{137}Cs, as well as a control group (no ^{137}Cs). The trees were grown in hydroponic conditions, with the growing medium being oxygenated water. Hydroponic growth conditions were chosen to minimise factors associated with the mixing and cycling of ^{137}Cs in soils or other solid media. Growth conditions were perfected through a pre-experiment trial, which was run for one month, with 20 trees being placed in hydroponic conditions. The trial helped to establish the method of oxygenating water, as well as identifying correct levels and types of nutrients needed for healthy growth. Consistency of growth conditions between each tree was important for two reasons; firstly to ensure ^{137}Cs uptake was not varied by changes in the growing conditions, and secondly so that any changes in spectral reflectance could be linked to ^{137}Cs contamination (as opposed to variations in growing conditions). The trees were split up across the growing area to prevent any spatial bias being introduced to the growing position of particular groupings and rotated each week, again to ensure all trees were grown in the same environmental conditions. In addition, the hydroponic solution was monitored weekly and nutrients added to maintain the same growing medium for each tree. The growing conditions and laboratory setup are illustrated below in Figure 6.1.

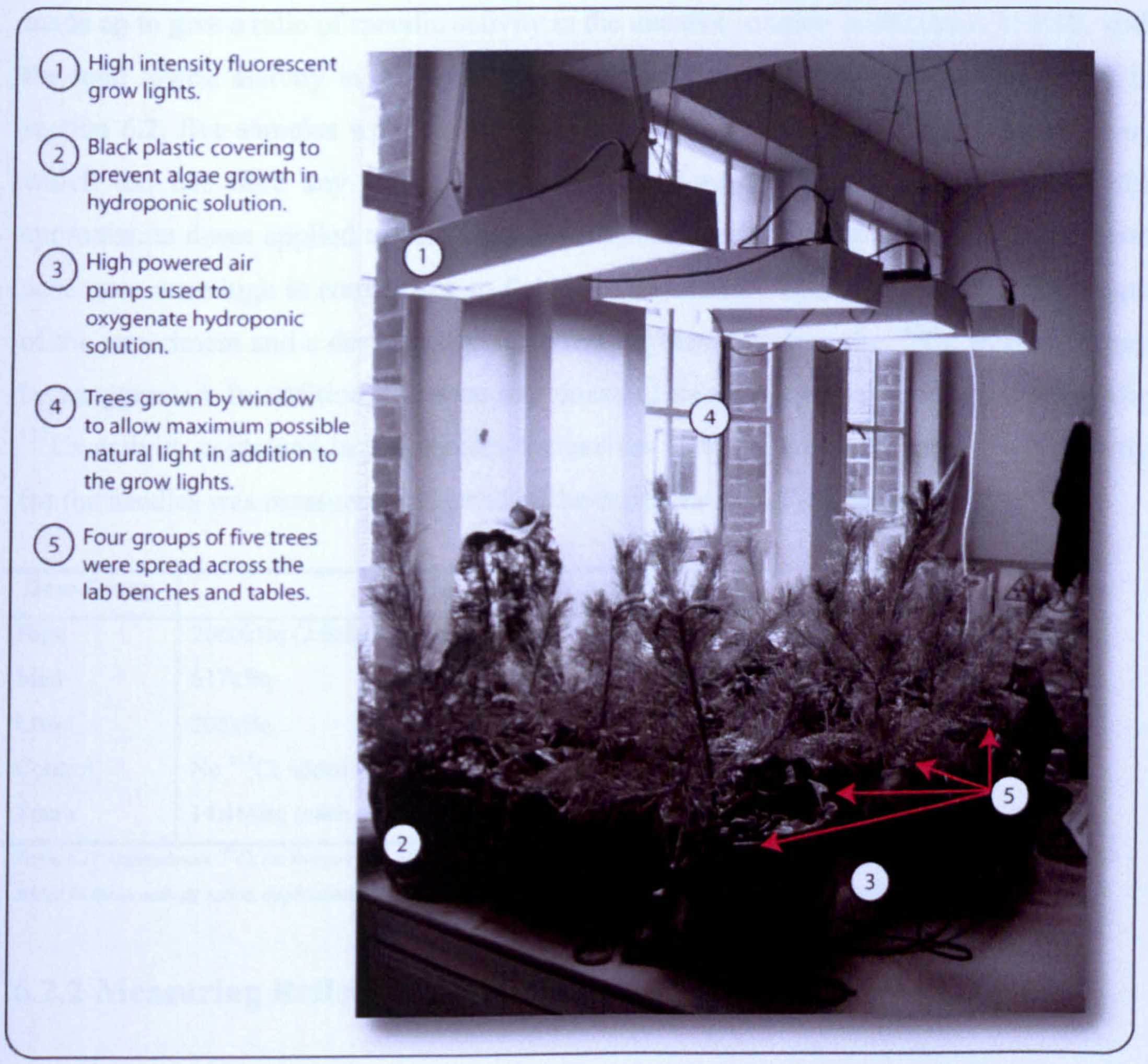

Figure 6.1. An annotated photo, summarising the laboratory conditions and setup during the experiment.

6.2.1 Dosing the Trees with ^{137}Cs

^{137}Cs was added to the trees from a stock solution of ^{137}Cs for which the activity was quantified using a National Physical Laboratory (NPL) ^{137}Cs standard (appendix A5). Gamma spectrometry was used to check each solution before it was added to the tree via a pipette. Having determined the activity of the stock ^{137}Cs solution, it was then possible to decide a suitable volume to be dispensed into each of the trees' hydroponic solution. Given that the top soil in the higher level contaminated regions of Belarus (where field radiometry was conducted, see chapters four and five) is typically about 100kBq/kg (Entwistle *et al.* 2005) it was appropriate to use a nutrient solution with specific activity at around this 100kBq/kg level, and above. The low, medium, and high ^{137}Cs doses were

made up to give a ratio of specific activity in the nutrient solution in the ratios 1: 3:10, with the total lowest activity in the nutrient solution of about 200kBq. As already stated in section 6.2, five samples were assigned to each activity level as well as a control group which did not have any ^{137}Cs added to the growing medium. Table 6.1 shows the approximate doses applied to each tree. It is important to note that the lowest experiment dose rates were high in comparison to field sites in Belarus. This is due to the short length of the experiment and a desire to see the effect on the trees from the ^{137}Cs, even if it may be exaggerated. In addition, the dose rate does not necessarily correspond to the specific ^{137}Cs activity contained in the needles themselves (section 6.2.3). Specific ^{137}Cs activity for the needles was measured at the end of the experiment and is reported in table 6.2.

Dose Group	Total Activity (Bqs)
High	2060kBq (2.06MBq)
Med	617kBq
Low	206kBq
Control	No ^{137}Cs added (0 Bq)
Totals	14.4MBq (each of the above multiplied by 5, since there are 5 trees in each group)

Table 6.1: Approximate ^{137}Cs (in Becquerels) added to the different groups of Pinus sylvestris. The three radioactive groups had ^{137}Cs added in three activity ratios, approximately 1: 3: 10, with the lowest level containing a total of 206kBq ^{137}Cs.

6.2.2 Measuring Reflectance Spectra

An Analytical Spectral Devices (ASD) Fieldspec Pro was used to collect reflectance spectra of the *Pinus Sylvestris* needles according to the method described in chapter three (section 3.3.1). Reflectance spectra were collected after one month of growth in the ^{137}Cs hydroponic solutions. Spectra were not collected throughout the experiment due to constraints in borrowing equipment from NERC FSF, but also because the focus of the experiment was in how the reflectance spectra were affected by ^{137}Cs *per se*, and not how the trees responded or changed over a short period of time. This is due to the experiment acting as a link and providing insight into field radiometry work already conducted in Belarus (chapters four and five), where the trees have been exposed to ^{137}Cs since the 1986 Chernobyl accident. As mentioned above, since the experiment was run over a short period of time, and with younger trees than in the fieldwork, the doses of ^{137}Cs added to the trees were elevated compared to dose rates found in the field. The low site in the laboratory experiment roughly matched the dose levels in the high field site. This was done to

promote an effect in the trees and subsequently the spectra, over the relatively short time scale of the experiment.

After one month in ^{137}Cs hydroponic conditions, all needles were harvested from each tree, and a sub-sample was selected randomly for spectral reflectance measurement. Figure 6.2 shows the mean absolute reflectance spectra collected for each group of trees. As the trees were small saplings (c. <3 years), there was not enough new growth over the one-month time scale of the experiment to provide material for biochemical assay as material was needed for ^{137}Cs specific activity measurement. This is a limitation of the laboratory experiment and highlights opportunity for further research.

6.2.3 Measuring Specific ^{137}Cs Activity

In section 6.2.1 dosing of the trees with ^{137}Cs was discussed. Whilst the dose rate provides an indication of ^{137}Cs levels contained within the trees' growing environment, it does not provide detail as to how much ^{137}Cs has been transferred from the growing medium into the physiologically active part of the tree (i.e. the needles). Central to the experiment was linking spectral response to levels of ^{137}Cs inside the needles, therefore a measure of ^{137}Cs specific activity was performed using gamma spectrometry as described in chapter three (section 3.3.10). These levels could then be linked to the spectra and the plant health. Specific ^{137}Cs activities for each tree are presented in Table 6.2 and Figure 6.2.

6.2.4 Measuring Plant Health using Chlorophyll Fluorescence

In addition to spectral reflectance measurements and gamma spectrometry, the needles were measured at intervals throughout the experiment using the technique of Chlorophyll Fluorescence (CF). CF (illustrated in figure 6.2) is a natural property of green plants which can be utilised to provide a quick, non-invasive and non-destructive way to monitor photosynthetic pathways, and in turn the health status of vegetation (Frankart *et al.* 2003). This technique allowed the health of the trees to be monitored throughout the experiment, with the possibility of linking ^{137}Cs levels to changes in CF and thus plant health. Since the experiment was run before all field data had been analysed, it was thought that chlorophyll may be impacted by ^{137}Cs and thus CF was considered to be a useful technique to

investigate the link between spectral reflectance, chlorophyll, and plant health as affected by ^{137}Cs. Chapters four and five show chlorophyll to be conditionally independent of ^{137}Cs however the technique was useful to give an indicator of plant health and to assess if chlorophyll was being affected by ^{137}Cs but being masked by other variables in the field data.

CF was measured using a pulse amplitude modulation (PAM) fluorometer; model PAM-210 (Waltz, GmbH). Parameters measured were Fv/Fm, Phi PSII (Fm'), electron transport rate (ETR), photochemical quenching (qP) and non photochemical quenching (qN). Each one of these parameters relates to the ways in which light energy is dissipated from the plant. Light emitted at longer wavelengths (fluoresced) is light which is dissipated by the plant and not used for photochemistry. Whilst a variety of CF parameters were measured, a key indicator of plant health is the ratio of variable to maximum fluorescence (Fv/Fm) (Kochevaa *et al.* 2004). The analyses in this paper therefore focus on the important parameter of Fv/Fm; the other CF parameters are beyond the scope of this research chapter.

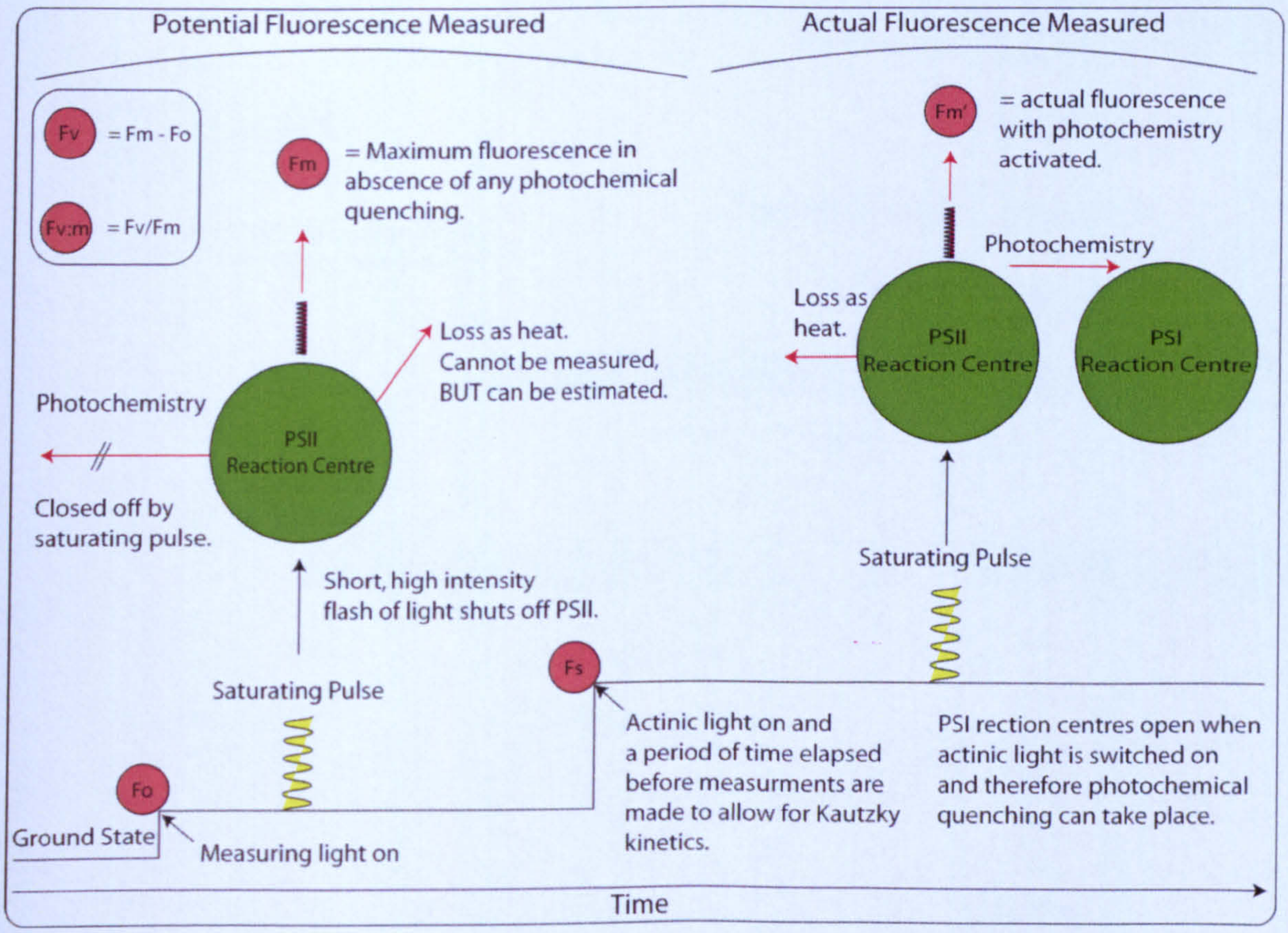

Figure 6.2: Conceptual illustration of the process of Chlorophyll Fluorescence (CF) and parameters measured.

6.3 Analysis and Discussion

This section is split into two main parts. Firstly the ^{137}Cs uptake by the plants as well as the health of the plants as measured by Fv/Fm, and secondly the analysis of the trees' spectral reflectance in relation to ^{137}Cs contamination and plant health.

6.3.1 Specific ^{137}Cs Activity and Plant Health

Table 6.2 shows specific ^{137}Cs activity for each tree, whilst figure 6.3 presents the mean specific activity for each group. One sample has been excluded in the calculation of the mean in the high group. The particular sample is 'high 4' which is highlighted in table 6.2 and is thought to be an anomalous result. This is due to the sample containing very few needles relative to the other samples and the resulting effects on efficiency of counting during the gamma spectrometry process.

Specific Activity of Needles							
Control	**Specific Activity (Bq/g)**	**Low**	**Specific Activity (Bq/g)**	**Medium**	**Specific Activity (Bq/g)**	**High**	**Specific Activity (Bq/g)**
1	0.07	1	86.06	1	177.55	1	1.86
2	0.36	2	35.34	2	19.46	2	0.65
3	0.10	3	36.41	3	836.27	3	399.25
4	0.08	4	61.47	4	7.39	**4**	**2792.04***
5	0.39	5	6.34	5	344.65	5	65.04
Average	0.20		45.12		277.07		116.70
StDev	0.16		30.08		341.42		190.75
Coefficient of Variance (%)	79.83		66.66		123.23		163.46

*Table 6.2: Specific ^{137}Cs activities for each sample, as measured by gamma spectrometry. * denotes the suspected anomaly ('high 4') which is included in the table for completeness of data, but which is excluded from calculation of mean and standard deviation and thus any subsequent analysis.*

The uptake of ^{137}Cs is non-linear despite all other growing conditions being kept constant. Unexpectedly, the medium group of trees have the highest specific ^{137}Cs activity, pointing to a higher transfer factor in this group, or perhaps a blocking mechanism (preventing ^{137}Cs uptake) at certain ^{137}Cs concentrations. This is corroborated by White and Broadley (2000) who suggest that in the presence of a constant Potassium (K) concentration (as in the hydroponic solutions in this experiment) an inhibitory effect limits Cs uptake as the Cs concentration increases. In essence the blocking mechanism is active due to the K uptake pathways in plants closing in high concentrations of Cs.

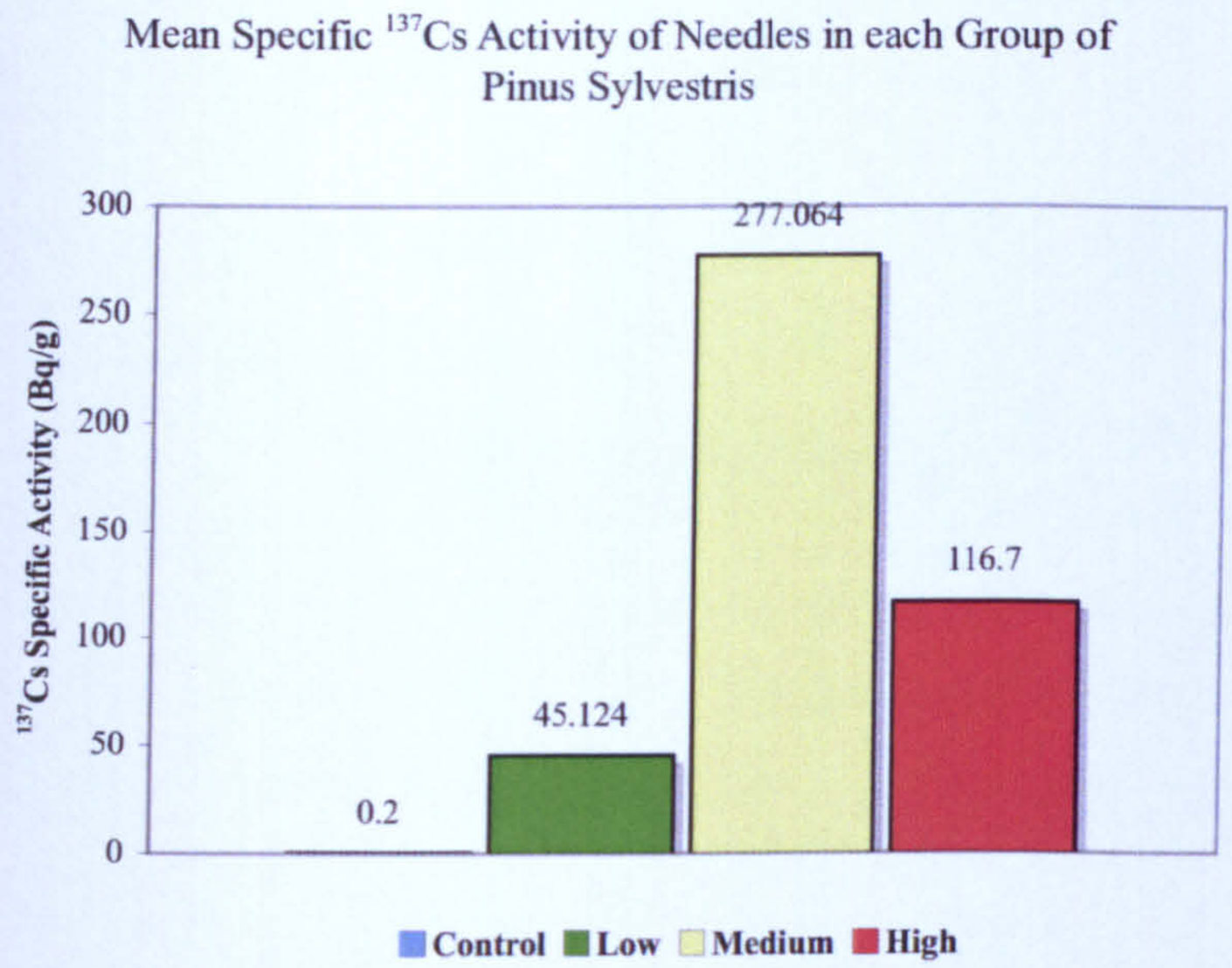

Figure 6.3: Mean specific ^{137}Cs activity in Bq/g for each group of trees as acquired by gamma spectrometry. n = 5 in each group except 'high' where n = 4 due to a likely anomaly being removed from the mean calculation.

The Fv/Fm values indicate that plant health is also non-linear in its response to ^{137}Cs contamination. Healthy green plants usually have an Fv/Fm value ranging from between 0.7 and 0.8, with the figure tending to decrease with stress (Rosso *et al.* 2005). Figure 6.4 shows mean Fv/Fm values for each group and according to this measure the medium group of trees are the least stressed, followed by the high and then the low and control groups. This is surprising in that the control group are the most stressed. This points to the possibility of a hormetic dose response rate. Hormesis is a dose response characterised by a stimulation at low doses and a high dose inhibition (Calabrese 2005).

In the case of this experiment, ^{137}Cs appears to have a positive effect on the health of the plants as the dose rate increases until a threshold is reached at the high level where health (as indicated by Fv/Fm) then begins to decline. Interestingly, the needles with the highest mean specific ^{137}Cs activity also have the highest mean Fv/Fm values. This may be partly explained by the blocking mechanism mentioned above which according to White and Broadley (2000) also inhibits uptake of other nutrients and thus trees in the highest dose group may be lacking in nutrients relative to the medium group because of this blocking mechanism. This provides interesting further opportunity for the experiment in terms of measuring the ^{137}Cs left in the solution to ascertain if ^{137}Cs is being stored elsewhere in the plant or if it is left in the solution. This highlights a limitation in the methodology of the

current experiment; that only ^{137}Cs needle specific activity was measured as opposed to the specific activity of the growing solution as well.

If the response by *Pinus sylvestris* to ^{137}Cs contamination is hormetic then it has important implications for remote sensing of radionuclide contamination and could effectively preclude sensing low-level radioactive stress which might be disguised as healthy forests rather than those being stimulated by low dose radiation. The analysis of the spectra is therefore key in determining whether changes in the spectra caused by ^{137}Cs can be isolated and detected. Having said this it is pertinent to remember that the ^{137}Cs levels in this artificial laboratory study are higher than those collected in Belarus (section 6.2.1).

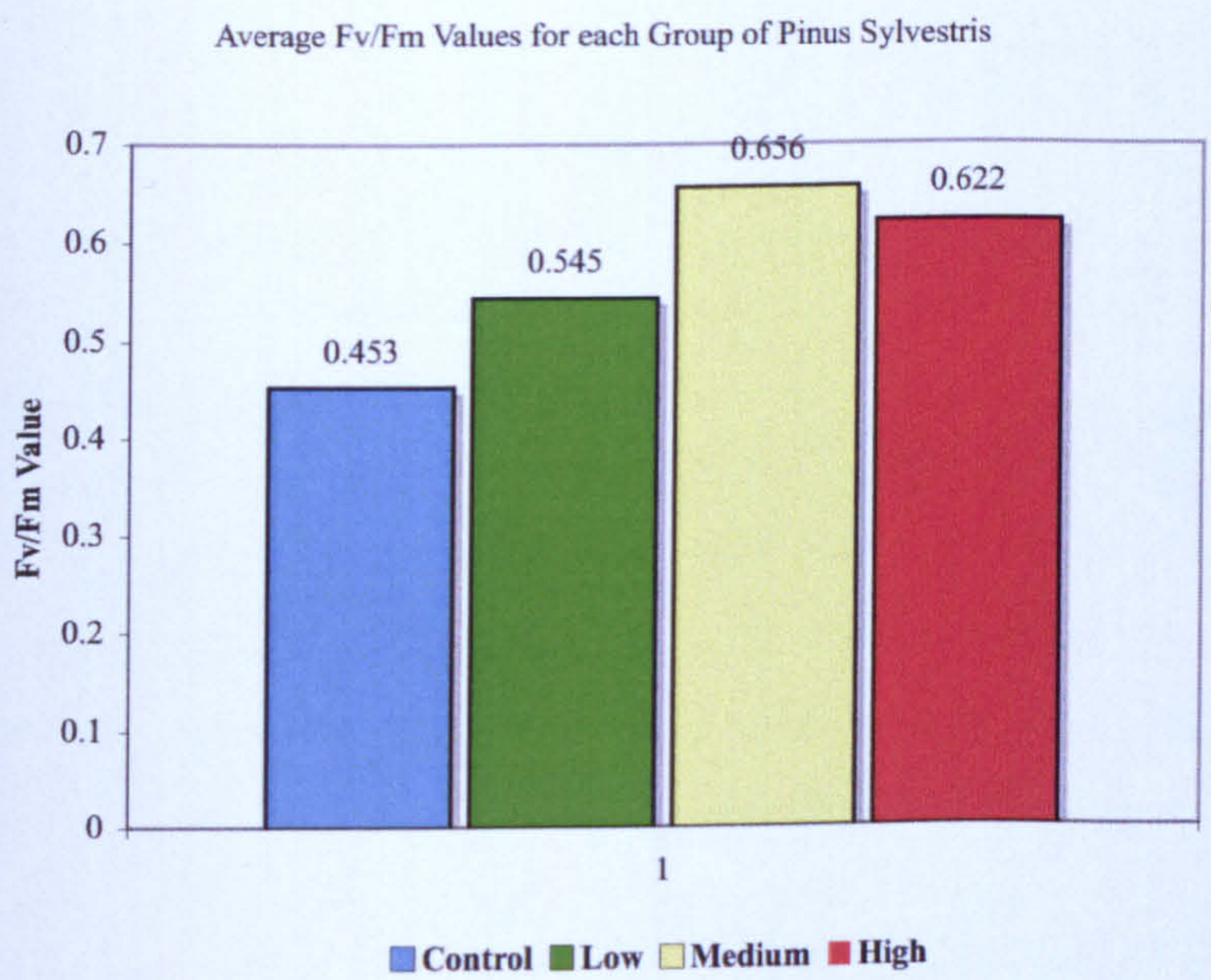

Figure 6.4: Average Fv/Fm values as measured by Chlorophyll Fluorescence.

6.3.2 Spectral Analysis

Spectra were collected on needles harvested at the end of the experiment. Figure 6.5 shows the average spectral reflectance for each group of trees and indicates that there are differences in spectra between groups. The next step in spectral analysis involved exploring the correlation between spectral reflectance and specific ^{137}Cs activity. Correlation was computed against absolute reflectance as well as two statistical transformations of the spectra, the first derivative and continuum-removed BDNA reflectance (described in chapter 3, section 3.3.4). Statistical transformation of the spectra

using derivative spectroscopy and continuum removal allowed subtle changes in spectral response to be resolved and assessed.

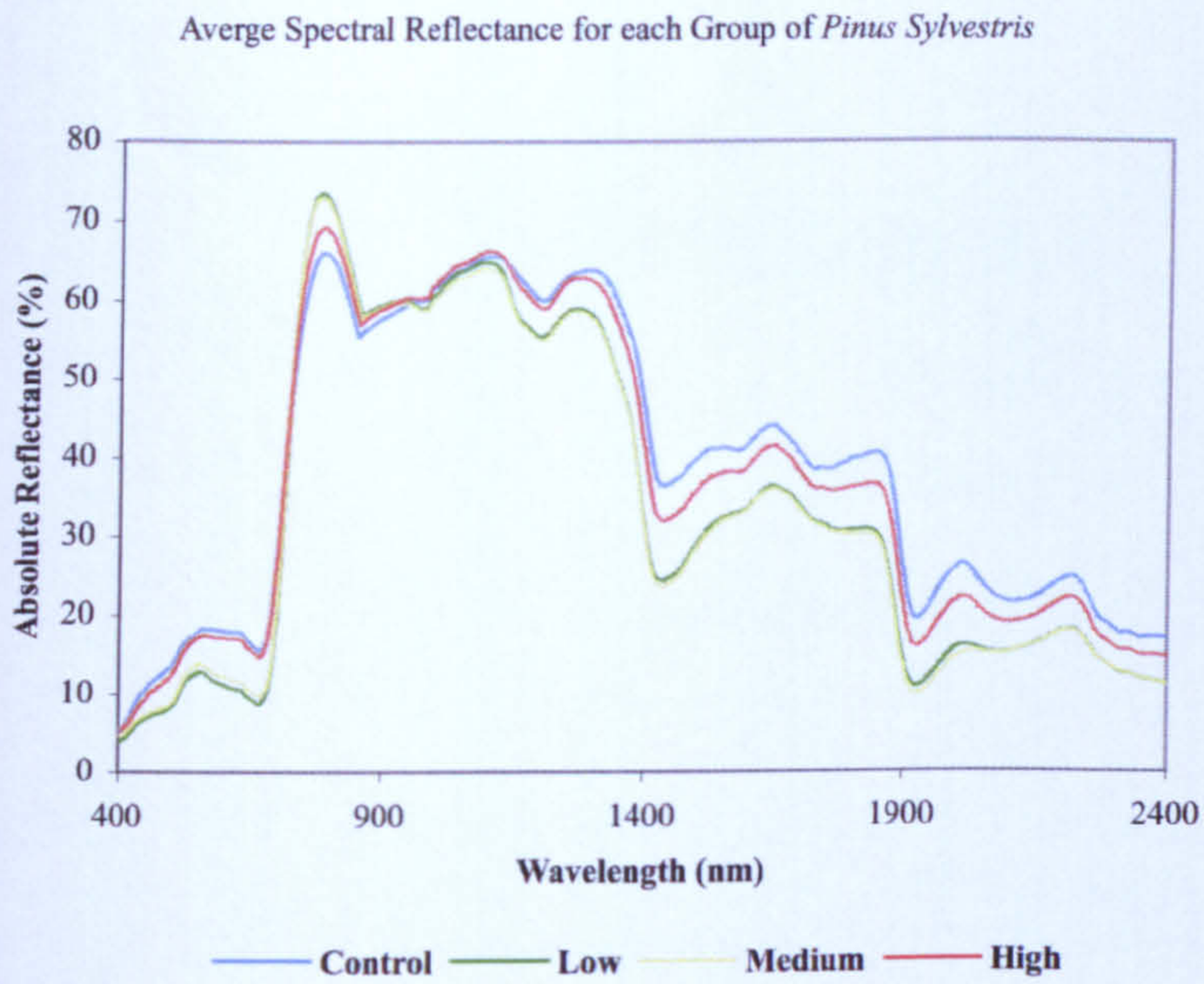

Figure 6.5: Mean spectral reflectance for each group of trees in the experiment (control, low, medium and high).

The correlation coefficient was squared to convert it to the coefficient of determination, allowing the strength of the correlation to be assessed as the percentage of reflectance that might be caused by changes in ^{137}Cs levels. After correlating spectral response with specific ^{137}Cs activity, Fv/Fm measurements were correlated with spectral reflectance, first derivative and continuum removed reflectance. This was to see if wavebands significantly correlated with ^{137}Cs might also be related to plant health (as determined by Fv/Fm) and whether any of these wavelengths are associated with key foliar biochemicals and their known absorption points. In addition, consideration was given to whether results from the laboratory were similar to those obtained in the field (chapters four and five).

Figure 6.6 shows the coefficient of determination between absolute reflectance and specific ^{137}Cs activity. At the 95% confidence level no bands are significantly correlated with ^{137}Cs, with a maximum of approximately 15% of spectral variation possibly being explained by ^{137}Cs (at bands 1390nm and 1874nm).

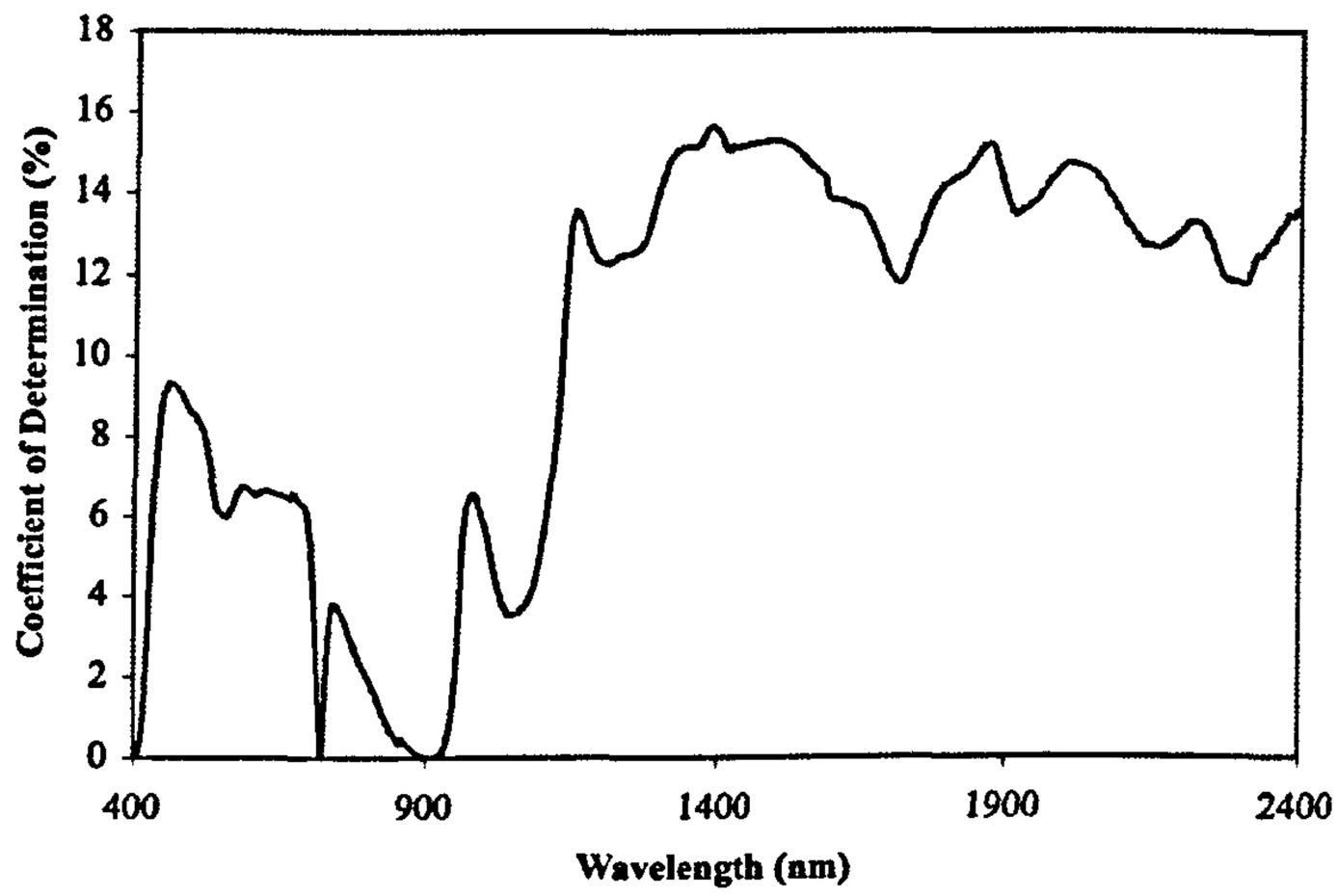

Figure 6.6: Coefficient of determination between raw spectra (absolute reflectance) and specific ^{137}Cs activity across the entire spectrum. The coefficient of determination is the squared correlation coefficient and is interpreted as the percentage of variation in one variable possibly caused by the other. n = 20. 95% confidence level is 19.7% (0.444^2).

Figure 6.7 illustrates the coefficient of determination between absolute reflectance and Fv/Fm values and it appears that there are many bands which have a statistically significant correlation with Fv/Fm values. This is perhaps somewhat expected, as Fv/Fm is a good indicator of plant health, which in turn would be expected to affect many wavelengths. Generally longer wavelengths from 1160nm onward have a higher proportion of variation that might be explained by changes in Fv/Fm. At the shorter wavelengths the 430-530nm region is significant. Again, this is expected given the known absorption by pigments/chlorophyll in this region and the direct impact on Fv/Fm these pigments would have.

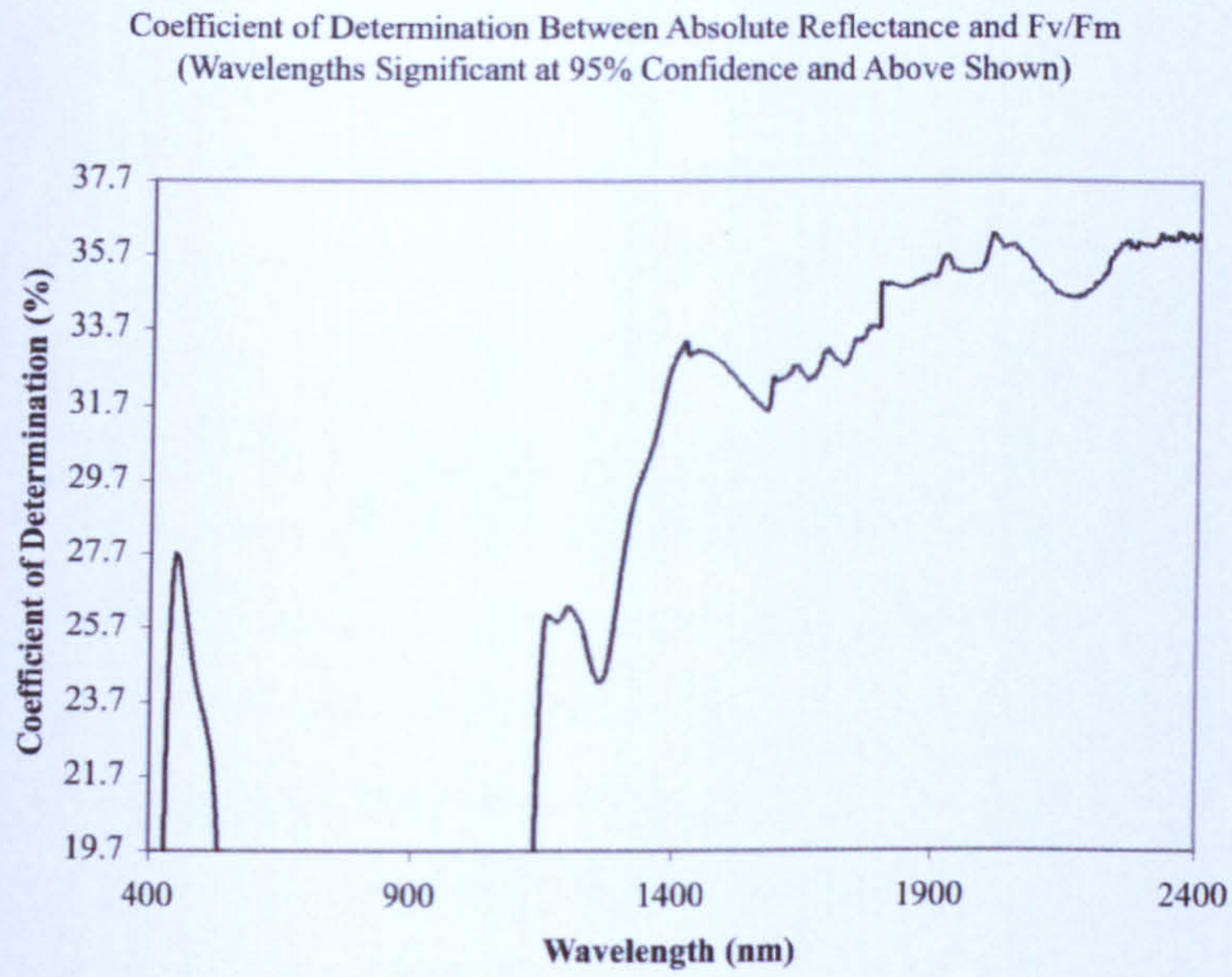

Figure 6.7: Coefficient of determination between raw spectra (absolute reflectance) and Fv/Fm values across the entire spectrum. The coefficient of determination is the correlation coefficient squared and is interpreted as the percentage of variation in one variable which is possibly caused by the other. n = 20.

The spectra were then transformed to the first derivative to determine if significant correlations existed. Demetriades-Shah (1990) indicates that the first derivative is suitable for removing background signals and resolving overlapping or complex absorption features. Figure 6.8 illustrates the mean first derivative at each wavelength for each group of trees.

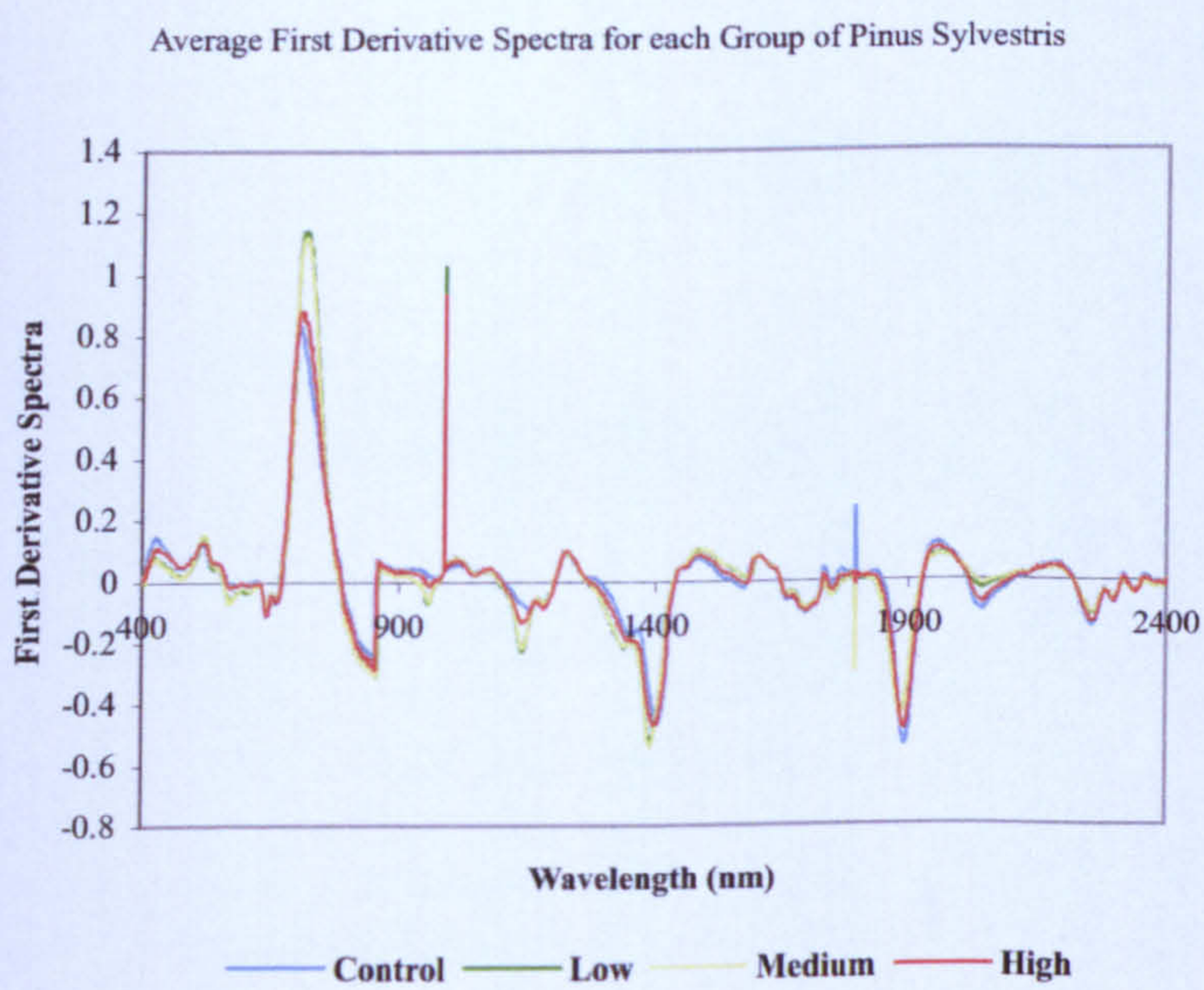

Figure 6.8: Mean first derivative spectra for each group of trees in the experiment (control, low, medium and high).

Correlation between the first derivative at each wavelength and specific ^{137}Cs activity (shown in figure 6.9) identified a variety of wavelengths significant at the 95% confidence level. The correlation analysis was performed on all samples (as there would not be enough samples to perform a statistically valid correlation for individual groups) with a total sample size of 20. Notably significant correlations exist at 424nm, 761nm, 1163nm, 1016nm, 1058nm, 1255nm, 1694nm, 1808nm and 2311nm. Some of these bands are close to known biochemical absorption features. For example 424nm is close to the chlorophyll absorption feature at 430nm, whilst the 1255nm band is close to the cellulose feature at 1275nm. The band with the highest correlation is 1163nm. 1163nm is close to a noted lignin absorption feature (1174nm). Some of these significant wavebands are similar to those identified in the field radiometry research (chapters four and five) (Boyd *et al.* 2006). It is interesting to note that ^{137}Cs is known to bind to lignin (e.g. Andolina and Guillitte 1990) and is postulated as a possible reason why fungi in radionuclide-contaminated areas seem to concentrate ^{137}Cs; they break down lignin (Nimis 1996). Whilst lignin content was not measured in the samples in this experiment (due to lack of needle material), needles collected in the field radiometry work have been assayed for lignin content and lignin has been highlighted by the foliar biochemical t-test (chapter five) to be significantly different based on changing ^{137}Cs levels.

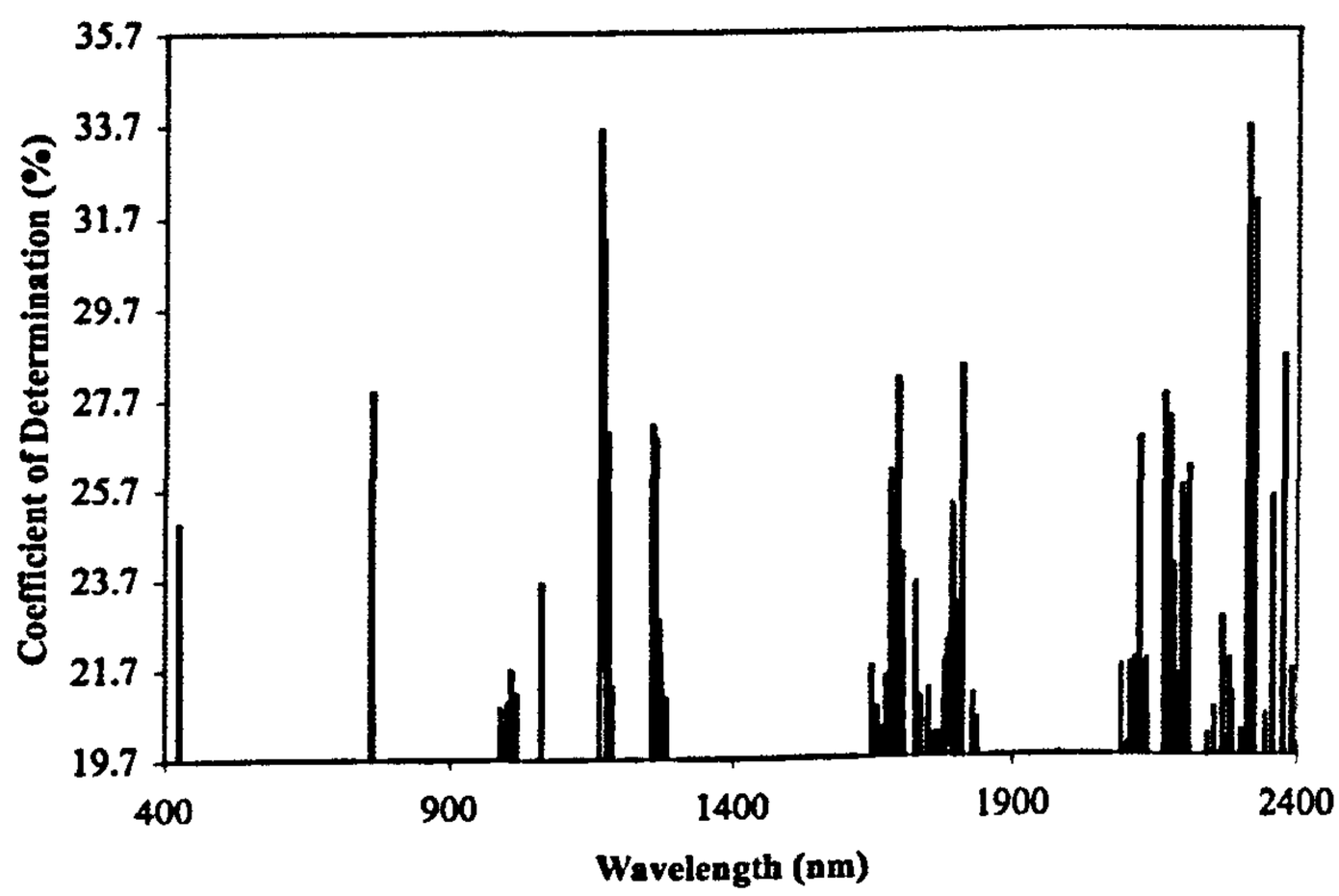

Figure 6.9: Coefficient of determination between first derivative transformed reflectance and specific ^{137}Cs activity. Values significant at the $\alpha = 5\%$ (95% confidence) level and above are shown. $n = 20$.

Figure 6.10 represents correlation between first derivative spectra and Fv/Fm values (plant health). As with the absolute reflectance correlation, there are many more bands that are statistically significant and the significance level of these bands is generally higher than for correlation between first derivative and specific ^{137}Cs activity.

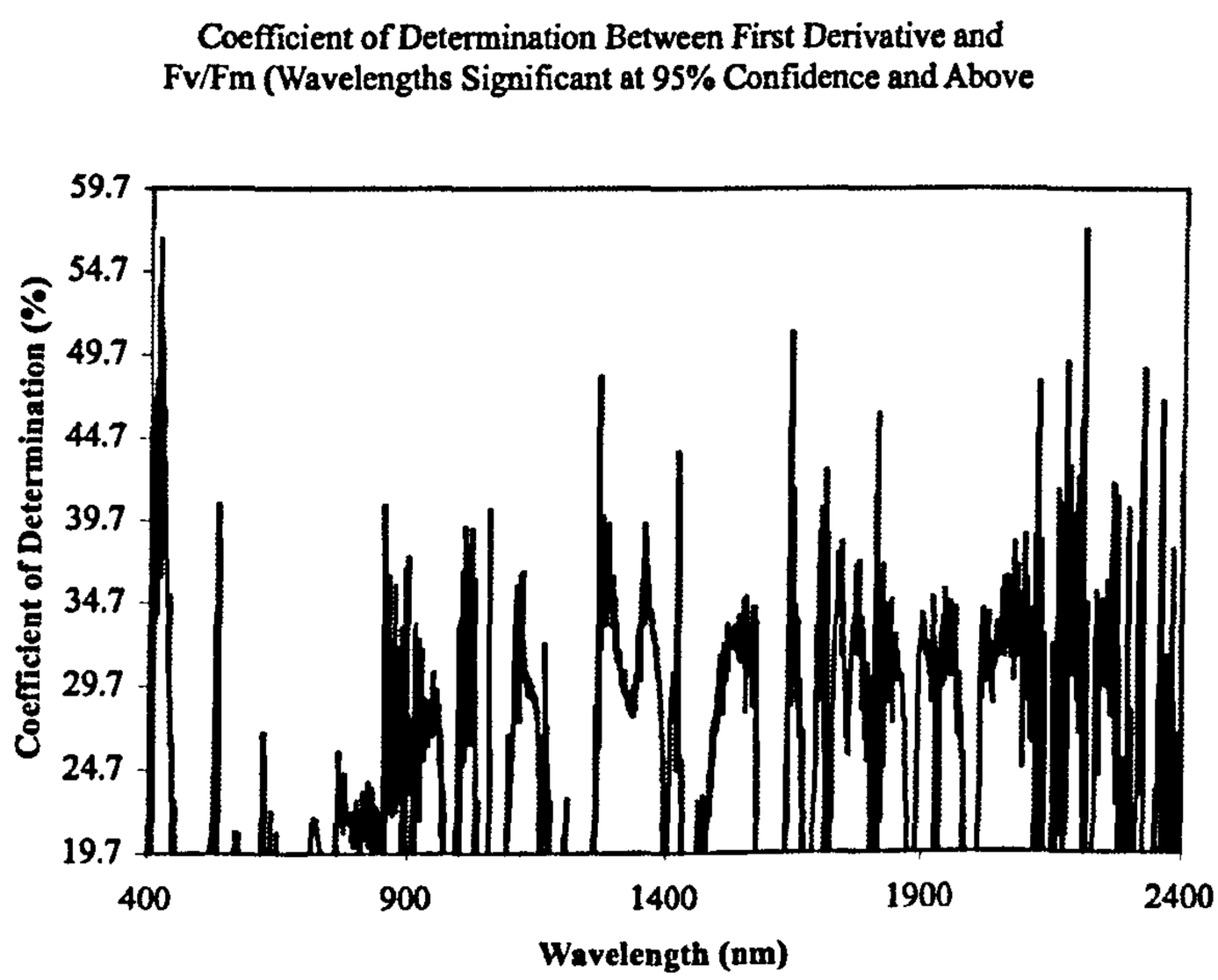

Figure 6.10: Coefficient of determination between first derivative transformed reflectance and Fv/Fm values. Values significant at the α = 5% (95% confidence) level and above are shown. n = 20.

As with absolute reflectance, these results are expected given that Fv/Fm is an indicator of overall plant function which would be expected to affect spectral reflectance (and its transformations) at the majority of wavelengths. Fv/Fm would therefore be expected to account for a large proportion of variation in reflectance. There are some significant wavelengths which are similar to the correlation between specific ^{137}Cs activity and first derivative, notably at 1163nm (lignin) and 424nm (chlorophyll). Interestingly 761nm is not significant in Fv/Fm correlation, but is significant in ^{137}Cs correlation and is located at the red edge shoulder. Additionally, 1058nm (starch/sugar) and 1255nm (cellulose) are not significant in Fv/Fm correlation, but are in the ^{137}Cs correlation.

The final correlations performed were between specific ^{137}Cs activity, Fv/Fm values and spectra which had been transformed into band depth normalised to area (BDNA). The BDNA is the end product of continuum removal (isolating spectral absorption features from the rest of the spectra) and is a function of a given wavelength within a particular

absorption feature. Continuum removal is reported by Curran *et al.* (2001) to provide a more accurate prediction of foliar biochemicals than the first derivative. Based on visual analysis of absolute reflectance as well as significant features in the literature and work in the pilot study (chapter four), six features were chosen for continuum removal, and ultimately, BDNA calculation. These were centred at 470nm, 670nm, 920nm, 1200nm, 1360nm and 1840nm. BDNA was calculated according to the method outlined in chapter three. Only one of the six continuum-removed absorption features contained significant correlations with Specific ^{137}Cs Activity. This was the 1200nm feature and is shown in figure 6.11.

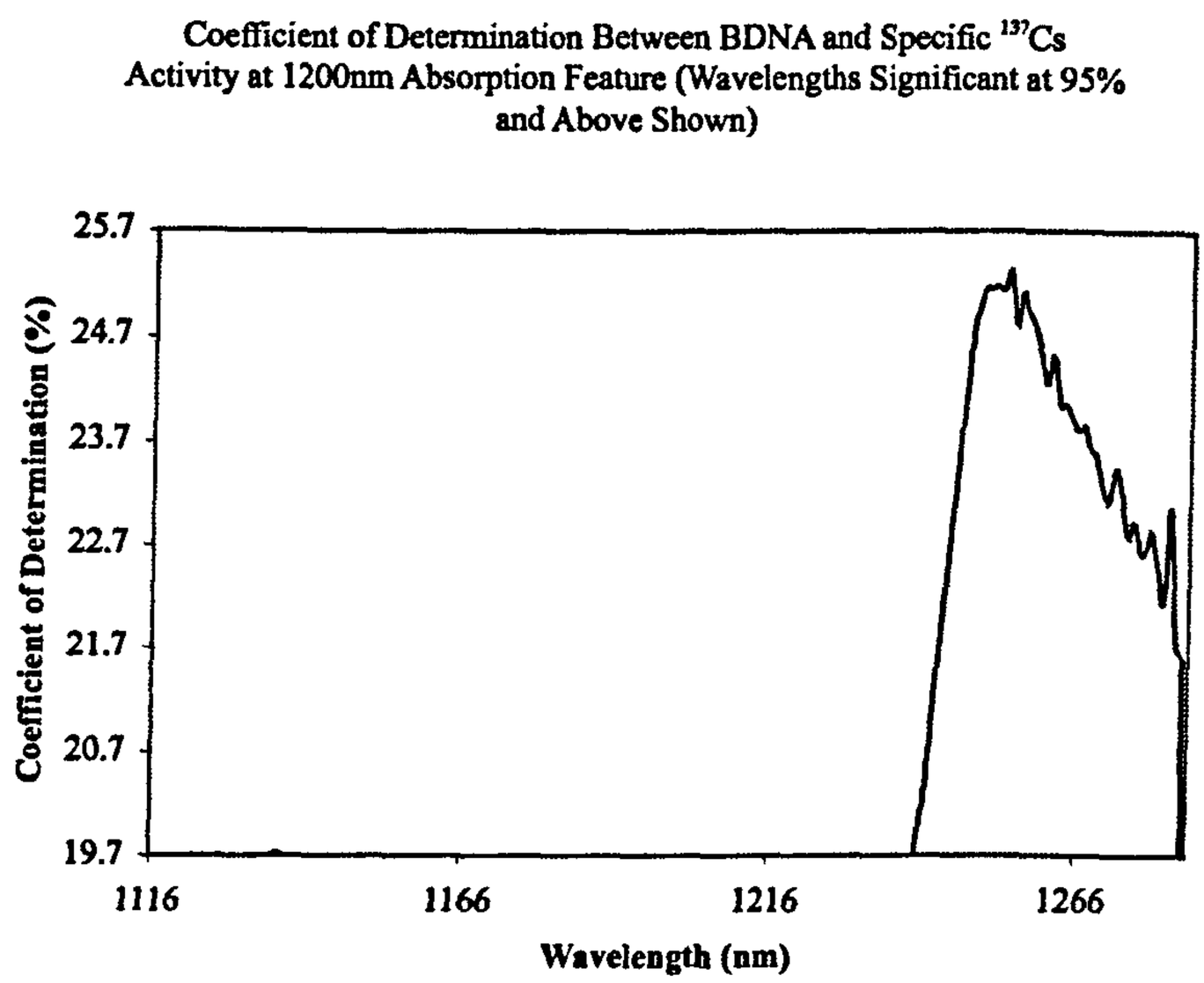

Figure 6.11: Coefficient of determination between band depth normalised to area reflectance and specific ^{137}Cs activity. This is at the 1200nm absorption feature. Values significant at the $\alpha = 5\%$ (95% confidence) level and above are shown. $n = 20$.

The coefficient of determination is lower than for similar wavelengths in the first derivative. A marginally significant waveband lies at 1136nm, close to the known absorption feature by water at 1140nm. 1240-1280nm are also significant bands and the peak of significance at 1255nm is close to (within 20nm) a known cellulose absorption point. This wavelength is also highlighted in first derivative correlation. Cellulose is related to lignin (Fioretto *et al.* 2005) and in turn may relate to the aforementioned binding of ^{137}Cs to lignin.

In figure 6.12, the coefficient of determination between BDNA and Fv/Fm values shows there are a number of significant wavebands, with particularly high coefficient of determination values at 1120nm (lignin) and bands (centred around 1260nm) which are also significant in the coefficient of determination for specific ^{137}Cs activity.

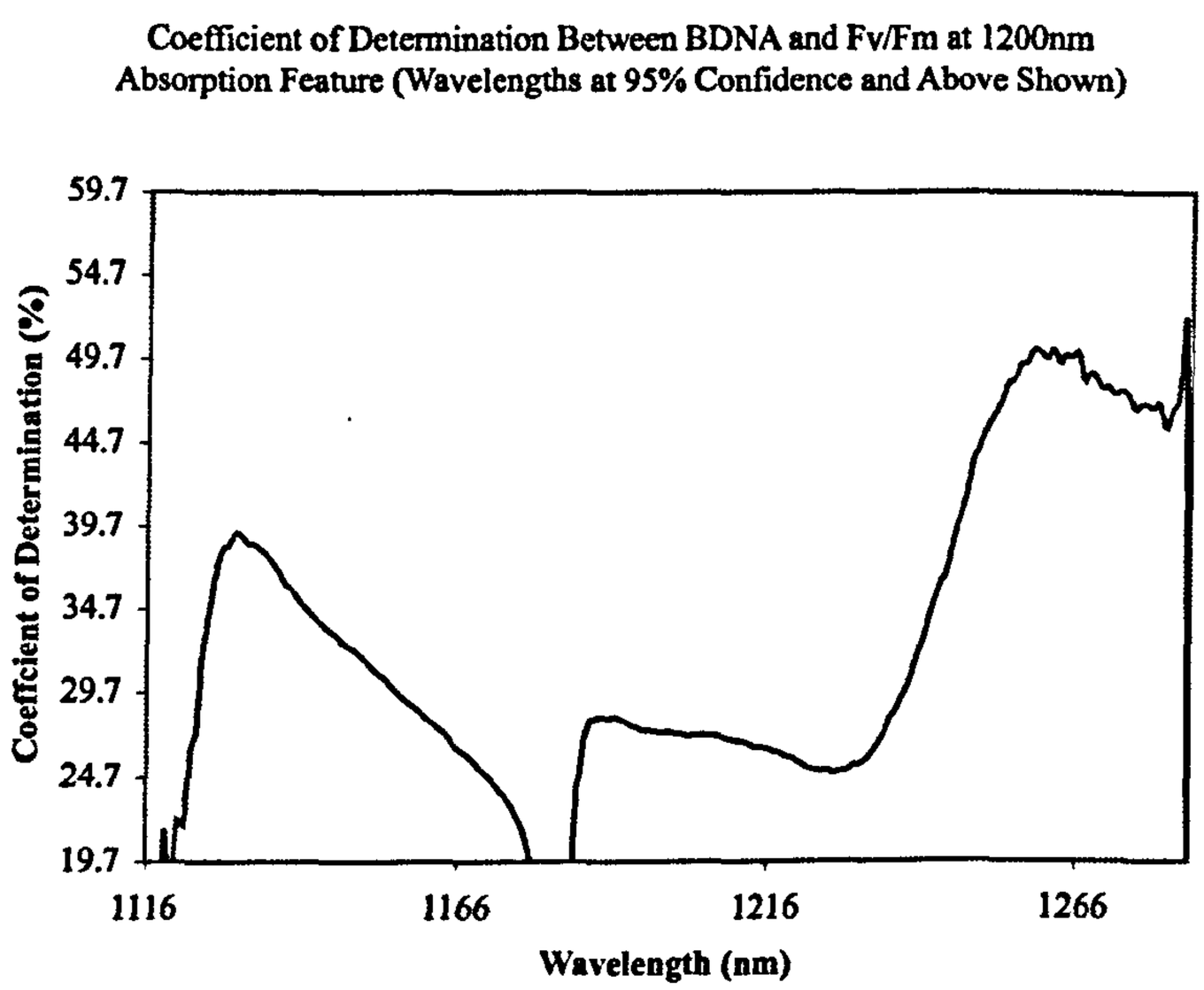

Figure 6.12: Coefficient of determination between band depth normalised to area reflectance and Fv/Fm values. This is at the 1200nm absorption feature. Values significant at the $\alpha = 5\%$ (95% confidence) level and above are shown. $n = 20$.

6.4 Summary

The findings of this experiment can be summarised as follows:

1. Uptake of ^{137}Cs by the plants has not been linear and the 'medium' group had the highest specific ^{137}Cs activity, suggesting the possibility of a blocking mechanism in ^{137}Cs uptake. In addition, the Fv/Fm values point to a non-linear, hormetic dose response to ^{137}Cs, with possible implications for remote sensing radionuclide contamination.

2. It has been shown through correlation with various manifestations of the spectra (absolute reflectance, first derivative, BDNA) and ^{137}Cs, that certain wavelengths vary in their reflectance, possibly as a function of specific ^{137}Cs activity. This is particularly at wavelengths associated with lignin and cellulose (structure of plant) and may be linked to the known binding of ^{137}Cs to lignin. There is also significant correlation between Fv/Fm values and spectra as well as at many more wavebands than specific ^{137}Cs activity,

although this is perhaps expected given that plant health is expected to affect spectral response across the entire spectrum. Of the three types of spectra, the first derivative exhibits the greatest number of significantly correlated bands in both ^{137}Cs specific activity and Fv/Fm values.

3. The value of the experiment has been in keeping all variables constant except the ^{137}Cs dose. Confidence that the changes in spectra and correlations are attributable to ^{137}Cs is therefore higher than for spectra collected in field studies (chapters four and five). It has also identified further research opportunity with a need to measure foliar biochemicals as well as ^{137}Cs and spectral reflectance. Overall the experiment has shown that spectra do differ based on changing ^{137}Cs levels and that wavelengths affected seem to be related to similar foliar biochemicals identified in the field studies (chapters four and five).

Several key lessons can be learned from the experiment described in this chapter and the strengths of the approach can be summed up as follows:

- An understanding of the relationship between spectral reflectance and ^{137}Cs concentration in *Pinus sylvestris* can be gained at its simplest level.

- Modifications to future fieldwork can be informed by the results of the experiment.

- Other data such as potassium and specific activity of the growing medium could be measured, thus further enhancing the usefulness of the experiment and in turn the fieldwork.

There are also several limitations which arise in the experimental approach and which should be considered for further research. These are:

- The lack of biochemical data is a hindrance to linking field and laboratory data and could be rectified in the future by prolonging the growing period in order to gain more needle material.

- The discrepancy between the age of trees in the laboratory experiment versus those in the field data prevent a true comparison of results between laboratory and field.

In the future older trees could be considered for use in the experiment, subject to logistical constraints.

- Measurement of ^{137}Cs specific activity in the needles along with spectral reflectance measurements could be undertaken at regular intervals throughout the experiment to gauge how trees respond through time and at what stage effects of ^{137}Cs concentration become visible in spectral reflectance data.

Despite these limitations, the experimental approach has provided useful data about how ^{137}Cs affects spectral reflectance of *Pinus sylvestris* and is useful for considering the implications of using remotely sensed imagery to attempt to measure ^{137}Cs contamination. Chapter seven describes research into hyperspectral imagery in relation to monitoring ^{137}Cs specific activity of *Pinus sylvestris*.

Chapter 7

Detecting ^{137}Cs from a Spaceborne Platform: Hyperion Imagery

7.1 Introduction

This chapter outlines research undertaken on hyperspectral imagery collected over the contaminated field sites described in chapter five. It begins by describing the processes of imagery collection and the radiometric and geometric correction routines applied to the imagery. It then details the extraction of spectra from certain pixels as well as the analyses of those spectra and finally compares spectra collected from space (imagery) to those spectra collected in the field. The chapter concludes by considering whether spaceborne hyperspectral imagery has the capability to detect changes in spectra caused by ^{137}Cs levels in *Pinus sylvestris*. It is important to note that this chapter is a brief scoping study assessing whether differences between ^{137}Cs contamination levels can be seen in spectra collected from space. This is mainly due to the limitation that the imagery was collected approximately one year after the field data (chapters four and five) and for further analyses, data collected coincidently with the imagery would be required. Political and logistical reasons prevented a return to Belarus to collect the necessary coincidental data. As such, the assumption was made that the forests from the hyperspectral images are identical in terms of their biophysical properties. The theme followed in this chapter is to link changes in spectra caused by varying foliar biochemicals in relation to ^{137}Cs content. Assumptions for the work centre around the accuracy of the atmospheric correction and biophysical factors. Both images were collected approximately two weeks apart and as such differences in scene illumination and radiometric quality exist. Whilst atmospheric correction was performed it is likely that some radiometric discrepancies remain. For the purposes of this research, biophysical factors were also assumed to be having no impact when comparing pixels from sites of differing contamination levels. In reality, biophysical

properties of forest canopies are likely to have large effects on differences in spectral response. These assumptions form opportunities to expand upon this work in the future.

7.2. The Hyperion Hyperspectral Instrument

High resolution spectral data is key to this research and therefore a spaceborne sensor capable of resolving detailed spectra was needed in order to make comparisons with field spectroscopy data from chapters four, five and six and to determine whether any subtle changes in spectral response, which might be related to ^{137}Cs content of vegetation, could be detected from space. Hyperion was chosen to collect spectra over the contaminated Belarusian landscape due to its technical attributes, which provided an ability to resolve detailed spectra at an appropriate spatial resolution.

The Hyperion sensor is one of three land imaging devices onboard the National Aeronautics and Space Administration (NASA) Earth Observation 1 (EO-1) satellite. Hyperion was the first civilian hyperspectral sensor to be deployed on a spaceborne platform and was originally conceived as an experimental technology demonstration mission (Pearlman *et al.* 2003). It is a tasking sensor with a spatial resolution of 30m, which is designed to match the spatial resolution of Landsat data in order to allow comparison and validation of EO-1 data. Spectrally, Hyperion is capable of resolving 242 spectral channels from 400 – 2500nm at 10nm intervals, though not all these bands are usable. Out of 242 channels, bands 1-7 (356-417nm) and 225-242 (2406-2578nm) are not calibrated. Bands 58-70 (VNIR) and 71-76 (SWIR) are also not calibrated. This leaves 198 calibrated bands but there is a small amount of overlap between the VNIR and SWIR instruments. These are bands 56-57 and 77-78. Therefore, out of 198 calibrated bands there are 196 unique usable channels. Hyperion is a pushbroom sensor with a ground surface cross-track width of approximately 7.5km with a typical scene length being 42km although this varies based on the data acquisition request (DAR) and can be up to 185km. The main technical attributes of the Hyperion instrument are summarised in table 7.1.

Hyperion Technical Specifications	
Spatial Resolution	30m
IFOV	42.4 micro radians
Number of Spectral Bands	242
Wavelength Range	400 – 2500nm
Spectral Coverage	VNIR 10.11 – 10.13nm SWIR 10.08 – 10.09nm
Band Width	VNIR 10.11-10.13nm SWIR 10.08 – 10.09nm
Swath Width	7.5km
Typical SNR	65-130
Data Quantization	12-bit
Altitude	705km (as of September 25th 2005, EO-1 orbit lowered by 5-6km)

Table 7.1: Summary of Hyperion technical specifications (adapted from Pearlman et al. 2003).

As mentioned above, Hyperion provides a suitably fine spectral resolution to characterise the spectral response of ^{137}Cs contaminated *Pinus sylvestris*, but is at the time of writing also the only spaceborne imaging spectrometer with a fine enough spatial resolution suitable for monitoring small scale changes over the Belarusian landscape. Hyperion was thus selected as the most appropriate spaceborne imaging spectrometer from which to collect data from the contaminated Belarusian landscape.

7.3 Data Acquisition over the Belarusian Landscape

Since Hyperion is a tasking sensor, a data acquisition request (DAR) was submitted to the United States Geological Survey (USGS). The centre coordinates of each of the three fieldsites mentioned in chapter 5 (section 5.2) were used to define the centre point of the required images. Three DARs were submitted (one for each of the fieldsites; control, medium and high). Nadir collection was specified to give maximum radiometric quality. Each DAR allowed three attempts to collect a scene with less than 25% cloud cover. If after three collections none of the resulting images had less than 25% cover the DAR was still considered fulfilled. The DARs for the medium and high sites provided two images with quality classified by the USGS as 'very good'. Each of the three attempts at acquisition over the control site resulted in images of 100% cloud cover and as a result the DAR was fulfilled although no image was provided for the control site. To collect spaceborne spectra from forests with no contamination an alternative was needed. To

gather such spectra, clean *Pinus sylvestris* stands were identified within the image which was acquired over the high ^{137}Cs contaminated field site and these were used to provide spectra from trees not contaminated with ^{137}Cs. The images collected along with the position of the medium, high and clean forests are shown in figures 7.1 and 7.2. In addition, the metadata for the medium and high images are shown in appendix A6. Once data had been collected, imagery was pre-processed to correct geometric and radiometric distortions.

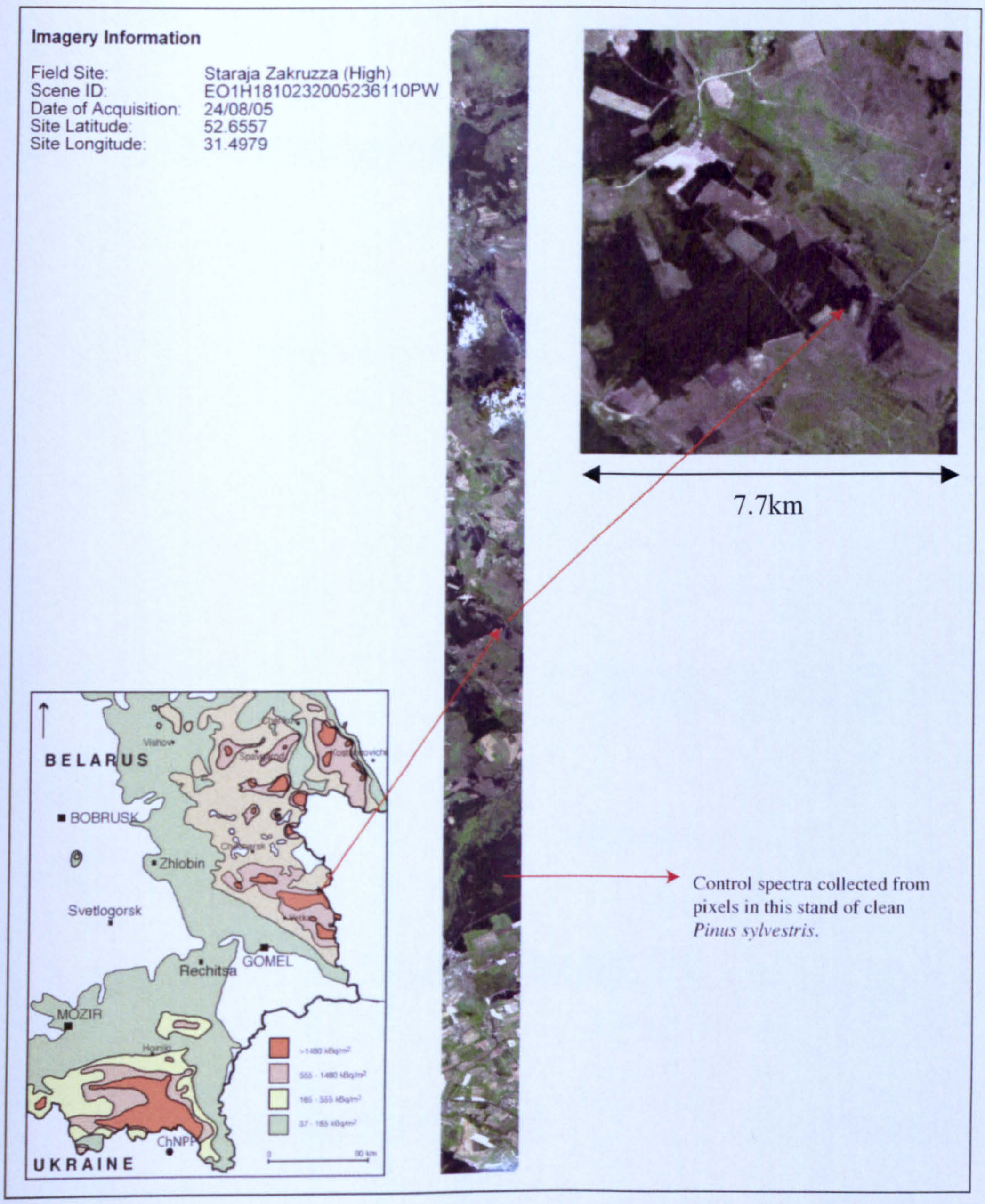

Figure 7.1: Approximate true colour display of Hyperion imagery collected from the high site along with its location in relation to Belarus and a zoom of the field area. The main Hyperion scene is approximately 7.7km wide and 185km long.

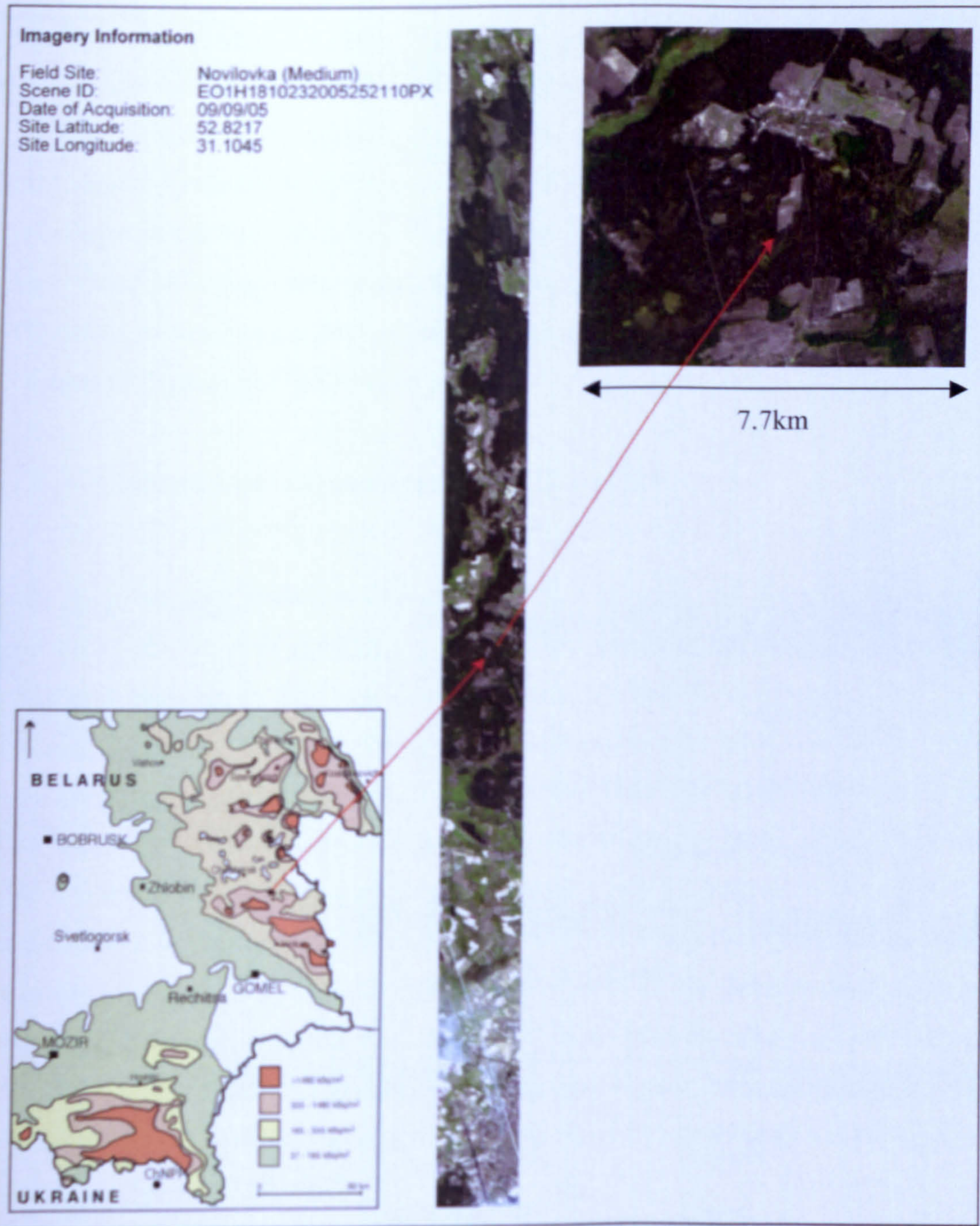

Figure 7.2: Approximate true colour display of Hyperion imagery collected from the medium site along with its location in relation to Belarus and a zoom of the field area. The main Hyperion scene is approximately 7.7km wide and 185km long.

7.4 Pre-processing of Imagery

Data was received from USGS in the hierarchical data format (HDF) and was already radiometrically calibrated (correction of known issues and nominal artefact removal) to a level 1R data product. In order to determine the spectral content of an image pixel, the atmosphere must be characterised to a sufficient accuracy (Sanders *et al.* 2001). In addition, effects of path radiance, water vapour and other trace gases can be removed and DN values of radiance could be converted to absolute reflectance (Goetz *et al.* 2002). This was important in this research so that spectra collected from field sites could be compared with those collected from space. The effects of the atmosphere on the imagery were characterised and corrected by utilising using the Fast Line-of-sight Atmospheric Analysis of Spectral Hypercubes (FLAASH) model.

7.4.1 Atmospheric Correction using FLAASH

The most accurate techniques for atmospheric correction are those based on empirical methods (Ben-dor *et al.* 2004) whereby field data is collected coincidentally with imagery and used to correct for atmospheric effects. In this work, imagery was collected approximately one year after the field data and so this precluded the use of empirically based techniques. The alternative to empirical methods rely on modelling the radiance at the sensor by using radiative transfer models (French *et al.* 2002). These models require basic information about the scene (e.g. site height, visibility, acquisition times) and use this information along with physical principles to correct for atmospheric effects. Several models exist (e.g. ATREM, HATCH, ACORN) but all are alike in their approach and derive similar results (Staenz *et al.* 2001). FLAASH is an atmospheric correction module which runs within RSI's ENVI image processing software. It was developed by Spectral Sciences Inc. under sponsorship of the U.S. Air Force Research Laboratory and utilises the MODTRAN model (RSI 2005).

The two Hyperion images were atmospherically corrected using ENVI 4.2 and the FLAASH module at the University of Southampton. FLAASH contained a built in spectrograph definition file to correct for the known spectral smile of Hyperion (Jupp *et al.* 2001). Full images (not subset) were entered into the FLAASH module. As only two

images required correction, computation time did not pose a problem and the finest resolution MODTRAN model was selected (5cm). In addition, spectral polishing was implemented to remove spectral artefacts from the spectra (RSI 2005). The output resulted in two atmospherically corrected Hyperion images which were then spectrally subset to the unique usable bands described in section 7.2 and were then ready for geometric correction.

7.4.2 Geometric Correction

Geometric correction was applied to the images so pixels could be chosen and extracted based on fieldwork locations. The method used was similar to that described by Dyk *et al.* (2002). A geometrically corrected Landsat image was used as the reference image and forty ground control points (GCPs) were selected for each image. A simple nearest neighbour polynomial transformation was then applied in ENVI resulting in a geometrically corrected Hyperion scene. For the high image, the RMS error was 0.311 pixels (9.3m) and for the medium image RMS error was 0.294 pixels (8.8m). Following this geometric correction and the atmospheric correction described in section 7.4.1 two Hyperion scenes were ready for extraction of pixels for spectral analysis.

7.5 Extraction of Spectra From Pixels

The focus of this chapter remained on old trees (c. >20 years) as these have been shown to have most potential for utilising imaging spectrometry to monitor their ^{137}Cs content as well as their inherent economic value. In addition, the images were collected to match data from the field sites in chapter five, which were also old trees (c. >20 years). Spectra were extracted from the pixels representing the medium and high field sites (described in chapter five, section 5.2) and also from an area of *Pinus sylvestris* in the Staraja Zakruzza (high) image which is known to be clean (little or no ^{137}Cs contamination). From each of the three image areas, spectra from 20 pixels were extracted. In addition, at the centre of each site a window of 5x5, 10x10 and 15x15 pixels was extracted to represent the average spectral response at each of the three locations. In the medium and high *Pinus sylvestris* stands, spectra were selected based on the GPS coordinates taken in the field. Pixels were selected based on their proximity to the field GPS coordinates collected. In the clean site, pixels were selected randomly since no fieldwork took place at this site. Ideally, each of

the spectral samples collected from the field (chapter 5) would have had a representative pixel in the image from which corresponding spectra could have been extracted. The spatial resolution (30m pixels) of Hyperion precluded this and meant that each pixel represented at least one field sample. Pixels were therefore chosen based on ^{137}Cs levels of field spectra which could be related to a particular pixel. This gave spectra which could be identified as having either low, medium or high levels of ^{137}Cs despite the inter-site variability of ^{137}Cs. Collection of 20 pixels from each site allowed a fair representation of the samples collected in the field. Once extracted, the spectra were then processed to first derivative spectra (FDS) and analysed to assess whether significant differences existed between spectra contaminated with relatively high and low ^{137}Cs levels.

7.6 Analysis of Image Spectral Information

The first analysis was to assess whether significant differences existed between spectra contaminated with high and low levels of ^{137}Cs. Splitting samples into relatively high and low levels of ^{137}Cs was straightforward in the field and laboratory samples since ^{137}Cs specific activity of *Pinus sylvestris* was measured using gamma spectrometry. In the imagery this presented a challenge since specific ^{137}Cs activity of pixels was not known. To overcome this, spectra were chosen and extracted from pixels that were spatially close to field samples of a known activity and as such, ^{137}Cs specific activity of the pixels could be inferred. Needles are likely to bioaccumulate ^{137}Cs differently to the rest of the tree and as such, using needle as opposed to whole wood concentration of ^{137}Cs may give a skewed indication of true ^{137}Cs concentrations in *Pinus sylvestris*. This is an additional limitation which warrants further investigation. There is thus a need to investigate the relationship between needle accumulations of ^{137}Cs and whole wood activity concentrations.

Domestic and lumber fuel wood limits used in chapters four and five could not be used to split spectra from pixels as the exact ^{137}Cs activity level was not known. Although each sample in chapters four and five had data for ground level ambient dose rate and specific ^{137}Cs activity of needles, the spatial resolution of Hyperion imagery (30m) precluded the use of extracting exact activities from known samples. As such spectra were split simply between high (nearest field samples above 1Bq/g) and low (nearest field samples below 0.5Bq/g). Analysing whether differences existed between high and low spectra was then

carried out by performing a two-tailed Student's t-test to see if statistically significant differences existed, at which wavelengths and whether these were in similar areas of the electromagnetic spectrum to those shown by the t-tests for the field (chapter 5) and laboratory (chapter 6) spectra. Student's t-tests were performed between FDS collected from each site and the results are presented below in figures 7.3, 7.4 and 7.5.

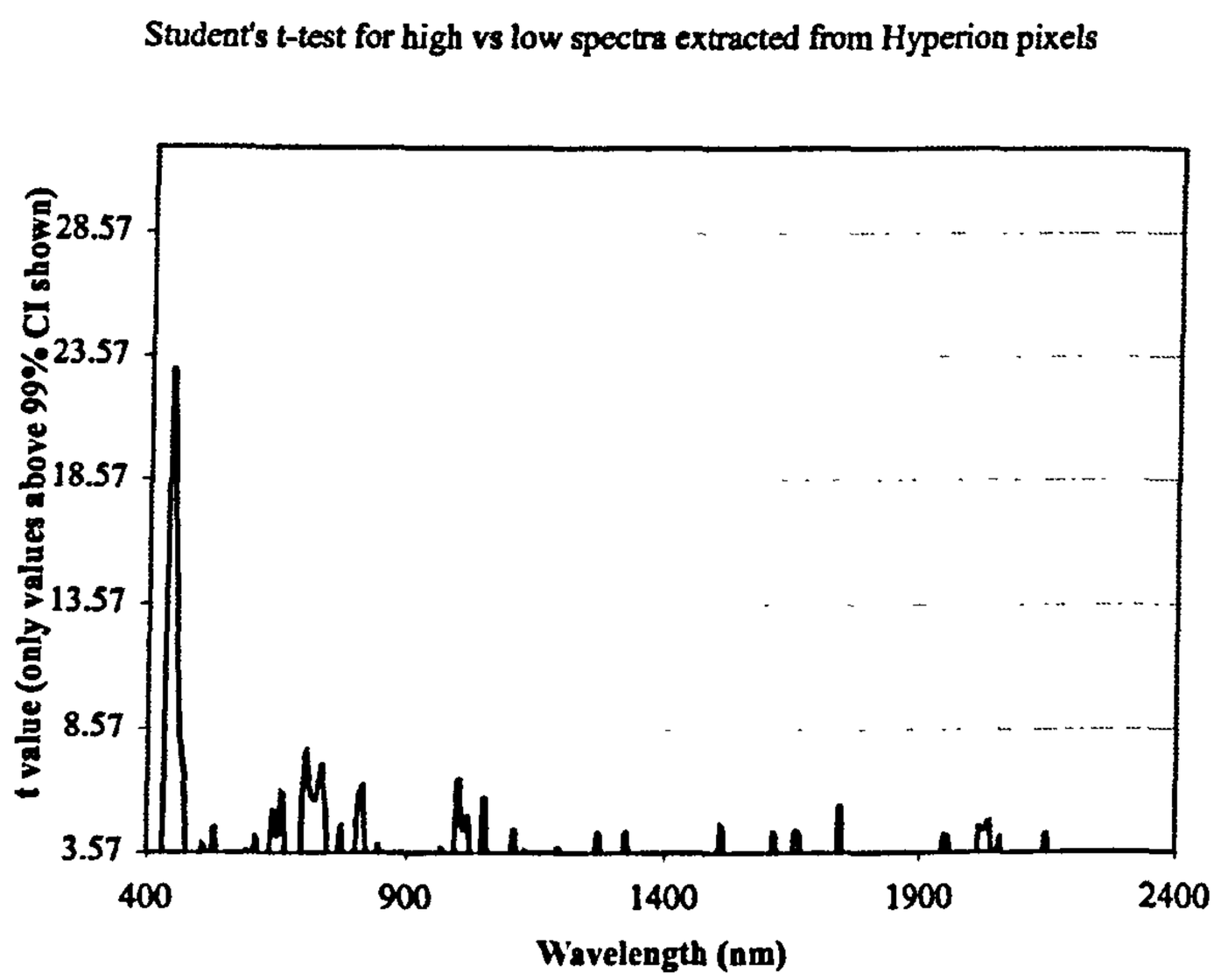

Figure 7.3: Student's t-test results for high versus low FDS extracted from Hyperion pixels. Only wavelengths significant at the 99% confidence interval are shown (3.57 is the minimum t-value required for a 99% significance level).

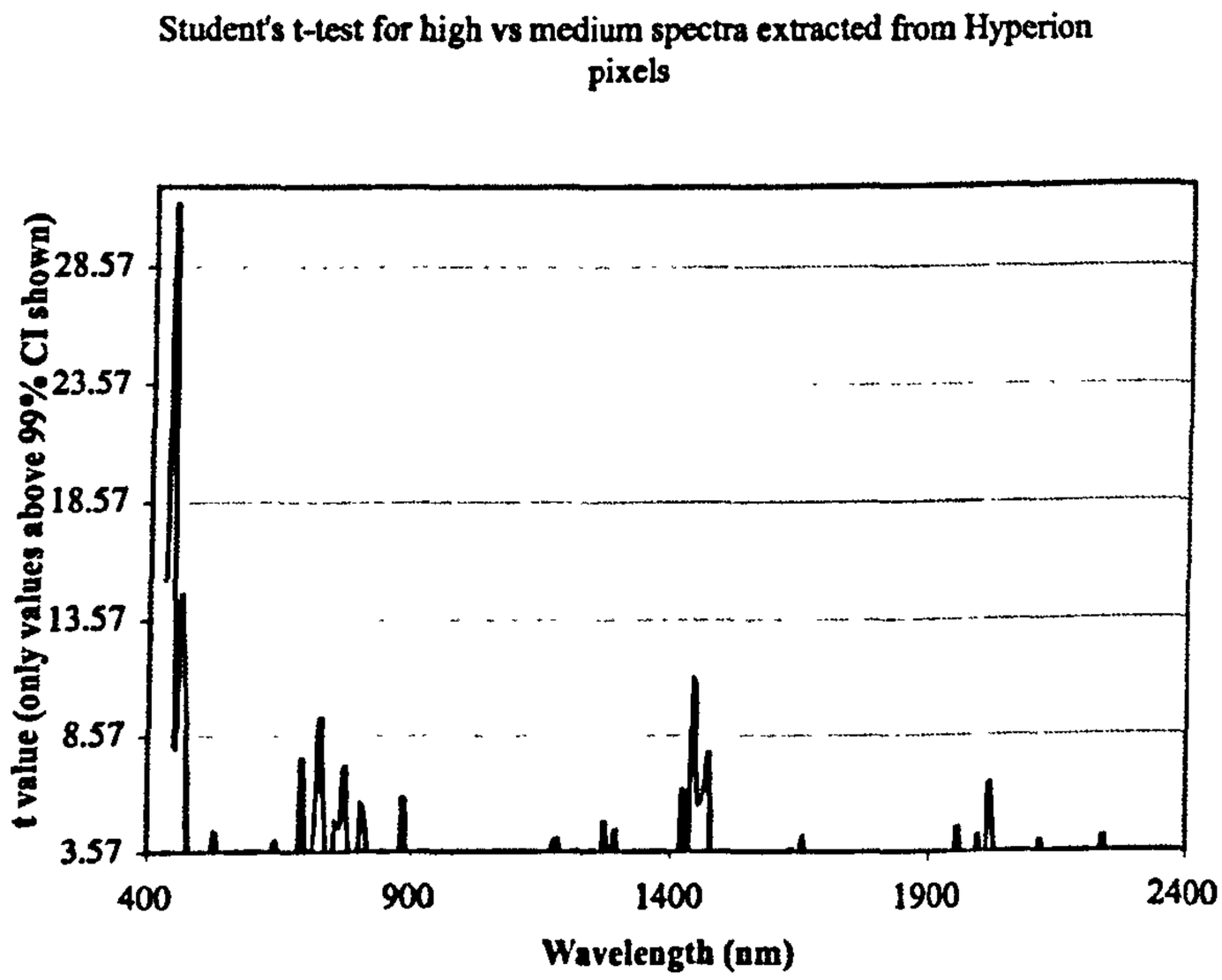

Figure 7.4: Student's t-test results for high versus medium ^{137}Cs FDS extracted from Hyperion pixels.

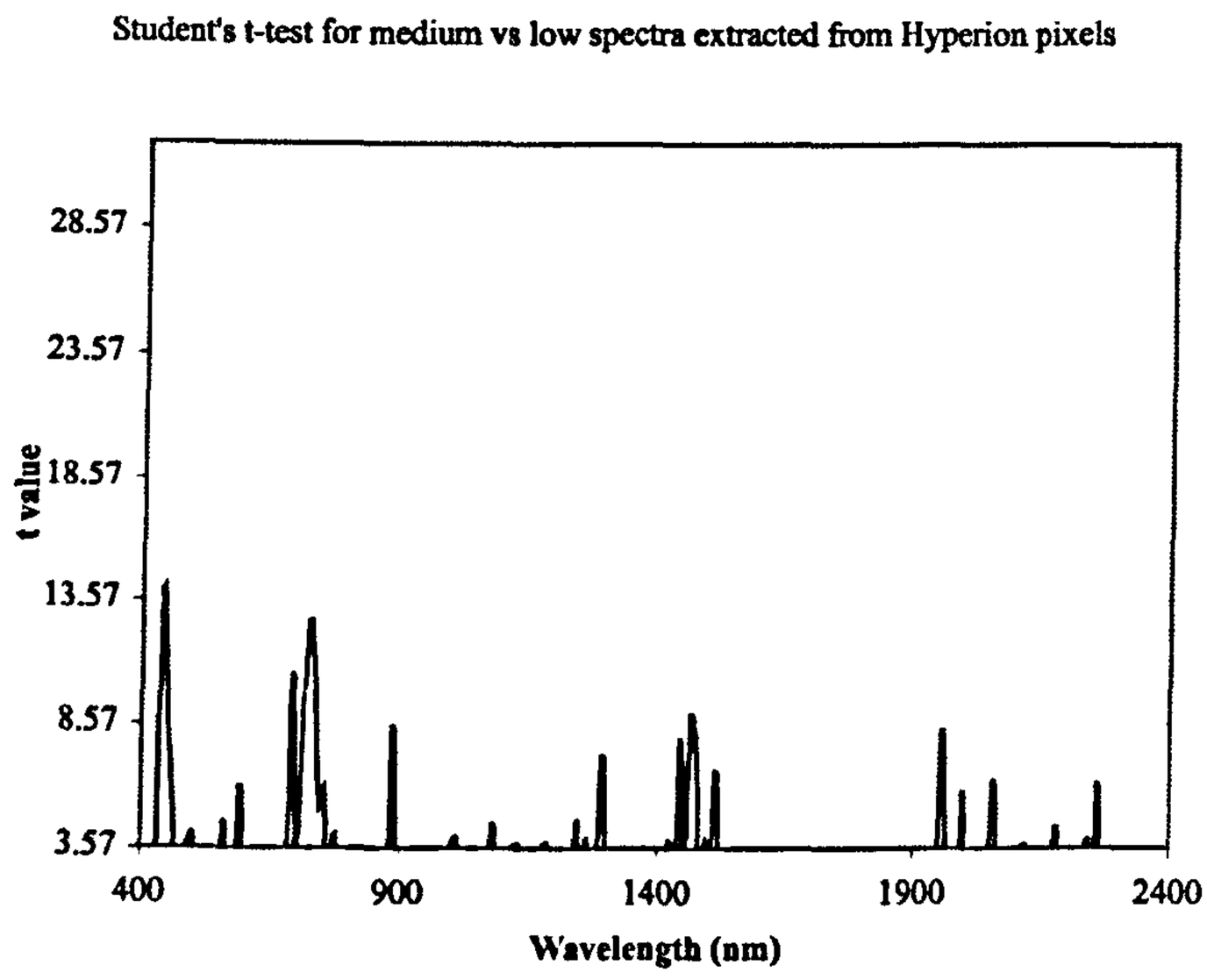

Figure 7.5: Student's t-test results for medium versus low ^{137}Cs FDS extracted from Hyperion pixels.

The t-test result in figure 7.3 shows statistically significant differences exist between Hyperion spectra from *Pinus sylvestris* forests contaminated with relatively high and low levels of ^{137}Cs. The high and low pixels in this t-test came from the same image (figure 7.1). As the high and low spectra have come from the same image, this helps to minimise differences that might otherwise be associated with radiometric or geometric image distortions. The wavelength of maximum difference is at 448nm and is associated with chlorophyll content. The second is at 702nm and is associated with the red edge region of the electromagnetic spectrum. This is followed by 998nm (associated with starch) and 814nm (unattributable). As spectra extracted from Hyperion imagery corresponded to low, medium and high levels of ^{137}Cs, the t-test was performed between each of these groups to assess whether the same wavelengths differed significantly and which might be related to certain foliar biochemicals.

The general pattern is shown by figure 7.4 to be similar as that for high versus low spectra, except the graph appears nosier than in high versus low. This maybe partly due to comparing spectra from differing images, which although should be feasible given the atmospheric correction employed, radiometric error and distortion cannot be completely eradicated. The wavelength of maximum significance is again at 437nm (associated with chlorophyll), followed by 1442nm (associated with lignin), 722nm (associated with chlorophyll), 692nm (associated with chlorophyll), 2017nm (associated with starch),

1291nm (unattributable), 1956nm (associated with water, lignin, protein, nitrogen, starch and cellulose), 529nm (associated with chlorophyll) and 2240nm (associated with cellulose). So far there appear to be significant differences between Hyperion spectra of different ^{137}Cs levels, though radiometric and geometric distortions (attempted to be minimised via corrections) may be accentuating such differences. This does not however account for differences between high and low ^{137}Cs pixels, which have been taken from the same image and show similar significant differences. Figure 7.5 shows the Hyperion spectra for medium versus low ^{137}Cs spectra to assess whether the pattern of difference is the same as in figures 7.3 and 7.4.

The general pattern of significant wavelengths is once again similar with 437nm (associated with chlorophyll) being the largest significant t-value. This is followed by 1442nm (associated with lignin), 722nm (associated with chlorophyll), 692nm (associated with chlorophyll), 2017nm (associated with starch), 1291nm (unattributable), 1956nm (associated with water, lignin, protein, nitrogen, starch, cellulose), 529nm (associated with chlorophyll) and 2240nm (associated with cellulose). There are more significant t-values in the medium versus low ^{137}Cs levels, which may be corroborated by the different transfer factors as shown by the laboratory experiment (chapter 6) whereby medium contamination levels contained more ^{137}Cs than the trees growing in greater levels of ^{137}Cs. Once again, these could be due to radiometric and geometric distortions since the spectra are taken from two different images. In all three t-tests, the chlorophyll waveband has emerged with the highest t-value. In chapter 5 however, chlorophyll is considered as conditionally independent of ^{137}Cs. In short, there are statistically significant differences across the spectra in all three t-tests, however it is difficult to isolate whether these differences are caused by changing ^{137}Cs levels or other environmental factors. Since there is no coincident biochemical data, environmental factors are difficult to rule out. To try to eliminate other environmental conditions and assess whether these differences follow a similar pattern to the field spectra, the t-test result from field spectra and imagery are presented on the same graph in figure 7.6 for ease of comparison.

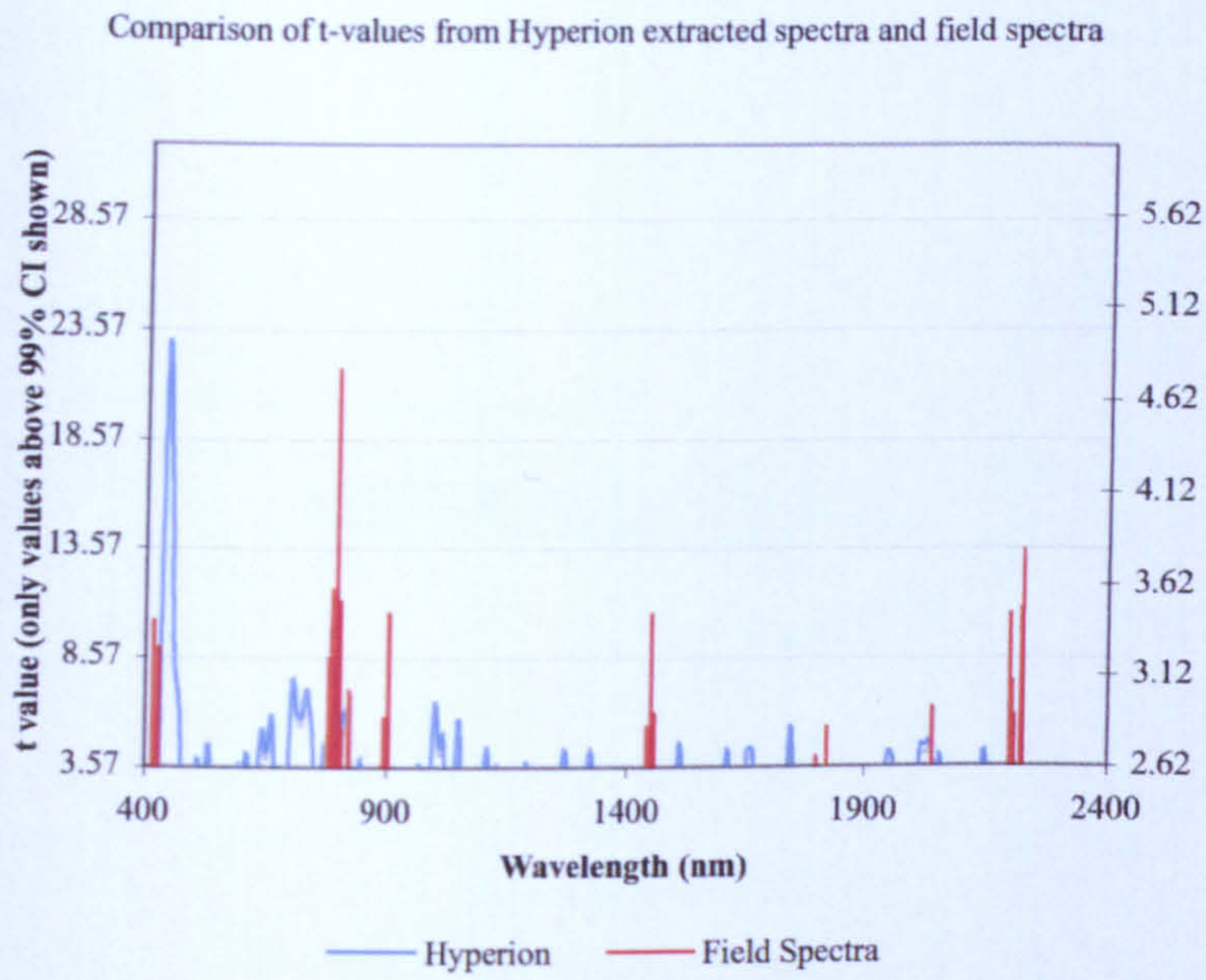

Figure 7.6: Comparison of statistically significant t-values for spectra taken from Hyperion pixels and spectra collected with the ASD field spectrometer in Belarus (Split according to the domestic fuel wood (0.74Bq/g) limit). Note that a secondary axis has been used to ease comparison and interpretation of results.

Figure 7.6 shows three areas of the spectrum where statistically significant differences from imagery and field spectra match. These are at approximately 430nm (associated with chlorophyll), from 770 – 815nm (red edge/unattributable) and finally at around 2040nm (associated with cellulose). The same comparison is shown in figure 7.7, however using the lumber fuel wood limit (1.85Bq/g) spectra as opposed to the field spectra separated according to the domestic fuel wood (0.74Bq/g) limit.

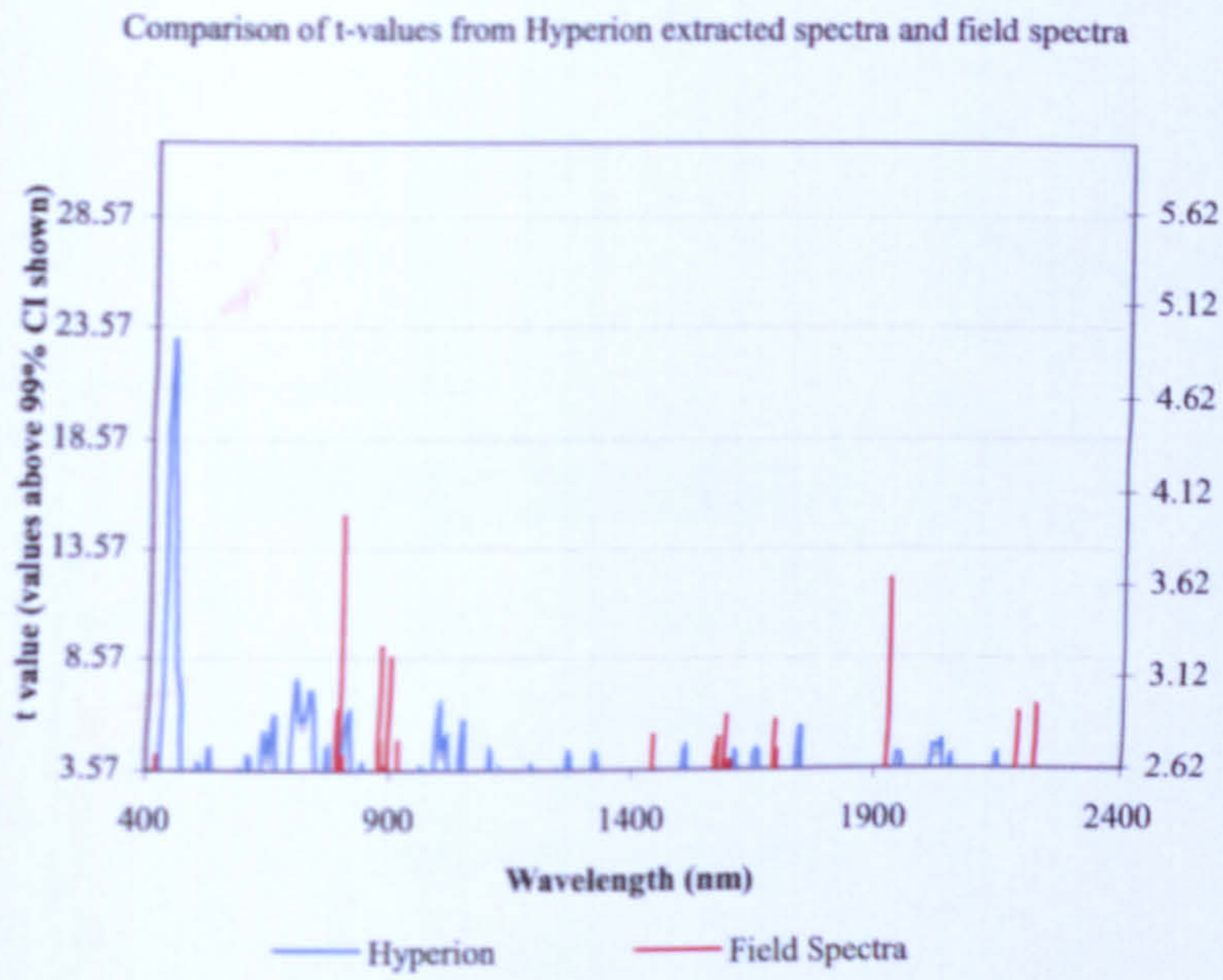

Figure 7.7: Comparison of statistically significant t-values for spectra taken from Hyperion pixels and spectra collected with the ASD field spectrometer in Belarus (Split according to the lumber wood limit (1.85Bq/g) limit). Note that a secondary axis has been used to ease comparison and interpretation of results.

Figure 7.7 shows there are four areas of the spectrum where there are statistically significant differences which match in terms of field spectra (lumber wood limit) and Hyperion extracted spectra. There are differences at 437nm (associated with chlorophyll) 804nm (unattributable), 1602nm (unattributable) and 1956nm (associated with water, lignin, protein, nitrogen, starch, cellulose). Chapter 5 showed that chlorophyll did not differ significantly based on changing ^{137}Cs levels, yet this region appears as the most statistically significant in terms of the t-value, possibly suggesting that the differences shown in the chlorophyll region of the spectrum are affected by another environmental variable (such as biomass) and not differing ^{137}Cs levels. A potential way to analyse if the differences are due to ^{137}Cs is to compare significant differences from imagery pixels with those from the laboratory experiment (chapter 6) where everything remained constant other than ^{137}Cs levels. This was performed and the results are shown in figure 7.8.

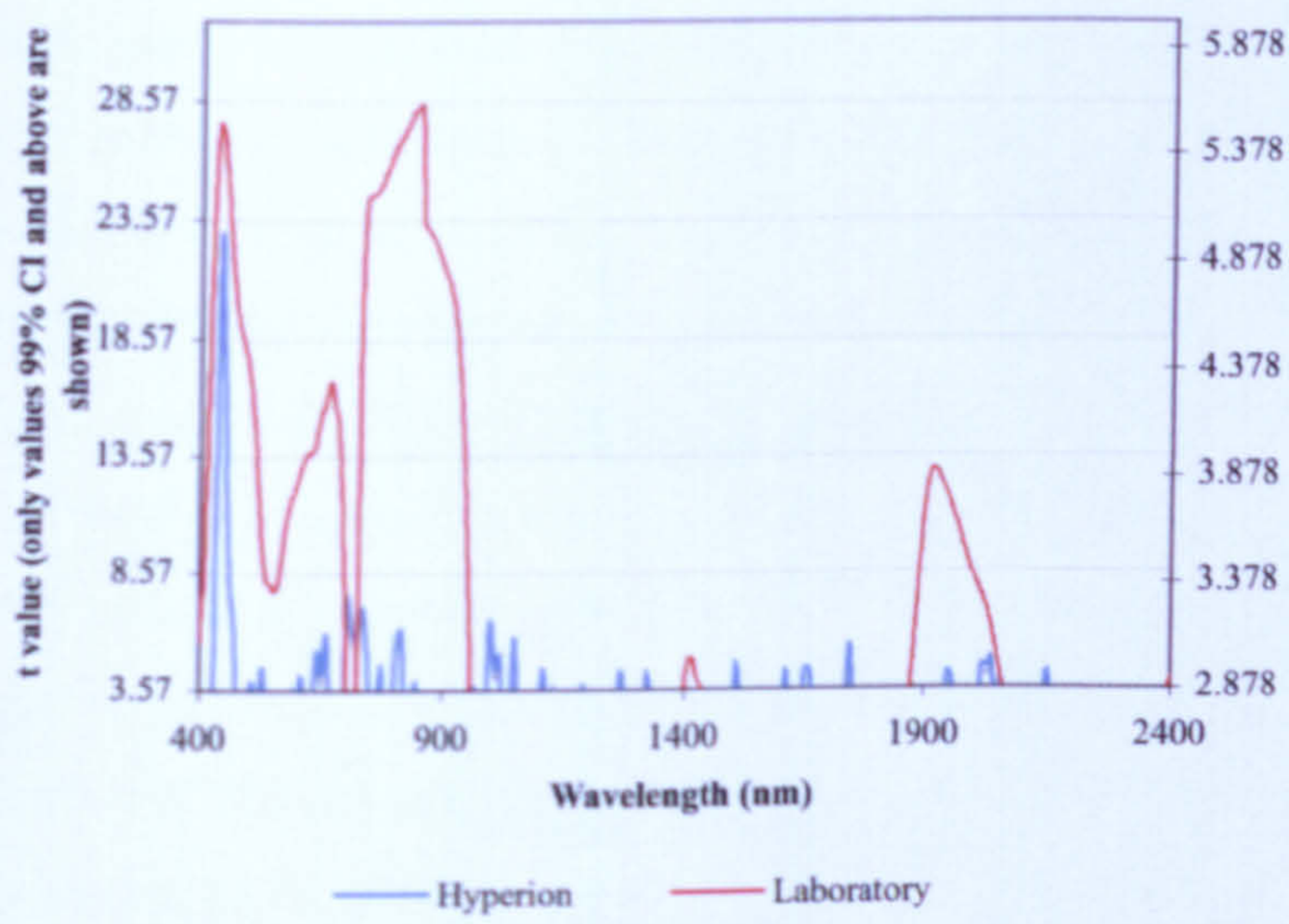

Figure 7.8: Comparison of statistically significant t-values for spectra taken from Hyperion pixels and spectra from the laboratory experiment. Note that a secondary axis has been used to ease comparison and interpretation of results.

Due to the magnitude of difference between ^{137}Cs levels used in the laboratory and those in the field as well as the spectral resolution of the Hyperion instrument versus the ASD spectrometer there are many more wavelengths in the laboratory spectra that are significantly different between high and low ^{137}Cs levels and these tend to occupy continuous parts of the spectrum rather than discrete wavelengths. Having said this, some areas of significant difference match. These are at 450nm (associated with chlorophyll), 697nm (associated with chlorophyll/red edge) 724nm (associated with chlorophyll), 830nm (unattributable), 1956nm (associated with water, nitrogen, starch, cellulose), and 2054nm (associated with nitrogen).

7.7 Summary

In analysing Hyperion extracted spectra, this chapter has shown that statistically significant differences do exist between spectra from relatively high and low levels of ^{137}Cs. Assuming no differences exist in biophysical properties, isolating whether these differences are causally related to ^{137}Cs or due to other environmental variables has been the research challenge in this chapter. By comparing the location of significant t-values from imagery with those collected in the field and laboratory it can be shown that some of these differences occur in the same position of the electromagnetic spectrum and some of

these areas are associated with key foliar biochemicals shown to be affected by ^{137}Cs. Ultimately, whilst this adds confidence that ^{137}Cs impacts can be seen in spectra collected from space, it is by no means conclusive. This is partly due to the results shown in chapters 4, 5 and 6 which do not identify any particular wavelengths or biochemicals that are definitively associated with ^{137}Cs. Further research whereby field spectra and biochemicals collected coincidentally with spaceborne imagery would help to solve research issues highlighted in this chapter and is an area worthy of further study. Collecting field data with due regard to spatial resolution of the imaging spectrometer would also help to assess implications for spatial variability of ^{137}Cs in *Pinus sylvestris*. In addition and perhaps most importantly, the assumption regarding forest biophysical properties would need to be addressed. Forests are challenging targets in terms of their biophysical properties due to the clumping of optically active surfaces, influences of understory, soil and bark as well as the effect of relief and shadow (Schlerf *et al.* 2005). The influence of ^{137}Cs on forest biometric properties and scaling these effects from the needle to the canopy represents a challenge for this research. This chapter however, does indicate potential in spaceborne hyperspectral imagery for monitoring ^{137}Cs levels in *Pinus sylvestris*. The assumptions and limitations represent opportunity for further investigation.

Chapter 8

Discussion and Conclusion

8.1 Introduction

This final chapter brings together results from each of the research chapters to assess how the aims and objectives set out in chapter one have been met and show the implications for using imaging spectrometry to monitor ^{137}Cs levels. It also considers limitations within the research as well as opportunities for further study.

The principal research aim of this thesis was set out in chapter one and was 'can ^{137}Cs contamination be detected by using imaging spectrometry techniques?' To answer this question, four specific research objectives emerged and these are revisited here, providing suitable headings under which to discuss and conclude the research.

8.2 Are Changes in Spectral Response Caused by Differing ^{137}Cs Levels?

Pilot study research (chapter four) has shown statistically significant differences exist between spectra of pine needles contaminated with relatively high and low levels of ^{137}Cs. These differences in spectra signified potential in using spectral response to delineate between ^{137}Cs specific activity of *Pinus Sylvestris*. Tree age was also investigated in this chapter and old trees (c. >20 years) were considered most appropriate for monitoring in terms of the effects of ^{137}Cs and the economic potential given by trees of this age. Subsequent fieldwork focused on old trees; however the laboratory study described in chapter six used *Pinus sylvestris* trees of approximately three years old. Logistically and practically, old trees could not have been dosed with ^{137}Cs and therefore there was no choice but to use young *Pinus sylvestris*. As a means to try to circumvent the inconsistency in tree age between fieldwork and laboratory, dose rates of ^{137}Cs were enhanced in the laboratory relative to those in the field. Time was essentially substituted with increased ^{137}Cs levels. In the laboratory study, spectra show differences, when all other variables were kept constant other than levels of ^{137}Cs. This corroborates what was discovered in the fieldwork chapters (four and five); that spectral reflectance (and various manifestations)

differ at statistically significant levels in response to ^{137}Cs. Hyperspectral imagery collected over the contaminated fieldsites also exhibit statistically significant differences in their spectral response. The research based on Hyperion hyperspectral imagery (chapter seven) makes several assumptions regarding biophysical properties which cannot be ignored, but which point to openings for further research. The fact that statistically significant differences do exist in hyperspectral imagery however does indicate potential in the ability to use spaceborne hyperspectral imaging to monitor ^{137}Cs levels in *Pinus sylvestris*. Each part of the overall investigation (fieldwork studies, laboratory experiment, and Hyperion hyperspectral imaging) has discovered that spectral reflectance and its manifestations (FDS, BDNA, BNC) show changes according to ^{137}Cs levels within *Pinus sylvestris*. Several factors are limiting the ability to compare results from each component of this work and are also preventing the relationship between spectral reflectance and ^{137}Cs from being fully understood. In data from the fieldwork (chapters four and five) there is the difficulty of isolating changes in spectra and attributing them to effects of ^{137}Cs concentration as opposed to other environmental variables. The laboratory experiment was designed to observe effects of ^{137}Cs concentration on spectral reflectance of *Pinus sylvestris* without any confounding environmental variables; essentially to investigate the system in its simplest form. Comparisons between laboratory and field data are however, hindered by differences in tree age between the laboratory (c. <3 years old) and field (c. >20 years old) samples and the lack of biochemical data in the laboratory study. Repeating this experiment and addressing these issues is a key area to follow should this work be continued. Comparing results from imaging spectrometry work (chapter seven) to other research results presents a major challenge in terms of the complexity of the biophysical parameters of *Pinus sylvestris* and their relationship to ^{137}Cs concentration. The hyperspectral Hyperion imagery will be affected by canopy structure, forest stand height and leaf area index (LAI) (Skowronski *et al.* 2007) all of which may be affected by ^{137}Cs concentration and require further investigation. Additionally, the lack of coincidental field data collected alongside the imagery as well as inherent radiometric and geometric distortions prevents a true comparison of imaging spectrometry data to field and laboratory results. Further work can focus on these limitations to provide data from field, laboratory and imagery that could be compared in order to confidently assess whether changes in spectral response are caused by differing ^{137}Cs levels and the mechanisms by which ^{137}Cs is causing these spectral changes (i.e. biophysical factors, biochemical factors, or a combination of both).

8.3 Does ^{137}Cs Contamination have any Effects on Key Foliar Biochemicals and at what Regions of the Optical Range of the Electromagnetic Spectrum are these Detectable?

The Student's t-test between content of nine key foliar biochemicals indicted that up to five exhibited statistically significant differences when grouped according to levels of ^{137}Cs. Depending on the method used to group the samples (lumber or domestic fuel wood limit) affected which biochemicals were highlighted by the t-test as being significant. In the domestic fuel wood limit (0.74Bq/g) grouping three biochemicals were highlighted as significant (lignin, cellulose and elemental N). In the lumber wood limit (1.85Bq/g) five biochemicals were shown to be statistically significant (AD fibre, lignin, cellulose, elemental nitrogen and ^{15}N). It might be expected that the domestic fuel wood (0.74Bq/g) grouping would show a greater number of statistically different biochemicals since the cut off between high and low is based on the limit for a low or non-radioactive material, meaning the difference between high and low levels of ^{137}Cs is greater in this group than the lumber (1.85Bq/g) limit. This suggests that the effect of ^{137}Cs on biochemicals is not necessarily detectable on a linear basis and suggests effects from ^{137}Cs do not occur until higher concentrations are reached. This is corroborated by results from the artificial laboratory experiment where uptake of ^{137}Cs and its effects on plant health are nonlinear. It also shows ^{137}Cs seems to stimulate plant health at relatively low to medium levels but at the highest level has an adverse impact on health. This again might explain why more biochemicals differ significantly in the grouping with a higher cut off limit between high and low levels of ^{137}Cs. Although the laboratory results have provided useful analyses it must be borne in mind that young trees (c. <3 years old) were used in the laboratory experiment for a relatively short period as opposed to old trees in the field (c. >20 years old). The main use of the laboratory experiment has been to assess whether differences in spectral reflectance of *Pinus sylvestris* occur when all other variables are held constant. This has been the case and has strengthened confidence in t-tests from the field spectra and spectra extracted from Hyperion pixels. In addition to the t-test between foliar biochemicals, partial correlation was used to indicate if ^{137}Cs was to blame for the differences between foliar biochemicals as highlighted by the t-test and additionally, to see which part of the spectrum was affected by the ^{137}Cs.

Partial correlations identified two sets of foliar biochemicals; those whose spectral response was affected by ^{137}Cs (conditionally dependent) and those whose spectral response remained unaffected by ^{137}Cs (conditionally independent). Elemental nitrogen, ^{15}N, AD Fibre, Lignin and Cellulose are all conditionally dependent but water and the three variants of chlorophyll are conditionally independent of ^{137}Cs concentration.

This is unexpected given that spectral response seems to be significantly different in regions of the electromagnetic spectrum associated with absorption by chlorophyll. In the laboratory study, and hyperspectral imagery spectra, wavebands in the chlorophyll region of the spectrum are affected by ^{137}Cs. It may be that the methods used to monitor chlorophyll concentration are not accurate enough or that ^{137}Cs has an indirect non-linear effect on chlorophyll. Also, since chlorophyll is comprised of nitrogen and nitrogen is affected by ^{137}Cs then this may be why ^{137}Cs seems to be related to spectral response in this part of the spectrum but not chlorophyll itself.

Water remains unaffected by ^{137}Cs according to both partial correlations and t-tests. This helps to eliminate water deficiency as an alternative variable causing changes in spectral response. Partial correlation and t-tests have shown the two forms of nitrogen and the structural components to be affected by ^{137}Cs. These two biochemicals are now discussed according to the literature and why they might be affected by ^{137}Cs.

In biomass production, lignins show variation depending on growth conditions of trees and not only are they a part of natural physiological development but they provide flexible metabolic responses to external factors such as environmental pollution (Chaplin 1991). Lignification is shown to protect plants against pathogens (Cook *et al.* 1995) and there is also evidence that increases in K concentration stimulates lignification (Mandre *et al.* 2006). In terms of ^{137}Cs this is of interest as Cs is illustrated by White and Broadly (2000) to behave in an analogous way to K. This suggests ^{137}Cs may be stimulating lignification through plant response to ^{137}Cs as a pathogen and/or in response to the ^{137}Cs *per se* as an alternative to K. Whilst the partial correlations and t-tests show significant differences between lignin based on different ^{137}Cs levels the laboratory experiment lacks biochemical data which would have allowed greater insight into the process of lignification with regards to ^{137}Cs.

When significant differences between spectral response of varying ^{137}Cs levels are considered alongside plant structural components (lignin, cellulose, AD fibre) the two results concur with each other. Differences in spectral response in fieldwork, artificial laboratory study and the Hyperion extracted spectra all show significant differences in wavelengths known to be associated with cellulose and lignin. In chapter five, the second highest t-value for the domestic fuel wood grouping is at a wavelength associated with cellulose. In the laboratory study the highest correlation between ^{137}Cs levels and spectral response is at a wavelength associated with lignin and is followed by a wavelength associated with cellulose. Despite limitations in the laboratory and hyperspectral imaging investigations, the collective results indicate that there is a relationship between ^{137}Cs, plant structural components and spectral reflectance. Understanding and utilising this relationship hinges on the ability to use spectral reflectance to predict lignin or cellulose and in turn predict ^{137}Cs. Results from the fieldwork (chapter five) and the laboratory study (chapter six) indicate that this prediction is not possible given the current understanding of the interplay between the three components of ^{137}Cs, plant structural components and spectral reflectance. To unravel this interplay, further research could investigate how ^{137}Cs affects plant structural components by comparing the effect of ^{137}Cs to that of stable Cs isotopes. This would allow an understanding of how the radiation is affecting plant structural components. In addition, the effects of alternative Chernobyl-derived radionuclides such as ^{90}Sr could be monitored in order to see if ^{137}Cs is causing changes in structural components or whether ^{90}Sr is responsible, or alternatively whether a combination of both ^{137}Cs and ^{90}Sr is causing changes to plant structure. If this is the case it may explain why the effects of ^{137}Cs on plant structural components cannot be fully understood from the current results since the effects of ^{90}Sr have not been measured. Comparing the influences of short lived radionuclides such as ^{134}Cs to the long lived isotopes such as ^{137}Cs may also provide useful evidence as to the effects of ^{137}Cs uptake on plant structural components and how this manifests itself in spectral reflectance.

The two variants of nitrogen (^{15}N and elemental N) were both shown by partial correlations and the foliar biochemical t-tests to be affected by ^{137}Cs specific activity. In the domestic fuel wood (0.74Bq/g) grouping, only elemental N was discovered as significant, but in the lumber limit (1.85Bq/g) both variants of N were identified as being affected by ^{137}Cs activity. In the artificial laboratory study (chapter six) and hyperspectral imagery research (chapter seven) some spectral wavelengths identified as being different in

relation to ^{137}Cs levels were associated with N although there were not as many bands as the structural components. Nitrogen has been previously shown to affect ^{137}Cs content in various plant species (e.g. Fuhrmann *et al.* 2003). In addition, Willey and Tang (2006) show that ^{137}Cs contamination may affect sources of N used by plants, hence the findings of this thesis; that ^{137}Cs either affects or is affected by N. In terms of using spectral reflectance (and ultimately, imaging spectrometry) to predict ^{137}Cs there is a requirement to be able to use spectral reflectance to predict changes in plant biochemicals (such as ^{15}N, elemental N, lignin, cellulose and AD Fibre) and in turn ^{137}Cs specific activity. This thesis has shown that ^{137}Cs affects spectral reflectance and that certain foliar biochemicals are conditionally dependent on ^{137}Cs, thus giving potential to indirectly estimate ^{137}Cs content from spectral reflectance, however this thesis has shown that prediction of biochemicals and indirectly, ^{137}Cs from spectra is not straightforward.

8.4 Can Key Foliar Biochemicals be Predicted from Spectral Response and in turn Used to Infer Levels of ^{137}Cs Contamination?

Chapter five has shown that foliar biochemistry of ^{137}Cs contaminated *Pinus sylvestris* can be predicted with accuracy comparable to other applications of field and imaging spectrometry in predicting foliar biochemistry (e.g. O'Neill *et al.* 2002, Grossman *et al.* 1996, Curran *et al.* 2001). Biochemicals shown to be conditionally independent of ^{137}Cs have regression equations with greater accuracy than those biochemicals which are conditionally dependent on ^{137}Cs. This suggests ^{137}Cs may be affecting biochemicals in a non-linear way and interfering with predictive ability. In particular, the concept of radiation hormesis is evident in the literature (e.g. Calabrese 2005). Hormesis, or hormetic response is well documented in toxicology (e.g. Calabrese 2005) and, as applied to radioecology, is the lack of, or stimulating effect of ionising radiation at low dose rates, but adverse effects at high dose rates. Hormesis appears to fit well with the results from the artificial laboratory study suggesting ^{137}Cs may have a stimulating effect at low doses with resulting implications for attempting to use imaging spectrometry to monitor ^{137}Cs. Aside from the differences in predictive ability of the regression equations between conditionally dependent (two forms of nitrogen, structural biochemicals) and independent biochemicals (water, chlorophylls), all can be predicted at a statistically significant level. Stepwise multiple linear regression (SWMLR) was used alongside the technique of partial least squares, but when considered side by side, SWMLR was most suitable for this research.

Forced entry stepwise regression allowed causality to be assigned to the wavebands selected by the statistical procedure. Transformations of spectral response using first derivative and continuum-removal techniques showed that prediction accuracy of particular biochemicals depended on the transformations of the spectral reflectance used and corroborate other research which utilises various spectral transformations to predict biochemicals (Curran *et al.* 2001, Kokaly and Clark 1999). Prediction of foliar biochemistry was central to being able to infer ^{137}Cs through the effects of ^{137}Cs on the foliar biochemicals and in turn spectral response. The ability however to use foliar biochemicals to predict ^{137}Cs has not been successfully demonstrated in this thesis. Using standard linear regression to predict ^{137}Cs from biochemicals did not result in any statistically significant model. Aside from standard linear regression, neural networks were employed to account for the possible non-linearity of the ^{137}Cs effect on foliar biochemicals. The maximum R^2 produced by the neural network was 0.83 but when applied to a test data set the R value was only 0.24 which is not statistically significant. Again, the lack of ability to predict ^{137}Cs specific activity from foliar biochemicals underlines current literature and understanding regarding the behaviour of ^{137}Cs with regards to plant physiology; it is not fully understood. This has implications for the use of imaging spectrometry as although subtle changes in spectra can be detected and foliar biochemicals predicted, the lack of any evident link between ^{137}Cs and foliar biochemistry presently precludes the use of spectra to infer ^{137}Cs specific activity. Having said this, further research opportunities may hep to refine understanding of the links between ^{137}Cs, foliar biochemicals and spectral reflectance and in turn may allow the use of imaging spectrometry. In particular, research into understanding the relationship between ^{137}Cs concentration and forest biophysical properties would complement results from this thesis and may help to understand the complexity of links between ^{137}Cs concentration, foliar biochemistry, biophysical properties and ultimately spectral reflectance of *Pinus sylvestris*. Biophysical variables such as leaf area index (LAI), tree height, tree girth, as well as canopy measures such as crown density and canopy structure would help to elucidate the effects ^{137}Cs is having on *Pinus sylvestris* and in turn may lead to a suitable method of using imaging spectrometry to measure ^{137}Cs concentration in that *Pinus sylvestris*.

8.5 Can any ^{137}Cs Impacts on Spectral Response and Foliar Biochemicals be Monitored from Space Using Imaging Spectrometry?

Hyperspectral remote sensing is a relatively new technology and has the ability to provide detailed spectral signatures of the Earth's surface (Liang and Fang 2004) and thus may be able to monitor changes in spectral reflectance caused by ^{137}Cs contamination. Chapters four, five and six have all demonstrated that spectral response changes based on differences in ^{137}Cs and this therefore gives potential in using spaceborne imaging spectrometers to monitor these changes. Foliar biochemistry is shown to vary in chapter five and all nine foliar biochemicals can be predicted at statistically significant levels, however when utilising foliar biochemistry to predict ^{137}Cs, no significant model can be generated. This means that although it is possible to use spaceborne imaging spectrometry to monitor changes in spectral response, it is currently not possible to link foliar biochemicals and ^{137}Cs. Since the links between spectral reflectance, ^{137}Cs and foliar biochemistry are not yet fully understood, it is impossible at present to use imaging spectrometry to monitor ^{137}Cs specific activity of vegetation. Not only are these links not fully understood, but limitations in chapter seven mean at present it can only be postulated that the differences in spectra caused by ^{137}Cs are visible from space and concur with spectral results from field radiometry (chapters four, five and six). The lack of coincident biochemical data and assumptions about biophysical properties when scaling from leaf to canopy mean that presently results of this research preclude the use of spaceborne imaging spectrometry, but with further research and understanding, this may be possible. In the artificial laboratory experiment the notion of hormesis was explored whereby ^{137}Cs seemed to stimulate plant health at low levels and in turn would have implications in using spaceborne imaging spectrometry in that ^{137}Cs contaminated forests may appear as healthy stands of *Pinus sylvestris*. Again, further research opportunities would enable this to be explored further in relation to foliar biochemicals, ^{137}Cs and spectra.

Spatially, spaceborne imaging spectrometry is also a challenge in that chapter five has shown ^{137}Cs to vary considerably over a field site. Chapter five also shows variability of ^{137}Cs over a single sample (tree) exists but is less than the variability over a field site. 30m spatial resolution of Hyperion is currently the finest spatial resolution of any spaceborne imaging spectrometer but given variability if ^{137}Cs over a field site, future imaging

spectrometers with finer spatial resolution may hold greater potential in mapping subtle differences in ^{137}Cs levels form spectra.

In short chapter seven has shown potential in using spaceborne imaging spectrometry to monitor ^{137}Cs, but further investigation and understanding is required before research can reach a definitive answer.

8.6 Research Limitations

The main limitations of this research come from chapters six and seven (artificial laboratory study and hyperspectral imaging). In chapter six an artificial laboratory experiment provided a unique opportunity to isolate the effects of ^{137}Cs on spectral response, however practical constraints meant young *Pinus sylvestris* trees (c. <3 years) were used when field radiometry work in chapter five focused on older trees (c. >20 years) which had been growing at the time of initial contamination (1986 Chernobyl accident). Dose rates in the laboratory were increased to try to overcome this limitation by substituting time with dose, but physiological differences between young and old trees mean when results from the laboratory and field are compared the differences in age must be borne in mind. Practically speaking, running an experiment with old trees could not take place in a laboratory experiment and application of ^{137}Cs to *Pinus sylvestris* in the natural environment would pose ethical and legal issues.

The laboratory experiment was run over a relatively short timescale (due to practical constraints such as equipment loan) and this resulted in small amounts of new growth needles which meant foliar biochemistry could not be measured due to lack of needle material. Provision of biochemical data may have elucidated the relationship between ^{137}Cs, foliar biochemicals and spectral response and presents an opportunity for further research (section 8.7).

In chapter seven, limitations arose from several areas. The lack of coincident biochemical and other field data created difficulty causally linking Hyperion extracted spectra to foliar biochemistry and ultimately ^{137}Cs. It also meant atmospheric correction of imagery had to be performed using mathematical models as opposed to the more accurate empirical line

method. Radiometric error could therefore potentially be responsible for some of the differences in spectra shown in chapter seven rather than ^{137}Cs. Additionally the collection of the image over the control site was never successful due to cloud cover, meaning secondary knowledge of field areas had to be used to choose clean forest stands where no fieldwork had taken place. When analysing spectra from hyperspectral images assumptions were made regarding biophysical properties which in future research would need more detailed consideration. Variability of ^{137}Cs is shown in chapter five to change over a field site with the spatial resolution of Hyperion possibly being too coarse to measure spectral changes of ^{137}Cs contaminated *Pinus sylvestris* over the Belarusian landscape. These limitations form the basis for further research opportunities.

8.7 Further Research Opportunities

Repeating the artificial laboratory experiment presents a particularly useful opportunity to unravel the relationship between spectral response, ^{137}Cs and foliar biochemistry. Measuring key foliar biochemicals as well as spectral response and ^{137}Cs specific activity would enable isolation of the effect of ^{137}Cs on spectra and biochemicals and could aid in understanding this same relationship in field data. Staged doses and running the experiment over a longer timescale are also factors which could be applied to the design of an experiment to some of the questions remaining from the current experiment and add value to field results.

With regards to fieldwork, further biochemical data could be collected alongside spectra to assess if ^{137}Cs is affecting these. For example literature shows similarities between Cs and K (e.g. White and Broadley 2000) and this suggests it may be beneficial to investigate K concentration and its relationship with ^{137}Cs and spectral response. Mutanga *et al.* (2004) investigate grass quality using K, P, Ca and Mg and this biochemistry could be added to further field radiometry work to improve understanding of ^{137}Cs effects and ultimately attempt prediction of ^{137}Cs from biochemistry.

Assessing potential of spaceborne imaging depends on the success of further field and laboratory work, but collecting imagery coincident with field data would allow increased radiometric accuracy of hyperspectral datacubes and could be linked with field data.

Additionally the consideration of biophysical parameters would enable greater confidence in spectral changes with relation to ^{137}Cs.

8.8 Conclusion

In conclusion, potential exists to monitor ^{137}Cs contamination of *Pinus sylvestris* using imaging spectrometry. With regards to the objectives set out in chapter one, this research has shown the following:

- Field radiometry and the artificial laboratory study has shown there are changes in spectral reflectance in response to differing ^{137}Cs levels.

- ^{137}Cs contamination affects the relationship between spectral reflectance and two forms of nitrogen (elemental N and ^{15}N) as well as lignin, cellulose, and AD Fibre. Total chlorophyll, chlorophylls *a* and *b* and water are not affected by ^{137}Cs contamination. The effects are detectable at wavelengths associated with these biochemicals and this is illustrated by partial correlations in chapter five.

- All foliar biochemicals can be predicted at a statistically significant level using spectral reflectance or a statistical transformation of it. Predicting ^{137}Cs specific activity from foliar biochemistry is not possible using methods and data in this research, though further research may change this.

- Changes in spectral response appear in spectra extracted from spaceborne hyperspectral imagery, however limitations and assumptions mean other variables cannot be excluded as being responsible for these changes. At present ^{137}Cs impacts on spectral response and foliar biochemicals are not fully understood and as such monitoring ^{137}Cs concentration of *Pinus sylvestris* from space using imaging spectrometry is not feasible. Opportunities identified for further research may clarify the relationship between ^{137}Cs, foliar biochemistry and spectral response ultimately allowing the use of imaging spectrometry to monitor ^{137}Cs specific activity.

This thesis has undertaken comprehensive and wide-ranging research with many methods and data (field radiometry, laboratory study, hyperspectral imagery) used to investigate whether *Pinus sylvestris* contaminated with ^{137}Cs can be detected using imaging spectrometry techniques. It has shown potential highlighted limitations and identified where further work is necessary. Current knowledge and results do not allow the use of imaging spectrometry techniques to map ^{137}Cs contamination but when results from this thesis are combined with further research the use of imaging spectrometry may well be a feasible method to monitor ^{137}Cs content of vegetation.

References

Abduragimov, I.M., and Odnolko, A.A. (1993) Fires on radioactively contaminated areas. *Priroda* **1**, 28-30.

Adler-Golden, S., Levine, R., Berk, A., Bernstein, L., Anderson, G. and Pukall, B. (1999) Detection of Cirrus Clouds at 1.13 Microns in AVIRIS Scenes Over Land. *SPIE Proceedings, Optical Spectroscopic Techniques and Instrumentation for Atmospheric and Space Research III*, 3756.

Alves, D., and Skole, D. (1996) Characterising land cover dynamics using multi-temporal imagery. *International Journal of Remote Sensing* **17**, 835-839.

Amiro, B., and Ipatyev, V., (1999) Special overview paper on forests and Chernobyl. *Journal of Environmental Radioactivity* **42**, 7-8.

Analytical Spectral Devices (ASD) (2004) The FieldSpec Pro family of portable spectroradiometers [Online] Available at: <http://www.asdi.com/asdi_t2_pr_sp_fsp.html> [Accessed 03/04/2007].

Andolina, J. and Guillettem, O. (1990) Radiocaesium availability and retention sites in forest humus. In Desmet, G., Nasimbeni, P. and Belli, M.(eds) Transfer of Radionuclides in Natural and Semi-natural Environments. Elsevier: London and New York, pp. 135-142.

Arnon, D. (1949), Copper enzymes in isolated chloroplasts. Polyphenoloxidase in Beta vulgaris. *Plant Physiology* **2**, 1-15.

Asner, G (1998) Biophysical and biochemical sources of variability in canopy reflectance. *Remote Sensing of Environment* **64**, 234-253.

Asner, G., Carlson, K. and Martin, R. (2005) Substrate age and precipitation effects on Hawaiian forest canopies from spaceborne imaging spectroscopy. *Remote Sensing of Environment* **98**, 457-467.

Baklanov, A., Mahura, A., Jaffe, D., Thaning, L., Bergman, R., and Andres, R. (2002) Atmospheric transport patterns and possible consequences for the European North after a nuclear accident. *Journal of Environmental Radioactivity* **60**, 23-48.

Barton F. (2002) Theory and principles of near infrared spectroscopy. *Spectroscopy Europe* **14**, 1, 12-18.

Bayari, C. and Kurttas, T. (2002) Coastal and submarine karstic discharges in the Gokova Bay, SW Turkey. *Quarterly Journal of Engineering Geology and Hydrogeology* **35**, 381-390.

Belluco, E., Camuffo, M., Ferrari, S., Modenese, L., Silvestri, S., Marani, A., and Marani, M. (2006) Mapping salt-marsh vegetation by multispectral and hyperspectral remote sensing. *Remote Sensing of Environment* **105**, 54-67.

Ben-dor, E. Kindel, B and Goetz, A. (2004) Quality assessment of several methods to recover surface reflectance using synthetics imaging spectroscopy data. *Remote Sensing of Environment* **90**, 389-404.

Blackburn, G. (2002) Remote sensing of forest pigments using airborne imaging spectrometer and LIDAR imagery. *Remote Sensing of the Environment* **82**, 311-321.

Blacksmith Institute (2007) The World's Worst Polluted Places [Internet] Available at <http://www.blacksmithinstitute.org> [accessed 20/09/07].

Boyd, D., Entwistle, J., Flowers, A., Armitage, A. and Goldsmith, P. (2006) Remote sensing the radionuclide contaminated Belarusian landscape: a potential for imaging spectrometry? *International Journal of Remote Sensing* **27**, 1865-1874.

Boyd, D., Foody, G. and Ripple W. (2002) Evaluation of approaches for forest cover estimation in the Pacific Northwest, USA, using remote sensing. *Applied Geography* **22**, 375-392.

Broadley M., Escobar-Gutiérrez A., Burns A., and Burns, I. (2000) What are the effects of nitrogen deficiency on growth components of lettuce? *New Phytologist* **147**, 519-526.

Brown, C., Nelson, R., and Fingas, M. (1996) Recovery of the Irving Whale oil barge: overflights with the laser environmental airborne fluorosensor. *Spill Science and Technology Bulletin* **3**, 231-234.

Brown, J., Alfonso, B., Avila, R., Beresford, N., Copplestone, D., Prohl, G. and Ulanovsky, A. (2008) The ERICA assessment tool. *Journal of Environmental Radioactivity* **in press.**

Cajaraville, M.P. (2000) Towards an integrative approach in environmental contamination and toxicology. *The Science of the Total Environment* **247**, 95-97.

Calabrese, E. (2005) Paradigm lost, paradigm found: The re-emergence of hormesis as a fundamental dose response model in the toxilogical sciences. *Environmental Pollution* **138**, 378-411.

Calabrese, E. and Baldwin, L. (2000) Radiation hormesis: the demise of a legitimate hypothesis. Human and Experimental Toxicology **19**, 76-84.

Campbell, J. (1996) Introduction to remote sensing. The Guildford Press, New York.

Carpenter, G., Gopal, S., Macomber, S., Martens, S., Woodcock, C. and Franklin, J. (1999) A Neural Network Method for Efficient Vegetation Mapping. *Remote Sensing Environment* **70**, 326-338.

Carter, G. (1993) Responses of Leaf Spectral Response to Plant Stress. *American Journal of Plant Botany* **3**, 239-243.

Chapin, F., (1991) Effects of multiple environmental stresses on nutrient availability and use. In: Mooney, H., Winner, W., Pell, E. (eds.) Response of Plants to Multiple Stresses. Academic Press, San Diego, pp.67-88.

Chavez, P. (1989) Radiometric calibration of Landsat Thematic Mapper multispectral images. *Photogrammetric Engineering and Remote Sensing* **55**, 1285-1294.

Chen, X. Zhao, H., Li, P. and Yin, Z. (2006) Remote sensing image-based analysis of the relationship between urban heat island and land use/cover changes. *Remote Sensing of Environment* **104**, 133-146.

Ciffroy, P., Beaugelin-Seiller, K., Luck, M. and Siclet, F. (2007) Protection of non-human biota against radiation in freshwater-Effect of time dependence in tiered exposure assessment. *Ecological Modelling* **206**, 360-368.

Clemente, H., Cerrillo, R., Hernandez Bermejo, J. and Gitas I. (2006) Modelling and monitoring post-fire vegetation recovery and diversity dynamics: A diachronic approach using satellite time-series data set. *Forest Ecology and Management* **234S**, S194.

Cook, D., Dreyer, D., Bonnet, D., Howell, M., Nony, E. and VandenBosch, K. (1995) Transient Induction of a Peroxidase Gene in Medicago truncatula Precedes Infection by Rhizobium meliloti. *The Plant Cell* **7**, 43-55.

Coops, N., Wulder, M. and White, J. (2006) Integrating remotely sensed and ancillary data sourced to characterize a mountain pine beetle infestation. *Remote Sensing of Environment* **105**, 83-97.

Copplestone, D., Howard, B. And Brechignac, F. (2004) The ecological relevance of current approaches for environmental protection from exposure to ionising radiation. *Journal of Environmental Radioactivity* **74**, 31-41.

Cresswell A., Sanderson, D. and White D.C. (2006) ^{137}Cs measurement uncertainties and detection limits for airborne gamma spectrometry (AGS) data analysed using a spectral windows method. *Applied Radiation and Isotopes* **64**, 247-253.

Crutzen, P. and Stoermer, E. (2000) The Anthropocene. *IGBP Newsletter* **41**, 17-18.

Curran, P. (1985) Principles of Remote Sensing. Longman, Harlow.

Curran, P. (1989) Remote sensing of foliar chemistry. *Remote Sensing of Environment* **30**, 271-278.

Curran, P., (1994) Imaging spectrometry - its present and future role in environmental research. In Hill, J., and Megier, J. (eds.) (1994) Imaging spectrometry: a tool for environmental observations. Kluwer Academic Publishers, Netherlands.

Curran, P., Dungan, J., and Peterson, D. (2001) Estimating the foliar biochemical concentration of leaves with reflectance spectrometry: testing the Kokaly and Clark methodologies. *Remote Sensing of Environment* **76**, 349-359.

Curran, P., Kupiec, J. and Smith, G. (1997) Remote sensing the biochemical composition of a slash pine canopy. *IEEE Transactions on Geoscience and Remote Sensing* **35**, 415-420.

Davids, C., and Tyler, A. (2003) Detecting contamination-induced tree stress within the Chernobyl Exclusion Zone. *Remote Sensing of Environment* **85**, 30-38.

Davies AMC (2001) Uncertainty testing in PLS regression. Spectrosopy Europe 13, 2, 16-19.

Dawson, T., Curran, P. and Kupiec, J. (1995) Causal Correlation of Foliar Biochemical Concentrations With AVIRIS Spectra Using Forced Entry Linear Regression. *Summaries of the Fifth Annual JPL Airborne Earth Science Workshop* **1**, 43-46.

Dawson, T., Curran, P., and Plummer, S. (1998) LIBERTY - modelling the effects of leaf biochemistry on reflectance spectra. *Remote Sensing of Environment* **65**, 50-60.

Debauche, A. (2004) Continuous radioactivity monitoring systems. From the pre-history of radioprotection to the future of radioecology. *Journal of Environmental Radioactivity* **72**, 103-108.

Demetriades-Shah, T. (1990) High resolution derivative spectra in remote sensing. *Remote Sensing of Environment* **33**, 55-64.

Disney, M., Lewis, P. and Saich, P. (2006) 3D modelling of forest canopy structure for remote sensing simulations in the optical and microwave domains. *Remote Sensing of Environment* **100**, 114-132.

Dobrowski, S., Pushnik, J. Zarco-Tejada, P. and Ustin, S. (2005) Simple reflectance indices track heat and water stress induced changes in steady state chlorophyll fluorescence at the canopy scale. *Remote Sensing of Environment* **97**, 403-414.

Dorigo, W., Zurita-Milla, R., de Wit, A., Brazile, J., Singh, R. and Schaepman, M. (2007) A review on reflective remote sensing and data assimilation techniques for enhanced agroecosystem modelling. *International Journal of Applied Earth Observation and Geoinformation* **9**, 165-193.

Du, Q., Chang, N., Yang, C. and Srilakshmi, K. (2008) Combination of multispectral remote sensing, variable rate technology and environmental modelling for citrus pest management. *Journal of Environmental Management* **86**,14-26.

Dungan, S., Gilmore, M. and Varekamp, J. (2007) Effects of mercury on visible/near-infrared reflectance spectra of mustard spinach plants. *Environmental Pollution* **148**, 301-311.

Dwyer, E., Pinnock, S., Gregoire, M., and Pereira, J.M. (2000) Global spatial and temporal distribution of vegetation fire as determined from satellite observations. *International Journal of Remote Sensing* **21**, 1289-1302.

Dyk .A, Goodenough, D., Bhogal, A. Pearlman, J. and Love, J. (2002) Geometric correction and validation of Hyperion and ALI data for EVEOSD. IEEE, presented at IGARSS 2002, Toronto, Canada, 579-583.

Eitel, J., Gessler, P., Smith, A. and Robberecht, R. (2006) Suitability of existing and novel spectral indices to remotely detect water stress in *Populus* spp. *Forest Ecology and Management* **229**, 170-182.

Entwistle, J., Flowers, A., Greenwood, J., Mellor, A. and Nageldinger, G. (2005) Determination of selected actinides (U, PU and Am) in Belarus soils using high resolution inductively coupled plasma mass and gamma spectrometry. *Geochemistry: Exploration, Environment, Analysis* **5**, 11-19.

Farias, S.S., Casa, V.A., Vazquez, C., Ferpozzi, L., Pucci, G.N., and Cohen, I.M. (2003) Natural contamination with arsenic and other trace elements in ground waters of Argentine Pampean Plain. *The Science of the Total Environment* **309**, 187-199.

Felde, G., Anderson, G., Cooley, T., Matthew, M., Adler-Golden, S., Berk, A. and Lee, J. (2003) Analysis of Hyperion data with the FLAASH atmospheric correction algorithm. *Geoscience and Remote Sensing Symposium, IGARSS Proceedings, IEEE International* **1**, 90 - 92.

Fioretto, A., Di Nardo, C., Papa, S. and Fuggi, A. (2005) Lignin and cellulose degradation and nitrogen dynamics during decomposition of three leaf litter species in a Mediterranean ecosystem. *Soil Biology & Biochemistry* **37**, 1083-1091.

Foster D. and Stine R. (2006) Honest Confidence Intervals for the error variance in stepwise regression. *Journal of Economic and Social Measurement* **31**, 89-102.

Frankart, C., Eullaffroy, P., Vernet, G. (2003) Comparative effects of four herbicides on non-photochemical fluorescence quenching in *Lemna minor*. *Environmental and Experimental Biology* **49**, 159-168.

French, A., Normanb, J., and Anderson M. (2003) A simple and fast atmospheric correction for spaceborne remote sensing of surface temperature. *Remote Sensing of Environment* **87**, 326-333.

Fuhrmann, M., Lasat, M., Ebbs, S., Cornish, J. and Kochian, L. (2003) Uptake and Release of ^{137}Cs by Five Plant Species as Influenced by Soil Amendments in Field Experiments. *Journal of Environmental Quality* **32**, 2272-2279.

Funk, C. and Brown, M (2006) Intra-seasonal NDVI change projections in semi-arid Africa. *Remote Sensing of Environment* **101**, 249-256.

Galvao, L., Ponzoni, F., Epiphanio, J., Rudorff, B. and Formaggio, A.R. (2004) Sun and view angle effects on NDVI determination of land cover types in the Brazilian Amazon region with hyperspectral data. *International Journal of Remote Sensing* **25** (10), 1861-1879.

Gaso, M., Segovia, N., Herrera, T., Perez-silva, E., Cervantes, M., Quintero, E., Palacios, J., and Acosta, E. (1998) Radiocaesium accumulation in edible wild mushrooms from coniferous forests around the nuclear centre of Mexico. *The Science of the Total Environment* **223**, 119-129.

Giardino, C., Brando, V., Dekker, A., Strombeck, N. and Candiani, G. (2007) Assessment of water quality in Lake Garda (Italy) using Hyperion. *Remote Sensing of Environment* **109**, 183-195.

Goetz, A., Ferri, M., Kindel, B. and Zheng, Q. (2002) Atmospheric correction of Hyperion data and techniques for dynamic scene correction. *Geoscience and Remote Sensing Symposium, IEEE* 1408 - 1410.

Goetz, A., Vane, G., Solomon, J., and Rock, B. (1985) Imaging spectrometry for Earth remote sensing. *Science* **211**, 1147 - 1153.

Gommers, A. Gafvert, T. Smolders, E Merckx, R. and Vandenhove, H. (2005) Radiocaesium soil-to-wood transfer in commercial willow short rotation coppice on contaminated farm land. *Journal of Environmental Radioactivity* **78**, 267-287.

Goor, F., and Thiry, Y. (2004) Processes, dynamics and modelling of radiocaesium cycling in a chronosequence of Chernobyl-contaminated Scotts pine (*Pinus sylvestris* L.) plantations. *The Science of the Total Environment* **325**, 163-180.

Grant, R., Zhang, Y., Yuan, F., Wang, S., Hanson, P., Gaumont-Guay, D., Chen, J., Black, T., Barr, A., Baldocchi, D. and Arain, A. (2006) Intercomparison of techniques to model water stress effects on CO_2 and energy exchange in temperate and boreal deciduous forests. *Ecological Modelling* **196**, 289-312.

Grime, J.P. (2001) Plant strategies, vegetation processes and ecosystem properties. Wiley: Chichester.

Grossman, Y., Ustin, S., Jacquemoud, S., Sanderson, E., Schmuck, G. and Verdebout, J. (1996) Critique of stepwise multiple linear regression for the extraction of leaf biochemistry information from leaf reflectance data. *Remote Sensing of Environment* **56**,182-193.

Guillot, L. (2001) Extraction of full absorption peaks in airborne gamma-spectrometry by filtering techniques coupled with a study of the derivatives. Comparison with the window method. *Journal of Environmental Radioactivity* **53**,381-398.

Gunzler, H., and Gremlich, H. (2002) IR spectroscopy: an introduction. Wiley, Weinheim.

Harrell, F. (2006) Regression modeling strategies: with applications to linear models, logistic regression, and survival analysis. Springer-Verlag, New York.

Heal G and Conrad K (2006) Incentive to reduce tropical deforestation. *Journal of Forest Economics* **11**, 201-203.

Hellweger, F., Scholosser, P., Lall, U. And Weissel, J. (2004) Use of satellite imagery for water quality studies in New York Harbor. *Estuarine, Coastal and Shelf Science* **61**, 437-448.

Herbert, S. (2002), A new regulatory role for the chloroplast ATP synthase. *Proceedings of the National Academy of Sciences* **99**, 12518-12519.

Hlavka, C., Peterson, D., Johnson, L. and Ganapol, B. (1997) Analysis of forest foliage using a multivariate mixture model. *Journal of Near Infrared Spectroscopy* **5**, 167-173.

Huanga, Z., Turnera, B., Durya, S., Wallisb, I. and Foley, W. (2004) Estimating foliage nitrogen concentration from HYMAP data using continuum removal analysis. *Remote Sensing of Environment* **93**, 18-29.

International Atomic Energy Agency (1996) Post-Chernobyl scientific perspectives: social health and environmental effects. *IAE Bulletin* **383**.

International Atomic Energy Agency (2006) Environmental consequences of the Chernobyl accident and their remediation: twenty years of experience. *Report of the UN Chernobyl Forum Expert Group.*

Ipatyev, V., Bulavik, I., Baginsky, V., Goncharenko, G., and Dvornik, A. (1999) Forest and Chernobyl: forest ecosystems after the Chernobyl nuclear power plant accident: 1986-1994. *Journal of Environmental Radioactivity* **42**, 9-38.

Jacquemoud, S., Verdebout, J., Schmuck, G., Andreoli, G. and Hosgood, B. (1995) Investigation of leaf biochemistry by statistics. *Remote Sensing of Environment* **54**, 180-188.

Jago, R., Cutler, M., and Curran, P. (1999) Estimating canopy chlorophyll concentration from field and airborne spectra. *Remote Sensing of Environment* **68**, 217-224.

Jayaraman, V., and Srivastava, S. (2002) The invariance of red-edge inflection wavelengths derived from ground based spectroradiometer and spaceborne IRS-P3: MOS-B data. *International Journal of Remote Sensing* **23**, 2741-2765.

Jiang, Z., Huete, A., Chen, J. and Chen Y., Jing Li, J., Yan, G. and Zhang, X. (2006) Analysis of NDVI and scaled difference vegetation index retrievals of vegetation fraction. *Remote Sensing of Environment* **101**, 366-378.

Jupp, D., Lovell J. King, E. (2001) The effects of spectral 'smile' on Hyperion data analysis and options for their reduction. *Unpublished CSIRO Earth Observation Centre Report.*

Kerr, J., and Ostrovsky M. (2003) From Space to Species: Ecological Applications for Remote Sensing. *Trends in Ecology and Evolution* **18**, 299-305.

Kochevaa, K., Lambrevb, P., Georgieva, G., Goltsevc, V. and Karabaliev, M. (2004) Evaluation of chlorophyll fluorescence and membrane injury in the leaves of barley cultivars under osmotic stress. *Bioelectrochemistry* **63**, 121-124.

Kokaly, R. and Clark, R. (1999) Spectroscopic determination of leaf biochemistry using band-depth analysis of absorption features and stepwise multiple linear regression. *Remote Sensing of Environment* **67**, 267-287.

Kooistra, L., Leuven, R., Wehrens, R., Nienhuis, P., and Buidens, L. (2003) A comparison of methods to relate grass reflectance to soil metal contamination. *International Journal of Remote Sensing* **24**, 4995-5010.

Kooistra, L., Salas, E., Clevers, J., Wehrens, R., Leuven, R., Nienhuis, P., and Buydens, L. (2004) Exploring field vegetation reflectance as an indicator of soil contamination in River Floodplains. *Environmental Pollution* **127**, 281-290.

Koponen, S., Pulliainen, J., Servomaa, H., Zhang, Y., Hallikainen, M., Kallio, K., Vepsalainen, J., Pyhalahti, T., and Hannonen, T. (2001) Analysis on the feasibility of multi-source remote sensing observations for chl-*a* monitoring in Finnish lakes. *The Science of the Total Environment* **268**, 95-106.

Kuchment L., Demidov V. and Startseva Z. (2006) Coupled modelling of the hydrological and carbon cycles in the soil-vegetation-atmosphere system. *Journal of Hydrology* **323**, 4-21.

Kwarteng, A. (1998) Multitemporal remote sensing data analysis of Kuwait's oil lakes. *Environment International* **24**, 121-137.

LaCapra, V., Melack, J., Gastil, M. and Valeriano, D., (1996) Remote sensing of foliar chemistry of inundated rice with imaging spectrometry. *Remote Sensing of Environment* **55**, 50-58.

Latifovic, R., Fytas, K., Chen, J. and Paraszczak, J. (2005) Assessing land cover change resulting from large surface mining development. *International Journal of Applied Earth Observation and Geoinformation* **7**, 29-48.

le Maire, G., Francois, C. and Dufrene, E. (2004) Towards universal broad leaf chlorophyll indices using PROSPECT simulated database and hyperspectral reflectance measurements. *Remote Sensing of Environment* **89**, 1-28.

Lee, S., Cohen, W. Kennedy, R., Maiersperger, T. and Gower, S. (2004) Hyperspectral versus multispectral data for estimating leaf area index in four different biomes. *Remote Sensing of Environment* **91**, 508-520.

Li, L., Ustin, S. and Lay, M. (2005) Application of AVIRIS data in detection of oil-induced vegetation stress and cover change ay Jornada, New Mexico. *Remote Sensing of Environment* **94**, 1-16.

Liang, S. and Fang, H. (2004) An improved atmospheric correction algorithm for hyperspectral remotely sensed imagery. *IEEE geosciences and remote sensing letters* **1**, 112-117.

Lichtenthaler, H. (1987) Chlorophylls and carotenoids: pigments of photosynthetic biomembranes. *Methods in Ezymology* **148**, 350-382.

Lillesand T., Kiefer, R. and Chipman J. (2004) Remote sensing and image interpretation. Wiley, New York.

Liu, J., Drummond, J., Li Q, Gille J., and Ziskin, D. (2005) Satellite mapping of CO emission from forest fires in Northwest America using MOPITT measurements. *Remote Sensing of Environment* **95**, 502-516.

Louchard, E., Reid, P., Stephens, P., Davis, C., Leathers, R., Downes, T., and Maffione, R. (2002) Derivative analysis of absorption features in hyperspectral remote sensing data of carbonate sediments. *Optics Express* **10**, 1573-1584.

Lu, X., Hu, Z., Liu, W. and Huang, X (2007) Vegetation growth monitoring under coal exploitation stress by remote sensing in the Bulianta coal mining area. *Journal of China University of Mining and Technology* **17**, 479-483.

Lunetta, R. Johnson, D. Lyon, J. and Crotwell, J. (2004) Impacts of imagery temporal frequency on land-cover change detection monitoring. *Remote Sensing of Environment* **89**, 444-454.

Malek, M., Hinton, T., and Webb, S. (2002) A comparison of ^{90}Sr ^{137}Cs uptake in plants via three pathways at two Chernobyl contaminated sites. *Journal of Environmental Radioactivity* **58**, 129-141.

Mandre, M., Parn, H. and Ots, K. (2006) Short-term effects of wood ash on the soil and the lignin concentration and growth of *Pinus sylvestris*. *Forest Ecology and Management* **223**, 349-357.

Martin, M. and Aber, J. (1997) Estimation of forest canopy lignin and nitrogen concentration and ecosystem processes by high spectral resolution remote sensing. *Ecological Applications* **7**, 431-443.

Metternicht, G. and Zinck, J. (2003) Remote sensing of soil salinity: potentials and constraints. *Remote Sensing of Environment* **85**, 1-20.

Michel, R. (2001) Environmental radioactivity measuring methods. *ECORAD Proceedings, in F. Brechingnac, B.J. Howard (eds.) Radioactive Pollutants – Impact on the Environment, Les Ulis, France 3-7 September 2001*, pp.27-62.

Miller, R. and Small, C. (2003) Cities from space: potential applications of remote sensing in urban environmental research and policy. *Environmental Science and Policy* **6**, 129-137.

Millington, A., Velez-Liendo, X., and Bradley, A. (2003) Scale dependence in multitemporal mapping of forest fragmentation in Bolivia: implications for explaining temporal trends in landscape ecology and applications to biodiversity conservation. *ISPRS Journal of Photogrammetry and Remote Sensing* **12**, 3-24.

Milton, E.J. (2003) Methods in field spectrometry. NERC Equipment Pool for Field Spectroscopy. [online] Available at: <http://www.soton.ac.uk/~epfs/>. [accessed 11/01/04].

Moran, J., Mitchell, A., Goodmanson, G. and Stockburger, K., (2000) Differentiation among effects of nitrogen fertilization treatments on conifer seedlings by foliar reflectance: a comparison of methods. *Tree Physiology* **20**, 1113-1120.

Morisette, J., Nickeson, J., Garrigues, S., Baret, F., Huete, A., Didan, K., Miura, T., van Leeuwen, W. and Friedl, M. (2006) Report from the CEOS Land Product Validation topical workshop on the Validation of global vegetation indices and their time series. *Earth Observation* **18**, 6.

Mutanga, O., Skidmore, A. and Prins, H. (2004) Predicting in situ pasture quality in the Kruger National Park, South Africa, using continuum removed absorption features. *Remote Sensing of Environment* **89**, 393-408.

Mutanga, O., Skidmore, A. and van Wieren, S. (2003) Discriminating tropical grass (*Cenchrus ciliaris*) canopies grown under different nitrogen treatments using spectroradiometry. *ISPRS Journal of Photogrammetry & Remote Sensing* **57**, 263-272.

Mutanga, O., Skidmore, A., Kumar, L. and Ferwerda, J. (2005) Estimating tropical pasture quality at canopy level using band depth analysis with continuum removal in the visible domain. *International Journal of Remote Sensing* **26**,1093-1108.

Mykhaylo, M., Vinichuka, C., Karl J. Johanson K., Rosen, K. and Nilsson, I. (2005) Role of the fungal mycelium in the retention of radiocaesium in forest soils. *Journal of Environmental Radioactivity* **78**, 77-92.

Nelson, D. (ed.) (1998) Dictionary of Mathematics. Penguin Reference Books, London.

NERC FSF (2004), ASD FieldSpec Pro System. [Online] Available at: <http://fsf.nerc.ac.uk> [Accessed 03/04/2004].

Nimis, P., (1996) Radiocaesium in plants of forest ecosystems. *Studia Geobotanica* **15**, 3-49.

O'Neill, A., Kupiec, J. and Curran P. (2002) Biochemical and reflectance variation throughout a Sitka spruce canopy. *Remote Sensing of Environment* **80**, 134-142.

Oron, G. and Gitelson, A. (1996) Real-time quality monitoring by remote sensing of contaminated water-bodies: Waste stabilization pond effluent. *Water Research* **30**, 3106-3114.

Oumeish, O. (2002) Hazards and threats from ionising and nuclear radiation. *Clinics in Dermatology* **20**, 330-335.

Ourcival, J., Joffre, R. and Rambal, S. (1999) Exploring the relationships between reflectance and anatomical and biochemical properties in *Quercus ilex* Leaves. *New Phytologist* **143**, 351-364.

Payne, K., Bowen, H., Hammond, J., Hampton, C., Lynn, J., Mead, A., Swarup, K., Bennett, M., White, P. and Broadley, M. (2004) Natural genetic variation in caesium (Cs) accumulation by *Arabidopsis thaliana. New Phytologist* **162**, 535-548.

Pearlman, J., Barry, P., Segal, C., Shepanski, J., Beiso, D. and Carman, S.L. (2003) Hyperion, a Space Borne Imaging Spectrometer. *IEEE Transactions on Geosciences and Remote Sensing* **41**, 1160-1173.

Penuelas, J. and Filella, I. (1998) Visible and near-infrared reflectance techniques for diagnosing plant physiological status. *Trends in Plant Science* **3**, 4, 151-156.

Pinar, A. and Curran, P., (1996) Grass chlorophyll and the reflectance red edge. *International Journal of Remote Sensing* **17**, 351-357.

Plant, J. Smith D., Smith B. and Williams L. (2001) Environmental geochemistry at the global scale. *Applied Geochemistry* **16**, 1291-1308.

Poiarkov, V., Nazarov, A. and Kaletnik, N. (1995) Post-Chernobyl radiomonitoring of Ukrainian forest ecosystems. *Journal of Environmental Radioactivity* **26**, 259-271.

Porra, R. (2002), The chequered history of the development and use of simultaneous equations for the accurate determination of chlorophylls *a* and *b*. *Photosynthesis Research* **73**, 149-156.

Quattrochi, D. and Goodchild, M. (eds.) (1997) Scale in remote sensing and GIS. CRC Press, Florida.

Raghuraj Rao, K. and Lakshminarayanan, S. (2007) Partial correlation based variable selection approach for multivariate data classification methods. *Chemometrics and Intelligent Laboratory Systems* **86**, 68-81.

Rahu, M. (2003) Health effects of the Chernobyl accident: fears, rumours and the truth. *European Journal of Cancer* **39**, 295-299.

Rajitha, K., Mukherjee, C. and Chandran, R. (2007) Applications of remote sensing and GIS for sustainable management of shrimp culture in India. *Aquacultural Engineering* **36**, 1-17.

Rautiainen, M. (2005) Retreival of leaf area index for a coniferous forest by inverting a forest reflectance model. *Remote Sensing of Environment* **99**, 295-303.

Rees, W.G. (1990) Physical principles of remote sensing. Cambridge University Press, Cambridge.

Research Systems Inc (RSI) (2005) ENVI FLAASH module user's guide, version 4.2 August 2005: Research Systems Inc.

Roberts, D., Keller, M. and Soares, J (2003) Studies of land-cover, land use and biophysical properties of vegetation in the large scale biosphere atmosphere experiment in Amazonia. *Remote Sensing of Environment* **87**, 377-388.

Rosenqvist, A., Shimanda, M., Chapman, B., Freeman, A., De Grandi, G., Saatchi, S., and Rauste, Y. (2000) The global rainforest mapping project: a review. *International Journal of Remote Sensing* **21**, 1375-1387.

Rosso, P. Pushnik, J., Lay, M. and Ustin, S. (2005) Reflectance properties and physiological responses of *Salicornia virginica* to heavy metal and petroleum contamination. *Environmental Pollution* **137**, 241-252.

Rowland, A., and Roberts, J. (1994), Lignin and cellulose fractionation in decomposition studies using acid-detergent fibre methods. *Communications in Soil Science and Plant Analysis* **25**, 269-277.

Salbu, B. (2001) Hot particles - a challenge within radioecology. *Journal of Environmental Radioactivity* **53**, 267-268.

Sandalls, F., Segal, M., and Victorova, N. (1993) Hot particles from Chernobyl: a review. *Journal of Environmental Radioactivity* **18**, 5-22.

Sanders, L., Schott, J. and Raqueno, R. (2001) A VNIR/SWIR atmospheric correction algorithm for hyperspectral imagery with adjacency effect. *Remote Sensing of Environment* **78**, 252-263.

Sanderson, D., Cresswell, A., Hardeman F. and Debauche A. (2004) An airborne gamma-ray spectrometry survey of nuclear sites in Belgium. *Journal of Environmental Radioactivity* **72**, 213-224.

SAS (2005) Jmp Design of statistical experiments. SAS Institute Inc., Cary, NC.

Sato. H, Itoh A. and Kohyama, T. (2007) A new dynamic global vegetation model using a spatially explicit individual-based approach. *Ecological modelling* **200**, 279-307.

Schaepman, M. (2007) Spectrodirectional remote sensing: From pixels to processes. *International Journal of Applied Earth Observation and Geoinformation* **9**, 204-223.

Schimel, D. (1995) Terrestrial Biogeochemical Cycles: Global Estimates with Remote Sensing. *Remote Sensing of Environment* **51**, 49-56.

Schlerf, M. Atzberger, C. and Hill, J. (2005) Remote sensing of forest biophysical variables using HyMap imaging spectrometer data. *Remote Sensing of Environment* **95**, 177-194.

Schmidt, K. and Skidmore A (2003) Spectral discrimination of vegetation types in a coastal wetland. *Remote Sensing of Environment* **85**, 92-108.

Senay G.B. and Elliott R.L. (2000) Combining AVHRR-NDVI and land use data to describe temporal and spatial dynamics of vegetation. Forest Ecology and Management **128**, 83-91.

Serrano, L., Penuelas, J. and Ustin, S. (2002) Remote sensing of nitrogen and lignin in Mediterranean vegetation from AVIRIS data: Decomposing biochemical from structural signals. *Remote Sensing Of Environment* **81**, 355-364.

Shaw, D., Malthus T. and Kupiec J. (1998) High-spectral resolution data for monitoring Scots pine (*Pinus sylvestris* L.) regeneration. *International Journal of Remote Sensing* **19**, 2601-2608.

Skowronski, N., Clark, K., Nelson, R., Hom, J. and Patterson, M. (2007) Remotely sensed measurements of forest structure and fuel loads in the Pinelands of New Jersey. *Remote Sensing of Environment* **108**, 123-129.

Smith A., Wooster, M., Drake, N., Dipotso, F., Flakowski, M. and Hudak, A. (2005) Testing the potential of multi-spectral remote sensing for retrospectively estimating fire severity in African Savannahs. *Remote Sensing of Environment* **97**, 92-115.

Smith, J., Comans, R., Beresford, N., Wright, S., Howard, B. and Camplin, W. (2000) Chernobyl's legacy in food and water. Nature **405**, p.141.

Smolandera, S. and Stenberg, P. (2003) A method to account for shoot scale clumping in coniferous canopy reflectance models. *Remote Sensing of Environment* **88**, 363-373.

Soukhova, N., Fesenko, S., Klein, D., Spiridonov, S., Sanzharova, N., and Badot, P. (2003) ^{137}Cs distribution among annual rings of different tree species contaminated after the Chernobyl accident. *Journal of Environmental Radioactivity* **65**, 19-28.

Sridhar, B., Han, F., Diehl, S., Monts, D. and Su, Y. (2007) Monitoring the effects of arsenic and chromium accumulation in Chinese brake fern (Pteris vittata). *International Journal of Remote Sensing* **28**, 5, 1055-1067.

Staenz, K., Nadeau, C., Neville, R. and Secker, J. (2001) Effect of radiative transfer codes for mineral mapping using hyperspectral data. *Proceedings of the 8th international symposium on physical measurements and signatures in remote sensing, France January 8-12.*

Steiger, J. (1980). Tests for comparing elements of a correlation matrix. *Psychological Bulletin* **87**, 245-251.

Su, Y., Sridhar, B., Han, F., Diehl, S. and Monts, D. (2007) Effect of bioaccumulation of cs and sr natural isotopes on foliar structure and plant spectral reflectance of Indian mustard (Brassica juncea). *Water Air and Soil Pollution* **180**, 65-74.

Tanaka, A. and Tanaka, R. (2006) Chlorophyll metabolism. *Current Opinion in Plant Biology* **9**, 248-255.

The World Bank (2006) Belarus: Addressing Challenges Facing the Energy Sector. [Internet] Available at <http://web.worldbank.org/> [accessed 13/09/07].

Thenkabail, P., Enclona, E., Ashton M., and Meer, B. (2004[a]) Accuracy assessments of hyperspectral waveband performance for vegetation analysis applications. *Remote Sensing of Environment* **91**, 354-376.

Thenkabail, P., Enclona, E., Ashton, M., Legg, C. and Dieu, M. (2004[b]) Hyperion, IKONOS, ALI, and ETM+ sensors in the study of African rainforests. *Remote Sensing of Environment* **90**, 23-43.

Thiry, Y., Goor, F., and Riesen, T. (2002) The true distribution and accumulation of radiocaesium in stem or Scotts Pine (*Pinus sylvestris* L). *Journal of Environmental Radioactivity* **58**, 243-259.

Tobias, R. (1997) An introduction to partial least squares regression. SAS Institute, Cary.

Tottrup, C. and Rasmussen, M. (2004) Mapping long-term changes in savannah crop productivity in Senegal through trend analysis of time series of remote sensing data. *Agriculture, Ecosystems and Environment* **103**, 545-560.

Treitz, P. and Rogan, J. (2004) Remote sensing for mapping and monitoring land-cover and land-use change-an introduction. *Progress in Planning* **61**, 269-179.

Tyler, A., Svab, E., Preston, T., Presing, M. and Kovacs, W. (2006) Remote sensing of the water quality of shallow lakes: A mixture modelling approach to quantifying phytoplankton in water characterized by high-suspended sediment. *International Journal of Remote Sensing* **27**, 1521-1537.

ud din, S., Dousari, A. and Literathy, P. (2008) Evidence of hydrocarbon contamination from the Burgan oil field Kuwait – Interpretations from thermal remote sensing data. *Journal of Environmental Management* **86**, 605-615.

Underwood, E., Mulitsch, M., Greenberg, J., Whiting M., Ustin, S. and Kefauver, S. (2006) Mapping invasive aquatic vegetation in the Sacramento-San Joaquin Delta using hyperspectral imagery. *Environmental Monitoring and Assessment* **121**, 1573-2979.

United Nations (2003) Declaration of principles on the CORE programme, Co-operation for rehabilitation of living conditions in Chernobyl affected areas in Belarus.[Internet] Available at: <http://www.un.org> [accessed 18/12/06].

Vagan, T. (2006) Remote sensing of complex land use change trajectories – a case study from the highlands of Madagascar. *Agriculture, Ecosystems and Environment* **115**, 219-228.

Vandenhove, H., Goor, F., O'Brien, S., Grebenkov, A., and Timofeyev, S. (2002) Economic viability of short rotation coppice for energy production for reuse of caesium-contaminated land. *Biomass and Bioenergy* **22**, 421-431.

Vargo, G. (2000) The Chernobyl accident: a comprehensive risk assessment. Battelle Press, Ohio.

Vignolo, A., Pochettino, A. and Cicerone, D. (2006) Water quality assessment using remote sensing techniques: Medrano Creek, Argentina. *Journal of Environmental Management* **81**, 429-433.

Vincent, R. (1997) Fundamentals of geological and environmental remote sensing. Prentice Hall, London.

Walker, P. (ed.) (1999) Chambers Dictionary of Science and Technology. Cambridge University Press, Cambridge.

Warner, T. and Shank, M. (1997) Spatial autocorrelation analysis of hyperspectral imagery for feature selection. *Remote Sensing of Environment* **60**, 58-70.

Webster, C., Davis, M., Escobar, D., and Everitt, J. (1999) Utilization of airborne photography in the investigation of PCB contamination in Donna Reservoir, Lower Rio Grande Valley, Texas. *Texas Journal of Science* **51**, 259-266.

White, P. and Broadley, M. (2000) Mechanisms of caesium uptake by plants. *New Phytologist* **147**, 241-256.

Willey, N. and Tang, S. (2006) Some effects of nitrogen nutrition on caesium uptake and translocation by species in the *Poaceae*, *Asteraceae* and *Caryophyllidae*. *Environmental and Experimental Botany* **58**, 114-122.

Williams, P. and Norris, K. (1987) Near-infrared technology in the agricultural and food industries. American Association of Cereal Chemists, Minneapolis.

Wittenberg, L., Malkinson, D., Beeri, O., Halutzy, A. and Tesler, N. (2007) Spatial and temporal patterns of vegetation recovery following sequences of forest fires in a Mediterranean landscape, Mt. Carmel Israel. *Catena* **71**, 76-83.

World Nuclear Association, (2001) Energy for sustainable development: Chernobyl. [Internet] Available at <http://www.world-nuclear.org/info> [Accessed 28 May, 2006].

Yamano, H. And Tamara, M. (2004) Detection limits of coral reef bleaching by satellite remote sensing: Simulation and data analysis. *Remote Sensing of Environment* **90**, 86-103.

Yoder B. and Pettigrew-Crosby, R. (1995) Predicting nitrogen and chlorophyll content and concentrations from reflectance spectra (400-2500nm) at leaf and canopy scales. *Remote Sensing of Environment* **53**, 199-211.

Zarco-Tejada, P., Miller, J., Harron, J., Hu, B., Noland, T., Goel, N., Mohammed, G., and Sampson, P. (2004) Needle chlorophyll content estimation through model inversion using hyperspectral data from boreal forest conifer canopies. *Remote Sensing of Environment* **89**, 189-199.

Zarco-Tejada, P., Pushnik, J., Dobrowski, S. and Ustin, S. (2003) Steady-state chlorophyll *a* fluorescence detection from canopy derivative reflectance and double-peak red-edge effects. *Remote Sensing of Environment* **84**, 283-294.

Zellmer, J. and Eastman, S. (1997) Incorporation of historical aerial photographs and land-use information into environmental site assessments. *Environmental and Engineering Geoscience* **3**, 431-441.

Zhao, C., Liu, L., Wang, J., Huang, W., Song, X. And Li, C. (2005) Predicting grain protein content of winter wheat using remote sensing data based on nitrogen status and water stress. *International Journal of Applied Earth Observation and Geoinformation* **7**, 1-9.

Zhu Y. and Smolders E. (2000) Plant uptake of Radiocaesium: a review of mechanisms, regulation and application. *Journal of Experimental Botany* **51**, 1635-1645.

Zhu, Y. and Shaw, G. (2000) Soil contamination with radionuclides and potential remediation. *Chemosphere* **41**, 121-128.

Appendix A1

Laboratory Report and Standards from Iso-Analytical

The nitrogen analysis (both elemental nitrogen and ^{15}N) were completed by elemental analyser isotope ratio mass spectrometry (EA-IRMS). The laboratory report and reference standards used are shown in this appendix.

ISO-ANALYTICAL Laboratory Report

Client: Kingston University

Contact: Paul Goldsmith

Analysis: Nitrogen-15 and elemental nitrogen of plant tissue

IA Ref. No.: 060713-2

Reported by: Charles Belanger

Date: 1 September 2006

We have completed nitrogen-15 and elemental nitrogen analysis of the supplied plant samples. The results of analysis can be found as an e-mail attachment in MS Excel format with the name 060713-2-results.XLS. The samples were measured with 20% duplication with all replicate results given. Nitrogen-15 results are presented in per mil notation (‰) versus the primary international reference standard of Air. Elemental nitrogen results are presented in percent notation (wt./wt.)

Nitrogen-15 Analysis

The technique used for analysis was EA-IRMS (elemental analyser isotope ratio mass spectrometry). In brief, tin capsules containing sample or reference material are loaded into an automatic sampler on a Europa Scientific elemental analyser. From where they are dropped in sequence into a furnace held at 1000 °C, where they are combusted in an oxygen rich environment. The tin capsules flash combust, raising the temperature in the region of the sample to ~ 1700 °C. The gases produced on combustion are swept in a helium stream over combustion catalyst (Cr_2O_3), copper oxide wires (to oxidize hydrocarbons), and silver wool to remove sulphur and halides. The resultant gases, N_2, NO_x, H_2O, O_2, and CO_2 are swept through a reduction stage of pure copper wires held at 600 °C. This step removes O_2 and converts NO_x species to N_2. A magnesium perchlorate chemical trap is used to remove H_2O and a Carbosorb trap is used to remove CO_2. Nitrogen is resolved using a packed column gas chromatograph held at an isothermal temperature of 100° C. The resultant chromatographic peak for N_2 enters the ion source of a Europa Scientific 20-20 IRMS where it is ionized and accelerated. Gas species of different mass are separated in a magnetic field then simultaneously measured using a Faraday cup collector array to measure masses 28, 29, and 30 for ^{15}N analysis.

Both references and samples are converted to N_2 and analysed using this method. The analysis proceeds in a batch process by which a reference is analysed followed by a number of samples and then another reference.

Elemental Nitrogen Analysis

The elemental nitrogen content of the samples is calculated using the total ion beam area (in units of ampere-seconds) generated from the IRMS. Each sample's total ion beam area (or TBA) is compared to the TBA of the reference standard which is Iso-Analytical Ltd. working reference standard IA-R001 wheat flour (1.88% nitrogen). IA-R001 is calibrated and traceable to IAEA-N-1 pure ammonium sulphate (21.21% nitrogen) supplied by the International Atomic Energy Agency, Vienna.

Reference Standards

The reference material used during analysis was Iso-Analytical Ltd. working reference standard IA-R001 (wheat flour) with a $\delta^{15}N$ value of 2.55 ‰ vs. Air. IA-R001 is traceable to IAEA-N-1 (ammonium sulphate) with an accepted $\delta^{15}N$ value of 0.40 ‰ vs. Air. IA-R001 was chosen as a reference material as it most closely matches both the isotopic and elemental composition of your samples.

For quality control of isotopic analysis, test samples of IA-R001, IAEA-N-1and IAEA-N-2 ($\delta^{15}N$ of 20.30 ‰ vs. Air) were measured along with the plant samples. The results for these analyses are given in the attached table.

The International Atomic Energy Agency, Vienna, distributes IAEA-N-1 and IAEA-N-2 as isotope reference standard materials.

The unused portions of each sample will be returned to you if you request us to do so, otherwise the samples will be placed in storage for a period of three months after which time they will be disposed of.

If you require any further information regarding the analysis or wish to discuss any related issues, please do not hesitate to contact me.

Analysed and Reported by: Checked by:

Charles Belanger, BSc. Steven Brookes, PhD.

For and on-behalf of:

Iso-Analytical Limited
Millbuck Way
Sandbach, Cheshire
CW11 3HT
UK
Tel: 44 (0)1270 766771 Fax: 44 (0)1270 766709
E-mail: info@iso-analytical.com

Appendix A2

National Physical Laboratory Pine Needle Standard

To accurately determine specific ^{137}Cs activity of *Pinus sylvestris* needles, a National Physical Laboratory (NPL) standard of known activity was used to create a pine needle standard. This enabled the efficiency of the detector to be calculated in turn allowing accurate determination of specific ^{137}Cs activity. The NPL certificate for the radionuclide solution used in the creation of the standard is shown in this appendix.

E/4DC/1
19/5/03

NATIONAL PHYSICAL LABORATORY
Teddington Middlesex UK TW11 0LW Switchboard 020 8977 3222

Certificate of Calibration

UKAS CALIBRATION 0478

MIXED RADIONUCLIDE
STANDARD SOLUTION

PARAMETER MEASURED:	Gamma rays emitted per second per gram of solution at each of twelve specified gamma-ray energies.
DATES OF CALIBRATION:	2 April 2003 to 12 April 2003
IDENTIFICATION	Ampoules A105/03 to A148/03 Product code R08-03
DESCRIPTION	A mixed radionuclide solution containing Americium-241, Cadmium-109, Cobalt-57, Cerium-139, Mercury-203, Tin-113, Strontium-85, Caesium-137, Cobalt-60 and Yttrium-88 as chlorides in 4 M hydrochloric acid. The carrier concentration is approximately 25 µg of each of the above elements, except Americium, per gram of solution. Supplied as 10 g nominal of solution contained in a flame-sealed 10 ml British Standard glass ampoule.

UNCERTAINTIES

The reported uncertainties are based on standard uncertainties multiplied by a coverage factor of $k=2$, which provides a level of confidence of approximately 95%. The uncertainty evaluations have been carried out in accordance with UKAS requirements.

Reference: E03050206/1

Date of issue: 14 May 2003

Checked by: Julian Roan

Signed: (Authorised Signatory)

Name: Mr S M Jerome for Managing Director

Page 1 of 4

[illegible] United Kingdom Accreditation Service. It provides [illegible] measurements made at the NPL or other recognised national [illegible] unless permission for the publication of an approved extract [illegible] the organisation may attributes beyond these stated [illegible]

NATIONAL PHYSICAL LABORATORY

Continuation Sheet

MEASUREMENTS

The samples were prepared by gravimetric dilution of a solution containing a mixture of the radionuclides concerned. The mixture solution had been previously standardised in a manner traceable to national standards of radioactivity. The gamma-ray emission rate per unit mass of the components of the mixture were confirmed using a hyperpure Ge γ-ray spectrometer. The accuracy of the dilution factor was checked using a 'well-type' NaI(Tl) gamma detector.

RESULTS

Gamma-ray emission rates per unit mass at 12:00 GMT on 1 May 2003

Nuclide	Gamma-ray energy (MeV)	Gamma rays per second per gram of solution	Overall uncertainty
Americium-241	0.060	19.2	± 2.7 %
Cadmium-109	0.088	10.2	± 6.3 %
Cobalt-57	0.122	8.8	± 1.6 %
Cerium-139	0.166	9.1	± 1.5 %
Mercury-203	0.279	12.9	± 1.5 %
Tin-113 (via Indium-113m)	0.392	25.6	± 3.6 %
Strontium-85	0.514	35.0	± 2.6 %
Caesium-137	0.662	41.4	± 2.0 %
Yttrium-88	0.898	72.7	± 1.7 %
Cobalt-60	1.173	57.7	± 1.6 %
Cobalt-60	1.333	57.7	± 1.6 %
Yttrium-88	1.836	76.8	± 1.4 %

UNCERTAINTIES

The reported uncertainties are based on standard uncertainties multiplied by a coverage factor of k=2, which provides a level of confidence of approximately 95%. The uncertainty evaluations have been carried out in accordance with UKAS requirements.

Reference: E03050206/1

Checked by: Julian Dean

NATIONAL PHYSICAL LABORATORY

Continuation Sheet

FOR:

School of Life Sciences
Kingston University
Penryhn Road
Kingston-Upon-Thames
Surrey
KT1 2EE

For the attention of: Dr Alan Flowers

AMPOULES SUPPLIED	WEIGHT OF SOLUTION
A107/03	10.63g ± 0.02 g

7/7/03 DISPENSED TO KU source ref. E/ABG/1 ,– 10·56g ± 0·02g.

DATE OF PACKING. 16th June 2003

UNCERTAINTIES

The reported expanded uncertainty is based on a standard uncertainty multiplied by a coverage factor of $k = 2$, providing a level of confidence of approximately 95%. The uncertainty evaluation has been carried out in accordance with UKAS requirements.

Reference: E03050206/1

Checked by:

Page 3 of 4

NATIONAL PHYSICAL LABORATORY

Continuation Sheet

GAMMA-RAY EMISSION PROBABILITIES

Nuclide	Gamma-ray energy (MeV)	Gamma rays per decay	Uncertainty
Americium-241	0.060	0.360	± 0.008
Cadmium-109	0.088	0.0363	± 0.0004
Cobalt-57	0.122	0.8560	± 0.0034
Cerium-139	0.166	0.7987	± 0.0012
Mercury-203	0.279	0.8148	± 0.0016
Tin-113(via Indium-113m)	0.392	0.6489	± 0.0026
Strontium-85	0.514	0.984	± 0.008
Caesium-137	0.662	0.851	± 0.004
Cobalt-60	1.173 1.333	0.99857 0.99983	± 0.00044 ± 0.00012
Yttrium-88	0.898 1.836	0.940 0.9936	± 0.006 ± 0.0006

HALF-LIVES

Nuclide	Half-life (days)	Uncertainty (days)
Americium-241	157850	± 480
Cadmium-109	462.6	± 1.4
Cobalt-57	271.79	± 0.18
Cerium-139	137.640	± 0.046
Mercury-203	46.595	± 0.026
Tin-113	115.09	± 0.08
Strontium-85	64.849	± 0.008
Caesium-137	11020	± 120
Cobalt-60	1925.5	± 1.0
Yttrium-88	106.630	± 0.050

UNCERTAINTIES

The reported uncertainties are based on standard uncertainties multiplied by a coverage factor of $k=2$, which provides a level of confidence of approximately 95%. The uncertainty evaluations have been carried out in accordance with UKAS requirements.

Reference: E03050206/1

Page 4 of 4

Checked by: Julian Dean

Appendix A3

Belarus Deports Chernobyl Expert

Whilst in Minsk, after the collection of field data, but whilst pre-processing biochemical material, Alan Flowers was arrested by the KGB and subsequently deported. This resulted in an early exit from Belarus. The BBC news story detailing the expulsion is contained in this appendix.

BBC NEWS

Belarus deports Chernobyl expert

A British scientist who studied the Chernobyl disaster in the former Soviet Union has been mysteriously deported from Belarus while on a lecture tour.

The decision to rescind his visa was made by the former Soviet republic's interior ministry.

Dr Alan Flowers, a specialist in radiology based at Kingston University, said he was being removed because of his contact with non-government groups.

The Foreign Office confirmed the deportation but declined to comment.

Dr Flowers reportedly started studying the effects of the disaster in 1992.

Radioactive rain

The Chernobyl power station, in Belarus' neighbouring former Soviet republic Ukraine, exploded on 26 April 1986.

The blast, which killed at least 30 people and forced the evacuation of 135,000 more people because of the level of nuclear contamination in the area, was the world's worst nuclear disaster

Vladimir Kuzura, an official from the Belarusian Interior Ministry, refused to explain the reasons behind the withdrawal of Dr Flowers' visa and the deportation order.

But Dr Flowers is said to have made a claim that, if proved right, would cause great embarrassment to former top Soviet officials.

According to Vera Rich, who was the Soviet correspondent of the scientific journal Nature at the time of the tragedy, many believe the then Soviet Union seeded clouds to make them rain on Belarus

Freedom of speech

The move was aimed at preventing winds from blowing contaminated material towards Moscow, theorists say.

But many scientists are highly dubious of claims for successful cloud-seeding. One of the problems is proving that any rain following experiments would not have fallen anyway.

According to Ms Rich, who is currently a freelance writer for the Ukrainian Weekly, Dr Flowers said he had many colleagues in Belarus who believe in this theory but would never admit it in public for fear of retaliation.

In her article, she quoted him as saying: "For a full understanding of the distribution and effects of the Chernobyl fallout, we need as much evidence as possible.

"What caused the rain is still an uncertainty in our knowledge about the intensity and nature of the contamination."

The Chernobyl disaster led to a dramatic rise in the number of cases of thyroid cancer, leukaemia and birth defects, especially in Belarus.

Up to seven million people are believed to have been affected.

Belarusian President Alexander Lukashenko has imposed strict controls on freedom of expression, and the country is being increasingly isolated by the west.

Story from BBC NEWS
http://news.bbc.co.uk/go/pr/fr/-/1/hi/world/europe/3943013.stm

Published: 2004/[illegible] 31 19:24:49 GMT

© BBC MMVII

Appendix A4

Wavebands Used for Forced Entry (Constrained) Regression

In chapter five, forced entry regression was used to produce predictive models of foliar biochemistry from reflectance data. The wavebands used in this constrained regression were not included in the chapter, but are listed in this appendix for reference. They include wavelengths known to be associated with a particular biochemical and wavelengths identified in the partial correlation analysis. The tables show the wavelengths retained by the forced regression and whether they are attributable to a particular biochemical, or from the partial correlation procedure (or both).

Moisture:

Wavelength (nm)	Association
970	Water
552	Chosen by partial
981	Chosen by partial
1436	Chosen by partial (attributable to water)
1942	Chosen by partial (attributable to water)

Lignin:

Wavelength (nm)	Association
1120	Lignin
1174	Lignin
1192	Lignin
1206	Lignin
1442	Lignin
1542	Lignin
1672	Lignin
1690	Lignin
1696	Lignin
1786	Lignin
1940	Lignin
2068	Lignin
2090	Lignin
2214	Lignin
2300	Lignin
439	Selected by partial correlation
857	Lignin
906	Selected by partial correlation
981	Selected by partial correlation
2181	Selected by partial correlation
434	Selected by partial correlation
807	Selected by partial correlation
820	Selected by partial correlation
1445	Selected by partial correlation (attributable to lignin)
1766	Selected by partial correlation (attributable to lignin)
1809	Selected by partial correlation
2129	Selected by partial correlation (attributable to lignin)
2201	Selected by partial correlation (attributable to lignin)
2303	Selected by partial correlation (attributable to lignin)
2373	Selected by partial correlation

Cellulose:

Wavelength (nm)	Association
1275	Cellulose
1448	Cellulose
1484	Cellulose
1490	Cellulose
1536	Cellulose
1540	Cellulose
1578	Cellulose
1924	Cellulose
1940	Cellulose
2084	Cellulose
2340	Cellulose
2356	Cellulose
439	Selected by partial correlation
540	Selected by partial correlation
820	Selected by partial correlation
876	Selected by partial correlation
909	Selected by partial correlation
1053	Selected by partial correlation
1257	Selected by partial correlation (attributable to cellulose)
1442	Selected by partial correlation (attributable to cellulose)
2043	Selected by partial correlation
2080	Selected by partial correlation (attributable to cellulose)
1259	Selected by partial correlation
2025	Selected by partial correlation

Chlorophyll *a*:

Wavelength (nm)	Association
540	Selected by partial correlation (attributable to chlorophyll)
577	Selected by partial correlation (attributable to chlorophyll)
613	Selected by partial correlation (attributable to chlorophyll)
849	Selected by partial correlation
895	Selected by partial correlation
1942	Selected by partial correlation
2043	Selected by partial correlation

Chlorophyll *b*:

Wavelength (nm)	Association
660	Chlorophyll
540	Selected by partial correlation (attributable to chlorophyll)
577	Selected by partial correlation (attributable to chlorophyll)
613	Selected by partial correlation (attributable to chlorophyll)
849	Selected by partial correlation
895	Selected by partial correlation
1942	Selected by partial correlation
2043	Selected by partial correlation
2100	Selected by partial correlation
2303	Selected by partial correlation

Total Chlorophyll:

Wavelength (nm)	Association
540	Selected by partial correlation (attributable to chlorophyll)
577	Selected by partial correlation (attributable to chlorophyll)
613	Selected by partial correlation (attributable to chlorophyll)
849	Selected by partial correlation
895	Selected by partial correlation
1942	Selected by partial correlation
2047	Selected by partial correlation

Elemental Nitrogen:

Wavelength (nm)	Association
910	Nitrogen
1020	Nitrogen
1030	Nitrogen
1060	Nitrogen
1426	Nitrogen
1456	Nitrogen
2060	Nitrogen
2168	Nitrogen
2180	Nitrogen
2274	Nitrogen
2294	Nitrogen
2300	Nitrogen
428	Selected by partial correlation
863	Selected by partial correlation
902	Selected by partial correlation (attributable to nitrogen)
916	Selected by partial correlation (attributable to nitrogen)
1441	Selected by partial correlation (attributable to nitrogen)
2039	Selected by partial correlation
2081	Selected by partial correlation (attributable to nitrogen)
859	Selected by partial correlation

^{15}N:

Wavelength (nm)	Association
910	Nitrogen
1020	Nitrogen
1030	Nitrogen
1060	Nitrogen
1426	Nitrogen
1446	Nitrogen
1456	Nitrogen
1510	Nitrogen
1694	Nitrogen
1974	Nitrogen
1980	Nitrogen
2054	Nitrogen
2060	Nitrogen
2180	Nitrogen
2274	Nitrogen
2300	Nitrogen
2342	Nitrogen
432	Selected by partial correlation
552	Selected by partial correlation
794	Selected by partial correlation
1260	Selected by partial correlation
1436	Selected by partial correlation (attributable to nitrogen)
1809	Selected by partial correlation
2379	Selected by partial correlation
1259	Selected by partial correlation
976	Selected by partial correlation
1385	Selected by partial correlation
1545	Selected by partial correlation
1768	Selected by partial correlation
1846	Selected by partial correlation
2062	Selected by partial correlation (attributable to nitrogen)
2209	Selected by partial correlation
2322	Selected by partial correlation
2361	Selected by partial correlation

Appendix A5

National Physical Laboratory Standard for ^{137}Cs Solution

When dosing the trees grown in the artificial laboratory environment, a ^{137}Cs standard was used to dose the *Pinus sylvestris* trees. This is shown in this appendix.

0/1

NATIONAL PHYSICAL LABORATORY

Teddington Middlesex UK TW11 0LW Switchboard 0181-977 3222

CENTRE FOR IONISING RADIATION AND ACOUSTICS

Certificate of Calibration

MIXED RADIONUCLIDE

STANDARD SOLUTION

PARAMETER MEASURED:	Gamma rays emitted per second per gram of solution at each of twelve specified gamma-ray energies.
DATES OF CALIBRATION:	2 July 1996 to 21 September 1996
IDENTIFICATION:	Ampoules A938/96 - A960/96 Product code R08-04
DESCRIPTION:	A mixed radionuclide solution containing Americium-241, Cadmium-109, Cobalt-57, Cerium-139, Mercury-203, Tin-113, Strontium-85, Caesium-137, Cobalt-60 and Yttrium-88 as chlorides in 4.0 M hydrochloric acid. The carrier concentration is 25 µg of each of the above elements, except Americium, per gram of solution. Supplied as 10 g nominal of solution contained in a flame-sealed 10 ml British Standard glass ampoule.

UNCERTAINTIES

The uncertainties are for a confidence probability of not less than 95%.

Reference: R1604

Page 1 of 4

Date of issue: 1 October 1996

Signed: for the Managing Director, NPL

Checked by:

Name: Dr J B Hunt

This certificate provides traceability of measurement to recognised national standards, and to the units of measurement realised at the NPL or other recognised national standards laboratories. This certificate may only be published in full, unless permission for the publication of an approved extract has been obtained in writing from the Managing Director. It does not of itself impute to the subject of calibration any attributes beyond those shown by the data contained herein.

NATIONAL PHYSICAL LABORATORY
Continuation Sheet

MEASUREMENTS

The solution was prepared by gravimetric dilution of a mixture of the radionuclides concerned, the component nuclides of which had been individually assayed using a high-pressure re-entrant ionisation chamber. The chamber had been previously calibrated for these radionuclides using absolute counting techniques. The activity concentrations of the components of the mixture were confirmed using a hyperpure Ge γ-ray spectrometer. The accuracies of dilutions were checked using a 'well-type' NaI(Tl) gamma detector.

RESULTS

Gamma-ray emissions at 12:00 GMT on 1 October 1996

Nuclide	Gamma-ray energy (MeV)	Gamma rays per second per gram of solution	Overall uncertainty
Americium-241	0.060	144	± 2.4%
Cadmium-109	0.088	103	± 1.8%
Cobalt-57	0.122	78.4	± 0.8%
Cerium-139	0.166	218	± 2.1%
Mercury-203	0.279	113	± 3.6%
Tin-113 (via Indium-113m)	0.392	249	± 1.5%
Strontium-85	0.514	530	± 4.2%
Caesium-137	0.662	311	± 2.3%
Yttrium-88	0.898	3785	± 1.0%
Cobalt-60	1.173	704	± 2.1%
Cobalt-60	1.333	705	± 2.3%
Yttrium-88	1.836	4001	± 3.8%

UNCERTAINTIES

The uncertainties are for a confidence probability of not less than 95%.

Reference: R1604
Checked by: Wendy Brosnan

Page 2 of 4

NATIONAL PHYSICAL LABORATORY

Continuation Sheet

FOR:

Kingston University
Penrhyn Road
Kingston Upon Thames
Surrey
KT1 2EE

For the attention of Mr N Varley

AMPOULES SUPPLIED	WEIGHT OF SOLUTION
A941/96	10.50 ± 0.02 g

DATE OF PACKING: 24 October 1996

UNCERTAINTIES

The uncertainties are for a confidence probability of not less than 95%.

Reference: R1604

Checked by:

Page 3 of 4

NATIONAL PHYSICAL LABORATORY

Continuation Sheet

GAMMA-RAY EMISSION PROBABILITIES

Nuclide	Gamma-ray energy (MeV)	Gamma rays per decay	Uncertainty
Americium-241	0.060	0.360	± 0.008
Cadmium-109	0.088	0.0363	± 0.0004
Cobalt-57	0.122	0.8560	± 0.0033
Cerium-139	0.166	0.7987	± 0.0012
Mercury-203	0.279	0.8148	± 0.0016
Tin-113 (via Indium-113m)	0.392	0.6489	± 0.0025
Strontium-85	0.514	0.984	± 0.008
Caesium-137	0.662	0.851	± 0.004
Cobalt-60	1.173 1.333	0.99857 0.99983	± 0.00043 ± 0.00012
Yttrium-88	0.898 1.836	0.940 0.9936	± 0.006 ± 0.0006

HALF-LIVES

Nuclide	Half-life (days)	Uncertainty (days)
Americium-241	1.5785×10^5	$\pm 0.0047 \times 10^5$
Cadmium-109	462.6	± 1.4
Cobalt-57	271.79	± 0.18
Cerium-139	137.640	± 0.045
Mercury-203	46.595	± 0.025
Tin-113	115.09	± 0.08
Strontium-85	64.849	± 0.008
Caesium-137	1.102×10^4	$\pm 0.012 \times 10^4$
Cobalt-60	1925.5	± 1.0
Yttrium-88	106.630	± 0.049

UNCERTAINTIES

The uncertainties are for a confidence probability of not less than 95%.

Reference: R1604

Checked by: Wendy Brosnan

Page 4 of 4

Appendix A6

Hyperion Imagery Metadata

The metadata for the two Hyperion images used in chapter seven are shown in this appendix. The metadata are split into high and medium and correspond to the specific details of each image described in chapter seven itself.

High Metadata:

Dataset Attribute	Attribute Value
Entity ID	EO1H1810232005236110PW_SGS_01
Acquisition Date	2005/08/24
NW Corner	53°04'58"N, 31°38'08"E
NE Corner	53°03'50"N, 31°44'46"E
SW Corner	52°11'47"N, 31°13'43"E
SE Corner	52°10'40"N, 31°20'14"E
Image Cloud Cover	10% to 19% Cloud Cover
Image Quality	9
Receiving Station	SGS
Scene Start Time	2005:236:08:38:39.307
Scene Stop Time	2005:236:08:38:55.307
Date Entered	2005/09/05
Target Path	181
Target Row	23
Orbit Path	181
Orbit Row	23
Browse Available	Yes
Look Angle	-1.3798
Sun Azimuth	152.211748
Sun Elevation	45.537296

Medium Metadata:

Dataset Attribute	Attribute Value
Entity ID	EO1H1810232005252110PX_SGS_01
Acquisition Date	2005/09/09
NW Corner	53°13'42"N, 31°13'42"E
NE Corner	53°12'35"N, 31°20'24"E
SW Corner	52°20'29"N, 30°49'46"E
SE Corner	52°19'23"N, 30°56'21"E
Image Cloud Cover	0% to 9% Cloud Cover
Image Quality	9
Receiving Station	SGS
Scene Start Time	2005:252:08:38:26.434
Scene Stop Time	2005:252:08:38:42.434
Date Entered	2005/09/20
Target Path	181
Target Row	23
Orbit Path	181
Orbit Row	23
Browse Available	Yes
Look Angle	-3.9515
Sun Azimuth	155.442771
Sun Elevation	40.039005